In vivo modelling of tumour suppressor gene function

JOANNA ZABKIEWICZ

PhD

Cardiff University

2005

ProQuest LLC
789 East Eisenhower Parkway
P.O. Box 1346
Ann Arbor, MI 48106-1346

Declaration

I hereby declare that this work has not previously been accepted in substance for any degree and is not being currently submitted in candidature for any degree.

This thesis is the result of my own investigations, except where otherwise stated within the text.

If accepted, I give consent for my thesis to be available for photocopying and interlibrary loan, and for the title and abstract to be made available to outside organisations.

Signature.....

Joanna Zabkiewicz

2005

Acknowledgements

With special thanks to Professor Alan Clarke whose guidance and patience over the last few years was much appreciated.

I would also like to acknowledge the contributions of Dr Owen Sansom for his practical advice and humorous words. Also everyone from the Alan Clarke group past and present, who made my everyday work and life so enjoyable.

I am eternally grateful to all those family and friends that guided and encouraged me during the highs and the lows, especially David Richardson for his continued support.

Table of contents

Abstract

The apoptotic response is mediated by a complex network of pathways, the correct execution of which is essential to the maintenance and general homeostasis of rapidly regenerating tissues such as the intestine. Loss or disruption of the apoptotic machinery and its regulatory genes is hypothesised to result in persistence of damaged or inappropriate cells and to play an important contributory factor in the onset of tumourigenesis and the development of chemoresistance.

This thesis focuses on investigating the modes of action of three proposed intestinal tumour suppressor genes: *MBD4* (a member of the methyl binding domain family), *LKB1* and the pro-apoptotic *DAPK* (both of which encode serine/threonine kinases). Loss of all three proteins has been reported in various sporadic and hereditary gastrointestinal neoplasias, and recent advances in knockout mouse models has provided useful tools with which to investigate the contribution of each gene to apoptosis and tumour prevention within the murine small intestine.

My data outlines an important role for Mbd4 and Dapk in mediating the apoptotic response to a wide variety of chemotherapeutic drugs. Additionally Mbd4 status can determine long term survival *in vivo* to specific types of cytotoxic damage. This may have wider implications for those patients harbouring mutations in the gene and the tailoring of appropriate chemotherapies.

LKB1 has been implicated in a wide range of cellular functions and is associated with many potential substrates in *in vitro* studies, however the *in vivo* role of LKB1 remains unclear and its precise contribution to the prevention of intestinal tumours in the hereditary Peutz-Jegers syndrome is as yet uncharacterised. Conditional deletion of LKB1 in the murine small intestine resulted in significant disruption of intestinal homeostasis, particularly that of the differentiation process, suggesting LKB1 plays a key role in intestinal differentiation and it is loss of this function that predisposes to tumourigenesis.

Abbreviations

ACF = Aberrant crypt foci
AT = Ataxia Telangiectasia
ATM = Ataxia Telangiectasia mutated
ATR = Ataxia Telangiectasia and Rad3 related
5Aza2dc = 5-aza-2-deoxycytidine
BER = Base excision repair
BNF = β-Napthoflavone
bp = base pair
BrdU = 2,5 Bromodeoxyuridine
BS = Blooms syndrome
CDDP = Cisplatin
CRCs = Colorectal Cancers
DD = Death Domain
DDW = deionised distilled water
DED = Death Effector Domain
DEPC = diethylpyrocarbonate
DISC = Death Inducing Signalling Complex
DNMT = DNA methyltransferase
dNTPs = deoxynucleotide triphosphates
DMSO = dimethyl Sulphoxide
DSB = Double Strand Break
dTMP = 2 deoxythymidine - 5- monophosphate
dUMP = 2 deoxythymidine - 5- triphosphate
ECM = Extracellular matrix
E.Coli = *Esherichia coli*
EM = Electron microscopy
ENU = N-ethyl-N-nitrosurea
FAP = Familial adenomatous polyposis
5FU = 5-Flurouracil
fdUDP = 5fluro-2-deoxyuridine-5-diphosphate
fdUMP = 5-fluro-2-deoxyuridine-5-monophosphate
HCC = Hepatocellular Carcinoma
H&E = Haematoxylin and Eosin
HNPCC = Hereditary non polyposis colorectal cancer
HR = Homologous Recombination
HRP = horseradish peroxidase
$3H^T$ = Radio labelled Thymidine
IAPs = Inhibitors of Apoptotic Proteins
IDL = Insertion/deletion loops
γ-IFN = gamma interferon
IHC = Immunohistochemistry
i.p = intra-peritoneal
γ-IR = gamma Ionising Radiation
JPS = Juvenile Polyposis Syndrome
LACs = Lung Adenocarcinomas
LOH = Loss of heterozygosity
MBD = Methyl binding domain
5MeC = 5-methylcytosine

MEFs = Mouse Embryonic Fibroblasts
O6MeG = O6-methylguanine
MGMT = O6-methylguanine DNA methyl transferase protein
MIN = Multiple Intestinal Neoplasia
MLC = Myosin Light Chain
MLCK = Myosin Light Chain Kinase
MMPs = Metalloproteinases
MMR = Mismatch repair
MSI = Microsatellite Instability
mTOR = mammalian target ot rapamycin
MWU = Mann Whitney U statistical test
NBS = Nijmegen Breakage Syndrome
NER = Nucleotide Excision Repair
NHEJ = Non homologous end joining
NLS = Nuclear Localization Signal
NMNU = N-methyl-nitrosurea
NSCLC = Non small cell lung cancer
PAR = Partitioning defective proteins
PARP = poly ADP-ribose polymerase
PBS = Phosphate Buffered Saline
PCD = Programmed Cell Death
PCNA = Proliferating Cell Nuclear Antigen
PCR = Polymerase Chain Reaction
PI3K = phosphoinositide 3-kinase
PIP2 = Phosphoinositol – 4,5-biphosphate
PIP3 = Phosphoinositol –3,4,5-triphosphate
PJS = Peutz-Jegers Syndrome
sPLA2 = Secretory Phospholipase A2
PTEN = phosphatase and tensin homolog
RB = Retinoblastoma
RER+ve = Replication Error positive
RT = room temperature
SEM = Standard error of mean
SDS = sodium dodecyl sulphate
TBST = Tris buffered saline/ Tween
TNF = Tumour Necrosis Factor
TRD = Transcriptional Repression Domain
TS = Thymidylate Synthase
TSA = Trichostatin
WS = Werners syndrome
WT = Wild type
XP = Xeroderma Pigmentosa

Chapter 1. Introduction

1.1.1 Intestinal morphology

The small intestine is a rapidly dividing tissue with a high turnover of cells. The outer layer is composed of a smooth muscle layer, contraction of which aids peristalsis and movement of the gut. The gut mucosa is lined with a sheet of epithelial cells arranged in glandular invaginations termed the crypts of Leiberkuhn that give rise to finger like projections into the lumen termed villi. The vascular lamina propria and muscularis mucosa give underlying support to the epithelial surface, in addition to the lamina propria which provides a supportive network to the epithelial cells containing fibroblasts, fibrocytes, myofibroblasts, endothelial and smooth muscle cells, all of which contribute to secreting growth factors and regulating epithelial cell function (Leedham *et al* 2005) (see figure 1.1A).

During embryogenesis the inner epithelial mucosa invaginates at day 14.5 into pockets within the epithelium forming the crypts of Leiberkuhn. The crypt population is then increased as a result of crypt fission, a process whereby crypts produce daughter crypts by basal bifurcation and longitudinal division (Totafurno *et al* 1987). Mesoderm tissue then differentiates into smooth muscle and connective stromal tissue as a result of anterior-posterior morphogenic waves at E18.5. The crypt/villus structures have a large surface area and a complex vasculature that aids maximum absorption of nutrients in the digestive system.

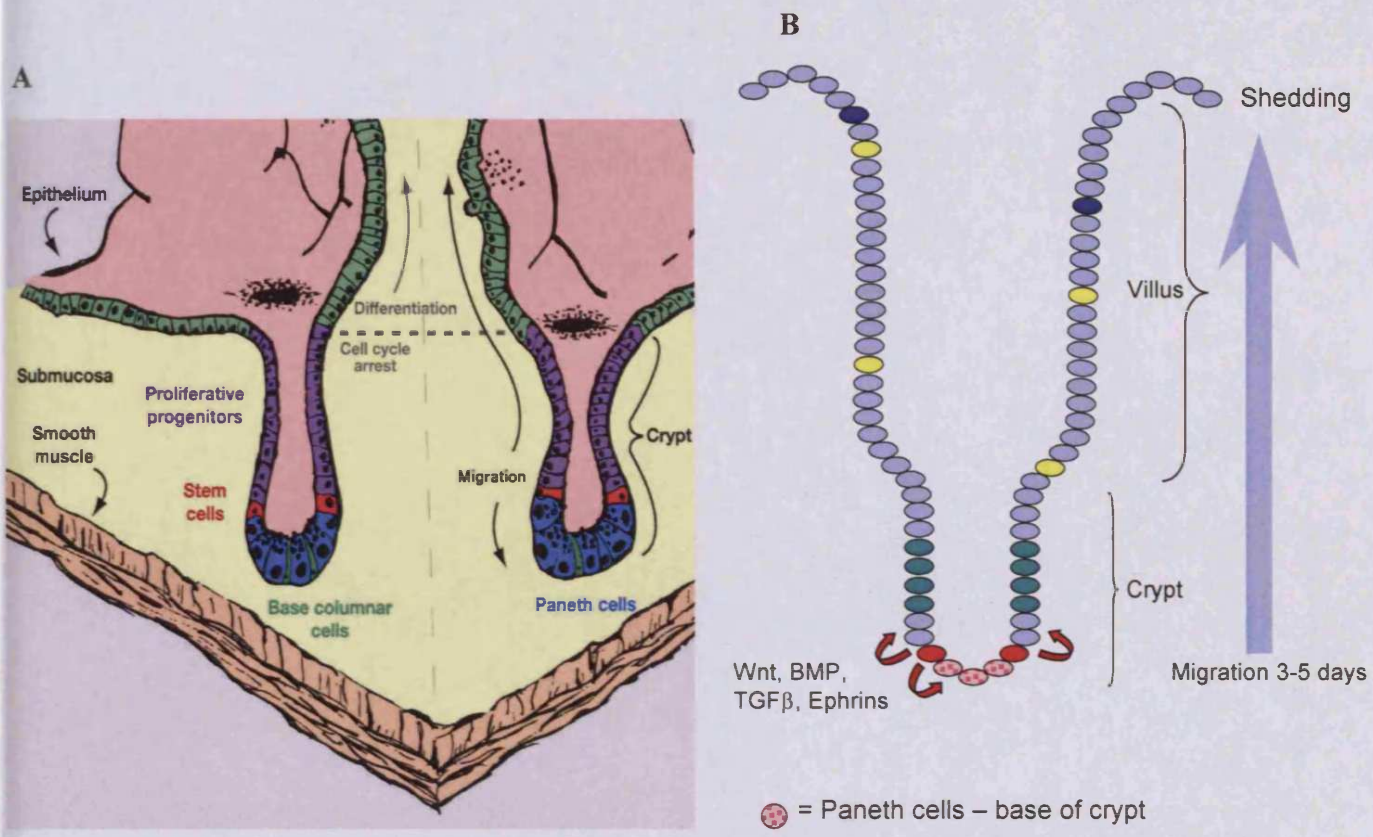

Figure 1.1 **A,** Overview of intestinal structural components (from Sancho *et al* 2004).
B, Schematic representation of cell lineages within the Crypt-villus axis. Stem cell region gives rise to a transit amplification zone in through which cells divide, exit and differentiate as they migrate up the axis

1.1.2 Intestinal Stem cells

A stem cell is defined as having an undifferentiated phenotype, is self maintained, can regenerate upon injury (Potten *et al* 1998), and is pluripotent - supplying a continual production of all the cell lineages (Sancho *et al* 2004). Intestinal stem cells are essential in maintaining homeostasis within the crypt, and epithelial contact with the surrounding mesenchyme contributes to non-autonomous paracrine signalling of cytokines and growth factors (Leedham *et al* 2005). These factors in conjunction with a defined set of epithelial signalling pathways control stem cell activity, proliferation, transit, differentiation and death of cells within the crypt (Sancho *et al* 2004).

$3H^T$ radio labelling and nuclear β-catenin have been used to try to source stem cells within the intestine, although other cell lineages such as paneth cells and proliferative progenitors also stain positive for β-catenin (Sancho *et al* 2003). As a result it is estimated that the adult gut is polyclonal containing between 1-6 active stem cells in each crypt structure, located at positions 4-6 above the base of the crypt.

Stem cells commonly undergo asymmetric division to produce an identical daughter cell and a committed progenitor cell. Symmetric division may produce both stem cell propagation and clonal dominance or stem cell loss through committed daughter cell differentiation. This process of niche succession of stem cells has been suggested to contribute to tumourigenesis via mutations in clonally dominant stem cells (Leedham *et al* 2005).

Previous work using $3H^T$ (radio labelled thymidine) incorporated during DNA replication revealed retention of the parental replicative strand in intestinal stem cells. Retention of the parental template strand circumvents acquisition of replicative errors frequently incurred during replication. Subsequently stem cells are highly sensitive to radiation damage at low doses to protect the parental strand from mutagenesis (Potten 2004). Interestingly progenitor daughter cells which migrate bi-directionally may dedifferentiate to the stem cell niche, suggesting that a hierarchy of stem cells exists providing regenerative capacity depending on age and position of stem cell within the crypt (Potten *et al* 1997).

Given the high levels of control in removing proliferative stem cells and high regulation of programmed cell death in the small intestine, it is not surprising that cancers of the small intestine are relatively rare in humans. This degree of regulation is not observed in the human colon, which frequently displays colorectal cancers (CRCS). However, this does not appear to be reflected in murine models where malignancies of the small intestine are most frequent (Potten 2004).

1.1.3 Intestinal homeostasis and spontaneous cell death

Programmed cell death plays an essential part in the remodelling and general homeostasis of a rapidly regenerating tissue such as the gut. The apoptotic response is crucial to the development of tissues and maintenance of tissue in the adult (Potten and Booth 1997). All cell lines (apart from paneth cells) once differentiated, migrate up the crypt-villus axis over a period of 3-5 days and are then shed into the lumen. Cell loss occurs in a defined hierarchy, and cellular age can be assessed by position of the cell along the axis.

Alterations in cell:cell adhesion induces anoikis based cell death. This process is key to regulating intestinal spontaneous cell death. Loss of anchorage at the tip of the villus is the process underlying the sloughing off into the lumen. Proteins such as laminins, integrins, cadherins and matrix metalloproteinases mediate this mechanism, loss of which contributes to progression of neoplasia (Potten *et al* 1997). Intestinal tumour cells are particularly anoikis resistant and can easily invade stromal tissue following oncogenic Ras/Src/TGF-β stimulation (Morin and Huot 2004).

In addition to cell death by Anoikis at the tip of the villus, spontaneous apoptosis is observed in the stem cell regions of the crypt, and this process occurs infrequently to regulate the number of stem cells. The apoptotic proteins Bcl-2 and p53 seem redundant in anoikis and spontaneous cell death in the small intestine and expression of both proteins is very low (Potten and Booth 1997). Much of the apoptotic process is mediated by Fas signalling and the death receptor pathways (Debatin 2004). The ability of a cell to undergo apoptosis therefore seems dependant upon its position in the crypt and the surrounding environment.

1.1.4 Intestinal cell lineages

The hierarchical crypt structure is organised with the stem cell niche at the base of the crypt, giving rise to a transit proliferative cell zone within the middle of the crypt. All cell division occurs in the transit amplification zone and cells divide every 12 hours. The proliferative and differentiation zones are distinctly separated along the crypt villus axis. Proliferating crypt cells eventually enter G1 cell cycle arrest and

subsequently differentiate and migrate up the villus (see figure 1.1B) (Leedham *et al* 2005).

There are 4 main terminally differentiated intestinal cell lineages, which provide the digestive, absorptive, protective and endocrine functions throughout the gut (Van den Brink *et al* 2001). Mucin secreting Goblet cells provide a protective and lubrication role, as do Paneth cells, which regulate crypt microenvironment via secretion of granules containing cryptidins, defensins, α peptides, sPLA2 and lysozymes, all of which provide a protective antimicrobial function (Porter *et al* 2002). Absorptive enterocytes secrete hydrolases and compromise the majority of crypt/villus cells. Finally enteroendocrine cells secrete neuropeptides and signalling hormones by endocrine or paracrine methods, and are sparsely distributed throughout the villus. In contrast to enterocytes, the secretory lineages are less abundant and typically reside in the villus region. Paneth cells however migrate downwards to the base of the crypt below the stem cell populations where they are phagocytosed after about 20 days (Sancho *et al* 2003).

1.2 Signalling pathways in the intestine

Integration of several signalling pathways within the intestine has been implicated in maintaining correct homeostasis. So far the precise interplay between Wnt, TGFβ, BMP, and Notch has yet to be elucidated but more details are emerging of their distinct roles and their contributions to intestinal tumourigenesis (Sancho *et al* 2004).

1.2.1 Wnt signalling

Wnts are a large family of secreted glycoproteins that play a key role in development of many tissues, in particular the intestine. The downstream transcriptional targets of Wnt - β-Catenin and TCF drive proliferation in conjunction with Myc expression and mediate the proliferative-differentiation switch along the crypt-villus axis as cells move away from the Wnt source (Giles *et al* 2003).

Wnt signalling is one of the best characterised signalling pathways within the intestine, and is seen up-regulated in intestinal stem and progenitor cells at the base of the crypt (Sancho *et al* 2004). Recently however, a mouse model overexpressing Dickkopf 1 (Dkk1), a secreted inhibitor of Wnt signalling, displayed severely reduced crypt structures and shortened villi, suggesting Wnt may actually be required for control of the entire crypt region rather than just at the base (Pinto *et al* 2003).

Downstream targets of Wnt signalling such as the Eph receptors and Ephrin ligands, are expressed in gradients along the crypt-villus axis and define cell positional information, for example to paneth cells which reside at the base of the crypt (Wong *et al* 2000). Adhesion proteins such as integrins, laminins, CD44, Matrix metalloproteinases (MMPs), and semaphorins have also recently been identified as downstream Wnt targets from transcriptome analysis of the Apc^{fl} mouse (Sansom *et al* 2004a), and these cell positioning and contact adhesion molecules help to maintain correct cell localizations within the crypt-villus structure. Remodelling of these junctions is essential during growth, differentiation and death and alterations in junctional proteins commonly links with cancer progression and metastasis.

1.2.2 PI3K/AKT survival signalling

PI3K signalling and its downstream effector protein AKT are involved in mediating cell proliferation, survival, growth and motility events within the intestine. PI3K is composed of 2 subunits: p85 and p110. The p85 domain is a substrate for many cytoplasmic receptor tyrosine kinases via its SH2 domain. Phosphorylation of the p85 subunit acts as a negative regulatory signal for activity of the adjacent p110 subunit. PI3K activity generates the secondary intracellular messenger PIP3 from PIP2, this process is tightly controlled by phosphatases such as PTEN and SHIP1/2, which reverse the process in a GTP dependant manner (Laprise *et al* 2002). PTEN regulates cell growth on 2 levels, firstly blocking post mitotic growth of differentiated cells and second at the cell cycle entry phase for undifferentiated cell types. Pten null mice show increased proliferation in the stem cell region but not in terminally differentiated cell types, suggesting cell type specificity in this process (Backman *et al* 2002).

PI3K signalling within the intestine has been shown to mediate intestinal differentiation by promotion of adheren junction assembly and p38/MAPK survival pathway activation (Laprise *et al* 2002). PI3K signalling is localized to the crypt region similarly to Wnt and inhibition of the pathway further up the villus induces Cdx2 expression, a homeobox protein with a key role in regulating intestinal polarisation and differentiation (Lynch and Silberg 2002).

1.2.3 TGFβ/BMP signalling

TGF-β and BMP signalling negatively regulate growth within epithelial cells and mediate morphogenesis, patterning and organogenesis during intestinal embryonic development (Chen *et al* 2004). Cytokines such as BMPs (bone morphogenic proteins) and Activins act as ligands in TGF-β cascades and signals are tranduced by a network of intracellular molecules: Smads and I-Smads. BMP signalling is inhibited by antagonists such as Noggin and Chordin, which define the inter-villus pockets, which subsequently transform into crypts during development (Sancho *et al* 2004). Mice mutant for BMP genes die during embryogenesis as do those mutant for soluble BMP inhibitors, confirming the critical role for BMP signalling during development (Haramis *et al* 2003).

1.2.4 Notch signalling

Spatial patterning and cell fate is controlled by Notch signalling in intestinal precursor cells. Although much remains to be characterised about the process of intestinal cell differentiation, Notch may be the underlying mechanism for determining cell fate in combination with Wnt signalling which is already known to control the stem cell proliferation/differentiation switch at the base of the crypt (Sancho *et al* 2004).

In the mouse there are 4 Notch receptors and five ligands of the delta and jagged type in addition to various other modifiers. Interaction of Notch receptors with their ligands induces a cleavage of the Notch intracellular domain, which directs cell fate by recruitment of various transcription factors such as Hes1. Cell fate between

adjacent precursor cells may be either cell-autonomous or non-autonomous depending on its surroundings (Schroder and Gossler 2002).

1.2.5 Hedgehog signalling

Hedgehog signalling coordinates with Wnt and Notch to regulate stem cell self-renewal and cell fate. Activation of receptors: smoothened, patched and hedgehog interacting protein by Sonic and Indian hedgehog ligands results in transcription of morphogens involved in cell fate specification and gut architecture modelling. Hedgehog directed cell specification induces the differentiation of smooth muscle and mesenchymal tissue surrounding the epithelium. Mice mutant for Hedgehog components show failure of gut maturation, shorter villi, decreased epithelial progenitors and die shortly after birth, strengthening a role for these genes in intestinal homeostasis (Ramalho-Santos *et al* 2000). Sonic and Indian hedgehog signalling is often upregulated in cancer and autocrine and paracrine signalling from meshenchymal tissue to surrounding cancer cells aids inappropriate cell growth (Sancho *et al* 2004).

1.3 Colorectal Cancer

At least 50% of the western population develops a colorectal polyp by the age of 70, and in about 1 in 10 of these individuals, progression to malignancy ensues (Kinzler and Vogelstein, 1996). Genetic alterations commonly underlie the formation of many tumours and can include: chromosomal changes (such as translocations, duplications, deletions or recombination events, genetic sequence changes (such as substitutions, deletions or insertions), loss of either paternal or maternal allele via loss of imprinting, Loss of heterozygosity (LOH), and gene amplifications (Lengauer *et al* 1998). Accumulation of these genetic changes is the underlying cause of the progression of colorectal cancers (CRCs) and develops via a complex multi-step process that can take many decades to accumulate. The precise contribution played by each mutation remains unclear, although many associations have been made between gene mutation and disease stage. A key challenge has therefore been to link individual genetic changes with the cellular mechanisms underlying disease (Sancho *et al* 2004).

1.3.1 Tumour suppressor genes

Genes found to protect cells from malignant transformation are termed tumour suppressor genes. Mutation of these important genes is usually associated with accelerated tumourigenesis (Kinzler and Vogelstein 1996).

Several classes of tumour suppressor genes have been now identified. The discovery that loss of death inducing genes contributes to cancer formation has lead to the notion of a global 'gatekeeping' role for several tumour suppressor genes, which prevent neoplasia either through the initiation of cell death or via regulation of the cell cycle and proliferation. Such genes include: *p53*, *Rb* and *APC*, all of which help to prevent overgrowth in cancer cells. Investigation of reactivation of these gatekeeper genes may be crucial in the prevention of tumourigenesis and the treatment of cancer cell growth (Kinzler and Vogelstein 1998).

Caretaker tumour suppressor genes indirectly guard against tumourigenesis by guarding genomic stability and help to prevent increased mutation rates. These genes are often DNA repair genes such as: *ATM, MSH* and *MLH1* loss of which may lead to increased mutation burden and acceleration of cancer. However mutations in these genes is rarely an initiating event and therefore restoration of caretaker gene function may do little to promote regression of tumours (Kinzler and Vogelstein 1996)

Our understanding of tumour suppressor genes has become increasingly more complicated over the last few years with the discovery that some tumour suppressor genes fail to conform to Knudson's 2 hit hypothesis, where mutation of the remaining wild type allele of a tumour suppressor gene initiates its tumourigenic potential. Additionally landscaping tumour suppressor function rather than the classical gatekeeper or caretaker function of a gene has been suggested in several cases where tumour microenvironment may play an essential role in tumour suppression. Several inherited tumour susceptibility genes (*PTEN, SMAD4* and *LKB1*) have been linked to hereditary polyposis syndromes and are providing insights into the signalling events between cancer cells and surrounding cells that constitute tumour mass (Kinzler and Vogelstein 1998).

1.3.2 Apoptosis and Disease

The process of apoptosis or cell suicide occurs in both normal and malignant tissues and was suggested to be a genetically controlled process subsequently named Programmed cell death (PCD), found to be critical in embryonic development, the aging process and disease (Wyllie *et al* 1980). Cells undergoing programmed cell death can be identified by their morphological appearance: cell rounding, nuclear condensation (pycnotic nuclei), fragmentation of DNA, chromatin shrinkage, membrane blebbing and formation of apoptotic bodies (Kerr *et al* 1972). Macrophages subsequently phagocytose apoptotic cell bodies to contain spillage of cell contents and prevent inflammatory responses commonly associated with explosive or necrotic cell death (Makin and Hickman 2000).

Loss of control of cell death mechanisms can manifest in several ways. Firstly excessive cell death culminates in deletion of essential cells and developmental abnormalities and in adult tissues is responsible for the onset of neurodegenerative diseases. Peptide inhibitors of apoptosis in neuronal cells are one of the current therapies under development to combat the disease (Pelled *et al* 2002). Secondly, inhibition of the death response in cells by evasion of a host of death inducing cues such as: lack of survival signals, pro-apoptotic signals and inhibition of proliferation, is an underlying mechanism by which cancer cells propagate. Traditionally tumourigenesis studies have focused on cell proliferation and the aberrant survival of mutant cancer cells, but the initiation of the apoptotic response appears to be an equally important event in the development of neoplasia and is frequently found perturbed at different stages of the disease.

The inappropriate persistence of cells unable to correct replicative errors or commit suicide inevitably creates a population of cells highly resistant to the DNA damaging agents used as chemotherapeutics (Potten and Booth 1997). This role for apoptosis in disease has lead to much research in trying to identify some of the key genes involved, and generate novel targets for therapy.

1.3.3 CRC genetics

Accumulation of genetic alterations in tumour suppressor genes or activation of oncogenes contributes to CRC tumourigenesis over a number of years depending on the order and time of inactivation. The canonical progression of CRCs incorporates a series of at least 7 different genetic alterations resulting in the adenoma to carcinoma progression sequence (figure 1.2).

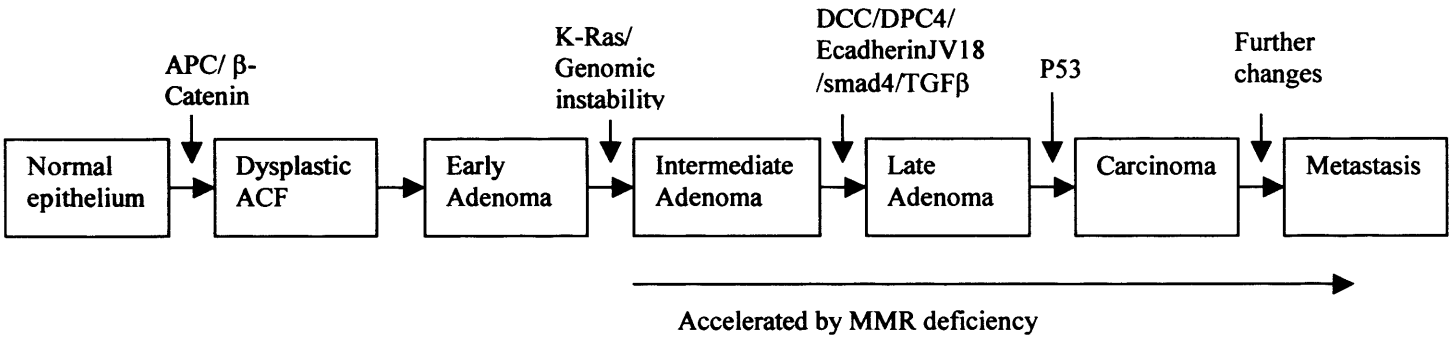

Figure 1.2 – The genetic changes associated with colorectal tumourigenesis. Invasive carcinoma formation is a multi-step process requiring a number of mutations of tumour suppressor and oncogenes in a particular order. (ACF = aberrant crypt foci) (adapted from Kinzler and Vogelstein 1996).

The multiple genetic lesions appear to occur in a specific order. Dysplastic or unicryptal lesions in the intestine are prone to *APC* mutation, which further predisposes to adenocarcinoma formation. Inactivation of both alleles of the tumour suppressor gene *APC* is a frequent initiating event in the process leading to the formation of dysplastic aberrant crypt foci (ACF) which are usually non malignant (Kinzler and Vogelstein 1996). Oncogenic Kras mediated progression of these lesions however is a relatively rare event in CRCs (Sancho *et al* 2004).

Migration of colorectal tumour cells to colonize other tissues in the body is known as metastasis. After the formation of malignancies, metastasizing tumour cells entering the circulatory system must evade a further host of death signalling mechanisms including: detachment of the extracellular membrane, immune system activation, cytokines, superoxides, nitric oxides and shearing forces. Many recently identified tumour suppressor genes function to prevent these late stage changes and induce apoptosis in metastasizing cells (Raveh *et al* 2001).

1.4 Hereditary Colorectal cancers

Inheritance of a single gene mutation can predispose an individual to cancer formation. Hereditary cancers manifest at an earlier age than sporadic cancers generally do as the patients usually harbour germline mutations in one copy of a tumour suppressor gene, the remaining copy of which may be easily lost and cancer ensues. In the intestine several hereditary cancer syndromes exist involving loss of tumour suppressor genes of Gatekeeper, Caretaker and Landscaper function. The 2 most common forms of hereditary CRCs are FAP (familial adenomatous polyposis) and HNPCC (hereditary non polyposis colorectal cancer), both of which are associated with intestinal polyposis and the adenoma to carcinoma progression sequence (Kinzler and Vogelstein 1996).

1.4.1 FAP and Intestinal polyposis syndromes

Familial Adenomatous polyposis (FAP) is one of the best-defined heritable forms of intestinal neoplasia. It is an autosomal dominant disease characterised by the formation of many thousands of benign tumours of the colon known as adenomas. Adenomas and colonic polyps are clonal outgrowths of the intestinal epithelium, additional mutations of which lead to the progression into invasive carcinomas (Reya and Clevers 2005). Other tumours associated with FAP occur in the retina, skin and brain. Patients are predisposed to developing these lesions at a young age and prognosis is poor (Kinzler and Vogelstein 1996).

FAP is caused by germline mutation of the gatekeeper gene tumour suppressor gene *APC* (Adenomatous Polyposis Coli), (Nishisho *et al* 1991), although *APC* has also been shown to be mutated in more common sporadic forms of CRCs mentioned above (Kinzler and Vogelstein 1996). APC loss follows Knudson's two-hit hypothesis, with the crucial step to malignancy being the inactivation of the remaining *APC* allele by somatic mutation (Kinzler and Vogelstein 1996). Loss of the remaining Apc allele by LOH, methylation or somatic mutation promotes tumour initiation and results in adenoma formation. Additional progression is slow and requires subsequent hits to tumour suppressor genes such as K-Ras and p53.

1.4.2 APC

The *APC* gene encodes a large protein of 2843 amino acids. This multi-domain protein is most commonly associated with Wnt signalling, in which it plays a key role in phosphorylating and down regulating β-Catenin via a central binding domain. Wnt signalling is suppressed when cytoplasmic β-Catenin stabilized by the APC/AXIN complex is phosphorylated by Casein Kinase I and GSK-3β and subsequently ubiquitinated and targeted to the proteosome for degradation. On addition of a Wnt ligand, APC scaffolding is blocked and β-Catenin accumulates and translocates into the nucleus where it activates TCF/LEF transcription factors (Giles *et al* 2003).

The APC and β-Catenin complex also binds to cadherins to mediate cell adhesion, therefore implicating APC in several other pathways including: cell-to-cell interactions, apoptosis and proliferation. Additionally the role of APC in mitotic spindle organisation and chromosome stability has been well documented (Bienz and clevers 2000, Giles *et al* 2003).

Inappropriate Wnt activation has been found in 90% of CRCs, making this pathway most important in the study of intestinal cancers. The majority of mutations occur at the c-terminus between codons 1250-1450 in the mutation cluster region causing truncation of the protein. The location and type of mutation directly impacts on the ability of the APC protein to regulate β-catenin levels and ultimately affects onset and severity of the disease. *β-Catenin* mutations are found in around 10% CRCs and are often in conjunction with *APC* mutations (Giles *et al* 2003).

1.4.3 The APC mouse models

The Apc^{MIN} (Multiple intestinal neoplasia) mouse was the first mouse model developed as an investigative tool of the genetic changes underlying FAP. The MIN mutation was developed using mutagenic ethylnitrosourea to introduce a germline nonsense mutation at codon 850 in the *Apc* gene, a mutation which is also commonly found in many FAP patients (Moser *et al* 1990).

Despite mice being predisposed to small intestinal adenoma formation compared to human colonic predisposition, this model largely reflects human FAP and has given an insight into the correlation between mouse and human colorectal cancers. Mice homozygous for the MIN mutation die during embryogenesis, however heterozygous mice with one truncated allele and one remaining wild type *Apc* allele are viable and develop multiple intestinal adenomas, intestinal blockage and anaemia (Moser *et al* 1990).

The genetic background of the mice was found to affect susceptibility to polyp formation, as mice on a Black 6 (BL6) background were found to be more resistant to tumourigenesis. This was later attributed to a dominant modifier locus associated with the *APC* locus termed MOM (Modifier of MIN). This gene encodes phospholipase A2, an enzyme involved in membrane remodelling and alteration of polyp microenvironment (Su *et al* 1992 Moser *et al* 1992, MacPhee *et al* 1995).

COX1 and COX2 are regulators of prostaglandin production as a result of cytokine, growth factor and oncogenic induction and are often over expressed in CRCs. Inhibition of COX2 using Non steroidal anti inflammatory drugs (NSAIDs) such as aspirin was found to suppress tumourigenesis on the Apc^{MIN} background (Mahmoud *et al* 1998, Sansom *et al* 2001a). Therefore COX2 inhibitors are proving useful in clinical trials for CRC patients to help slow tumour formation and aid in regression treatment (Peek 2004).

Conditional inactivation of *Apc* in the adult mouse intestine with Cre-Lox technology and the Apc^{fl} allele has helped to elucidate part of the mechanism of Apc tumour suppressor action (Shibata *et al* 1997). Heterozygote Cre recombinase mediated excision of *Apc* resulted in adenoma formation within 4 weeks (Ghebranious *et al* 1998, Sansom *et al* 2004a). Short-term homozygote *Apc* loss resulted in nuclear accumulation of β-catenin, activated Wnt signalling and disruption of differentiation, migration and intestinal crypt homeostasis. The resultant increase in progenitor-like cells and inability to delete these aberrant cells through migration and apoptosis has been suggested to contribute to the undifferentiated cell type observed in adenomas associated with *Apc* loss (Sansom *et al* 2004a).

1.5 Hamartomatous polyposis

Several other hereditary syndromes manifest with intestinal polyps and studies from polyposis syndromes have been crucial in identifying potential cancer susceptibility genes such as *SMAD4* and *BMP1, LKB1* and *PTEN* (Kinzler and Vogelstein 1998, Sancho *et al* 2004).

Hamartomatous polyps are best described as the overgrowth of cells native to the tissue area. In the intestine these may be mesenchymal, stromal, endodermal or ectodermal and are usually always benign compared to the malignant potential of adenomas (Bosman 1999). These benign stromal polyps are thought to require additional genetic hits for further progression to malignancy, although hyperproliferative states often accompany polyp overgrowth (Marignani 2005).

Polyp formation arises from the mucosal surface of the epithelial tissue and elongated crypts and glands are arrayed in frond like structures on a core of muscle fibres forming a stalk and polyp head (Jansen *et al* 2005 in press). Recently it has been suggested that hamartomas may arise as a result of mucosal prolapse. Mucosal prolapse, cloacogenic polyps and rectal ulcers (all of which are considered to be rare occurrences), were considered to be separate syndromes from heritable polyposis. These syndromes are collectively characterised by protrusion of the mucosa into the lumen. Consequently invagination of the intestinal tissue and polyp formation in early adulthood is associated with bleeding, intussusception and obstruction, leading to ulceration of the gut, anaemia and general malnutrition (Rossi *et al* 2002).

The recent debate on the malignant potential of hamartomas focuses on the parallel suggested between adenoma to carcinoma sequence in CRCs, with hamartoma progression to carcinoma requiring an additional hit. The relatively low levels of adenoma and carcinoma lesions within hamartomatous polyps and the observation that hamartomas fail to show any preneoplastic changes, has cast doubt on this sequence theory. Some reports suggest that polyps decrease with age, furthermore newborn babies have been found with intestinal polyps, again arguing against a step wise accumulation of alterations such as that observed with FAP (Jansen *et al* 2005 in press.

1.5.1 Peutz-Jeugers syndrome

Patients with the inherited autosomal dominant Peutz-Jeugers syndrome (PJS) develop multiple gastrointestinal hamartomatous polyps with associated mucocutaneous pigmentation of the lips, bucal mucosa and didgits (Tomlinson and Houlston 1997). Although polyps have low-level neoplastic capability, the disease is associated with a 15 fold increased risk of colorectal and other cancers in tissues such as: Stomach, Lung, Pancreas, Breast, Testis, Cervix and Ovaries, all of which present at relatively early onset (50-60 years) (Tomlinson and Houlston 1997).

PJS hamartomas are benign polyps, composed of differentiated glandular epithelium and a normal lamina propria in conjunction with a well-developed smooth muscle component. Germline mutations in *LKB1* at the 19p13.3 locus have been identified as the genetic alteration underlying PJS (Hemminki *et al* 1997, Jenne *et al* 1998, Yoo *et al* 2002), and as such LKB1 has been described as a recessive gatekeeper tumour suppressor gene in the intestine (Hemminki *et al* 1997). Unusually PJS patients develop hamartomas as a result of LKB1 loss in epithelial rather than stromal tissue (Sancho *et al* 2004).

LKB1 is rarely mutated somatically in sporadic tumours (Sanchez-cespedes *et al* 2002), although low expression levels of LKB1 have been found in PJS and sporadic breast cancer, correlating with a poor prognosis (Nakanishi e*t al* 2004). Loss of the 19p13 region of the genome occurs at a high frequency in breast cancer and may result in loss of an area around 250kb, including loss of the LKB1 gene, or several other genes. Discontinuous LOH of multiple tumour suppressor genes or concurrent inactivation may be a contributing factor to breast cancer development (Yang *et al* 2004).

Several reports differ in their observations of *LKB1* status in PJS, with anywhere between 50-80% of PJS patients harbouring inactivating *LKB1* mutations. This has lead to the proposal that genetic heterogenecity or indeed a secondary locus may be associated with PJS, possibly through PKA and CKII, which both share homology to LKB1 (Marigani 2005). Additionally mutation studies have focused on those patients with point mutations of *LKB1*, but large scale or entire gene deletions may have gone undetected (Le Meur *et al* 2004).

Epigenetic inactivation of LKB1 in somatic cells has been implicated in sporadic tumourigenesis, although this appears to be a relatively rare event with only 8% of sporadic CRCs showing LKB1 promoter hypermethylation and 13% with LOH (Trojan *et al* 2000). PJS patients show heterogeneity of epigenetic modification, and LOH due to promoter hypermethylation was considered a rare event in PJS polyps (Bosman *et al* 1999). In contrast, investigations by Esteller *et al* into *LKB1* promoter methylation in PJS breast and intestinal tumours yielded a higher frequency of hypermethylation in PJS patients than in sporadic tumourigenesis (Esteller *et al* 2000). LKB1 is also frequently silenced in pancreatic carcinomas. Restoration of LKB1 expression in cancer cell lines using demethylating agents (5Aza2dc) was found to induce p53-independant mitochondrial mediated apoptosis (Qanungo *et al* 2003).

Loss of LKB1 status was also reported to correlate with increased *COX2* expression in a similar manner to FAP. Furthermore when treating PJS patients with a known COX2 inhibitor Celecoxib, intestinal tumour burden was found to decrease (Udd *et al* 2004). However, the fact that overexpression of COX2 was found in 82% of PJS hamartomas and nearly all carcinomas, suggests a relatively late stage induction during carcinoma progression, rather than as a direct result of LKB1 loss or haploinsufficiency (Wei *et al* 2003).

As limited work has been performed on hypermethylation at the LKB1 locus in PJS patients and similar sporadic tumours, epigenetic silencing may responsible for the discrepancies reported in LKB1 status between patients and polyps. Mutation screening of LKB1 mRNA has revealed splicing variations, truncated proteins and novel mRNA isoforms in a subset of PJS patients (Abed *et al* 2001), analysis of which may provide some insight into the genetic regulation of PJS and other similar syndromes.

1.5.2 LKB1

LKB1 (STK11) is 55KDa Serine/Threonine kinase, highly conserved between species, with murine *Lkb1* showing strong sequence homology to human *LKB1*. Upstream kinases such as cAMP/PKA and p90S6K/RSK activate LKB1 via Ser431 phosphorylation, although many other *in vivo* regulators may also exist (Collins 2000).

Several levels of regulation exist including: autocatalytic activation, prenylation modification, phosphorylation activation sites and a variety of binding partners. Preferential binding complexes may also act to alter the subcellular localization of the protein, thereby adding an additional level of regulation.

A putative NLS (nuclear localisation signal) gives rise to several key interactions within the nucleus (Smith *et al* 1999). Most well documented being that of LKB1 induced G1 cell cycle arrest, which was determined upon reintroduced of wild type LKB1 into tumour cell lines (Tiainen *et al* 1999). BRG1 (product of the brahma related gene) is part of the chromatin remodelling complex, and uses ATPase activity to disrupt nucleosome structure for transcriptional access. LKB1 has been shown to increase BRG1 ATPase activity and mediate RB induced cell cycle arrest and senescence again at the G1 phase (Marignani *et al* 2001). LKB1 has also recently been found in complex with cell cycle check point and DNA repair proteins: p53, BRCA1 and ATM *in vivo*, with both p53 and LKB1 recruited and phosphorylated by ATM following chromatin alterations as a result of DNA damage (Ferrandes *et al* 2005).

Phosphorylation of LKB1 is considered essential for cell cycle arrest and growth suppression functions, and several groups have suggested this to be in conjunction with nuclear localisation of LKB1 (Collins *et al* 2000, Sapkota *et al* 2001, Baas *et al* 2003). However, loss of kinase function in LKB1 mutants resulted in nuclear retention, thereby suggesting cytoplasmic localization of LKB1 is critical for its phosphorylation activities (Wei *et al* 2003). The identification of two different isoforms of LKB1 in PJS patients, aberrantly localized to the nucleus suggests that

correct localization of this protein to be key to its tumour suppressor functions (Boudeau *et al* 2003a). LKB1 activation by PI3K and DNAPK has also been reported *in vitro* and *in vivo* (Sapkota *et al* 2002). This cytoplasmic process may be linked to LKB1 interactions with an FLIP, which negatively regulates NF-κB signalling, suggesting an important role for LKB1 in mediating cell survival signals (Liu *et al* 2003).

1.5.3 LKB1 and metabolic cascades

STRAD has been identified as an LKB1 substrate *in vivo* and is a pseudokinase member of the Ste20 kinase family. STRAD forms a complex with LKB1 and MO25 resulting in dual phosphorylation of both LKB1 and STRAD before translocating from the nucleus to the cytoplasm (Boudeau *et al* 2003b).

In addition to phosphorylation of STRAD, LKB1 was found to be a homologue of the Pak1, TOS3, and Elm1 in *Saccharomyces cerevisae*, all of which activate Snf1 kinase (sucrose non fermenting protein). As a result, the search broadened to indentify a mammalian homologue of Snf1 and AMPK was considered to be a suitable candidate and confirmed to be a downstream substrate for LKB1 *in vivo* (Hong *et al* 2003, Hedbacker *et al* 2004). AMPK is composed of 3 subunits and contains potential glycogen and AMP binding sites. LKB1 phosphorylates AMPK on Thr172, although PKB may be capable of similar AMPK activation (Carling 2004). AMPK is activated when the cellular AMP: ATP ratio is increased and subsequently activates the stress cascade resulting in utilization of fatty acid stores by Acetyl Co A Carboxylase mediated oxidation during times of low cellular ATP or glucose (Shaw *et al* 2004a). The glycogen binding domain of AMPK is of unknown function. When glycogen levels are depleted, AMPK is activated to metabolise blood glucose and fatty acids, suggesting glycogen binding may act as a repressive mechanism (Hardie 2005).

Many processes exert energy stress on a cell including: oxidative damage, heat shock, osmotic stress, muscle contraction, hypoxia, glucose deprivation and starvation (Hawley *et al* 2003). AMPK can also act at a whole body level to increase fatty acid oxidation via hormonal control. Adipocytes secrete hormones such as: Leptin and

Adiponectin to signal starvation or low energy throughout the whole body (Luo *et al* 2005). AMPK also exerts an effect on inhibiting the cell cycle via Cyclin A and B1 mRNA degradation. P53 is stabilized as a result and energy consuming proliferation is halted (Marignani 2005).

Further evidence to support the role of LKB1 in metabolic signalling has been reported from *Lkb1*$^{-/-}$ MEFs, which displayed increased mTOR signalling. mTOR (mammalian target of rapamycin) controls growth and proliferation (G1 progression) in response to mitogenic stimuli, insulin and amino acid availability (Kimura *et al* 2003). Activated AMPK has been shown to inhibit mTOR via phosphorylation of the *TSC2* gene product Tuberin (Shaw *et al* 2004b), although AMPK can also directly phosphorylate and inhibit mTOR (Cheng *et al* 2004), and S6 Kinase, independently of the mTOR priming switch. This provides an override mechanism by which AMPK can regulate energy consuming processes such as cell proliferation, protein synthesis and cell growth (Kimura *et al* 2003).

The net result of the process is inhibition of EF2/S6K phosphorylation and consequently reduced cell size and growth (Kyriakis *et al* 2003). Feedback loops involving direct p90RSK and ERK phospohorylation of downstream mTOR effectors provides another input for LKB1 regulation. LKB1 may activate ERK induced mTOR in certain tissue types and therefore play both positive and negative regulatory roles depending on cell type or binding partners (Kimball *et al* 2004).

The link between AMPK, mTOR and LKB1 suggests integration of cellular energy control with proliferation and cell growth pathways (see figure 1.3) (Shaw *et al* 2004 a).

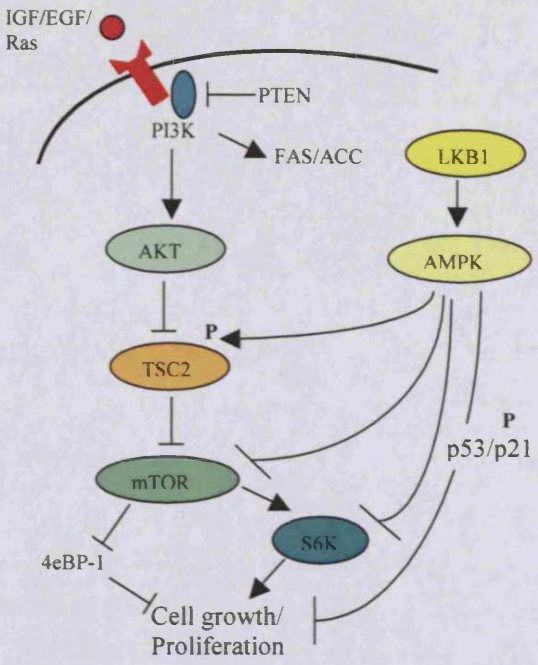

Figure 1.3 – LKB1 signal integration into cell survival and growth pathways. AMPK activation blocks PI3K induced mTOR and survival signals. The multiple inputs and integration of AMPK and mTOR pathways makes LKB1 a key upstream regulator of this process (adapted from Luo *et al* 2005).

Glucose repression mediated by AMPK provides an interesting link between the proposed tumour suppression function of LKB1 and insulin resistance in type 2 diabetes. Therefore AMPK activation may protect against cancer and insulin resistance/metabolic syndromes (Kimura *et al* 2003). AICAR (an AMP analogue) can mimic AMP activation of AMPK *in vivo* independently of LKB1 status, and has been suggested a promising therapy to both diabetic and PJS patients alike. However, there is now increasing evidence that LKB1 activation of AMPK is only required under a subset of stress conditions (Taylor *et al* 2005, Altarejos J *et al* 2004, Sakamoto *et al* 2004).

1.5.4 LKB1 and cell death

Karuman *et al* 2001 found LKB1 to directly associate with p53 and hence regulate p53 dependant apoptosis. This interaction may stabilize and activate p53 in a subset of cell types, although the primary role for this interaction is suggested to be cell cycle inhibition rather than induction of apoptosis (Karuman *et al* 2001).

With an increasing body of evidence proposing LKB1 as a inhibitor of proliferation, it is interesting that *Lkb1*$^{-/-}$ MEFs became resistant to transformation following oncogenic Ras stimuli (Bardeesy *et al* 2002). These cells appeared to be extremely sensitive to cell death, giving rise to suggestions that LKB1 activation of AMPK may also act as an inhibitor of cell death and hence protect from stress induced apoptosis during times of high energy demand such as oncogenic transformation (Shaw *et al* 2004a).

MO25/STRAD interactions with LKB1 induce translocation of the complex to the mitochondria, implicating LKB1 in mediating cytochrome C release and mitochondrial apoptosis, and this may be p53 dependent and independent (Karuman *et al* 2001, Qanungo *et al* 2003). Given that AMPK activation can block caspase 3 activation and protects a subset of LKB1 null cells from apoptosis, there maybe a number of tissue specific AMPKKs that may substitute for LKB1 (Shaw *et al* 2004a). Indeed TSC2 is also involved in protecting against glucose deprivation induced apoptosis as unregulated growth causes stress and cell death (Shaw *et al* 2004b).

These findings suggest *LKB1* $^{-/-}$ tumours may be sensitive to changes in AMP levels, and agents that modify this signal such as AICAR or Rosiglitazone may be suitable therapies to reactivate this pathway and induce apoptosis in PJS tumours (Shaw *et al* 2004a).

1.5.5 LKB1 and Polarity

In addition to AMPK, LKB1 may have more than 13 other *in vivo* substrates in the AMPK family, many of which have been identified as MARK proteins (Par homologues involved in polarity regulation) (Lizcano *et al* 2003). Studies in *C.elegans* (Watts *et al* 2000) and *Drosophila* (Martin and St Johnston 2003) have identified *LKB1* as a mammalian homologue of *PAR4*. The Par proteins (partitioning defective proteins) were originally identified in *C.elegans* and are involved in Anterior-Posterior formation in conjunction with Wnt signalling during development. Cellular polarity is organised by asymmetry of the actin cytoskeleton, mitotic spindle, correct localisation of mRNAs, cell junctional control, secretory granule localization, and correct sorting of plasma membrane markers.

The reorganisation of the actin framework is mediated via Rac and the Rho GTPase Cdc42. As Cdc42 is found to localize with the Par3-Par6 and PKCζ complex, it is suggested that these proteins may act as downstream effectors of LKB1 (see figure 1.4) (Baas *et al* 2004). Recent work has implicated LKB1 in spontaneous apical brush border formation in the intestine following differentiation and actin cytoskeleton rearrangement. LKB1 reactivation and STRAD binding in isolated intestinal epithelial culture resulted in apical brush border formation and actin cytoskeleton rearrangement even in the absence of junctional contacts. This process additionally relocalizes junctional proteins such as ZO-1 and other membrane proteins to the brush border where they are correctly sorted (Baas *et al* 2004). LKB1 has also been implicated in binding PAPK and translocating to the cytoplasm, where it fulfils a role in tight junction and cell-to-cell contact regulation (Brajenovic *et al* 2004). This observation has implications for transformation as loss of polarity is considered a key step in neoplastic progression (Baas *et al* 2004).

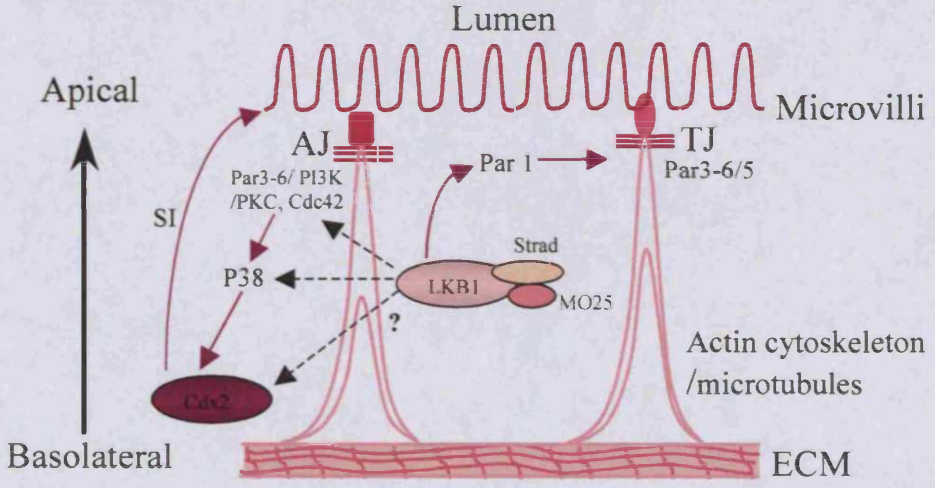

Figure 1.4– Model of intestinal polarity. Correct polarity is maintained by formation of apical microvilli brush borders on the luminal surface, correct actin cytoskeleton organisation and presence of both Adheren junctions (AJ) and Tight junctions (TJ). LKB1 may play several roles in maintaining correct polarity and differentiation status via PKC, PI3K, Cdx2, p38 and sucrase isomaltase (SI)(adapted from Baas *et al* 2004, Laprise *et al* 2002).

Additionally, yeast 2 hybrid screening using LKB1 as bait has also pulled down AGS3 (activator of G protein signalling) as a phosphorylation target involved in cell polarity and membrane signal transduction (Blumer *et al* 2003).

1.5.6 LKB1 and Wnt signalling

In mammalian Wnt signalling LKB1 is thought to compete with dishevelled (DV1) for PAR1A and consequently down regulate Wnt by allowing degradation of β-Catenin (see figure 1.5) (Sun *et al* 2001). LKB1 was subsequently found to affect cell cycle progression through redirection of Par1A and repression of Wnt signalling in adult tissue (Spicer *et al* 2003). Conversely, the *LKB1* homologue *XEEK1* has also been implicated as a positive regulator of Wnt during xenopus development by phosphorylation and inhibition of GSK3 (Ossipova *et al* 2003).

Regulation of Wnt signalling therefore appears to be dependant on cell type and developmental stage, indeed LKB1 is highly expressed in developing fetal and malignant tissue, and only at low levels in adult tissue (Rowan *et al* 2000), suggesting expression may be controlled in a temporal and/or tissue specific manner similarly to mTOR. *In situ* analysis of LKB1 mRNA found expression was localized to the base of the crypt associated within the proliferative zone rather than the villus region, again supporting a role for LKB1with integration into the Wnt pathway (Rowan *et al* 2000).

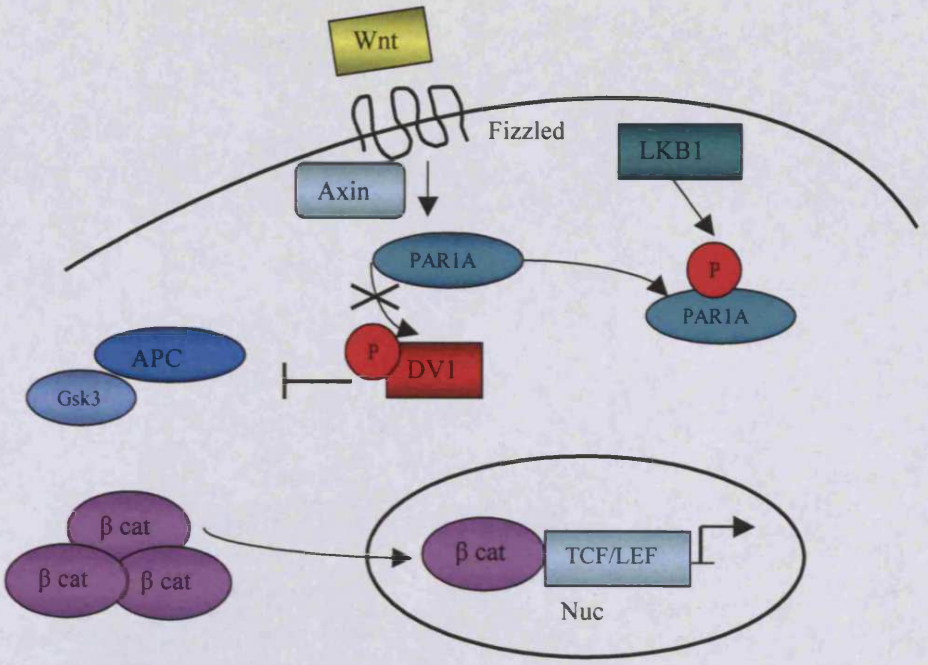

Figure 1.5– Mechanims of Wnt signalling. Inhbition of the APC/ GSK3/ Axin complex allows accumulation and translocation of β-Catenin to the nucleus and upregulation of Wnt effector genes. LKB1 redirection of Par1A allows degradation of β-Catenin and hence inhibits expression of Wnt effectors (adapted from sun *et al* 2001, Spicer *et al* 2003).

1.5.7 Mouse models of PJS

Previously constitutive homozygote knockouts of *Lkb1* have resulted in embryonic lethality at E9.5 due to neural tube defects and aberrant vessel formation in the yolk sac and placenta. This was attributed to down regulation of VEGF and angiogenesis (Ylikorhala *et al* 2001, Jishage *et al* 2002). Heterozygote mice were viable and developed benign gastrointestinal polyps in a similar pattern to PJS patients from 20-50 weeks of age (Miyoshi *et al* 2002, Nakau *et al* 2002, Bardeesy *et al* 2002). Other neoplastic changes observed in heterozygote mice include: Lung adenocarcinomas (LACs) (Jimenez *et al* 2003), Hepatocellular carcinoma (HCC) (Nakau *et al* 2002, Bardeesy *et al* 2002), multiple liver adenomas and breast carcinomas (Shen *et al* 2002), and endometrial carcinomas (Rossi *et al* 2002), all of which are constituents of the human disease in PJS patients.

Analysis of polyps from *Lkb1*$^{+/-}$ mice produced variable results, with the majority reporting haploid mRNA in polyps, although some LOH and depleted protein levels were observed, much reflecting the human PJS situation (Rossi *et al* 2002, Baas *et al* 2004). Classical tumour suppressor genes follow Knudson's 2 hit hypothesis of biallelic inactivation. Recessive tumour suppressor genes such as p27^{kip} and SMAD4 only require a decrease in protein levels to predispose to tumourigenesis. *LKB1* does not appear to act as a classical tumour suppressor gene, and therefore in combination with haploinsufficiency in both the human and mouse models, *LKB1* would appear to conform to recessive tumour suppressor genetics.

1.5.8 Jeuvenile polyposis syndrome

Similarly to PJS, Juvenile polyposis syndrome (JPS) is a hereditary syndrome displaying similar hamartomatous intestinal polyps and increased risk of malignancy. Associated inflammatory disease can be observed as mucinous cysts and stromal outgrowth appear frequently in connection with JPS polyps.

JPS has been linked to defects in the TGF-β signalling pathway. Mutations in both *BMPR1A* in stromal tissue and *SMAD4* in epithelial tissue have been identified as major genetic defects in JPS patients (Haramis *et al* 2003). Disruption of the TGF-β pathway can induce a hyperproliferative state, growth advantage, inflammation and microsatelite instability (MSI), all of which contribute to adenocarcinoma transformation.

Mice heterozygote for *Smad4* develop polyps similar to those of JPS patients, and show accelerated tumourigenesis when crossed to the *Apc*^{MIN} background (Takaku *et al* 2000).

1.5.9 Tuberous sclerosis

Tuberous sclerosis (TS) is characterised by benign hamartomatous lesions of the heart, lung, kidney, brain, skin and nervous system, caused by germline mutations in *TSC1* and *TSC2*. The respective gene products Hamartin and Tuberin protein inhibit the mTOR survival pathway, and also mediate β-Catenin, TGF-β and AMPK stress signalling (Mak and Yeung 2004).

1.5.10 Cowdens disease

Mutations in the tumour suppressor gene PTEN (phosphatase and tensin homolog) are frequently found in cancers such as breast, thyroid, glioblastoma, prostate, GI tract, trichilemmonas (skin polyps) and the hereditary Cowdens syndrome and JPS (Luukko *et al* 1999, Wang *et al* 1998). PTEN inhibition of the PI3K survival cascade provides a protective function against inhibition of cell death, and hence loss of PTEN leads to overexpansion of cell lines normally deleted. PTEN signalling may also control translation and feed into *TSC* gene regulation, both of which can be linked to regulation of cell size and growth commonly associated with hamartoma development (Backman *et al* 2002). *PTEN* mutations result in constitutively activated PI3K and predisposes to transformation. PI3K cascades are also downstream of receptor tyrosine kinases (RTKs) and Ras signalling, so may be novel targets for new cancer therapies (Laprise *et al* 2002).

Pten deficient mice are embryonic lethal, although heterozygotes are viable and are predisposed to a variety of cancers including endometrium, thyroid, prostate, breast, liver and intestine (podsypanina *et al* 1999).

Loss of function of tumour suppressor genes involved in suppressing the mTOR growth/metabolic pathway links many of these syndromes (see figure 1.3) and has been suggested to contribute to the overgrowth of tissue seen in polyps (Tee and Blenis 2005). The overlapping similarities between the hamartomatous polyposis syndromes suggests that *LKB1, PTEN, BMP1A, SMAD4* and the *TSC1* and *TSC2* genes may have similar molecular functions, however the many variations between

diseases suggests these genes have independent tumour suppressor functions (Brugarolas and Kaelin 2004).

1.6 Genetic instability in cancer

Malignant cells may have the ability to survive carrying unstable genetic alterations. Genetic instability can lead to malignancy by the result of deletion or suppression of the damage surveillance, repair and cell death processes, or by amplification of survival signals (Makin and Hickman 2000). Clonogenic cells may then acquire a selective advantage that leads to expansion and propagation of inappropriate cells. Further genetic hits as a result of genetic instability may then lead to progression and transformation (Giles *et al* 2003).

1.6.1 Chromosomal instability (CIN)

Large scale chromosomal instability is a common feature of CRCs and is found in about 85% of cases. Changes in chromosome numbers either by loss or gain of chromosomes (Aneuploidy), or aberrant increases in unpaired chromosome numbers (hyperploidy), contribute to large scale chromosomal instability. These features may arise from abnormal mitotic spindle assembly, chromosome segregation and subsequent breakage, loss, gain, and/or chromosomal translocation (Makin and Hickman 2000).

1.6.2 Microsatellite instability (MSI)

Genomic instability and MSI occur as a result of DNA replication slippage, which induces non-paired misalignment in the DNA sequence at small repetitive genetic loci called microsatellites (1-5 base pairs repeated 15-30 times)(Wheeler *et al* 2000). Insertion or deletion of these units predisposes replication machinery to slippage and errors looping out the DNA. In conjunction with mismatch repair (MMR) deficiency, these loops are not repaired and persist in the genome. Failure to correct replicative mismatches leads to an increase in the basal mutation rate and is said to confer a mutator or replication error positive (RER+) phenotype (Riccio *et al* 1999).

Inactivation of both alleles of a MMR gene causes MSI according to Knudson's two hit hypothesis for tumour suppressor genes and this may be by genetic or epigenetic intervention, increasing the probability that other genes such as: caretaker genes *Apc, Tgfβ, Bax*, and gatekeeper genes such as *Brca1* and *Brca2, p53, Rb* and *IGF-IIR* may additionally become inactivated causing the progression of tumourigenesis (Buermeyer *et al* 1999).

MSI is observed at low rates in sporadic CRCs at a rate of approximately 15%, however MSI is a common feature in hereditary MMR deficient CRCs such as hereditary non-polyposis colorectal cancer (HNPCC), where over 90% of tumours exhibit MSI (Wheeler *et al* 2000).

1.6.3 HNPCC

Hereditary non-polyposis colorectal cancer (HNPCC) is an autosomal dominant early onset inherited disorder, which accounts for 2-4% of the western worlds CRCs (Kinzler and Vogelstein 1996). HNPCC is distinct from the more common sporadic CRCs as malignancies are mostly found in the right colon and at an earlier onset age (Wheeler *et al* 2000). HNPCC in contrast to FAP is relatively slowly initiated, but exhibits rapid progression due to germ line mutations in caretaker tumour suppressor genes of the MMR machinery such as *MlLH1* and *MSH2* (Buermeyer *et al* 1999).

The disease is characterised according to the 'Amsterdam' criteria including: at least 3 relatives with CRCs, at least 2 successive generations affected, at least one diagnosed before the age of 50, FAP excluded, and ultimately histological diagnosis (Bocker et al 1999). Differing phenotypes present with each class of the disease, which include: Lynch syndrome, Turcots syndrome, and Muir-Torre syndrome. The main symptoms include: carcinomas of the colon, endometrium, ovary, stomach, pancreas, small bowel, hepatobiliary tract, ureter, renal pelvis and skin (Wheeler *et al* 2000).

1.6.4 DNA mismatch repair

Genomic DNA has evolved a system for basic maintenance of its sequence and protection against persistence of base-to-base mismatches and insertion/deletion loops (IDL) which are frequent occurrences in the genome following replication. The MMR proteins function to repair DNA lesions which arise as a result of oxidative, alkylating or base cross-linking damage and stop these potentially harmful changes from persisting for any further rounds of replication. Bacterial MMR is relatively well characterised and involves a series of DNA repair enzymes (Drummond and Bellacosa 2001).

1.6.5 Long patch nucleotide excision repair (NER)

The NER response is capable of repairing many exogenous DNA lesions, most commonly those induced by UV mutagenesis (Lengauer *et al* 1998). NER can respond to transcriptionally active and inactive areas of the genome following DNA damage recognition. In the case of transcriptionally coupled NER, this response is mediated by proteins that arrest transcriptional machinery (Friedberg *et al* 2004).

Studies of bacterial NER identified repair complexs containing the mismatch repair proteins MutS, MutL and MutH, which recognise and bind DNA mismatches before recruiting endonucleases and polymerases to excise the tract and resynthesize the sequence. MutL binds and stimulates the endonuclease activity of MutH, which induces cleavage of the newly synthesised stand. Strand discrimination is determined by the ability of MutH to recognise the unmethylated adenosine nucleotides at hemimethylated GATC sites (Buermeyer *et al* 1999). The endonuclease activity cleaves out a long tract between the mismatch and the GATC site, prior to DNA polymerase III resynthesizing the strand across the gap, which is then resealed by ligases (Modrich 1994). The whole process is reliant upon MutL enhancing MutS ATPase activity. ATP hydrolysis by MutS facilitates translocation along the DNA strand, and mutations in this ATPase activity have been found to inactivate MMR machinery *in vivo* (Buermeyer *et al* 1999).

1.6.6 Base excision repair (BER)

BER removes individual DNA base mismatches in a lesion specific manner. The key enzymes involved in this pathway are the DNA N-glycosylases, which cleave N-glycosylic bonds between bases and excise the damaged or mispaired base. These enzymes are specific to different types of DNA damage depending on the lesion created. After excision of the base, DNA polymerse-β and repair ligases fill the single base gap (Drummond and Bellacosa 2001).

1.6.7 Mammalian Mismatch Repair

Several mammalian homologues of the bacterial MMR system exist. Human mismatch repair genes include: *MLH1*, *MSH2, PMS1*, *PMS2, MSH6 and MSH3*. Inactivation of each MMR gene has been linked to human neoplasia, most convincingly through the association with the hereditary cancer syndrome HNPCC (Buermeyer *et al* 1999).

MSH6 is the mammalian homologue of MutS, and appears to contain similar ATPase activity in complex with either MSH2 or MSH3 (additional MutS homologues). MSH6 forms a heterodimers with either MSH2 or MSH3 depending on the type of lesion created. MSH2/MSH6 heterodimers recognise base-to-base mismatches and single base pair insertion/deletion loops (IDLs) (see figure 1.6), whereas the MSH3/MSH6 complex can bind and repair larger 2-4 base pair lesions. There are 3 mammalian homologues of MutL: MLH1, PMS1 and PMS2, all of which may function as MutL in stimulating lesion excision, although some level of redundancy is observed in this system (Wheeler *et al* 2000).

Adenine methylation does not occur in mammalian cells and a mammalian homologue of MutH has yet to be identified, therefore the mechanism of strand discrimination in mammalian systems is still undetermined (Drummond and Bellacosa 2001). However, recent advances suggest Proliferating cell nuclear antigen (PCNA) and 5 prime ends of discontinuous DNA synthesis in the lagging strand (Okazaki fragments) during replication help to guide strand discrimination for MMR proteins (Buermeyer *et al*, 1999, Wheeler *et al* 2000).

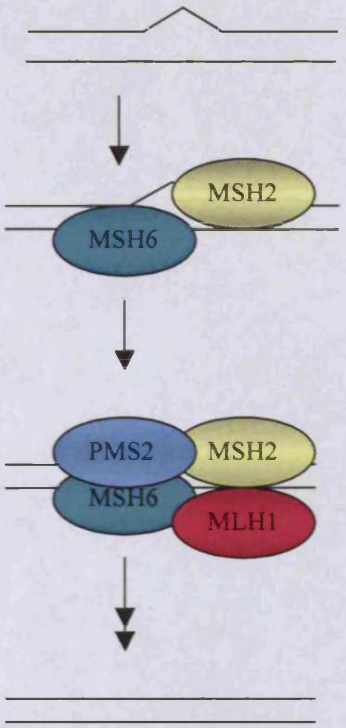

Figure 6 - BER and MMR pathway in mammalian cells. Misincorporation of inappropriate base during replication leads to slippage and looping out of bases. Mismatch is recognised by MSH6 and MSH2 or MSH3 heterodimer. MLH1 and PMS2 are then recruited to the site, and the mismatch repaired by exonuclease, helicase and ligase activity (adapted from Kinzler and Vogelstein 1996)

1.6.8 MMR and apoptosis

An additional role for the MMR system in eliciting apoptosis was first suggested by the observation of reduced sensitivity to cytotoxic DNA damaging agents in MMR defective tumours (Fishel *et al* 1999). This raised the hypothesis that MMR deficiency may predispose to neoplasia through failed apoptosis as well as failed DNA repair (Fedier *et al* 2004).

The precise mechanism by which MMR mediates cell death remains unclear, with both futile cycles of repair and direct signalling proposed (Fishel *et al* 1999). Persistent attempts by MMR machinery to cleave and repair mis-incorporated bases which are then reincorporated following successive rounds of replication, results in futile cycling and can signal cell cycle arrest and subsequently apoptosis. This is demonstrated by the tolerance of MMR deficient cells to O-6meG lesions, which are removed but then replaced again by the MMR machinery (Meyers *et al* 2004).

There is clear evidence for mediation of MMR dependant apoptosis through p53, for example with the MMR machinery proposed to activate p53 in response to radiation damage, and recently the MLH1–PMS1 heterodimer linked to regulation of p53 (Luo *et al* 2004).

1.6.9 MMR and Mouse models

The initial finding that *mutS* and *mutL* mutants in *E.Coli* were resistant to some types of cytotoxic damage and that human MMR components could recognise cytotoxic apoptosis (Duckett *et al* 1996), has lead to further investigations into MMR and chemoresistance using mouse models.

Analysis of the apoptotic response following exposure to DNA damage shows defective responses in *Pms2, Msh2* and *Mlh1* null mice, but with damage-specific and gene dose-dependent differences in the requirement for each of these MMR components (Toft *et al* 1999). For example, at high levels of alkylation damage, Msh2 is required for signalling the apoptotic response whereas Mlh1 and Pms2 appear redundant. In contrast, lower levels of damage appear dependent on Mlh1 and Pms2 (Sansom *et al* 2003a). These studies therefore show clear reliance upon functional MMR for the *in vivo* induction of apoptosis, but reveal significant complexity in this reliance.

With regard to MMR and p53 directly signalling apoptosis results are somewhat contradictory, with very clear p53 dependency for the response to alkylation damage (Toft *et al* 1999), but with cells from mice mutant for *Pms2* and *p53* reported showing additive apoptotic decreases only in the response to radiation damage, suggesting independent roles for p53 and MMR (Zeng *et al* 2000).

MMR null mice have been shown to be susceptible to both lymphoma and intestinal tumourigenesis reflecting that of the human HPNCC syndrome, although the predisposition to intestinal neoplasia is gene-dependent, with the lowest susceptibility seen in mice singly mutant for Pms2, and highest in Msh2 and Pms2 nulls. This again highlights the functional redundancy seen in mammalian MMR, although the degree of redundancy may vary in different tissues (Prolla *et al* 1998, Buermeyer *et al* 1999).

In terms of mutation and tumour predisposition, there is very clear data showing MMR deficiency to lead to increased mutability and neoplastic predisposition in the intestine (Sansom *et al* 2001b, Baross-Francis *et al* 2001, Sansom *et al* 2003a). Indeed *MSH2* deficiency appears to accelerate tumourigenesis when crossed to the Apc^{MIN} background (Reitmair *et al* 1996). However, precisely which elements of these increases relate to the failed engagement of apoptosis as opposed to failed repair remains to be elucidated.

1.7 DNA damage induced death

Cells that fail to repair DNA damage enter into senescence or undergo apoptosis. Deletion of DNA damaged cells is of vital importance to eliminate cells harbouring possible DNA mutations (Hickman and Samson 1999). DNA damage may occur by endogenous oxidative species or by exogenous cytotoxic agents and may include: DNA crosslinking, double or single strand breaks, carcinogen induced DNA cyclic adducts and lesions (Petronzelli *et al* 2000a). Double stranded breaks can be repaired either through homologous recombination or by direct fusion of the broken ends (Friedberg *et al* 2004).

1.7.1 DNA repair proteins

A network of DNA repair and damage sensing proteins exists to delete inappropriately damaged cells from the system. Part of this process is linked to inhibition of the cell cycle upon detection of damage. DNA damage activates $p16^{Ink4b}$ (CDK4 inhibitor), which subsequently blocks expression of the major proliferative control genes *Rb* and *E2F* (Lee and Schmitt 2003). E2F controls the progression of the cell cycle through G1 to S phase and is upregulated by CHK2 in response to DNA damage. E2F activation induces $p14^{ARF}$ and the p53 pathway in addition to Apaf1 activation and intrinsic cell death pathways (Crighton and Ryan 2005).

ATR (ataxia telangiectasia and Rad3 related) and ATM (ataxia telangiectasia mutated) are kinases that phosphorylate and activate DNA damage sensors such as: CHK1 and CHK2, BRCA1, p53 and RAD17 which in turn inhibit the cell cycle and signal DNA repair and/or cell death effectors (Friedberg *et al* 2004).

1.7.2 DNA repair gene cancer syndromes

Many of these DNA damage sensing proteins are mutated in hereditary and spontaneous cancer syndromes such as ataxia telangiectasia (AT), Fanoni anaemia and Li-Fraumeni, where cells commonly fail to detect and repair DNA double strand breaks (see figure 1.7).

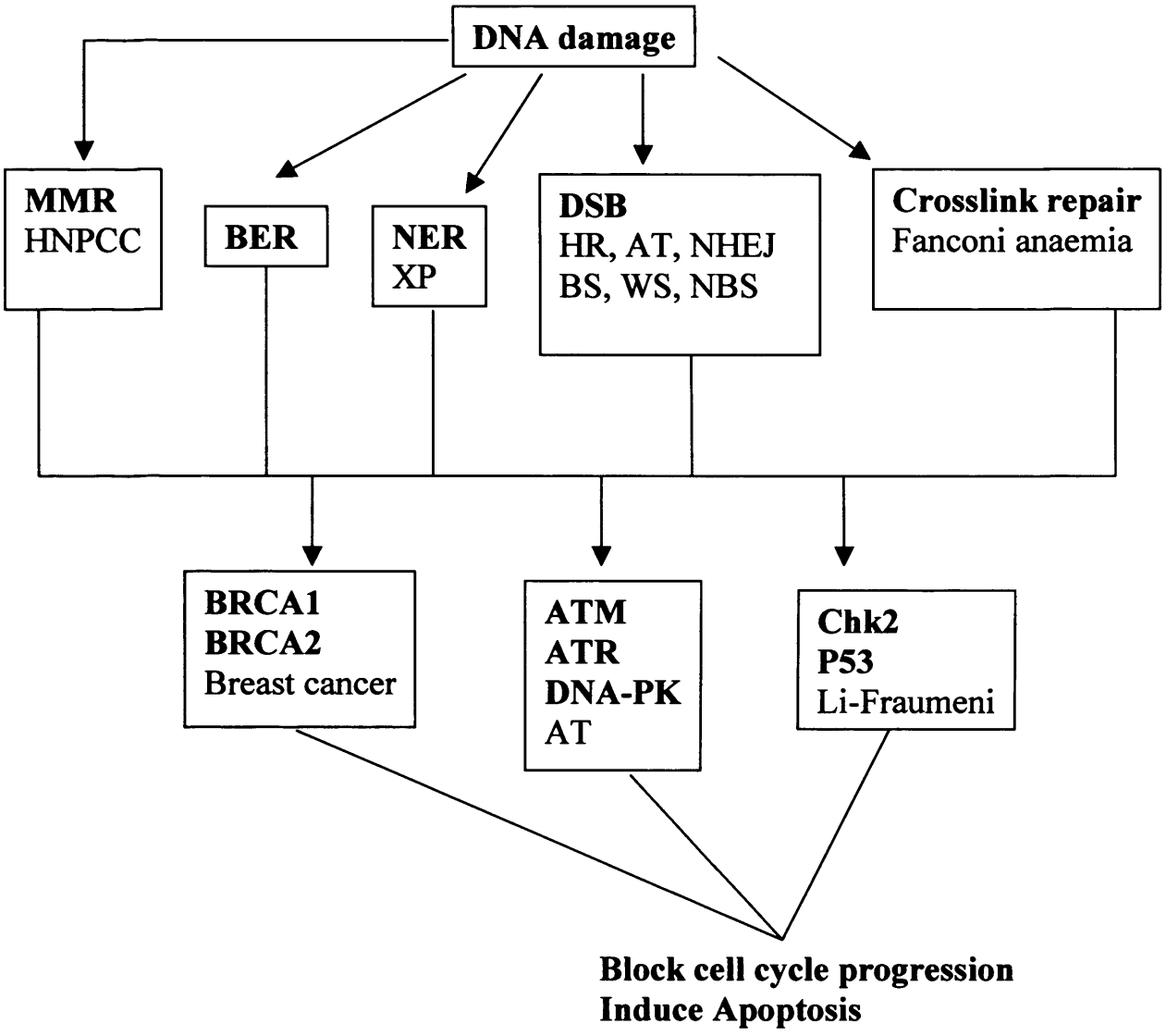

Figure 1.7- DNA repair processes linked to cell cycle checkpoint control. DSB=double stranded breaks, BS=Blooms syndrome, BER= base excision repair, NER = Nucleotide excision repair, HR=homologous recombination, NBS=nijmegen breakage syndrome, NHEJ=non homologous end joining, WS= werners syndrome, XP=xeroderma pigmentosa, AT = ataxia telangiectasia (adapted form Levitt and Hickson 2002).

1.8 P53

P53 was first identified in SV-40 cells by Lane and Crawford 1979, subsequently various studies have shown inactivation of p53 results in resistance of cells to apoptosis when exposed to death inducing conditions such as: oncogene activation, hypoxia, telomere erosion, matrix detachment and DNA damaging agents (Yonish – Rouach *et al* 1991, Raveh *et al* 2001). Consequently, the nuclear phospho-protein p53 has been identified as a tumour suppressor gene and described as 'a guardian of the genome' as a consequence of its multiple roles in DNA repair, senescence, genome integrity and both spontaneous and damage induced apoptosis (Lowe 1999).

1.8.1 P53 and Cell cycle arrest

Phosphorylation and stabilization of p53 is critical to its pro-apoptotic function, and activation by ATM and CHK2 in response to double stranded DNA breaks forms part of the G-S cell cycle checkpoint. P53 is capable of directly binding DNA mismatches via exonuclease activity and its C terminal domain (Mummenbrauer *et al* 1996, Degtyareva *et al* 2001). Induction of p21, an inhibitor of Cyclin E and activator of retinoblastoma protein Rb, is a key function of activated p53 in blocking cell cycle progression and implimenting G1 arrest (Motoyama and Naka 2004).

P53 is also activated by oncogenic Ras or Myc activation, or by loss of Rb function. This negative feedback loop acts to minimise the effects of oncogenic activity by co-expression of p16 and p53 to block the cell cycle and promote death (Lee and Schmitt 2003).

1.8.2 P53 and the Apoptotic response

P53 functions as a transcription factor to repress anti-apoptotic growth regulatory genes such as *BCL-2, MAP4, PCNA* and *Survivin* (Makin and Hickman 2000). Most importantly to its role in the apoptotic response p53 up-regulates pro-apoptotic genes: *BAX, BAK, BAD, BID,* and BH domain proteins: *NOXA, PUMA* in addition to various other components of the intrinsic apoptosome: *IGF-BP3, CytoC, APAF1, DIABLO* (Slee *et al* 2004). P53 also targets the death receptor pathways: CD95/Fas and *DR5* to amplify the death signal (Crighton and Ryan 2005).

P53 does not, however, exclusively mediate death through transcriptional control, as experiments using transcriptionally inactive p53 mutants show clear uncoupling of its transcription factor function from the apoptotic response (Slee *et al* 2004). Similarly, there is evidence for the translocation of stress-induced p53 directly to the mitochondria to induce apoptosis via Bcl-2/Bcl-xl-mediated cytochrome *c* release, demonstrating multiple roles for p53 in mediating cell death (Mihara *et al* 2003).

1.8.3 Regulation of p53

The tumour suppressor functions of p53 are mostly post-translationally regulated by phosphorylation, although further modifications such as acetylation, glycosylation and sumoylation have all been implicated in the regulatory control of p53 (Crighton and Ryan 2005). Furthermore p53 protein levels are normally kept to a low level and this is regulated by MDM2, which sequesters and signals p53 degradation (Ghebranious *et al* 1998). Inactivation of MDM2 is dependant on stress activated signalling cascades such as $p14^{ARF}$/$p19^{ARF}$, which bind and degrade the protein releasing p53 from inhibition (Crighton and Ryan 2005).

Given the central nature of p53 to the apoptotic response, it is perhaps not surprising that perturbations of p53 regulatory proteins also impacts on the apoptotic programme. Thus, the 14-3-3 protein, which can stabilize p53 after DNA damage and which also antagonises MDM2 function, can inhibit oncogene-induced tumourigenesis *in vivo* (Yang *et al* 2003). Similarly, mice null for the p53 activator CHK2 show defects in ionising radiation-induced apoptosis (Hirao *et al* 2002) and cells deficient for the upstream regulator PML (promyelocytic leukaemia gene), show decreased senescence and apoptosis in response to death cues (de Stanchina *et al* 2004).

Tissue specific differences exist in the activity and dependency for p53 induced apoptosis. This can even be seen between rather similar cell types, such as the small and large intestine, with the only the latter showing increased p53-dependence for clonogenic survival (Hendry *et al* 1997). Therefore p53 activation seems to be highly dependant on cell type, microenvironment and hence interacting networks, binding partners, regulatory mechanisms and transcriptional targets may be activated accordingly (Samuels –Lev *et al* 2001).

1.8.4 P53 and Cancer

Loss of p53 leads to increase in cell proliferation, suppressed apoptosis, genomic instability and contributes to tumourigenesis. Heterozygous germline mutation in p53 underlies the hereditary Li-Fraumeni syndrome (figure 1.7), suffers of which show an increased frequency of lymphomas, sarcomas and breast carcinomas (Potten and Booth 1997). P53 inactivating mutations are found in a variety of spontaneous tumours and over 80% of Colorectal carcinomas contain p53 mutations (Attardi and Jacks 1999). Most mutations are base substitutions of the DNA binding domain leading to expression of abnormal p53 protein (Makin and Hickman 2000).

Whereas MMR deficiency is associated with MSI, p53 loss is associated with gross chromosomal instability (Toft *et al* 2002). Deficiency of both *p53* and MMR genes predisposes to lymphomagenesis *in vivo* (Toft *et al* 2002), and the majority of CRCs display chromosomal instability as a result of p53 loss (Reichmann *et al* 1981). However, p53 has also recently been implicated in preventing MSI at a dose dependent level in $Msh2^{-/-}$ $p53^{+/-}$ mice. Additional loss of p53 on this MMR deficient background resulted in acceleration of lymphomagenesis via increased MSI (Toft *et al* 2002), suggesting the normally redundant p53 steps in to monitor MSI in the absence of MMR.

In terms of drug resistance, p53 loss can be shown to confer *de novo* resistance to drug and ionising radiation induced damage *in vitro* and *in vivo* (Lowe *et al* 1993). P53 null tumour cells have also been reported to be extremely resistant to 5FU-induced damage (Bunz *et al* 1999). However, as may be inferred from the complexity of tissue specificity discussed above, the true clinical situation is inevitably complex with p53 status not directly predicting chemoresistance (Debatin and Krammer 2004).

1.8.5 P53 mutant mice

To test the function of p53 *in vivo*, p53 null mice have been generated by several different groups, all of which show essentially similar patterns of spontaneous tumour predisposition, particularly lymphomagenesis. P53 heterozygous knockout mice

exhibit similar symptoms to human Li-Fraumeni patients (Ghebranious *et al* 1998, Attardi and Jacks 1999).

The availability of these mouse models has allowed a clear demonstration of the *in vivo* requirement for p53 in mediating apoptosis following DNA damage, and raised the hypothesis that p53 deficiency leads to the inappropriate survival of cells that carry an increased DNA damage burden and are therefore predisposed to develop into neoplasia (Lowe *et al* 1993, Clarke *et al* 1993). However the role of p53 in intestinal tumourigenesis is unclear as p53 null mice failed to exhibit increased cell survival or increased mutation burden at spontaneous levels of damage (Buettner *et al* 1997) and only small increases at extreme levels of damage (Clarke *et al* 1997). Together these finding perhaps explain why p53 deficiency only weakly predisposes to increased intestinal neoplasia on the Apc^{MIN} background, despite showing strong co-operativity with Apc deficiency in other tissues such as the pancreas (Clarke *et al* 1995) and the mammary gland (Meniel *et al* 2005).

1.9 Extrinsic and Intrinsic cell death

1.9.1 Extrinsic cell death

The molecular events underlying receptor initiated cell death (or extrinsic cell death) are relatively well characterised when compared to DNA damage induced death. Death receptor induced apoptosis may be induced by a variety of sources: Cytokine signalling (TNFα, γ-IFN and Fas/Apo-1), depletion of soluble growth or survival factors, ceramides, and also loss of cell-to-cell adhesion or detachment from the extracellular matrix (termed anoikis) (Potten *et al* 1997). Death receptor ligation and subsequent intrinsic apoptotic cascades are activated in response to several death stimuli including: stress, cytotoxic drugs, ionising radiation, and withdrawal of survival factors.

The use of organisms such as *Caenorhabditis elegans* and *Drosophila melanogaster* has been useful in identifying the genes responsible for programmed cell death and the human homologues of receptor mediated death genes (Hengartner and Horvitz 1994). Additionally, the yeast two-hybrid system has also been valuable in identifying

genes involved in mediating the apoptotic response to Tumour necrosis factor (TNF) family of cytokines and also the Fas/APO-1 pathways. As a result a large network of death signal mediators have been identified (outlined in figure 1.8).

Fas or TNF ligand binding to the appropriate receptors evokes trimerisation and transmission of the death signal via interaction of proteins containing death domains (DDs) or death effector domains (DEDs) (Ng *et al* 2001). Death domain aggregation recruits the FADD containing DISC complex (death inducing signalling complex), which leads to activation of the major effectors of apoptosis – the caspase family (Kissil and Kimchi 1998). Initiator caspases 8 and 9 are at the head of the caspase cascades and can be activated by cleavage of precursor domains. Downstream effector caspases (3, 6 and 7) cleave many substrates that bring about the morphological features of apoptosis such as chromatin condensation and membrane blebbing (Crighton and Ryan 2005).

Ceramides are also known to induce cell death in many cell types. Hydrolysis of sphingomyelin in the cell membrane generates a secondary ceramide messenger that acts to propagate cell death in response to other death stimuli such as: PIP3, TNF-α, Fas and X rays. Ceramides then activate the SAPK/JNK stress induced death pathway, which may play Pro and anti-apoptotic functions depending tissue specificity, microenvironment and caspase cleavage of its components (Crighton and Ryan 2005)(see figure 1.8). TNF induced cell signalling may also have pro and anti-apoptotic effects. TRAF recruitment can activate the NF-κB survival pathway, which inhibits apoptosis by upregulating IAPs (inhibitors of apoptotic proteins) and decoy death receptors (Crighton and Ryan 2005).

1.9.2 DAPK family of Pro-apoptotic proteins

Death associated protein kinase (DAPK) was first identified by its Ser/Thr kinase pro-apoptotic activities (Deiss *et al* 1995). This was confirmed by using a novel technique called technical knockout (TKO), which relies on random inactivation of gene expression by RNA targeting. This technique was used to screen antisense cDNA libraries for genes relevant to cell death. The inactivation of any gene significantly involved in mediating the death response would confer a selective advantage to cells

exposed to an apoptotic stimulus such as γ-interferon (γ-IFN). Forward selection then rescues any relevant cDNA clones for sequencing (Levy-Strumpf and Kimchi 1998). The TKO experiments produced several genes involved in mediating the γ-IFN response including: DAP1, DAPK, DAP3, DAP4, DAP5, CathepsinD (a lysosomal protease) and thioredoxin (redox regulatory protein) (Levy-Strumpf and Kimchi 1998).

DAP1 is a small 15kDa proline rich basic protein containing 2 potential CDK phosphorylation sites although the biochemical function remains unknown (Levy-Strumpf and Kimchi 1998). DAP3 may function as a nucleotide binding protein via a phosphate binding loop interaction and is a positive mediator of death. This function has recently been further characterised and DAP3 was found to assist in mitochondrial fragmentation during the death response to stimuli such as TNF-α and Fas (Mukamel and Kimchi 2004). Furthermore DAP3 has been identified as a possible suppression target of AKT survival signalling to prevent aniokis based death (Miyazaki *et al* 2004). DAP5 shows high homology to the translation initiation factor eIF4G1, and is a caspase activated self-regulating translation factor that aids translation of apoptosis related proteins (Henis-Korenblit *et al* 2000).

Death associated protein kinase (DAPK) is a Ca^{2+}/Calmodulin dependant Serine/Threonine kinase. Over expression of wild type DAPK was found to induce apoptosis in cell culture and conversely, mutations of the catalytic domain resulted in resistance to apoptosis *in vitro* (Cohen et al 1997). DAPK is widely expressed in many tissues and subsequently DAPK has been implicated in mediating the apoptotic response to a variety of apoptotic stimuli including: interferon -γ, Fas, TNF-α, TGF-β, anoikis and C_2, C_6 C_8 ceramides (Deiss *et al* 1995, Cohen *et al* 1999, Inbal *et al* 1997, Raveh and kimchi 2001, Jang *et al* 2002, Pelled *et al* 2002, Yamamoto *et al* 2002) (discussed further in chapter 4).

The remaining DAPK family consists of DAPK, DRP-1 (DAPK related protein –1), DlK/ZIP kinase, DRAK1 and DRAK2 (DAPK related apoptosis inducing proteins). All proteins share strong homology of the kinase domain, but have distinct cellular functions and localizations (Levy-Strumpf and Kimchi 1998).

1.9.3 Intrinsic/Mitochondrial cell death and the *Bcl-2* family

One of the first apoptosis related genes to be identified by Tsujimoto *et al* was cloned and isolated as anti-apoptotic gene *Bcl-2* (Tsujimoto *et al* 1984), subsequently a whole gene family related to *Bcl-2* has emerged. The Bcl-2 family of proteins are key players in the intrinsic death pathways and comprise both anti-apoptotic and pro-apoptotic members. It is thought that the ratio of these family members is critical to the cellular decision to live or die. Thus, Bcl-2, Bcl-xL and Bcl-w inhibit apoptosis and promote cellular growth (Potten *et al* 1997), hence predicting their oncogenic role if overexpressed. Pro-apoptotic members of the family include Bax, Bak, Bok and the BH3 subfamily comprising Bik, Bad, Bid, Bim, Noxa and Puma (Herzig *et al* 2002).

Fas signalling components are widely expressed in many cell types, both normal and neoplastic, initiating the death response via mitochondrial activity. Mitochondrial activation of caspases amplifies the death signal and converges with various other inputs on the caspase effector cascade to disassemble the cell (Makin and Hickman 2000). Pro-apoptotic proteins Bax, Bid and Bad are proposed to undergo conformational change and mediate formation of pores in the mitochondrial membrane analogous to the diphtheria toxin, releasing Cytochrome c (Makin and Hickman 2000). Apoptotic protease activating factor 1(Apaf-1) interacts with Cytochrome c release from the mitochondrial membrane and processes procaspase 9 and activation of the caspase pathway directly (see figure 1.8). Additional pro-apoptotic mitochondrial components are released including exonucleases and caspase enhancing proteins AIF, DIABLO and Omi (Crighton and Ryan 2005).

The anti-apoptotic protein Bcl-2 can prevent this whole process of cytochrome c release, effectively blocking cell death (Makin and Hickman 2000). Additionally pro-apoptotic Bad can be inactivated and sequestered by Akt phosphorylation and the 14-3-3 protein. The resultant release of another Bcl-2 family member; Bcl-xl also aids to block cytochrome c release and inhibition of cell death (Makin and Hickman 2000).

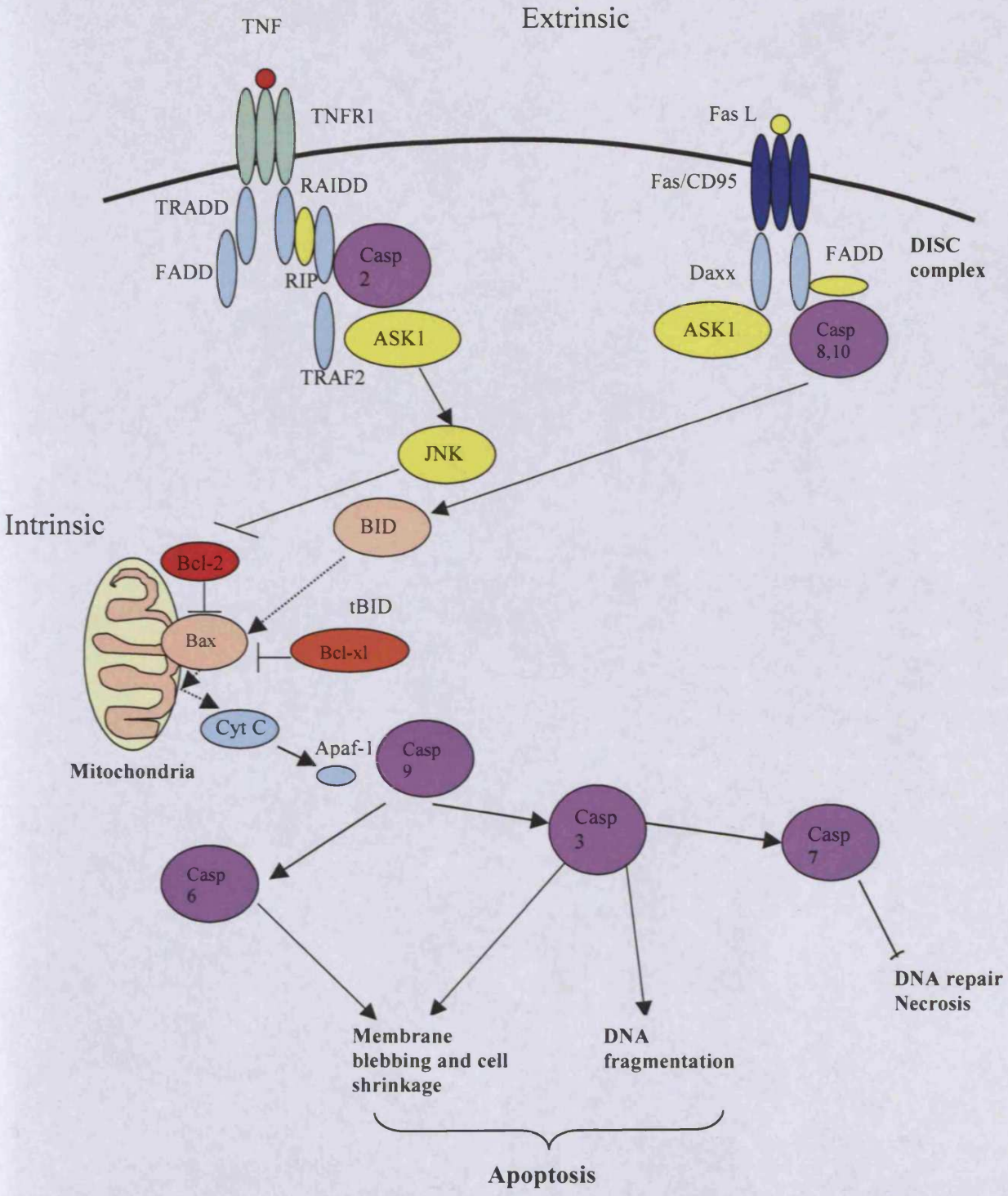

Figure 1.8- Extrinsic and Intrinsic cell death pathways. Death receptor stimulation leads to extrinsic activation of the apoptotic process via DISC complex formation and activated caspase cascade. Intrinsic cell death initiated by mitochondrial membrane changes is controlled by Bcl-2 family members, and feeds into effector caspase cascades (adapted from Crighton and Ryan 2005).

Tumour cells also often exhibit defects in receptor mediated death pathways by mutation of Receptors and ligands such as CD95 or by inactivation of the caspase members or upregulation of their inhibitors (Crighton and Ryan 2005). Mutations of any of the components involved in the Fas pathway may cause inhibition of death by formation of abnormal DISC complexes (Shin *et al* 2002). Many cancer cells have evolved to be Fas resistant due to mutations in the death domain containing genes of the pathway. Indeed mutations in Fas, FADD, Caspases 8 and 10 are associated with metastasis of cancer cells in non-small cell lung caner (NSCLC) (Shin *et al* 2002).

1.9.4 Bcl-2 family mouse models of tumourigenesis

The concept of loss of control of the intrinsic apoptotic response in tumourigenesis was first demonstrated by Tsujimoto *et al,* who identified that Bcl-2 was commonly mutated and overexpressed in B cell lymphomas, thereby blocking the death pathway (Tsujimoto *et al* 1984). Bad knockout mice also develop B cell lymphomas, and showed clear acceleration of lymphomagenesis following exposure to γ-irradiation (Ranger *et al* 2003). Similarly, Bim or Bax deficiency accelerates neoplasia in the context of overexpression of oncogenes such as E1A, Sv40, or c-Myc (Cory *et al* 2003).

Mouse models of Bcl-2 family members have been essential in characterising their role in apoptosis, with overexpression of *Bcl-2* conferring a distinct cell survival advantage *in vivo* (McDonnell *et al* 1998), this was accelerated with co-expression of other oncogenes such as c-Myc (Strasser *et al* 1990). Contrastingly, *Bcl-2* knockout mice exhibit a vast increase in spontaneous apoptosis (Potten and Booth 1997).

In terms of clonogenic survival within the small intestine, Bcl-2 deficiency in mice has been reported to reduce crypt survival following low dose-rate radiation, although this was reported only following a low dose-rate regime (Hendry *et al* 2000). At higher dose rates, no difference in clonogenic survival was noted in the small intestine, although reduced survival was seen in the bone marrow (Hoyes *et al* 2000).

These *in vivo* models have revealed a complexity of reliance upon individual Bcl-2 family members for the apoptotic response, particularly in the intestine. Bcl-2 expression in the epithelium of the large intestine protects the stem cell region from

spontaneous apoptosis, as Bcl-2 null animals showed elevated sensitivity within the stem cell compartment of the large intestine (Watson and Pritchard 2000). By contrast, apoptosis within the small intestine is regulated by the anti-apoptotic family member Bcl-w, with elevated levels of apoptosis following either 5FU or ionising radiation (Pritchard *et al* 2000). Such differential reliance upon the Bcl-2 family members may reflect the differential patterns of expression of each family member (Cory *et al* 2003).

At least part of the association between Bcl-2 proteins and cell death may arise as a consequence of p53 status, as several members of the Bcl-2 family including Bax, Noxa and Bid are regulated by p53. Consistent with this, both Bax and Noxa null MEFs show resistance to oncogene-induced p53-dependent apoptosis (Fridman and Lowe 2003, Villunger *et al* 2003). Noxa null mice also show resistance to irradiation-induced apoptosis of the small intestine, reinforcing the role of Noxa in p53-mediated apoptosis (Shibue *et al* 2003).

1.9.5 Drug resistance

The contribution of endogenous apoptotic signalling to drug-induced cell death is still unclear. Certainly cisplatin, 5FU and other cytotoxic agents have been shown to invoke auto and paracrine signalling to tumour cell death receptors to stimulate apoptosis. Indeed, p53 has been shown to up-regulate CD95, FADD, Procaspase8 and the DISC complex proteins. *In vivo*, *Fadd*$^{-/-}$ and *Casp8*$^{-/-}$ MEFs are still drug-sensitive, although clearly independently of death receptor stimulation. In contrast, *Apaf1*$^{-/-}$ and *Casp9*$^{-/-}$ MEFs are sensitive to death receptor triggers but show resistance to cytotoxic drugs (Debatin *et al* 2004).

Mutations in members of the Bcl-2 family also often results in drug resistance, as overexpression of Bcl-2 within a model of Myc-driven lymphomagenesis, produced multi-drug resistance (Schmitt *et al* 2000). Furthermore Bax-deficient tumours also show marked resistance to therapy, although is reliant upon genetic environment and type of oncogenic stimulation (Pritchard *et al* 1999, Cory *et al* 2003). Similarly, cell lines can be rendered chemosensitive *in vitro* by overexpressing Bcl-xL, yet prove to be chemoresistant *in vivo*, a phenomenon which may indicate that tumour

microenvironment is all critical in predicting response to chemotherapy (Johnstone *et al* 2002). This may in part be affected by death receptor density and/or NFκB signalling, which provides a regulatory balance between the decision of life or death. Alterations of these subtle regulatory elements may affect sensitivity or threshold of check-point mediated drug activation of apoptosis when treating cancers (Lee and Schmitt 2003).

1.10 Epigenetic modifications

1.10.1 Methylation

Changes that occur to the genome but do not alter the DNA sequence itself such as methylation patterns are referred to as epigenetic modifications. DNA methylation is essential for normal development in mammals. Methylation occurs at the 5'carbon of cytosine residues and globally throughout the genome at CpG dinucleotides (areas of GC rich bases stretching about 1kb). Methylation patterns are most dense at sites proximal to the centomeres on chromosomes (Hendrich and Bird 1998).

DNA methylases are responsible for generating and maintaining the methylation signal. The mammalian DNA methyltransferase DNMT1 is responsible for maintaining methylation in mammalian cells. Knockout mice lacking DNMT1 die mid-gestation, suggesting an important role for methylation signals during development (Li *et al* 1992). Other DNA methylases such as DNMT3a and DNMT3b are important for *de novo* methylation and generation of the methylation signal and overexpression of these regulatory genes has been linked with many human cancers (Esteller and Herman 2002, Esteller 2005).

Many essential roles exist for DNA methylation including: transcriptional regulation, positive suppression of foreign sequences such as viral DNA, X-chromosome inactivation, chromatin structure and organisation and genomic imprinting, all of which may be species and tissue specific (Mcburney 1999, Esteller and Herman, 2002) (see figure 1.9).

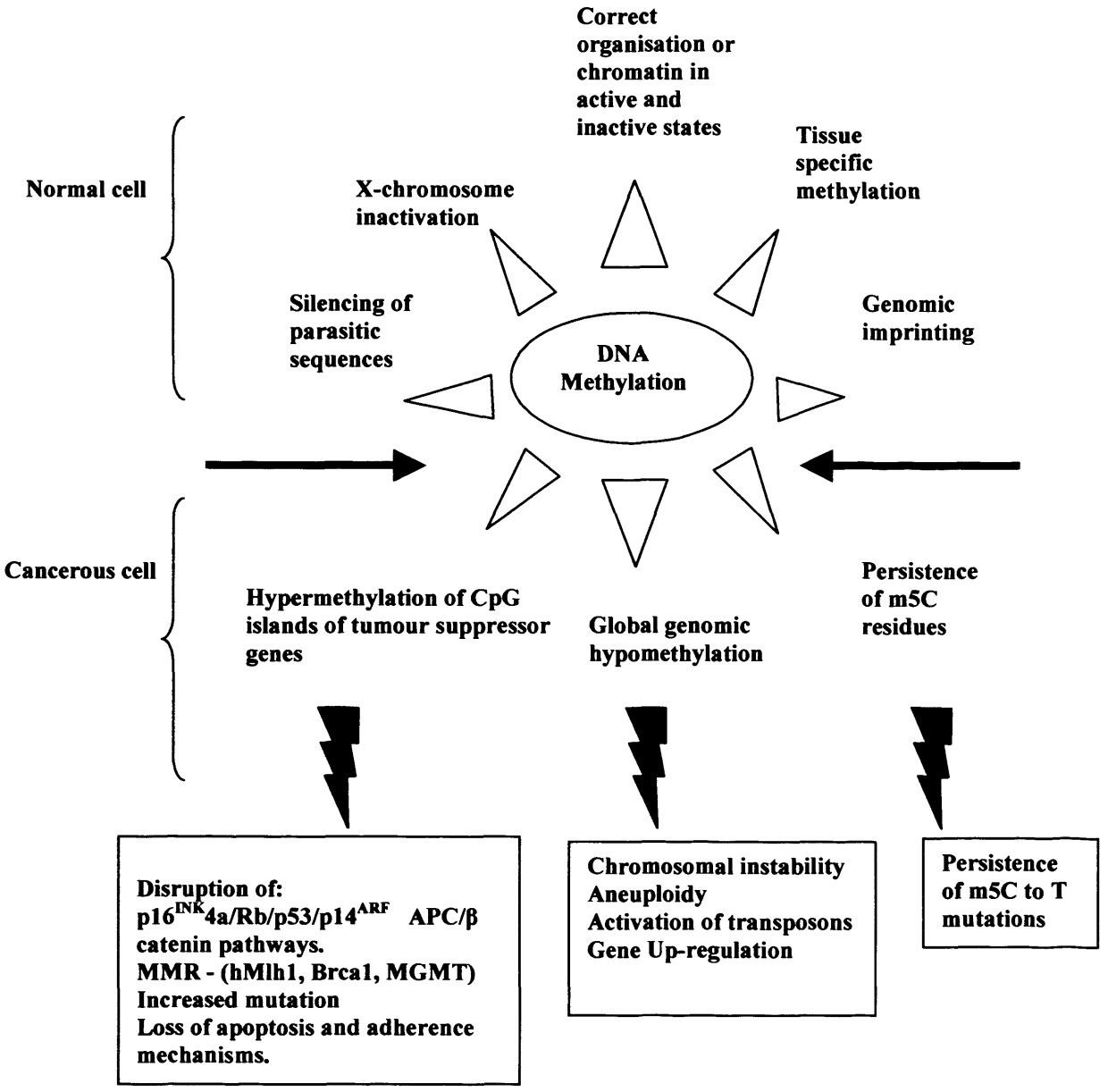

Figure 1.9- Roles of Mammalian DNA methylation. Correct DNA methylation is at the centre of both normal and malignant behaviour of the cell. Loss of control of these processes results in loss of tumour suppressor genes, increased mutation burden, inappropriate survival of damaged cells and ultimately tumourigenesis (adapted from Esteller and Herman 2002).

1.10.2 Spontaneous deamination and mutability of CpG sites

At least 50% of all somatic mutations in colorectal cancer arise from G:C to A:T deaminations of the highly mutagenic 5-methylcytosine (5MeC) at CpG sites (Drummond and Bellacosa 2001) and occur following endogenous damage or

exogenous mutagen exposure (Kinzler and Vogelstein 1996). Inactivation of caretaker genes such as *APC* may accelerate accumulations of mutations in genes such as *P53* and other tumour suppressor genes (Drummond and Bellacosa 2001). As base-to-base mismatches occur frequently throughout the genome during the normal process of replication, the ancestral RNA derived genome evolved a mechanism of replacing Uracil with Thymine in DNA. This allows the distinction to be made between C-T transitions and normal thymidine residues in DNA. Accordingly glycosylase enzymes involved in BER, have evolved to recognise these specific lesions so as not to remove legitimate thymines from the genome (Millar *et al* 2002).

1.10.3 Promoter Hypermethylation and transcriptional repression

Promoter sequences of genes are often flanked by CpG islands (Ballestar and Wolffe 2001). CpG rich islands surrounding the promoter regions of genes are usually protected from methylation, however once methylated these change DNA structure and render the gene inactivated and inaccessible (Esteller and Herman 2002). CpG islands may be misread by methylation enzymes for imprint boxes and randomly silenced by mistake (Mcburney 1999). However, it is still unclear whether methylation is the actual process responsible for gene silencing, or if it simply marks the fact that the event has occurred (Baylin and Herman, 2000).

Nuclear factors bind differentially to methylated genes and therefore alter the structure of chromatin and consequently transcriptional machinery is denied access to the promoter regions (Esteller and Herman 2002). Low levels of acetylaton (Hypoacetylation) in histones H3 and H4 are also associated with chromatin silencing. Methylation of CpG islands in conjunction with deacetylation of histones causes a closed chromatin state that is nuclease resistant and hence transcriptional repression (Mcburney 1999).

1.10.4 DNA Mehtylation and cancer

CpG island methylation may be a key step in the early stages of tumour development, hence Knudson's two hit hypothesis has been expanded to include allelic loss via methylation (Wheeler *et al* 2000). Consequently many tumour suppressor genes have

been found to be silenced due to promoter hypermethylation including: *p53, Rb, APC* apoptotic and adhesion genes such as *DAPK, APAF-1, TIMP3* (Esteller *et al* 2001), cell cycle genes $p16^{INK4a}$, $p14^{ARF}$, $p15^{INK4b}$, DNA repair genes *MLH1, BRCA1, MGMT, VHL* (Von Hippel Lindau) and several others *LKB1, p73, GSTP1* (Bellestar and Wolffe 2001, Esteller and Herman 2002). Methylation has been detected at early stages in lung carcinomas and many other cancers, and methylation patterns may provide some prognostic indictor in the early development of cancers (Soria *et al* 2002).

The finding that the *MLH1* promoter was found to be hypermethylated in 77% of RER+ve endometrial carcinomas, and 100% of gastric carcinomas suggests promoter hypermethylation to be the underlying cause of protein deficiency in sporadic CRCs. Indeed many RER+ve cancers have no detectable mutations in MMR genes, and therefore it was proposed that epigenetic mechanisms such as methylation maybe responsible for the MSI phenotype. However, in hereditary CRCs such as HNPCC (which also exhibits a RER+ve phenotype), hypermethylation of *MLH1* does not occur, suggesting differences in tumourigenesis (Wheeler *et al* 2000).

Altered expression of DNMT1 has been found to play a critical role in intestinal tumourigenesis as hypomorphic mice reduced the rate of CpG island methylation and polyp formation on an Apc^{MIN} background, therefore suppressing the intestinal MIN phenotype (Eads *et al* 2002).

In addition to promoter hypermethylation, global levels of DNA methylation are usually lower in tumour cells than in normal tissue, even though high levels of methyltransferases are detected. The process of hypomethylation allows inappropriate expression of oncogenes and loss of silenced or imprinted genes such as IGF-II and is associated with tumour growth (Mcburney 1999).

Proteins that recognise and mediate the methylation signal could provide clues to the process and novel targets for drugs to interact in the pathway (Bellestar and Wolffe, 2001). The drug trichostatin (TSA) partially relieves transcriptional repression by inhibiting histone deacetylase activity (Baylin and Herman 2000). However

methylation complexes may associate at a number of different promoters, and may be dependant on particular DNA templates or sequences, therefore specificity to date has been a major set back in the development of such drugs (Baylin and Herman, 2000).

1.10.5 Methyl binding Proteins

Given the involvement of methylation in cancer formation, investigations began to identify possible mediators of transcriptional repression, CpG deamination and the methylation signal. Among the first to be identified were a family of methyl binding proteins. Methyl binding proteins appear to have a novel function as interpreters and mediators of the methylation signal (Hendrich and Bird 1998). Each complex of proteins may in this way be targeted to and regulate a specific subset of genes (Ballestar and Wolffe 2001).

The first CpG binding proteins to be identified were MeCp1 and MeCp2 (Meehan *et al* 1989). MeCp1 distinguishes between methylated and non-methylated DNA sequences by binding to stretches of CpGs often found within the promoter regions of the genes. Mecp1 and MeCp2 have a large subunit structure and both bind to DNA in a methylation dependant fashion to inhibit transcription (Hendrich and Bird 1998).

The MeCp2 protein binds to single symmetrically methylated CpG sites across the whole genome. Point mutations in the MBD of MeCp2 have been found to underlie patients with Rett syndrome. This disease is characterised by childhood neurodevelopmental disorders and digestive problems (Ballestar and Wolffe 2001). MeCp2 is a chromatin associated nuclear protein containing a transcriptional repression domain (TRD) (Hendrich and Bird 1998). The TRD can repress transcription through long -range interactions with basal transcription machinery such as TFIIB (Bellastar and Wolffe 2001). MeCp2 can bind directly to DNA, and either directly repress or co-repress chromatin assembly in order to block transcription in addition to the transcriptional repression from the methylation signal itself, which stops transcriptional factors recognising and binding sequences (Wade 2001).

Database searches for MeCp1 homologues pulled up other MBD containing proteins, including: MBD1, MBD2, MBD3, and MBD4. The conserved Methyl binding domain (MBD) is a common feature to all family members at the N- terminus and MBD proteins are expressed in a wide range of tissues (Ballestar and Wolffe 2001). Alternative transcripts affecting the MBD exist for many of the MBD family, which may also suggest tissue specific isoforms (Wade 2001). Family members appear to differ in their cellular localization and methylation binding ability and specificity, with MBD2 and MBD4 binding heavily methylated DNA *in vivo*, whereas MBD1 binds lightly methylated DNA sequences (Hendrich and Bird 1998).

There is large divergence at the C terminus of the family, MBD1 contains several cystiene rich repeats (CxxC motifs) in addition to its TRD (Ballestar and Wollfe 2001). MBD2 is proposed to contain DNA demethylase activities and may act in complexes with MeCp1 and MBD1 to recruit co-repressor complexes to methylated sequences (Bellestar and Wolffe 2001, Sansom *et al* 2003b). Promoter methylation and repression during tumourigenesis may involve MBD proteins and MBD2 is overexpressed in many cancers. Loss of MBD2 has been shown to suppress intestinal tumourigenesis in a knockout mouse model by loss of transcriptional repression (Sansom *et al* 2003b).

MBD3 has 12 glutamic acid repeats and may be associated with the Mi-2NuRD chromatin remodelling complex which contains histone deacetylases and ATPases (Bellestar and Wolffe 2001). This links MBD proteins and the methylation signal to histone modification enzymes such as the histone deacetylases, and provides a dual function for MBD proteins. As MBD protein activity and DNA methylation can be relieved by inhibitors of histone deacetylases, many anticancer drugs are being developed to target this process (Bellastar and Wolffe 2001).

Finally MBD4 has a recognised thymine glycosylase activity, with the ability to recognise and remove G:T mismatches as a result of spontaneous deamination of CpG sites. MBD4 has high homology to MeCp2, and has recently been confirmed as having histone deactylase and transcriptional repressor activities similar to the other

family members (Kondo *et al* 2005). Further details of the structure and function of MBD4 will be discussed in chapter 3.

1.11 Mouse models of Tumourigenesis

The first transgenic mouse models of human neoplasia were generated through pronuclear injection and relied upon overexpression of oncogenic sequences (Adams *et al* 1985). This strategy provided the first real insights into genetic predisposition to tumourigenesis and since then increased knowledge of the mouse genome has progressed studies into inactivation of tumour suppressor genes.

Targetting and inactivation of alleles may be achieved by homologous recombination followed by transfection into embryonic stem cells to create a knockout mouse. In this situation the mouse is deficient for that particular gene from embryogenesis throughout all tissues. However, mice expressing exogenous gene sequences or homozygously deficient for essential tumour suppressor gene functions were often found to be embryonic lethal due to severe developmental defects.

Constitutive heterozygous gene deletion for tumour suppressor genes such as *p53*, *MSH2,* and *APC* have been particularly useful in creating representative models of hereditary human cancers such as Li-Fraumeni, HPNCC and FAP respectively. Furthermore homozygous gene loss in mice resulting in embryonic lethality has given insight into the importance of certain genes to embryonic development (Ghebranious *et al* 1998).

1.11.1 Conditional knockouts

Whole body deletion of genes although a useful tool does not reflect sporadic tumourigenesis in the human where initiation is often centred around a single lesion or clone in a relatively normal cellular environment.

Our understanding of the relevance of apoptosis to disease initiation and progression has been tempered by both the limitations of *ex vivo* studies and the complexities of *in vivo* analysis. The advent of genetically defined murine models has alleviated some of these problems, and the generation of models by targeted disruption of genes such as *Apc, p53, Bcl-2* and the MMR genes, that allows both spatial and temporal control of transgenes and endogenous genes has provided remarkable insights into the role of apoptosis during tumourigenesis.

Some of the more recent technologies include the delivery of conditional transgene expression by the Tetracycline on/off system. This relies of fusion of the *E.Coli* tetracycline responsive gene to a tissue specific promoter, and is controlled by administration of tetracycline or its analogue doxycycline (figure 1.10 Gossen *et al* 1992). A similar method for controlling transgene activity is via fusion to a tamoxifen sensitive mutant of the Estradiol Receptor. The latter approach has proven particularly successful in studying conditional c-Myc, with extremely rapid transgene activation in tissues such as skin, pancreas and lymphocytes (Giuriato *et al* 2004).

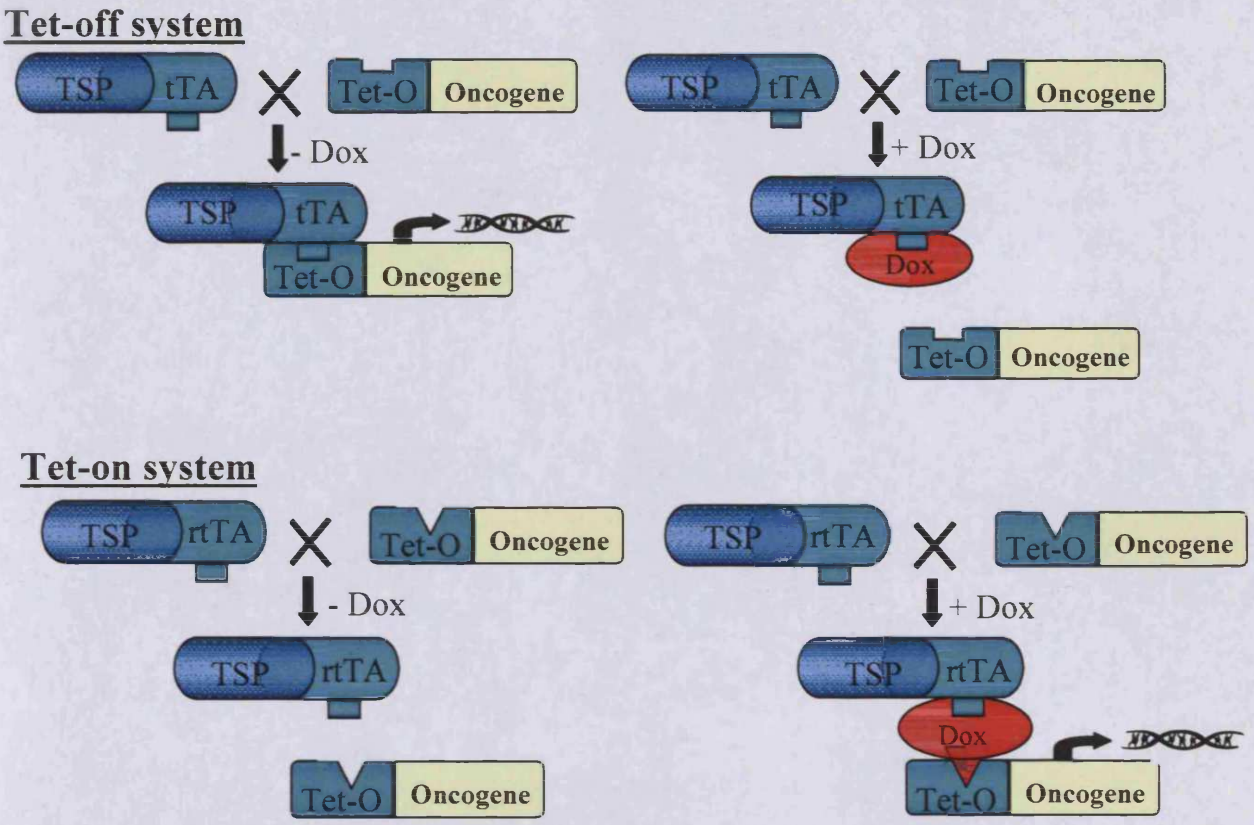

Figure 1.10 – Schematic of conditional Tet on/off system for oncogene expression. In the Tet off system, the Tet responsive DNA binding domain is fused to a transactivation domain from a herpes simplex viron protein gene (tTA) and linked to a tissue specific promoter (TSP). Additionally, a construct containing the gene of interest driven by the human CMV virus promoter and the tet operator Tet-O, binds the tTA in the absence of Dox (doxycycline), thereby expressing the oncogene constitutively. In the Tet-on system, a mutant version of the transactivation construct (rtTA) cannot bind and drive oncogene expression. The addition of Dox induces conformational change and Tet-O is activated (adapted from Gossen *et al* 1992, Giuriato *et al* 2004).

1.11.2 C-Myc mutant mice

This system has been used to study the effects of oncogene activation in spontaneous neoplasia from Myc and Ras oncogene activation. High levels of oncogenic c-Myc are found in 70% of colon cancers, and this has been attributed to activated Wnt signalling and mutation in the *APC* gene. Importantly cells with amplified Myc expression are sensitive to 5FU-induced apoptosis, which may induce apoptosis by a range of mechanisms, including the Bax-mediated release of cytochrome *c*, and the activation of a wide range of pro-apoptotic molecular targets, such as Arf and FADD (Arango *et al* 2001).

Adaptation of the Tet on/off system created the Eμ-Myc mouse transgene, which detailed that overexpression of c-Myc resulted in T cell lymphomas and acute myeloid leukaemia. Subsequent inactivation of c-Myc led to 90% tumour regression via terminal differentiation and apoptosis (Felsher *et al* 1999, Pelengaris *et al* 1999, 2000). D'cruz *et al* 2001 have also shown similar full reversal of Myc-induced invasive mammary carcinomas. Parallel experiments in pancreatic β cells showed Myc expression to drive both apoptosis and proliferation, but only to result in neoplasia following co-expression of Bcl-xL, which inhibited apoptosis (Pelengaris *et al* 2000, 2002). The precise role played by c-Myc-driven apoptosis in initiation and regression remains somewhat unclear, but is clearly context-dependent.

1.11.3 K-Ras mutant mice

Activating Ras mutations are very common in many cancers and are found in around 20% of CRCs. In the intestine Ras plays a role in proliferation and survival signalling and increases in K-ras have been shown to elevate PI3K, mTOR and S6K activities which contribute to transformation. This can be associated with MMR deficiency and in combination drives cancer progression rather than initiation (Sancho *et al* 2004).

Somewhat similar data to that of Myc activation has been generated in mice with mutant *Ras* alleles, with several different groups using conditional strategies to control mutant *Ras* gene expression and identify its role in tumour initiation and progression. Thus, Chin *et al* used the Tet system to drive expression of the mutant H-ras V12G allele, which resulted in melanoma development within 2 months. Upon doxycycline withdrawal, tumours spontaneously regressed showing high levels of apoptosis, but rapidly re-established if doxycycline was readministered (Chin *et al* 1999). Furthermore, a model dependent upon p53-deficient fibroblasts transfected with a doxycycline and a regulable tet-o-K-Ras4b^{G12D} allele, was subsequently infected with avian retrovirus carrying the rtTA component. In these circumstances, withdrawal of doxycycline resulted in reduced expression of the mutant K-ras allele and initiated regression of tumours *in vivo* (Pao *et al* 2003).

1.11.4 Cre-Lox P technology

Conditional expression of endogenous alleles has also been achieved with the Cre–LoxP and Flp–Frt systems driven by a tissue specific promoter to allow spatial and temporal and dose dependent gene inactivation (Kühn *et al* 1995). Cre/Lox P technology utilizes a site-specific recombinase, which recognises sites on the P1 bacteriophage genome called Lox P sites (locus of X-over P1)(Guo *et al* 1997). Mice integrating these sites flanking a gene of interest can then be crossed mice expressing a tissue specific Cre recombinase which mediates excision of the gene between the 34 bp LoxP sites (Campbell *et al* 1996)(see figure 1.11).

1.11.5 The inducible CYP1A promoter

CYP1A is a gene encoding members of the cytochrome p450 family, which catalyse oxidation of a wide range of compounds. They are inducible by a range of drugs such as polycyclic aromatic hydrocarbons. The CYP1A promoter has a dioxin response element, which can mediate induction of the gene by the compound β-Napthoflavone (BNF). Promoter function is enhanced by the AH (aryl hydrocarbon) receptor and its cofactor ARNT, both of which act as transcription factors. CYP1A can be used to drive expression of a targeted allele flanked by lox P sites specifically to the intestine (see figure 1.11). Using this tissue specific regulated expression system, removal of genes from the gut can be controlled in a dose and time dependant manner (Ireland *et al* 2004).

Combinations of all of the above conditional transgenic systems are now being successfully used for the analysis of tumourigenesis. These strategies, allied with the use of viral delivery systems and reporter genes such as LacZ and luciferase, are proving invaluable in monitoring tumour initiation, development, metastasis and regression (Giuriato *et al* 2004).

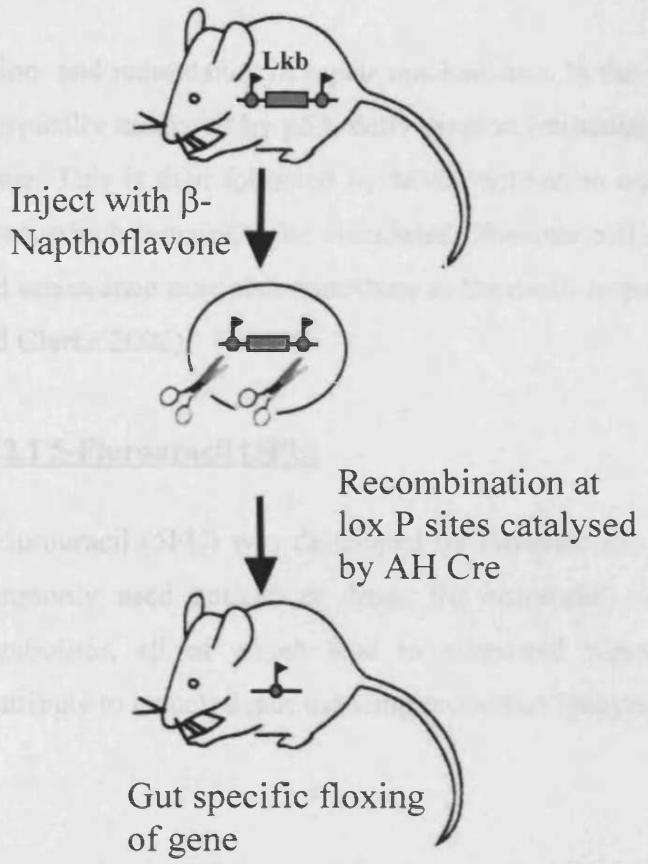

Figure 1.11 - Induction of cre recombinase by β-Napthoflavone results in gut specific recombination of LoxP sites (black flags). This gives 100% floxing of the flanked gene within the intestine.

1.12 Cytotoxic drug treatment

The intestinal apoptotic response to cytotoxic agents has been under much investigation to try to elucidate therapeutic targets and mechanisms of drug resistance. These agents commonly initiate the apoptotic response in tumour cells, although they can cause significant toxicity to normal cells in the process (Crighton and Ryan 2005).

Many cancer chemotherapy drugs induce apoptosis through activation of p53, p21, MDM2 and GADD45 (Makin and Hickman 2000). Treatment increases the immediate apoptotic response, depresses cell cycle progression and alters mature cell function and migration. Many cytotoxic drugs are aimed at incorporation during the S phase of the cell cycle causing rapid induction of apoptosis (Ijiri and Potten 1987).

The apoptotic response to DNA damaging agents is complex and still under investigation due to the complicated process of reactive metabolites, types of DNA

lesion, and redundancy in repair mechanisms. In the intestine drug induced cell death is typically mediated by p53, delivering an immediate apoptotic wave throughout the tissue. This is then followed by MMR activation and finally a p53-independent late wave, which remains to be elucidated. Necrotic cell death and p53/p16 growth arrest and senescence may also contribute to the death response to cytotoxic agents (Sansom and Clarke 2002).

1.12.1 5-Flurouracil (5FU)

5-Flurouracil (5FU) was developed by Heidelberger in 1957 and is one of the most commonly used anticancer drugs for colorectal cancers. 5FU has several active metabolites, all of which lead to mispaired bases and DNA strand breaks and contribute to its cell death inducing properties (Meyers *et al* 2004).

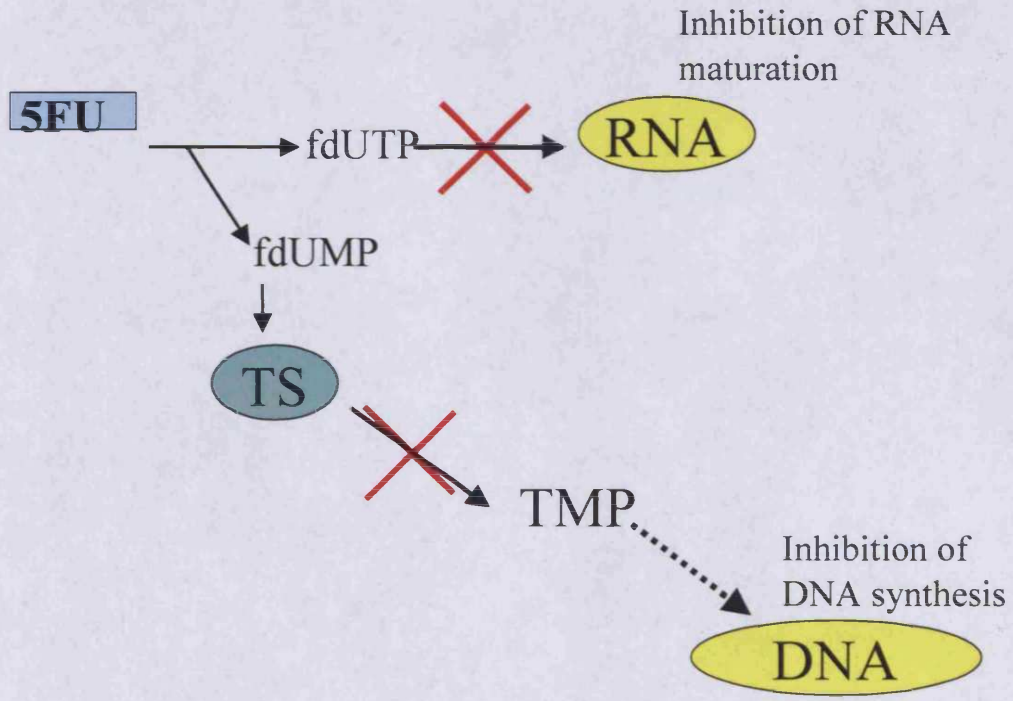

Figure 1.12- Mechanisms of action of the anti-tumour effect of 5Flurouracil. 5FU may block DNA synthesis and repair by Thymidylate synthase (TS) inhibition. RNA maturation is also blocked by 5FU incorporation. fdUMP = FdUrd-5'monophosphate, fdUTP = FdUrd5'triphosphate, TMP = Thymidine- 5-monophosphate (adapted from Tanaka *et al* 2000).

Thymidylate synthase (TS) is an essential enzyme in the synthesis of 2-deoxythymidine-5-monophosphate (dTMP) from the methylation of 2-deoxyuridine-5-monophosphate (dUMP). Many cancer therapeutic drugs including 5FU target and inhibit TS, especially those of folate derivative and nucleotide. Cells with low p53 levels are particularly sensitive to 5FU compared to those expressing mutant forms of the protein (Peters *et al* 2002). Inhibition of TS by Flurodeoxy-Uridine-5'monophosphate (fdUMP) leads to a depletion in dTMP levels and consequently DNA strand breaks (Tanaka *et al* 2000). Direct strand breaks by 5FU are mediated by Flurodeoxy-Uridine-5'triphosphate (fdUTP) incorporation into DNA. Finally incorporation of fdUTP into the RNA uracil pool results in perturbation of RNA maturation (see figure 1.12).

1.12.2 Cisplatin treatment

Also known as Cis-diamminedichloroplatinumII (CDDP) is another drug commonly used to treat CRCs. CDDP inhibits transportation of methionine into the cytoplasm from the extracellular space leading to depletion of intracellular methionine levels. This depletion increases synthesis from homocystiene and consequently tetrahydrofolate and 5,10-methylene-tetrahydrofolate, both of which add to the inhibition of TS. Cisplatin causes GG crosslinks between adjacent purines and consequently DNA strand breaks (Meyers *et al* 2004). This mechanism of action is similar to that of 5FU and the two drugs are often administered together to enhance 5FU anti-tumour effects. Resistance to cisplatin has been linked to mutation in the MMR gene *MLH1* (Strathdee *et al* 1999).

1.12.3 NMNU and Temozolomide

Alkylating agents such as NMNU, ENU, Temozolomide and their reactive metabolites are capable of producing many DNA lesions and ultimately double strand breaks. Alkylation occurs at oxygen and nitrogen sites of DNA at the N^3 position on purines and particularly the N^7 and O^6 positions of guanine (Petronzelli *et al* 2000a). The cytotoxic action of Temozolomide largely depends on the methylation of DNA and O^6 methyl guanine lesions (O-6meG), which mimic the endogenous G:T

mismatches thought to induce apoptosis through MMR signalling and inhibition of S phase (Duckett *et al* 1996, Newlands *et al* 1997). O6meG:T mismatches within the DNA following replication are recognised preferentially by MMR machinery rather than p53, which then channels cells toward arrest and apoptosis (Hickman and Samson 1999). Expression of O6-methylguanine DNA methyl transferase protein (MGMT) also repairs these adducts and reduces the apoptotic response to such alkylating agents (Zak *et al* 1994).

1.12.4 Ionising radiation

Ionising radiation (γ-IR) produces many types of DNA damage including: crosslinking, modified nucleotides and single and double stranded DNA breaks (Meyers *et al* 2004). The apoptotic response to γ-IR has been reported to be independent of MMR mechanisms (Sansom and Clarke 2002, Meyers *et al* 2004), and much of the death response centres on p53 and p73 dependent pathways (Bellacosa *et al* 2001a). P53 deficiency has been found to sensitise mice to higher doses of ionising radiation, causing lethal gastro-intestinal syndrome characterised by accelerated cell death and destruction of the villi. This has been interpreted as a consequence of failure of the protective p21-dependent cell cycle arrest, indicating the importance of p53 in the radiation induced apoptotic response (Komarova *et al* 2004).

Stem cells appear to be more resistant to certain types of damage than other cells and upon cytotoxic assault, repopulate the crypt structure, following the death of the transit proliferative cells at higher positions up the crypt (Potten *et al* 1997). Intestinal cells are killed within a few hours following high dose γ-IR and this response peaks at 6 hours at the base of the crypt. Remaining crypt structures are destroyed within 2-3 days. Isolated individual surviving clonogenic cells divide rapidly to repopulate the crypt and regenerate the intestinal structure (Potten and Booth 1997). This response is highly lesion and dose specific and radiation induced damage differs from that of cytotoxic drugs as it is capable of hitting the stem cell region at very low doses of radiation damage (1Gy) but not at high doses (15Gy). Further research has revealed that at low doses of radiation, dying stem cells co-opt up to 6 new replacement daughter cells to undergo dedifferentiation to repopulate the crypt. This number increases to approximately 22 at higher levels of DNA damage (Potten *et al* 1997).

1.13 Aims and objectives

This thesis aims to use constitutive mouse models to characterise the roles of two key cell death related genes; *Mbd4* and *Dapk* in mediating DNA damage induced apoptosis in the intestine. Mice harbouring mutant pro-apoptotic genes may be predicted to show reduced levels of cell death compared to wildtype mice in conjunction with increased clonogenic survival. Taken together these studies will help to elucidate mechanisms by which Mbd4 and Dapk signal apoptosis, either initiating a response directly or via p53 and MMR pathways. Consequently these studies may have further implications for accelerated tumourigenesis and chemoresistance in the intestine.

I also aim to outline a functional role for the tumour suppressor gene *LKB1* in the murine small intestine. I will use conditional inactivation of the $Lkb1^{fl}$ allele using the AHCre transgene to monitor the immediate effects of complete loss of Lkb1 on intestinal homeostasis and focus on potential *in vivo* functions of the protein. Given its varied roles in growth arrest, apoptosis and Wnt signalling, deletion of *Lkb1* should cause severe disruption to proliferation, cell growth, apoptosis and positional cues along the crypt –villus axis. Additionally, I will address the long-term consequences of the phenotypes observed to assess the contribution of homozygote and heterozygote Lkb1 loss to hamartoma formation and tumourigenesis.

Chapter 2. Materials and Methods

2.1 Mouse colonies

Mbd4$^{-/-}$ mice (supplied by Jacky Guy, Adrian Bird Laboratory) and *Mlh1*$^{-/-}$ mice (supplied by M Buermeyer, see Prolla *et al* 1997) were bred from an out bred colony segregating for Ola/129a and C57BL6 genomes (approximately 92% C57BL6). *Lkb1*^{fl} mice (supplied by Alan Ashworth Laboratory) were crossed to AHCre+ mice (supplied by Doug Winton) and were outbred segregating for C56BL6, Ola/129a and C3H genomes. Animals were maintained on Harlan standard diet (scientific diet services) and water provided *ad libitum*.

Cohorts of mice aging for *Lkb1*AHCre and *Lkb1*DelCre tumourigenesis studies were monitored daily for signs of disease (hunched back, poor coat quality, weight loss associated with intestinal neoplasia), and sacrificed for organs and gut preparations (see section 2.3).

2.2 Genotyping of mice

2.2.1 DNA extraction

Mice were genotyped by polymerase chain reaction using DNA extracted from Puregene DNA extraction kit (Gentra systems, inc., Minneapolis, MN). Briefly, a 2mm tail sample was lysed with 10µl Proteinase K (20mg/ml Roche) in 500µl cell lysis buffer overnight at 37°C. 200µl protein digestion solution was then added and samples centrifuged at maximum (14,000rpm) for 10 minutes. Supernatant was then discarded and DNA precipitated in 500µl propan-2-ol. The samples were finally centrifuged at maximum speed for 15 mins, supernatant discarded and samples allowed to air dry to 10-15 minutes before resuspending in 500µl DDW. All subsequent PCR reactions were carried out using 2µl (approx 200ng) of tail DNA preparation.

2.2.2 Preparation of Agarose gels

The majority of PCR reactions were run on 2% agarose gels containing 3g of Agarose dissolved in 150ml 1xTBE buffer (5x TBE 10L: 540g Tris base, 275g Boric acid, 37.2g Disodium EDTA pH8.3) by boiling in a microwave on full power for 2 minutes. Solution was allowed to cool slightly before adding 15µl ethidium bromide (10mg/ml Sigma), and pouring into gel cast. Those PCR reactions with small products (<200bp) were run on 4% agarose gels using 6g of argarose in 150ml 1x TBE buffer. All gels were run in 1xTBE buffer for 1 hour at 75V and bands visualised under UV.

2.2.3 Mbd4 PCR

PCR reactions contained:
5µl 10x RedTaq Buffer (Sigma)
1µl each primer (10pmoles/µl) (OSWEL)
1µl dNTPs (40mM)(Sigma)
2.5µl $MgCl_2$ (50mM) (Sigma)
30µl double distilled water (DDW)
1µl RedTaq (D4309 sigma)
2µl sample DNA

Reaction conditions were as follows:

Initial denaturation 94°C for 5 mins

94°C for 1 minute
65°C for 1minute } 30 cycles
72°C for 1 minute

Final extension 72°C for 10 minutes

Products were run on a 2% Agarose gel giving a wild type 322bp band and a homozygous 469bp band.

Primers:

1. 5'AAGGTGGCACCTAGAGCTCTGTCG'3
2. 5'GGATATTCGGTGCTGTCGCTCG'3
3. 5'GTCGGTTTATGCAGCAACGAGACG'3 (HOM)
4. 5'CAAACTGGCAGATGCACGGTTACG'3 (HOM)

Designed by Millar *et al* 2002

2.2.4 Mlh1 PCR

PCR reaction contained:

5µl 10x RedTaq Buffer (Sigma)
2.5µl W1 detergent (Gibco)
1µl each primer (10pmoles/µl) OSWELL
1µl dNTPs (40mM)(Sigma)
2.5µl $MgCl_2$ (50mM)(Sigma)
30µl DDW
1µl RedTaq polymerase (D4309 Sigma)
2µl of sample DNA.

Cycling conditions were as follows:

Initial denaturation 94°C for 5 minutes,

94°C for 1 minute
60°C for 1minute } 30 cycles
72°C for 1 minute

Final extension 72°C for 10 minutes

Products were run on a 2% Agarose gel. Wild type product was 258bp and homozygotes generated a 198bp fragment.

Primers:

1. 5'AGGAGCTGATGCTGAQGGC'3
2. 5'GATCTCGACGGTATCGATAAGC'3
3. 5'TTTCATCTTGTCACCCGATG'3

2.2.5 Dapk PCR

PCR reactions contained:

5µl 10x RedTaq Buffer (Sigma)
1µl each primer (10pmoles/µl) (OSWELL)
1µl dNTPs (40mM)(Sigma)
4µl $MgCl_2$ (50mM)(Sigma)
34µl DDW
2µl RedTaq polymerase (D4309 Sigma)
2µl of sample DNA.

Cycling conditions were as follows:

Initial denaturation 95°C for 3 min

94°C for 30 secs
54°C for 30 secs } 32 cycles
68°C for 2 minutes

Final extension 68°C for 10 minutes

Amplified fragments were separated on a 2 % Agarose gel. WT and HOM alleles gave PCR fragments of 531bp and 637bp respectively.

Primers:

WT alleles: 5'GTC CCT CCA GTT GCA GTT AGA ATC'3

5'CTT TCA GAG GTC TGC GGC TTG GTG CAT GAG'3

Hom allele 5' AGG ATC TCG TCG TGA CCC ATG GCG A'3

2.2.6 Lkb1 PCR

PCR reactions contained:

5µl 10x RedTaq Buffer (Sigma)
1µl each primer (10pmoles/µl) (OSWELL)
1µl dNTPs (40mM)(Sigma)
5µl $MgCl_2$ (50mM)(Sigma)
33µl DDW
2µl RedTaq polymerase ((D4309 Sigma)
2µl of sample DNA.

Cycling conditions were as follows:

Initial denaturation 94°C for 3 min

94°C for 30 secs
52°C for 30 secs } 32 cycles
72°C for 1 minute

Final extension 72°C for 10 minutes

Amplified fragments were separated on a 2 % Agarose gel, WT and HOM alleles giving PCR fragments of 320bp and 280bp respectively.

Primers: F 5'GTATTCCGCCAGCTGATTGA'3

R 5' AGTGTGACCCCAGCTGACCA

2.2.7 Lacz /AHCre PCR

PCR reactions contained:

5µl 10x RedTaq Buffer (Sigma)
0.1µl each primer (10pmoles/µl) (OSWELL)
1µl dNTPs (40mM)(Sigma)
5µl $MgCl_2$ (50mM)(Sigma)
32.3µl DDW
2µl RedTaq polymerase ((D4309 Sigma)
2µl of sample DNA.

Cycling conditions were as follows:

Initial denaturation 94°C for 3 min

94°C for 1 minute
55°C for 1 minute } 35 cycles
72°C for 1 minute

Final extension 72°C for 10 minutes

Amplified fragments were separated on a 2 % Agarose gel, Lacz and AHCre giving PCR fragments of 500bp and 1kb respectively.

Primers:

LacZ: P3 5'TACCACAGCGGATGGTTCGG'3

P4 5'GTGGTGGTTATGCCGATCGC'3

AHcre: CreA 5'TGACCGTACACCAAAATTTG'3

CreB 5'ATTGCCCCTGTTTCACTATC'3

2.2.6 Non-responder PCR

PCR reactions contained:

5µl 10x RedTaq Buffer (Sigma)
0.1µl each primer (10pmoles/µl) (OSWELL)
1µl dNTPs (40mM)(Sigma)
5µl $MgCl_2$ (50mM)(Sigma)
36.5µl DDW
0.3µl PIC Taq polymerase (CRUK)
2µl of sample DNA.

Cycling conditions were as follows:

Initial denaturation 94°C for 3 min

94°C for 1minute
56°C for 1 minute } 35 cycles
72°C for 1 minute

Final extension 72°C for 10 minutes

Amplified fragments were separated on a 4 % Agarose gel. Yes responder and No responder status giving bands of 196 and 180bp respectively.

Primers:

AHR6 5'AGGTTCCCTGGGACTTGTTT'3

AHR7 5'TCACCAAACCCTCCATCAGT'3

2.3 Dosing of DNA damaging agents

All reagents were administered at the same time of day, as mice display significant disturbance in apoptosis in accordance to their circadian rhythms.

Interperitinal (i.p) injections of 5FU were administered at 40 and 400mg/kg (David bull laboratories/faulding pharmaceuticals 10mg/ml stock). In experiments with 2 doses of 5 FU, the second injection was given after a 6hour interval (according to Pritchard *et al* 1998). Cisplatin was injected at a concentration of 10mg/kg (David Bull laboratories 10mg/ml stock). Temozolomide was used at 100mg/kg (dissolved in DMSO (10%v/v) and diluted in PBS, gift from Malcolm Stevens). NMNU / ENU used at 50mg/kg diluted in PBS with 0.05% glacial acetic acid.

Animals exposed to γ-irradiation were placed in a perspex holding container and irradiated depending on dose required, using a γ-IR source ^{137}Cs of 0.423 Gy/minute. Animals were dosed with 5Gy γ-IR for irradiation time courses of up to 48 hours. Clonogenic assays used 15Gy γ-irradiation.

Mice were dosed with i.p injection of 10μg Anti mouse Fas (0.5mg/0.5ml stock PharMingen diluted with PBS) and harvested 6 hours later.

2.4 Tissue preparations

2.4.1 Tissue Isolation

Mice were harvested at the appropriate time point and guts flushed with water. 3x1cm distal end sections were bound in surgical tape and quick fixed in formalin for a maximum of 14 hours at 4°C. Subsequent sections were taken for western and RNA analysis and the remaining gut section for BrdU analysis was left to fix overnight in methacarn (4 parts methanol, 2 parts chloroform, 1 part acetic acid), before rolling the gut for sectioning. Intestinal tumours were counted, graded by size and fixed in methacarn. All fixed samples were embedded in paraffin and sectioned to 5-6μm on polyL-lysine slides for histological examination or immunohistochemical analysis.

2.4.2 Lac Z analysis of recombination

The Rosa 26 lacz reporter system was recently developed by Sorriano *et al* 1999 to monitor Cre activity in tissue specific inducible mouse models and check that Cre has not been activated previously in development. The construct contains a Neo stop cassette flanked by lox p sites upstream of the lacZ reporter gene. Activation of AH Cre causes recombination of loxp sites in the targeted allele and in the Rosa26 construct. This leads to removal of the stop floxed cassette and subsequently expression of the Lac Z reporter gene (see figure 2.1). Gut tissue can then be stained blue with X gal substrate to report Cre activity and successful recombination. Floxing in intestinal stem cells allows repopulation of the crypt-villus axis over 5 days and upon X-gal staining, crypts stain blue.

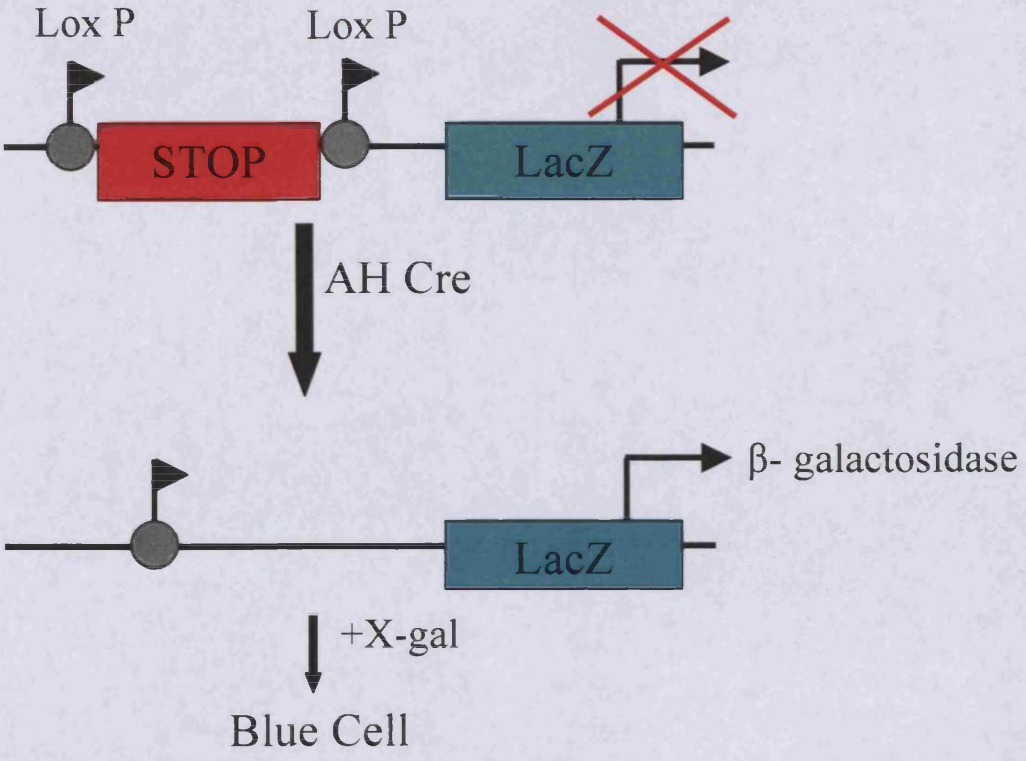

Figure 2.1- Diagram of Rosa26 LacZ reporter system. Cre mediated removal of LoxP-stop cassette from the Lacz Rosa26 transgene drives expression of β-galactosidase in recombined cells. Addition of X-gal substrate allows identification of blue cells.

β-Napthoflavone preparation

1g β-Napthoflavone was dissolved in 100mls corn oil (Sigma) by heating to 99.9 °C in a light resistant container in a water bath with stirring for approximately 1 hour. β-Napthoflavone was then aliquoted and stored at -20 °C and defrosted at 65 °C for 10-15 minutes prior to injection.

Mice were interperitoneally injected with high dose 80mg/kg β-Napthoflavone once daily for up to 4 days to induce recombination of the *Lkb1*^{fl} allele (for targeting see figure 5.1A). Lower level recombination regimes of 1 injection 80mg/kg β-Napthoflavone and 1 injection 0.8mg/kg β-Napthoflavone were used for Day 13 and 6 month time points respectively. A feeding regime was established to avoid recombination in the liver, with mice receiving 0.8mg/kg β-Napthoflavone from food

stuff coated in the solution and contained in a light proof vessel. Mice were allowed to feed *ad libitum* for 3 days before β-Napthoflavone coated food was replaced with standard feed. 7cm sections of tissue taken from the proximal 2nd fifth of the small intestine and flushed with cold water prior to opening and pinning out on a wholemount wax plate.

Whole mount wax plates

800g Ralwax was melted over a bunsen burner in a Pyrex beaker. Once melted 0.1 vols of paraffin oil was added to the beaker and liquid poured into large plastic culture plates (Gibco).

Once tissue was harvested, guts were guick fixed in cold 2% formaldyhyde (Sigma) /PBS/ 0.1%gluteraldehyde (Sigma) for 1 hour and then demucified for 30 minutes, before pipetting off debris under the microscope.

50mls Demucifying solution:

170mgs DTT (Dithiothreitol)
1 vol Glycerol: 5 mls
1 vol 0.1m Tris pH 8.2: 5ml
2 vol 100% ethanol: 10mls
6 vol sterile saline: 30ml

Wholemount gut sections were left to stain in X-gal solution overnight

500mls X-Gal solution:

2% X-Gal in DMF (Promega)
0.1g $MgCl_2$
0.48g K ferricyanide
0.64g K ferrocyanide
500mls PBS

Blue clones displaying recombined cells were visualised under the microscope and scored per field (according to Ireland *et al* 2004).

2.4.3 Preparation of quick fix gut parcels and Clonogenic microcolony assay

For clonogenic assays: 8-12 week old mice were given i.p Cisplatin (10mg/kg – 20mg/kg Ijiri and Potten 1983), Temozolomide (100mg/kg) and 5-FU (400mg/kg x 2). For γ-IR clonogenics, mice were exposed to γ-irradiation using a ^{137}Cs source delivering 0. 423 Gy per minute. Animals were dosed with 15Gy γ-IR and tissue harvested 72 hours later. 2cm sections of gut taken from the proximal top third of small intestine and rolled in 3M surgical tape to make gut parcels before being fixed in 10% formalin for 12-20 hours at 4°C. Sections taken across the circumference were counted for number of live crypts remaining after 72 hours (previously described Potten 1990, Hendry *et al* 1997).

2.4.4 Frozen sections

Liver samples or gut parcels (prepared as described for clonogenic assays) were fixed in 4% cold paraformaldehyde and sunk in 30% sucrose solution for 12 hours. Tissue was then embedded in OCT compound (Sakura) on frozen chucks sitting in dry ice and stored at -80 °C until ready to section. 5-10μm thick sections were cut using a cryostat, transferred onto polyL-lysine slides and allowed to dry at RT for 30 minutes before storage at -80 °C.

2.4.5 Scoring of Apoptosis

At each indicated time point following injection, a minimum of three animals were sacrificed and the small intestine immediately removed, flushed with water and fixed overnight in Methacarn (4 parts methanol, 2 parts chloroform, 1 part acetic acid). Slides were then stained with Haematoxylin and Eosin (H&E), dehydrated in graded ethanol, cleared in xylene and mounted using DPX (distrene dibutayl phthalate xylene) mounting medium (Sigma). Scoring for apoptosis was carried out on the Olympus BX41 microscope according to previously well described criteria including: chromatin condensation and pycnotic nuclei, apoptotic bodies and cell shrinkage producing a halo appearance around cell (Potten 1990, Hendry *et al* 1997, Toft *et al* 1999). A minimum of fifty half crypts were scored per animal.

2.5 Immunohistochemistry

All Paraffin wax embedded tissues (methacarn fixed or quick fixed sections) were dewaxed using 2x 10 mins xylene followed by rehydration down an ethanol gradient (2x 5mins 100%, 1x 5mins 95%, 1x 5 mins 75%), and rinsed in tap water prior to immunohistochemistry.

2.5.1 BrdU immunohistochemistry

Mice were injected with 0.25ml of BrdU (bromodeoxyuridine) (Amersham) 2 or 24 hours prior to harvesting. Mice were then sacrificed and gut tissue harvested and fixed in methacarn overnight. Paraffin wax embedded tissue was rehydrated as above. Slides were then treated with 1M HCl for 10 minutes at 60°C, allowed to cool for 20-30mins, then blocked with 1.5% H_2O_2 for a further 20 minutes. Samples were washed 3 times in 1% Tris buffered saline (Sigma)/ 0.1% Tween (Sigma)(TBST) and incubated for 20 minutes in 20% normal rabbit serum/TBST (DAKO). Sections were then incubated with Brdu antibody (Serotec rat anti-brdu MCA2060) at a dilution of 1 in 50 for 1 hour at room temperature (RT). Slides were then washed 3 x 5 minutes in TBST and further incubated with rabbit anti rat secondary antibody (1 in 200 in 20% rabbit serum) (Rabbit IgG ABC kit Vectastain) for 30 minutes at RT. Immediately after exposure to secondary antibody, ABC reagent (horse radish peroxidase HRP) was made up and left to incubate for 30 minutes at RT, prior to addition to slides after 3x TBST washes. Visualisation of positives was performed using DAB kit (2 drops DAB (diaminobenzidine) chromophor to 1ml DAB buffer)(DAKO) for 10-15 mins, and counterstained in haematoxylin followed by dehydration up the alcohol gradient and xylene washes prior to mounting in DPX (Sigma).

2.5.2 Ki-67 immunohistochemistry

Quick fixed sections were blocked in 0.5% hydrogen peroxide in methanol for 20 minutes before boiling in diluted citrate Buffer (Labvision) (1 in 10 DDW) at 99.9°C for 20minutes for antigen retrieval and then allowed to cool at RT for 30 minutes. Slides were then incubated in 20% normal rabbit serum/TBST (DAKO) for 30 minutes and primary antibody (vector anti-Ki67 1 in 20 dilution) was added for 1 hour at RT. Samples were washed 3x5 minutes in TBST and secondary antibody

(DAKO anti mouse biotinylated 1 in 200 dilution) for a further hour at RT. Sections were then visualised using the vectastain ABC and DAB kit as detailed above (section 2.5.1).

2.5.3 Caspase 3 immunohistochemistry for apoptosis

Rehydrated Methacarn fixed slides were immersed into preheated diluted citrate buffer (Labvision) (1 in 10 DDW) at 99.9°C for 20 minutes and cooled at RT for a further 30 minutes. Sections were then blocked for endogenous staining using 2.5% hydrogen peroxide in PBS (Gibco) with agitation for 45 seconds. This was followed by 3 washes in PBS and a subsequent 45 minute block in 10% normal goat serum/PBS (DAKO). Primary antibody was added (anti-caspase 3 rabbit polyclonal: AF835, R&D systems) at 1 in 750 dilution and slides incubated overnight at 4°C. Secondary antibody and HRP linked visualisation using the Rabbit ABC kit (Vectastain) and DAB (DAKO) was as previously described in Brdu protocol (section 2.5.1). Slides were then counterstained in haematoxylin, dehydrated, cleared and mounted in DPX.

2.5.4 P53 immunohistochemistry

Rehydrated quick fixed slides were immersed in preheated diluted EDTA buffer (labvision 1 in 10 DDW) at 99.9°C for 20 minutes for antigen retrieval and allowed to cool at RT for 30 minutes. Sections were then blocked for 20 minutes in hydrogen peroxide (H_2O_2, Mouse Envision$^+$ System DAKO kit), and washed 3 times in TBST. Primary antibody (p53 Ab mouse polyclonal Pab240 MS-104 Neomarkers) 1 in 50 in 20% rabbit serum/TBST, was incubated for 1 hour at RT. Samples were then washed 3x 5mins in TBST before peroxidase labelled polymer (HRP-conjugate, Envision+ system DAKO kit) was added for 1 Hour at RT. Positives were then visualised by DAB kit (DAKO), finally washed in TBST and counterstained in haematoxylin. Slides were then dehydrated, cleared and mounted in DPX.

2.5.5 P21 $^{CIP/WAF}$ immunohistochemistry

Rehydrated quick fixed slides were peroxidase blocked (citrate peroxidase 20L stock = 83.2g citric acid, 215.2g disodium hydrogen phosphate 2 hydrate, 20g sodium azide + 1.5% hydrogen peroxide) for 15 mins at RT. Sections were then boiled in preheated citrate Buffer (Labvision) (1 in 10 DDW) at 99.9°Cfor 20minutes for antigen retrieval and cooled rapidly by transferring slides to preheated solution in plastic coplin jars and running under cold water for 15 minutes. Sections were washed 2x5 mins PBS and blocked for 30 minutes with 5% goat serum/PBS (DAKO). Samples were washed twice more in PBS and incubated with P21 primary antibody (M-19 SC471 santa cruz rabbit polyclonal) at 1 in 500 dilution (5% goat serum/ PBS) for 1 hour at RT. Following 2x5 mins PBS washes, secondary antibody and HRP linked visualisation using Rabbit ABC kit (Vectastain) with DAB (DAKO) was carried out as previously described in BrdU protocol (see section 2.5.1).

2.5.6 CD44 immunohistochemistry

Rehydrated quick fixed slides were immersed into preheated diluted citrate Buffer (Labvision) (1 in 10 DDW) at 99.9°Cfor 20minutes for antigen retrieval and then allowed to cool at RT for 30 minutes. Sections were then blocked for endogenous staining using 1.5% hydrogen peroxide in PBS, and blocked for 20 minutes in 20% rabbit serum (DAKO)/PBS. Primary antibody (rat-anti mouse CD44, BD Pharmingen 550538) was added (1 in 50 dilution in 20% rabbit serum), and slides left to incubate for 1 hour at RT. Slides were then washed and processed with the mouse vectastain ABC kit in conjunction with DAB (DAKO) as described above (see section 2.5.1).

2.5.7 β-Catenin immunohistochemistry

Rehydrated quick fixed slides were blocked with citrate peroxidase (section 2.5.5) for 20 minutes, washed in 3x 5 minutes PBS and then boiled for 50min in Tris EDTA Buffer.

STOCK 1 L:

Tris 242g
EDTA 18.6
Working solution: 30ml stock to 1500ml DDW PH 8.0.

Sections were subsequently left to cool for an hour and washed 3x5 minutes PBS before incubation with blocking solution 1% BSA/PBS for 30 minutes. Primary antibody (Transduction laboratories anti β-catenin 1 in 50 dilution in 1%BSA/PBS) was added for 2 hours at RT. Slides were washed again 3x5 minutes in PBS and secondary HRP antibody (Envision Plus mouse DAKO kit) added for 1 hour. Finally sections were rinsed in PBS and positives visualised using DAB and counterstained in haematoxylin (section 2.5.1).

2.5.8 Math1 immunohistochemistry

Quick fixed sections were blocked with citrate peroxidase (1.5% hydrogen peroxide) (section 2.5.5) for 30 minutes. Slides were then boiled in citrate buffer (Labvision) (1 in 10 DDW) at 99.9°C for 20minutes and left to cool for 30 minutes. Samples were then washed 3x10 minutes in PBS and slides blocked in 10% BSA/PBS for 15 minutes. Slides were incubated with primary antibody overnight at 4°C (Math1 antibody 1:250 dilution kind gift from Dr Jane Johnson). Following a further 3x10 minute washes in PBS, the rabbit ABC vectastain and DAB kits were used to visualise as described previously (section 2.5.1).

2.5.9 Cell signalling antibodies: p-Akt, p-mTOR, p-GSK3,p-S6 ribosomal protein

All cell signalling antibodies followed the same protocol. Briefly, quick fixed sections were boiled for 10 minutes in 500mls Citrate buffer (Labvision) (1 in 10 DDW) in a microwave at full power and allowed to cool for 30 minutes. Slides were then washed in tap water and blocked in 1.5% hydrogen peroxide for 30 minutes, washed 3x5 minutes in TBST and incubated in 10% goat serum (DAKO)/PBS for 20 minutes. Primary antibodies were all used at a 1 in 50 dilution in 10% goat serum/TBST and left overnight at 4°C (p-GSK3 Ser 9 (9336), p-Akt ser 473 (9277), p-mTOR ser 2448 (2971), P-S6 ribosomal protein Ser 240/244 (2215) all cell signalling). Slides were then washed 3x10 minutes PBS and the rabbit ABC vectastain and DAB kits used to visualise as described previously (section 2.5.1).

2.6 Histological Tissue stains

Details of most procedures can be found at:
http://www.nottingham.ac.uk/pathology/protocols/.

2.6.1 Alcian Blue staining for intestinal Goblet cells

Alcian Blue staining is used to identify acidic mucin secreting cells. Mucin positive cells are bright blue in contrast to red nuclei of the gut epithelial cells. Paraffin embedded quick fixed sections were dewaxed and rehydrated as described above. Slides were then stained in Alcian blue (pH 2.5, 1g alcian blue + 3% acetic acid/100mls DDW) for 5 minutes, rinsed in tap water and counter stained in 0.1% nuclear fast red for a further 5 minutes. (0.1g nuclear fast red + 2.5g aluminium sulphate/100mls DDW). Sections were finally washed in water, dehydrated, cleared and mounted in DPX.

2.6.2 Periodic acid-schiffs (PAS) staining for acidic and neutral mucins

PAS staining is used to identify the different types of mucin secreting cells. Again acidic mucin cells stain blue, nuclei stain pale blue and glycogen/periodate reactive carbohydrates stain neutral mucins magenta. Paraffin embedded quick fixed sections were dewaxed and rehydrated as previously described. Slides were then stained with Alcian blue for 5 minutes, washed in DDW, then treated with 1% Periodic acid (Sigma) for a further 10 minutes. Slides were again rinsed in DDW and treated with Schiffs reagent (Sigma) for 20 minutes. Following treatment sections were washed in running tap water for 10 minutes and counterstained in haematoxylin prior to 'blueing' in 1% lithium carbonate (Sigma). Slides were subsequently dehydrated, cleared and mounted in DPX.

2.6.3 Grimelius stain for intestinal enteroendocrine cells

Grimelius staining relies on Agyrophil staining by silver nitrate to identify enteroendocrine cells within the gut structure. Positive staining cells are black on a yellow background. Following dewaxing and rehydration, slides were treated with silver solution for 3 hours at 65°C:

3mls 1% silver nitrate (Fisher)
87mls Ultrapure water
10mls acetate buffer (4.8mls 0.2M acetic acid, 45.2mls 0.2M sodium acetate, 50mls DDW pH 5.6)

Silver solution was drained from slides and sections then treated with freshly prepared reducing solution (2.5g sodium sulphite, 0.5g hydroquinone, 50mls DDW) at 45°C for approx 1 minute. Slides were then washed, dehydrated, cleared and mounted in DPX.

2.6.4 Oil red-O staining for intracellular fat

1g Oil red-O (Sigma) was dissolved in 100mls 60% Tri ethyl phosphate/DDW and boiled at 100°C for 5 minutes. Oil red solution was then hot filtered prior to use. Frozen sections were cut from liver samples and left to defrost at RT for 30 minutes. Slides were stained for 10 minutes with Oil red-O before rinsing in 60% Tri ethyl phosphate/DDW followed by water and counterstaining in haematoxylin for 45 seconds and mounting in DPX.

2.7 Western Blotting

2.7.1 Extracting Protein samples for western blots

Approximately 6 cm of gut tissue from the 3rd fifth of the intestine was flushed with water and snap frozen in liquid nitrogen. Liquid nitrogen was then poured onto half of the tissue in a mortar bowl and just before the liquid N2 had dispersed the frozen tissue was ground down with a pestle. This was repeated twice more until a fine power was obtained. 400µl of RIPA buffer was then added and tissue was sheared through increasingly fine needles. Protein concentration of samples was then determined using Bradfords reagent (Biorad) using 5-10µl protein to 1ml Bradford reagents before measuring absorbance at 595nm. Bovine serum albumin (BSA) standards (5-50µg/µl) were used to construct a standard curve. Samples were then equalised using RIPA buffer and stored at -80°C until ready for use.

RIPA buffer:	100mls
50mM Tris HCL pH 7.5	5mls of 1M solution
150mM NaCl	0.88g
1% Nonidet p40	1ml
0.5% sodium deoxycholate	0.5g
0.1% SDS	1ml of 10% solution
DDW	93ml

Stored at 4°C, 1 complete mini protease cocktail inhibitor tablet (Amersham) was added per 10mls before use.

2.7.2 Making and running western gels

P21 protein is a low molecular weight (21KDa) and therefore was run on a 15 % gel. Whole β-Catenin extract was also run on a 15% and ran at 82KDa. Gels were poured and overlaid ultrapure water until set (approx 20 mins). Water was removed and stacking gels were subsequently poured on top and combs inserted to set for 5 minutes.

Gels

	15%	10%
Ultrapure water	3.33ml	6.77mls
30% acrylamide (Biorad)	11.69mls	8.35mls
1M Tris HCL pH8.8	9.37mls	9.37mls
10% SDS	250µl	250µl
25% Ammonium persulphate	72µl	72µl
Temed	13.2µl	13.2µl

Stacking gel

Ultrapure water	3.33ml
30% acrylamide (biorad)	1.70mls
1M Tris HCL pH6.8	0.625mls
10% SDS	50µl
25% Ammonium persulphate	33µl
Temed	3.6µl

Samples were equalised with RIPA buffer and 30µg of each sample added to 5µl 4x loading buffer. Samples were then heated to 100°C for 2-3 minutes and immediately put on ice. After a brief spin, samples were loaded onto gels using the Biorad mini protean 3 gel rig and 10µl Gibco prestained molecular weight marker (Gibco). Gels were run at 150V for 1-2 hours at RT in 1x running buffer.

4x Loading buffer

200mM Tris HCL pH6.8
400mM Dithiothreitol (DTT)
8% SDS
0.4% Bromophenol Blue
40% glycerol

Running buffer (10x) 1L

30.2g Tris
188g Glycine
900ml DDW
10g SDS

Transfer Buffer 1L

800ml DDW
200ml Methanol
2.9g Tris
14.5g Glycine

PDVF membrane (Amersham) was soaked for 10 minutes in 100% methanol prior to transfer. Gels were transferred to membrane overnight at 20mV. Membranes were then blocked in TTM (TBST/ 10% marvel dried milk powder – dissolved with gentle heating) for 1 hour at RT. Primary antibody was then added (1 in 200 p21 M19 santa cruz, 1 in 1000 β-catenin BD PharMingen) in TTM for 1 hour at RT. Blots were then washed 3 times in TTM, and exposed to secondary antibody (p21 = anti-rabbit HRP IgG, β-catenin = anti-mouse HRP IgG, both Amersham) 1 in 2000 for 1 hour at RT. Blots were washed 3 x 10 minutes in TTM followed by 3 x 10 minutes TBST and subsequently developed for 5 minutes using ECL Plus western blotting detection system (Amersham) (3ml solution A and 75μl solution B). Blots were drained and exposed to photographic film for 1-5 minutes before developing.

2.8 RNA analysis

2.8.1 RNA Extraction

6-10 week old littermate mice were used for array analysis. 2x1cm sections from the 3rd fifth of the small intestine were taken into RNA Later (Sigma), taking care to avoid intestinal Peyer's patches. All RNA based procedures were performed using RNA free filter tip pipettes and tips and autoclaved solutions and plasticware. Intestinal tissue was homogenised for 30 seconds in 1ml cold TRIzol (Invitrogen) (cleaning homogeniser between each sample with 4M NaOH, followed by H_2O and 70% EtOH) and RNA extracted using standard Phenol-chloroform protocol:

Homogenised RNA in TRIzol was transferred into 2ml eppendorf tubes and left to stand at RT for 5 mins. 0.2ml chloroform was then added to each sample, mixed well and left at RT for a further 5 mins.

Samples were then centrifuged at full speed (14,000rpm) for 15 minutes at 4 °C, and supernatant transferred into fresh 2ml tubes. 0.5ml isopropanol was added and mixed before standing at RT for 10 mins. Following a 15 minute spin at max speed, supernatant was discarded and pellets washed twice in 75% ethanol with 5 minute spins at 7,500g (10,000rpm). Pellets were then left to air dry for 10-15 minutes and then resuspended in 100μl DEPC H_2O. Finally samples were heated to 65°C for 10 minutes and stored on ice.

2.8.2 RNeasy cleaning of RNA (Qiagen kit)

Briefly, 100µg of total RNA was used per column with 350µl RLT buffer and 250µl 100% ethanol added to the column. Samples were then centrifuged for 15 seconds at 10,000rpm and flow discarded. 500µl RPE buffer was then added and column spun at 10,000rpm for 15 seconds. Once more the flow was discarded and a further 500µl RPE buffer added. The column was then spun for 2 minutes at 10,000rpm and then once flow removed spun empty for 1 minute to remove any final solution. RNA was eluted by addition of 2x 40µl aliquots RNase free H_2O and a final spin for 1 minute at 10,000rpm before quantifying by spectrophotometer at 260/280nm.

2.8.3 RNA sample quality and RNA gels

Following RNA isolation, quality of RNA was investigated by spectrophotometer measurement and running RNA on a denaturing gel. Samples were diluted 2µl in 98µl DDW and optical density (OD) measured at 260 and 280nm. For this dilution Absorbance at 260 x 2 = Conc µg/µl

Denaturing formaldehyde gel

150ml DEPC H_20 + 2.5g Agarose was boiled in microwave for 2 minutes. Agarose was allowed to cool and 6µl ethidium bromide, 17.5mls 10x MOPS, 7mls Formaldehyde was added before casting and setting in a fume cupboard.

10 x MOPS

41.8g MOPS (3N-morpholino-propane sulfonic acid)
0.8l DEPC H_2O
16.6ml NaOAc
20mls 0.5M EDTA

RNA loading buffer

100µl saturated bromophenol blue
80µl 0.5M EDTA pH8
720µl formaldehyde (38% stock)
2mls glycerol
3.1mls of formamide
4mls of 10xMOPS

5µl loading buffer was added to RNA samples prior to heating to 65 °C for 10-15mins and cooling on ice. Samples were run with RNA marker ladder (invitrogen) on gels in 1x MOPS at 100V for an hour, and bands visualised under UV.

2.9 Preparation of Biotinylated target cRNA for Affymetix arrays

RNA samples were then used to make Biotinylated target cRNA according to http://www.paterson.man.ac.uk/facilities/mbcf/protocols.jsp and the following protocol:

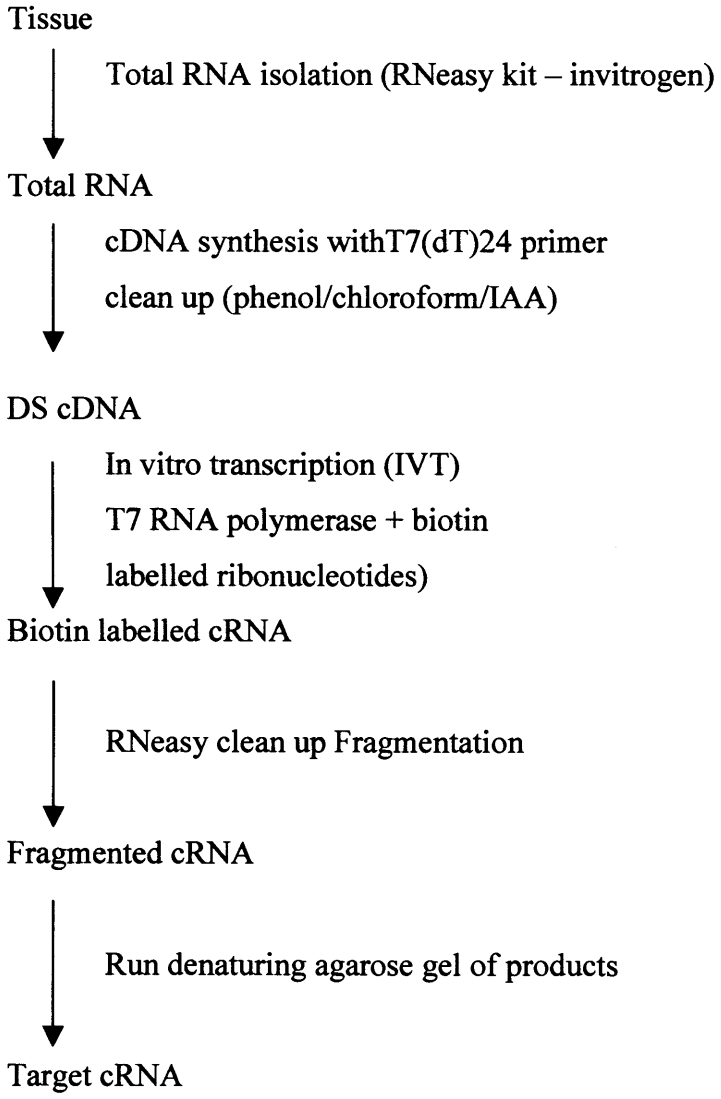

First strand cDNA synthesis

1µl of T7$(dT)_{24}$ primer (100pmol/µl) was added to **10µg** of purified RNA and made up to 11µl with depc H_2O.

T7(dT)24 primer:
5'GGCCAGTGAATTGTAATACGACTCACTATAGGGAGGCGG-$(dT)_{24}$-3'

Samples were mixed by pipetting and incubated at 65-70 °C for 10 minutes and then placed on ice. 7µl of master mix was added to each reaction and following 2 minutes at 42 °C, 2µl Superscript II reverse transcriptase (Invitrogen 200U/µl) was added. Samples were incubated for a further hour at 42 °C and stored on ice.

Master mix (Invitrogen double stranded cDNA synthesis kit)

4µl 5x first strand buffer
2µl DTT (Dithiothreitol)
1µl dNTPs (10mM)

Second strand synthesis

Reaction mixtures from the first strand synthesis step were transferred into new 200µl reaction tubes and 130µl master mix added and mixed.

Master mix (Invitrogen double stranded cDNA synthesis kit)

91µl depc H_2O.
30µl 5x second strand buffer
3µl dNTPs (10mM)
1µl *E.Coli* DNA Ligase (10U/µl)
4µl *E.Coli* DNA polymerase I (10U/µl)
1 µl *E.Coli* RNAse H (2U/µl)

Samples were then incubated at 16 °C for 2 hours before addition of 2µl T4 DNA polymerase and a further 5 minutes at 16 °C. Reactions were stopped by the addition of 10µl 0.5M EDTA, and samples stored on ice.

Clean up of Double stranded cDNA

Phase–lock tubes (Helena biosciences) were prespun at maximum speed for 30 seconds. 160µl of buffer saturated phenol/chloroform/IAA(indoleacetic acid) was added to reaction samples from second strand synthesis, and solution added to phase-lock tube. Tubes were then centrifuged at maximum speed (14,000rpm) for 2 minutes and the upper aqueous layer transferred to a new tube. 0.5 vols ammonium acetate, 4µl Glycogen (5mg/ml) and 2.5 vols 100% ethanol were added and samples spun at RT for 20 minutes at maximum speed. The resulting supernatant was discarded and the pellet washed twice with 160µl Cold 80% ethanol (centrifuged for 5 minutes each time). The pellet was air-dryed for 10-15 minutes and resuspended in 12µl depc H_2O. Samples were stored at -80 °C.

***In vitro* transcription - synthesis of cRNA**

Reactions were carried out using the Enzo bioarray high yield transcription labelling kit.

Master mix

10µl depc H_2O
4µl 10x HY reaction buffer
4µl biotin labelled ribonucleotides
4µl DTT (Dithiothreitol)
4µl RNase inhibitor mix
1µl T7 RNA polymerase

28µl master mix was added to each 12µl double stranded cDNA sample. This reaction was incubated at 37 °C for 5 hours, mixing gently ever hour. Samples were then placed on ice and cleaned using the RNeasy kit (Qiagen) as detailed above in section 2.8.2. Quantification was then performed by spectrophotometry at 260/280nm.

cRNA fragmentation

25µg cRNA was required for the fragmentation process, in addition to 10µl 5x fragmentation buffer (200mM Tris acetate pH8.1, 500mMKOAc, 150mMMgOAc) and made up to 50µl with depc H_2O. Samples were then heated to 94 °C for exactly 35 minutes. A 3µl aliquot was run on a gel to check fragmentation, before samples were

sent to Affymetrix CRUK facility at the Paterson institute to be run using the MOE430 2.0, 46,000 gene set chip.

2.10 RT-PCR and qPCR analysis

2.10.1 DNase treatment

Rneasy cleaned samples were Dnase treated using 10µl RQ1 enzyme (RQ1 kit Promega) per 10µg RNA. Additionally 3µl RQ1 enz buffer was added to each sample and samples made up to 30µl with depc treated H_2O. Following incubation at 37 °C for 30 mins, 3µl STOP solution was added and samples heated to 65 °C for 10 mins before putting sample on ice

2.10.2 RT-PCR

RT-PCR was performed using the Superscript II kit (Invitrogen) on all samples plus and minus Superscript II enzyme (Invitrogen) under the following reaction conditions: 6µl DNase treated RNA + 3µl depc H_2O was set up in duplicate and heated to 70 °C for 10 mins, then allowed to cool to 42 °C before 10µl of master mix was added.

Master Mix (from invitrogen kit)

2 µl N_6 primers (100ng/ µl)
4 µl First strand buffer
2 µl DTT (Dithiothreitol)
0.4 µl 40mM dntps
1.6 µl depc treated H_2O

Samples were then maintained at 42 °C for 1-2 mins before addition of Superscript II enzyme to positive samples only. Samples remained at 42 °C for a further 50 mins and enzyme inactivated at 70 °C for 15mins before storing samples at -20 °C.

PCR for cDNA was performed using HPRT control:

1 µl cDNA
5 µl Buffer (10x sigma)
5 µl MgCl (25mM)
1 µl dNTPs (25mM)
1 µl each primer (10pmoles/µl) (OSWEL)
2 µl Red Taq (Sigma)
33.5 µl H_20

Cycling conditions were as follows:

Initial denaturation 94°C for 2 mins 30 secs

94°C for 1 minute
52°C for 1 minute } 25 cycles
72°C for 1 minute

Final extension 72°C for 10 minutes

Products were run on a 2% Agarose gel and a 350bp product was detected in + Superscript II samples only.

2.10.3 qRT-PCR

cDNA was amplified by qPCR to validate array targets using MJ research Chromo4 PCR cycler to visualise Sybr green incorporation.

Reaction mixtures contained:

1 µl 10pM of each primer
2µl cDNA
18.5 µl Sybr Green (Biorad)
1 µl 10mM dntps

Samples were made up to 20µl with dH_2O. β-actin primers were used as a control housekeeping gene in both WT and HOM Lkb1 samples, and C_T values compared to those of other genes of interest:

β-actin 5'CTTCCTCCCTGGAGAAGAGC'3
5' AAGGAAGGCTGGAAAAGAGC'3

Lkb1 5' CTCCGAGGGATGTTGGATA'3
5'CTTGGTGGGATAGGTACGA'3

Math1 5'ACATCTCCCAGATCCCACAG'3
5'GGGCATTTGGTTGTCTCAGT'3

Claudin 2
5'TATCTCTGTGGTGGGCATGA'3
5'GCCACCAAGGATGAAAAAGA'3

BMP1 5'CGTCCTGCTCCTTTCTCTTG'3
5'GACCAGCATGGGAACCTCTA'3

TNF 5'CCAGTGTGGGAAGCTGTCTT'3

5'AAGCAAAAGAGGAGGCAACA'3

Adipsin

5'CCAGCGATGGTATGATGTGC'3

5'AACGAGGCATTCTGGGATAG'3

PCR conditions were as follows:

Initial denaturation 94°C for 3 minutes

94°C for 1 minute
60°C for 1 minute } 35 cycles
72°C for 1 minute

Final extension 72°C for 10 minutes

Fold change was determined as previously described using $2^{-\Delta\Delta C}{}_T$ (Livak *et al* 2001). All primers were designed using primer 3^{TM} software, with specified optimal melting temperature to avoid primer dimers, >50%GC content at 100 Bp and spanning intron/exon junctions.

Statistical analysis

Where possible, experiments were performed using a minimum of 3 replicates. Statistical analysis of data was carried out using the Mann Whitney U test (unless otherwise stated) to assess the significance of the differences between genotypes given the non-parametric nature of the data and the small data sets. The resultant p-value from this test indicates the probability that the null hypothesis is true – i.e. the difference observed occurred by chance and that there is no difference between the sample groups. A low p-value of <0.05 was taken as significant to reject the null hypothesis.

All other chemicals standard laboratory stock: Sigma, Novagen, Biorad, Promega, Fisher and BDH.

Chapter 3. Mbd4 deficiency reduces the apoptotic response to DNA-damaging agents in the murine small intestine.

3.1.1 Introduction to MBD4

The human DNA repair protein MBD4 (also known as MED1 (methyl CpG binding endonuclease 1) is a 62-kDa thymine glycosylase involved in base excision repair (BER). Originally identified by its N-terminal MBD, *MBD4* shows significant homology to the bacterial DNA repair glycosylase enzyme *MutY* and endonuclease III (*Escherichia coli)* (Ballestar and Wolffe 2001). Recently work has shown that MBD4 can recognise and remove G:T or G:U mismatches produced by $5^{Me}C$ deamination at methylated CpG sites *in vitro* and shows affinity for both methylated and unmethylated CpG sites (Hendrich *et al* 1999). The MBD of the protein and methylation status does not appear to influence thymine glycosylase activity (Petronzelli *et al* 2000b, Drummond and Bellacosa 2001) and therefore serves to reduce the mutability at methyl CpG sites by directing MBD4 to methyl CpG rich regions of the genome (Ballestar and Wolffe 2001).

3.1.2 MBD4 and cancer

Mutability of CpG sites causes genomic instability and progression to cancer. It is therefore proposed that *MBD4* acts as a caretaker gene as mutations in *MBD4* have been linked to MMR deficient CRCs, although this loss is rarely biallelic (Riccio *et al* 1999, Bader *et al* 2000). Defects in MBD4 activity may contribute to aberrant homeostasis response, accumulation of DNA damage and consequently predispose to tumourigenesis (Petronzelli *et al* 2000b). Recent work by Millar *et al* investigated mutation frequencies and spectra of *Mbd4* loss *in vivo* by using the excisable lacI mutational target gene, also known as the big blue mouse transgene (Stiegler and Stillwell 1993). Results showed that $Mbd4^{-/-}$ mice showed significantly increased C-T transitions at CpG sites and therefore concluded that Mbd4 does indeed function to reduce mutability and maintain genomic integrity at 5Me CpG sites *in vivo* (Millar *et al* 2002). Furthermore when $Mbd4^{-/-}$ deficient mice were crossed to the Apc^{MIN} background, accelerated tumourigenesis was also observed (Millar *et al* 2002).

3.1.3 MBD4 and MMR

MMR proteins have an additional role to the repair mechanism by signalling the apoptotic response to DNA damage *in vivo* via futile cycling (continued unsuccessful repair of the mismatch resulting in apoptosis) or via direct signalling (Fishel *et al* 1999, Buermeyer *et al* 1999). Indeed a decreased apoptotic response is seen *in vivo* in MMR deficient mice following several DNA damaging treatments (Toft *et al* 1999). It is thought that the selection for cells to escape from entering apoptosis is the most important feature in the evolution of MSI cancers (Wheeler *et al* 2000) and MMR deficient mammalian cells have been shown to be resistant to the DNA damage induced by Cisplatin, Temozolomide and gamma radiation. The persistence of such damage in MMR deficient cells leads to increased mutagenesis (Buermeyer *et al* 1999).

Using the yeast two hybrid screen MBD4 was found to interact with the mismatch repair protein MLH1. Co-immunoprecipitation studies in human cells confirmed that the two proteins interact *in vivo*, suggesting MBD4 may several roles in MMR, via the MLH1 interactions (Petronzelli *et al* 2000a, Drummond and Bellacosa 2001). Additionally MBD4 was also found capable of recognising and removing 5-Fluro-2-deoxyuracil (5FU) in G:5FU mismatches (Petronzelli *et al* 2000a) and O-6meG:T base mismatches from alkylating agents (Cortellino *et al* 2003), outlining a role for MBD4 in mediating cytotoxic induced apoptosis.

3.1.4 Intestinal mechanisms of drug induced apoptosis

In the intestine, p53 mediates the immediate apoptotic response to various forms of DNA damage, including ionising radiation, alkylation agents and 5FU (Clarke *et al* 1994, Pritchard *et al* 1998, Toft *et al* 1999). In the absence of p53, there is almost no detectable apoptotic response to these agents immediately following exposure, which was assumed to reflect a complete abrogation of the response. However, closer analysis of the kinetics revealed this not to be the case, with a delayed p53-independent response identified from clonogenic survival studies, which appears specific to the intestine (Clarke *et al* 1994, Pritchard *et al* 1998). There is growing evidence that this delayed response may be mediated by the p53 family members' p63

and p73, overexpression of either of which induces apoptosis and up-regulates various p53 targets. Indeed, p73alpha was recently proposed as a candidate to mediate p53-independent death in colonocytes following exposure to cisplatin (Oniscu *et al* 2004).

3.2 AIM

MBD4 deficiency increases mutability, accelerates tumourigenesis and is often mutated in MMR deficient cancers (Millar *et al* 2002). Previous studies of drug induced apoptosis in p53 and MMR doubly deficient mice found further reduction in the apoptotic response and increased intestinal clonogenic survival albeit in a lesion dependent fashion (Toft *et al* 1999, Sansom and Clarke 2002). *Mlh1*$^{-/-}$ mice have been found to be resistant to 5FU induced apoptosis *in vivo* (Meyers *et al* 2001) and MMR deficiency leads to resistance in the chemotherapeutic treatment of colorectal cancers (Petronzelli *et al* 2000a, Wheeler *et al* 2000). Therefore given the Mbd4-Mlh1 interaction and the ability of MBD4 to recognise double 5FU:G DNA mismatches and double stranded breaks in a similar manner to p53 (Petronzelli *et al* 2000a), this poses the question could Mbd4 status effect 5FU treatment of CRCs? I therefore decided to investigate the *in vivo* role of MBD4 in mediating the apoptotic response to a variety of cytotoxic agents in *Mbd4*$^{-/-}$ mice.

Initial experiments have shown that Mbd4 signals death in response to a wide variety of DNA damaging agents such as Cisplatin, γ-ioning radiation (γ-IR), and the alkylating agent Temozolomide at 6 hrs. Furthermore, clonogenic survival using the micro colony assay (Potten 1990, Hendry *et al* 1997) revealed Mbd4 deficient mice show increased long term crypt survival in response to Cisplatin but not to gamma radiation (work by Owen Sansom Appendix 1 - Sansom *et al* 2003c). This lesion specific Mbd4 dependency remains to be further characterised and this chapter aims to clarify the role of Mbd4 in mediating the apoptotic response to DNA damage (in particular to 5FU induced damage), with an overall aim to predict if Mbd4 status would be an important predictor of chemotherapeutic response.

3. 3 Results

3.3.1 Investigating Mbd4 loss and cytotoxic treatment

Preliminary data indicated a decrease in the apoptotic response in *Mbd4*$^{-/-}$ mice at 6 hours with Temozolomide, Cisplatin and 5FU treatment (see appendix, Sansom *et al* 2003c). To further characterise the kinetics of these responses and the role of Mbd4 in mediating apoptosis to these agents, I decided to investigate an extended time course following DNA damage. All experiments were performed using a minimum of 3 animals of 6-12 weeks of age for each genotype, and 50 half crypts were scored for apoptosis according to previous criteria ((Potten 1990, Hendry *et al* 1997, Toft *et al* 1999).

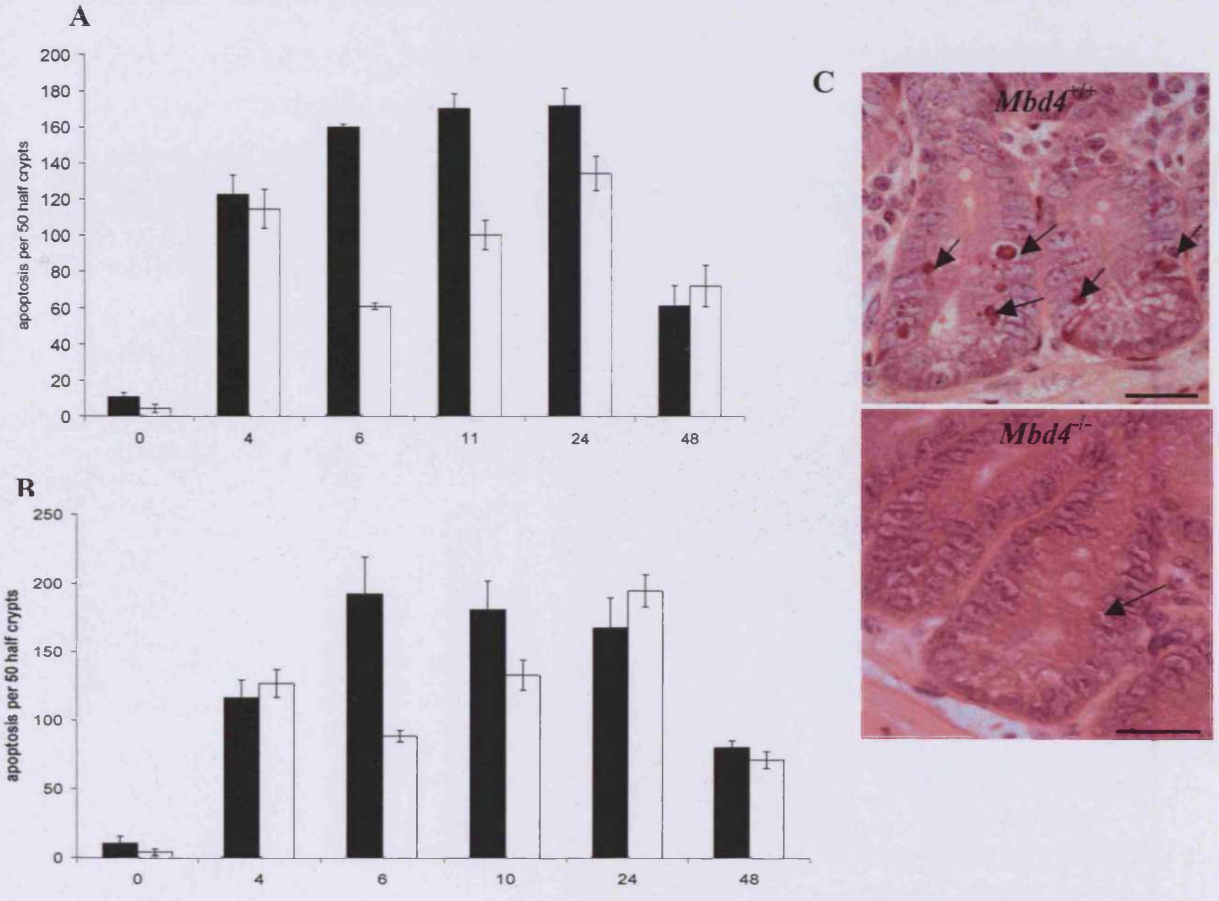

Figure 3.1 – **A,** Apoptosis scored per 50 half crypts over a 48 h period following 100 mg/kg temozolomide. Black bars, *Mbd4*$^{+/+}$ mice; open bars, *Mbd4*$^{-/-}$ mice **B,** Apoptosis scored per 50 half crypts over a 48 h period following 10 mg/kg cisplatin treatment. Black bars, *Mbd4*$^{+/+}$ mice; open bars, *Mbd4*$^{-/-}$ mice (N=3 for every time point and error bars = SEM). **C,** H&E histology of *Mbd4*$^{+/+}$and *Mbd4*$^{-/-}$ mice 6 hours after 100mg/kg Temozolomide (Arrows denote apoptotic bodies, scale bars = 50μm).

Figure 3.1 outlines the course of the apoptotic response to Temozolomide (3.1A) and Cisplatin (3.1B). *Mbd4*$^{-/-}$ mice show reduced apoptosis when compared to *Mbd4*$^{+/+}$ controls and a dependency for Mbd4 in mediating apoptosis in response to these agents is found at 6 and 11 hours when mice were dosed with Temozolomide ($p=<0.01$ MWU test) and 6 and10 hours Cisplatin treatment ($p=<0.04$ MWU test). Figure 3.1C illustrates the suppressed apoptotic response in *Mbd4*$^{-/-}$ mice, with clearly less apoptotic bodies present.

3.3.2 Mbd4 loss and response to 5FU induced damage

P53 activity is essential for the intestinal epithelial response to 5FU, and previous work in p53 null mice showed significant reduction in apoptosis, increases in cell proliferation and clonogenic survival when exposed to 2 injections of 400mg/kg 5FU 6 hours apart (Pritchard *et al* 1998). To further investigate reports that MBD4 can bind and signal G:5FU mismatches (Petronzelli *et al* 2000a), I followed an extended timecourse of 5FU treatment to observe if indeed Mbd4 plays a role in signalling 5FU damage *in vivo*.

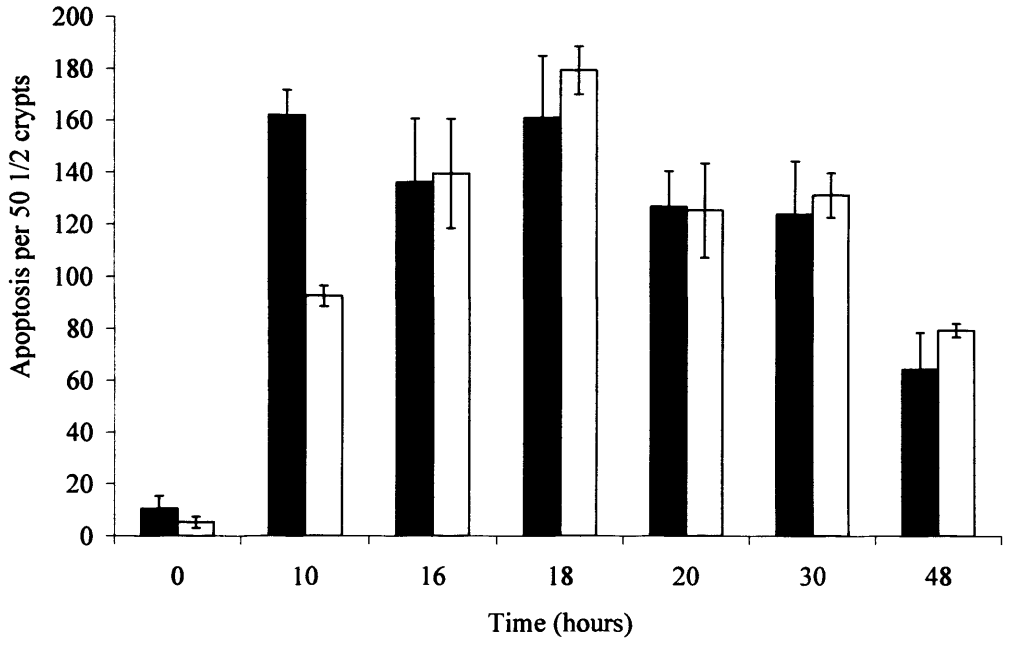

Figure 3.2 Apoptosis per 50 ½ crypts following 2x400mg/kg 5-FU treatment. Black bars, wild type mice; open bars, *Mbd4*$^{-/-}$ mice. At least 3 mice were used for every time point and error bars represent SEM. MBD4 deficiency caused a significant reduction in apoptosis at 10 hours following 5-FU treatment ($p=0.001$, $N=8$ MWU).

A maximal apoptotic response to 5FU is seen at the early time point of 10 hours in *Mbd4*$^{+/+}$ mice. This response is severely perturbed in *Mbd4*$^{-/-}$ deficient mice at the same time point (figure 3.2, p=0.001, N=8 MWU), with a maximal apoptotic response delayed until 18 hours post treatment. No further differences between the 2 genotypes were observed thereafter with the death response paralleling wildtypes, with low levels of apoptosis at 48 hours as the crypt deteriorates (figure 3.3).

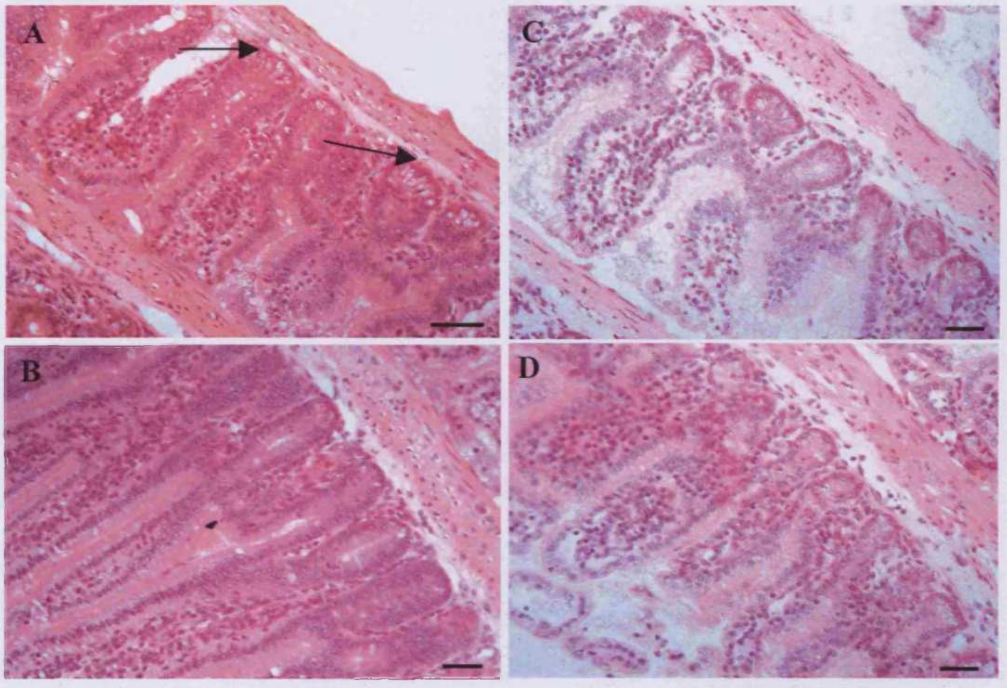

Figure 3.3– Haematoxylin and Eosin (H&E) staining of murine intestinal crypts following 2x400mg/kg 5FU treatment Significant loss of crypt integrity can be seen in *Mbd4*$^{+/+}$ controls compared to the *Mbd4*$^{-/-}$ mice. **A,** *Mbd4*$^{+/+}$ Crypt integrity begins to deteriorate at the base of crypts at 10 hours post treatment (see arrows) **B,** *Mbd4*$^{-/-}$ shows significantly less crypt disruption than controls at 10 hours **C,** *Mbd4*$^{+/+}$ at 48 hours post treatment, cell number has declined and crypts are destroyed **D,** *Mbd4*$^{-/-}$ at 48 hours, some viable crypts remain within the structure (see arrows) (scale bars = 50μm).

As 5FU induced apoptosis shows complex kinetics in the intestine and targets transit cells at positions 6-10 (Pritchard *et al* 1998), accompanying aberrant changes in crypt proliferation may contribute to crypt survival and ultimately tumourigenesis. I therefore looked at S phase BrdU incorporation as a measure of cell proliferation. Mice were injected with Brdu 2 hours prior to tissue harvesting from the 5FU time course. (Brdu injections are not thought to affect the apoptotic response). Percentage labelling was then determined relative to the number of cells in the crypt.

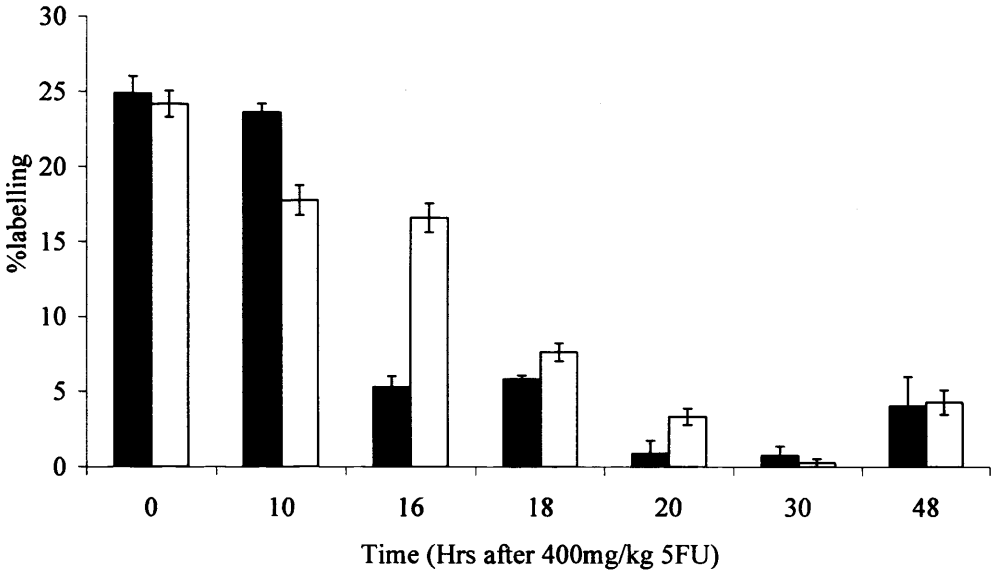

Figure 3.4 – S phase BrdU incorporation per 50 ½ crypts following 2 x 400mg/kg 5-FU treatment. Black bars, *Mbd4*$^{-/-}$ mice; open bars, *Mbd4*$^{+/+}$ mice. (N=3 and error bars = SEM). MBD4 deficiency caused a significant increase in BrdU labelling at 16, 18 and 20 hours following 5-FU treatment ($p=<0.05$ MWU).

Figure 3.4 indicates 5FU administration causes a decrease in proliferation when compared to untreated crypts. This decrease in proliferation was not as marked in *Mbd4*$^{-/-}$ mice. Indeed increased proliferation in Mbd4 nulls compared to controls was seen at 16,18 and 20 hrs following 5FU injections (figure 3.4, N=3, $p=<0.05$ MWU). After these time points however, proliferation temporarily drops in both genotypes before a proliferative burst or recovery is observed at 48 hours.

As the early time points show relatively high turnover in the crypts in response to 5FU, I therefore counted cell number to check that any proliferative increase was not as a consequence of increased crypt size over the time course.

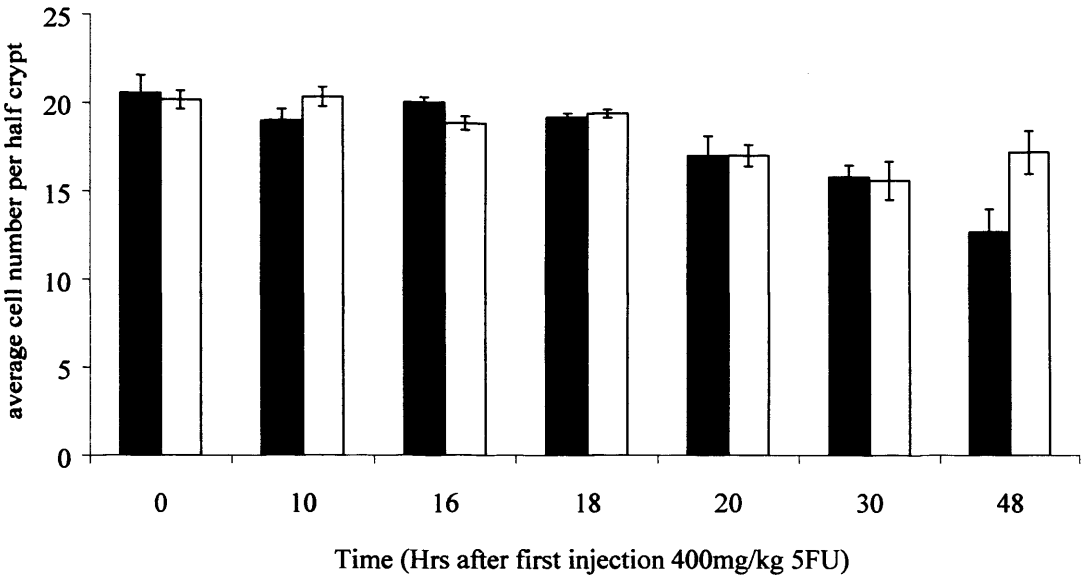

Figure 3.5 Average epithelial cell number per half crypt. Black bars, *Mbd4*$^{-/-}$ mice; open bars, *Mbd4*$^{+/+}$ mice. (N=3 for every time point and error bars = SEM). Mbd4 deficiency caused a significant increase in epithelial cell number 48 hours following 5-FU treatment ($p<0.05$ MWU).

Figure 3.5 shows that cell number remains fairly constant at 16, 18, and 20 hours in both groups, at an average of 22 cells ($p=>0.05$ MWU). However, by 48 hours *Mbd4*$^{-/-}$ mice have a significantly higher cell number than *Mbd4*$^{+/+}$ control mice ($p=<0.05$,n=3 MWU). No difference in proliferation is seen at this time point, suggesting the effect of increased cell number at this time point is a result of cumulative survival from decreased apoptosis and earlier increased proliferation (detailed in figures 3.2 and 3.4). This again reflects the higher level of destruction observed in *Mbd4*$^{+/+}$ control mice at 48 hours when compared to Mbd4 nulls (histology figure 3.3).

3.3.3 5FU and Thymidine/Uridine dosing

5FU action relies on blockage of RNA maturation and inducing DNA double strand breaks by inhibition of thymidylate synthase. (Tanaka *et al* 2000, section 1.12.1). Pritchard *et al* 1998 previously reported no change in 5FU induced apoptosis in p53 null mice between low doses of 40mg/kg and 400mg/kg 5FU, and indeed preliminary work using a single 400mg/kg dose of 5FU failed to show a significant Mbd4 dependency for apoptosis following 5FU treatment. Addition of Uridine during 5FU

dosing was found to relieve apoptosis levels induced by 5FU by quenching the uracil pool, however addition of Thymidine could not relieve thymidylate synthase inhibition, therefore authors concluded 5FU action in the gut is through RNA synthesis blockage (Pritchard *et al* 1997).

Following the observation that Mbd4 mediates 5FU induced apoptosis (Petronzelli *et al* 2000a), I decided to look at the Thymidine/ Uridine quenching of 5FU damage on the Mbd4 null background. Both compounds were injected in excess along with 5FU according to the protocol described in Pritchard *et al* 1997.

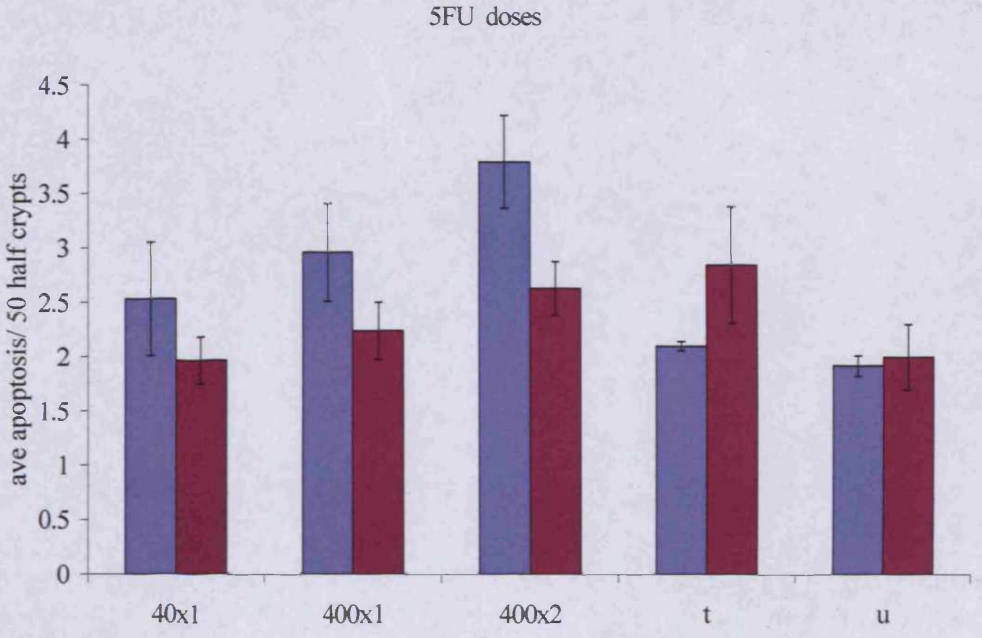

Figure 3.6– Apoptosis scoring following treatment with 5FU at 40mg/kg, 400mg/kg, 400x2mg/kg, 400x2mg/kg 5FU+ 400mg/kg thymidine (t) and 400x2mg/kg 5Fu + 3500mg/kg uridine (u). Mice were harvested at 10 hours after treatment. Purple bars = *Mbd4*$^{+/+}$, burgundy bars = Mbd4$^{-/-}$. N=3 all time points, error bars = SEM).

Significant suppression of apoptosis in Mbd4 null mice was seen at 2x400mg/kg dose (p=0.001, n=8 MWU), as previously seen in figure 3.2. The lower 40mg/kg and 400 mg/kg doses gave no difference between genotypes at 10 hours (p=>0.05 MWU, N=3), similarly to results in the p53 null mice by Pritchard *et al* 1998. Initial results suggest thymidine addition significantly suppressed *Mbd4*$^{+/+}$ control apoptosis response (figure 3.6, p=<0.01 MWU,n=3), although not the response of the Mbd4 nulls (p=>0.05 MWU). This failure to quench DNA based damage with thymidine

confirms the suggestion that Mbd4 mediates 5FU induced DNA damage. However, Uridine addition did decrease the apoptotic response in both *Mbd4*$^{+/+}$ (p = 0.04MWU) and Mbd4 nulls (p=<0.05MWU) compared to 2x400mg/kg 5FU alone, suggesting that 5FU RNA based damage in the cytoplasm is independent of Mbd4 status.

3.3.4 Clonogenic survival

It is not possible to directly address clonogenic survival using intestinal cultures, but an indication of survival can be gained from the microcolony assay, which essentially scores the ability of an entire crypt structure to survive insult (Potten 1990, Hendry *et al* 1997). Previous work on this project revealed that *Mbd4*$^{-/-}$ mice fail to show increased survival when treated with 15Gy γ-IR, however increased survival was observed when *Mbd4*$^{-/-}$ mice were treated with 15mg/kg cisplatin (see appendix Sansom *et al* 2003c). Following the decreased apoptotic response to 5FU in *Mbd4*$^{-/-}$ mice, I investigated the effects of Mbd4 loss on long-term survival following dosing with 2 x 400mg/kg 5FU as previously reported (Pritchard *et al* 1998).

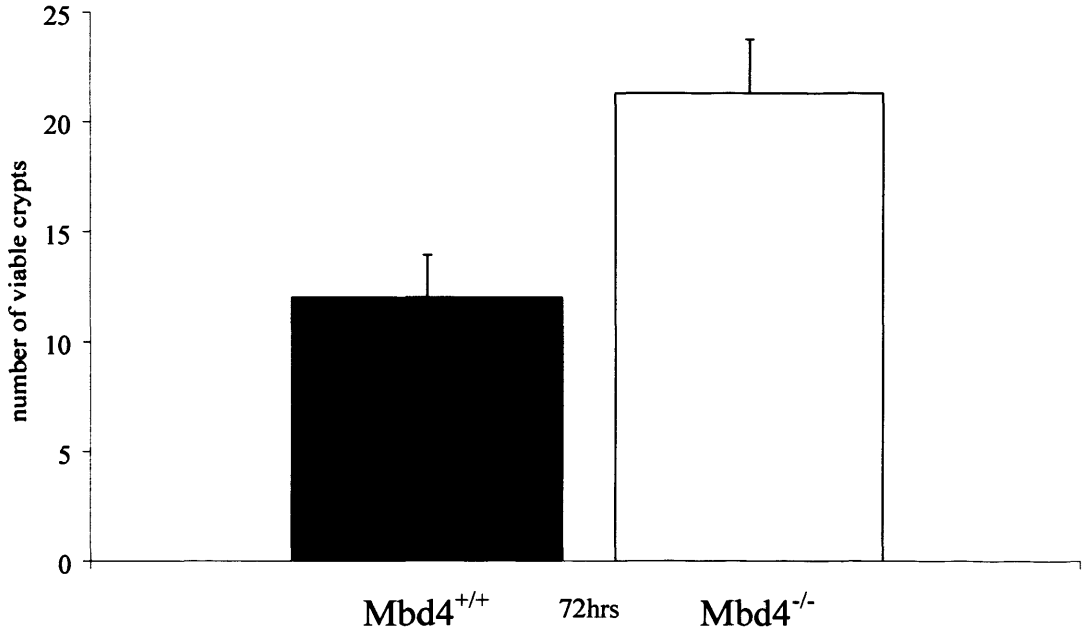

Fig 3.7 – Clonogenic survival of intestinal crypts 72 hours crypts following 2 x 400mg/kg 5-FU treatment. Black bars, *Mbd4*$^{+/+}$ mice; open bars, *Mbd4*$^{-/-}$ mice. MBD4 deficiency caused a significant increase crypt survival following 5-FU treatment (error bars= SEM, p=0.02 MWU, N=6).

A significant increase in clonogenic survival was seen in Mbd4 deficient mice 72hours following 5FU dosing (figure 3.7 p=0.02, MWU, N=6), indicating that *Mbd4*$^{-/-}$ crypts tolerate 5 FU damage more than *Mbd4*$^{+/+}$ controls and hence persist for longer time periods. Work done in conjunction with this study showed that Mbd4 null mice also showed increased clonogenic survival following cisplatin treatment (see appendix Sansom *et al* 2003c).

3.3.5 Double null investigations

As Mbd4 shows similar lesion dependant apoptotic and proliferative changes to those described in MMR deficient mice (Toft *et al* 1999, Sansom and Clarke 2002) and also interacts with Mlh1, this gives rise to the question - Does Mbd4 mediate apoptosis via MMR dependent death pathways?

I therefore decided to investigate the apoptotic deficiency in *Mbd4*$^{-/-}$ mice in the context of MMR deficiency by creating the doubly mutant *Mbd4*$^{-/-}$ *Mlh1*$^{-/-}$mouse.

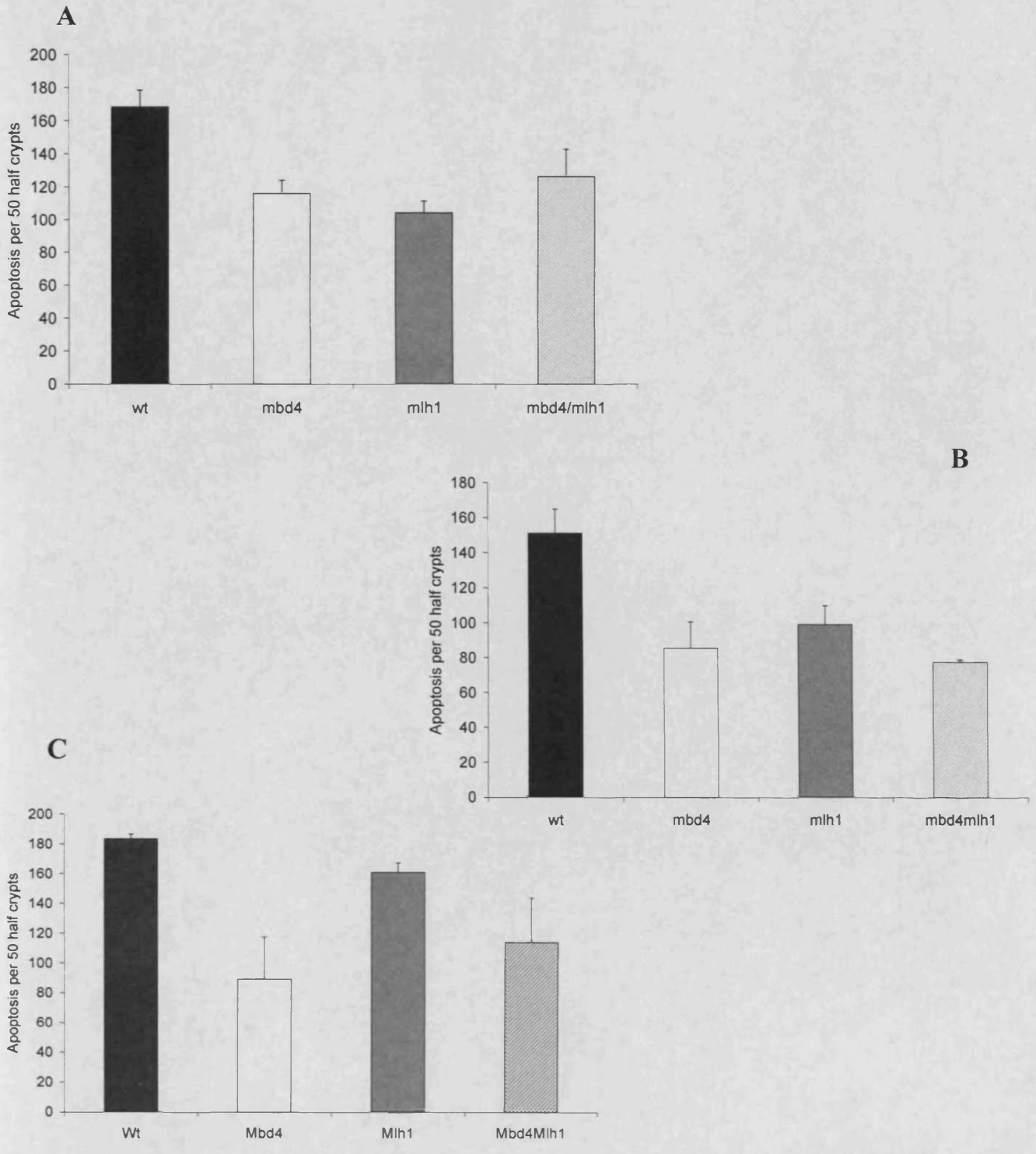

Figure 3.8 - Apoptosis per 50 ½ crypts **A**, 10 hours following 2x400mg/kg 5-FU treatment. **B**, Apoptosis per 50 ½ crypts 6 hours following 100mg/kg Temozolomide treatment. **C**, Apoptosis per 50 ½ crypts 6 hours following 10mg/kg cisplatin treatment. (N=3 minimum for every time point and error bars = SEM. Black bars, *Mbd4*$^{+/+}$ mice; open bars, *Mbd4*$^{-/-}$ mice; grey bars, *Mlh1*$^{-/-}$ mice and bars with diagonal stripes, *Mbd4*$^{-/-}$ *Mlh1*$^{-/-}$ mice.

Both *Mbd4* and *Mlh1* deficiency caused a significant reduction in apoptosis 10 hours following 5-FU treatment (figure 3.8A p=<0.01 MWU, n=6). The double mutants showed significantly reduced apoptosis compared to wild type mice (p = 0.04 MWU, n=3), but no significant reduction compared to either singly mutant *Mlh1*$^{-/-}$ (p = 0.38 MWU, n=3) or *Mbd4*$^{-/-}$ mice (p = 0.65 MWU, n=3). This data indicates that the additional loss of Mlh1 does not affect Mbd4 null cell death in response to 5FU.

Similar results were observed with Temozolomide treated animals (figure 3.8B), whith single *Mbd4* and *Mlh1* deficiency resulting in a significant reduction in apoptosis at 6 hours following Temozolomide treatment (p = 0.01 MWU, n=5). Double mutants again showed reduced apoptosis compared to wild type mice (p = 0.04 MWU, n=3), but no significant reduction compared to either *Mlh1*$^{-/-}$ (p = 0.765 MWU, n=3) or *Mbd4*$^{-/-}$ mice (p = 0.365 MWU, n=3).

Finally, single *Mbd4* and *Mlh1* deficiency caused a significant reduction in apoptosis at 6 hours following Cisplatin treatment (figure 3.8C, p=0.04 MWU). Interestingly *Mbd4*$^{-/-}$ mice showed significantly reduced levels of apoptosis compared to *Mlh1*$^{-/-}$ mice (p = 0.04 MWU, n=3). Double mutants showed significantly reduced apoptosis compared to wild type and *Mlh1*$^{-/-}$ mice (p = 0.04 MWU) but once more there was no significant reduction compared to *Mbd4*$^{-/-}$ mice (p = 0.45MWU). Together these data indicate that Mbd4 plays a more significant role than Mlh1 in mediating the apoptotic response to these agents and that this role is independent of its role in MMR.

3.4 Discussion

3.4.1 Mbd4 deficiency and the death response

Throughout the various time courses, all agents showed a typical early peak of apoptosis similar to that observed in previous studies in MMR deficient backgrounds (Toft *et al* 1999, Sansom and Clarke 2002). My extended studies of the Mbd4 dependency for the death response to several agents over a 48 hour period, has helped to identify a role for Mbd4 that stretches beyond the initial maximal response. This is shown in figure 3.1 where both Temozolomide and Cisplatin exhibit a reduced or lagging apoptotic response in *Mbd4*$^{-/-}$ mice compare to controls at 6-11 ($p=<0.01$) and 6-10 hours ($p=<0.04$) respectively. However this deficit is regained by the 24hour period and no difference was observed between genotypes by 48 hours.

3.4.2 Mbd4 and mediating the 5FU induced death response

One of the major focuses of this chapter was to characterise the role of Mbd4 *in vivo* in recognising and mediating the response to 5FU induced damage. Figure 3.2 highlights Mbd4 dependency for apoptosis in response to 5FU at the 10hour time point, with *Mbd4*$^{-/-}$ mice showing considerable reduction in cell death compared to controls ($p=<0.001$ MWU). This may well be p53 dependent, as similar profiles in 5FU induced apoptosis were observed in p53 null animals at this time (Pritchard *et al* 1998). Furthermore, the full apoptotic response is subsequently restored by 48 hours in Mbd4 null mice and a delayed wave of cell death peaking at 18 hours is observed in *Mbd4*$^{-/-}$ mice in comparison to the 10hour peak observed in *Mbd4*$^{+/+}$ mice (figure 3.2).

Time courses for Temozolomide, Cisplatin and 5FU (figures 3.1, 3.2) indicate that Mbd4 independent apoptosis occurred at later time points and no differences between genotypes was observed by 48 hours. This late wave of compensatory apoptosis was also observed by Toft *et al,* who showed a similar delayed apoptotic wave in γ-IR treated p53 null mice 72 hours following γ-IR treatment (Toft *et al* 1999). Further to this experiment, recent data suggests this wave to be p53 and MMR independent through similar experiments in knockout animals (Sansom and Clarke 2002). As my data suggests this wave to also be independent of Mbd4 (figures 3.1, 3.2), an

alternative death signalling pathway such as induction of the p53 family member p73 may signal this late apoptotic wave, although it is unclear whether this pathway is dependent or independent of MMR signalling (Shimodaira *et al* 2003, Sansom and Clarke 2002)

In addition to the induction of apoptosis in response to 5FU, a drop in cellular proliferative often accompanies cell death in wild type animals. The differences observed between genotypes in apoptosis at 10 hours (figure 3.1) are not reflected in the proliferative response until 16-20 hours after 5FU treatment (figure 3.3). I observed an increase in the proliferative capacity of *Mbd4*$^{-/-}$ mice compared to controls at 16, 18 and 20 hours ($p=<0.05$ for all, N=3), with *Mbd4*$^{-/-}$ mice failing to follow the suppressed proliferative phenotype of control mice. My results also show that the changes in apoptotic and proliferative responses translates into a significant increase in cell number (and hence crypt viability) by the 48 hours time point in Mbd4 null mice (figure 3.5 $p=<0.05$), indicating Mbd4 deficient cells are more resistant to 5FU induced cell death and carry a distinct survival advantage over wildtype cells.

3.4.3 Thymidine and Uridine relief of 5FU damage

Figure 3.6 sheds some light on the mechanism of action for Mbd4 mediated 5FU damage. The lack of quenching of 5FU induced DNA damage upon thymidine addition in *Mbd4*$^{-/-}$ mice ($p = >0.05$MWU) when compared to the significant quenching of apoptosis in the *Mbd4*$^{+/+}$ samples ($p = <0.01$ MWU), suggests that contrary to the report by Pritchard *et al* 1997, 5FU can induce DNA damage albeit at high doses of 5FU treatment and that Mbd4 may mediate apoptosis in response to 5FU DNA damage. The interesting finding that a reduction in apoptosis is observed when adding uridine to quench the RNA pool of 5FU damage, suggests that Mbd4 may be more crucial in mediating 5FU DNA damage rather than RNA damage in the gut following 5FU exposure via its role in recognising 5FU:G DNA mismatches (Petronzelli *et al* 2000a). Therefore Mbd4 deficiency appears contrary to that of the p53 null experiments, in which 5FU RNA damage induced p53 (Pritchard *et al* 1997). Recent data by Meyers *et al* has outlined a role for the MMR proteins MLH1 and MSH2 in binding and signalling G:5FU mismatches in the DNA component of 5FU damage by investigating thymidylate synthetase activity (Meyers *et al* 2005). This

finding may provide a novel situation where by MMR components and Mbd4 bind and signal 5FU induced DNA damage, in addition to p53 mediating the 5FU induced RNA damage. Clearly further questions must be answered about the exact mechanism of 5FU action in the intestine, indeed Tanaka *et al* 2000 report opposite observations to Pritchard *et al 1997,* with respect to 5FU RNA mediated toxicity in the gut. These differences may be dependent on time, dose and genetic background of mice and humans. In support of this, promoter polymorphisms of TS associated with stability of the TS transcript have been identified in humans and have been linked to carcinogenesis in relation to folate intake (Ulrich *et al* 2002).

3.4.4 Mbd4 loss and Clonogenic survival

Inappropriate survival of cells following treatment with DNA damaging agents is of great importance as potentially damaged cells may show long-term persistence and hence may contribute to tumourigenesis (figure 3.9). However, the increased survival of cells in association with suppressed apoptosis does not necessarily translate into an increase in clonogenic survival.

In the case of 5FU damage and Mbd4 deficiency, it appears that the depressed apoptotic response, increased proliferative drive and subsequent increase in cell number does translate into increased clonogenic survival at 72 hours when compared to $Mbd4^{+/+}$ mice (Figure 3.7 p=0.02 MWU, N=6). Treatment with Cisplatin also resulted in increased clonogenic survival in $Mbd4^{-/-}$ mice (Sansom *et al* 2003c appendix). The ability of Mbd4 loss to predict increased long-term survival appears to be damage type dependant, as additional data for publication showed Mbd4 null mice did not show increased clonogenic survival following 15Gy γ-IR. However, data for clonogenic survival from MMR deficient mice showing dependency for apoptosis with Cisplatin, nitrogen mustard and NMNU, observed that only NMNU gave increased survival at the clonogenic assay (Sansom and Clarke 2002). Similarly p53 null animals showed decreased apoptosis to a wide range of agents (Hendry *et al* 1997), but further clonogenic investigation in mice showed either weak or absent dependence on p53 for survival to a range of insults (Hendry *et al* 2000, Pritchard *et al* 1998, Sansom and Clarke 2002).

This failure to directly relate apoptosis with crypt survival may arise as a consequence of the assay system itself. This is clearly the case with ionising radiation, as survival of the endothelial cells rather than of the crypt epithelium itself appears to be the determinant of whole crypt survival (Paris *et al* 2001).

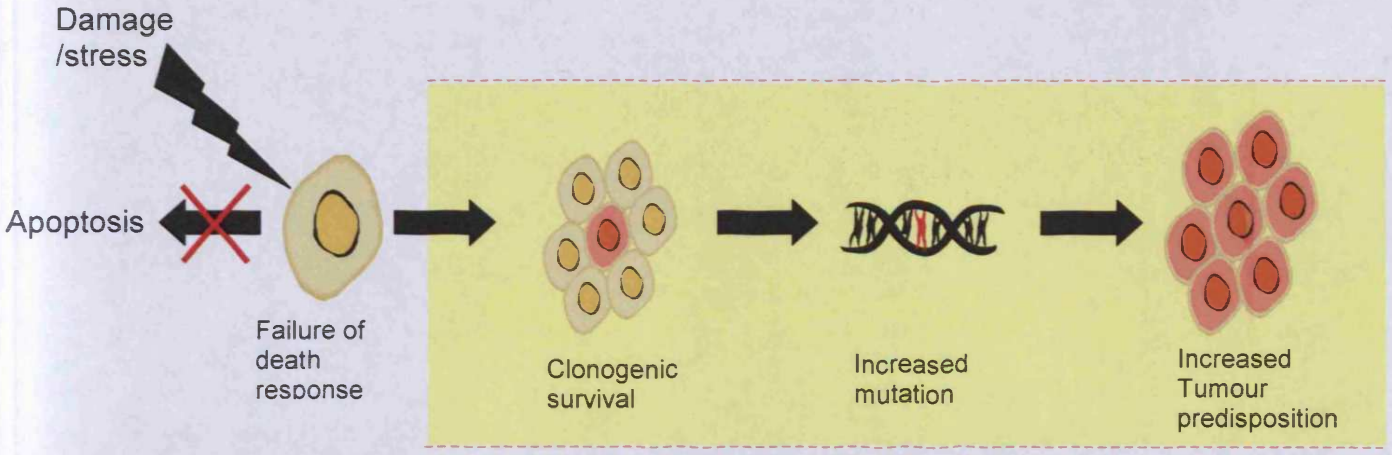

Figure 3.9- Schematic diagram illustrating the hypothesis that defects in the apoptotic programme can underlie tumour predisposition. This hypothesis has a number of predictions if apoptosis is compromised: first, increased clonogenic survival; second, increased mutation burden, and finally increased tumour predisposition.

3.4.5 *Mbd4*$^{-/-}$ *Mlh1*$^{-/-}$ Double null investigation

If Mbd4 and Mlh1 were to act on the same pathway to induce apoptosis we would expect no additive decrease in apoptosis in the double nulls. Additional loss of Mlh1 did not appear to reduce the apoptotic response when compared to single deficiency of either gene in response to 5FU or Temozolomide (figure 3.8A-C, p = >0.05 MWU for both). However a small reduction in the double nulls was observed compared to wild type and *Mlh1*$^{-/-}$ mice when treated with Cisplatin (p = <0.04 MWU), but this reduction was not seen when compared to Mbd4 null mice. Furthermore, *Mbd4*$^{-/-}$ mice showed greater suppression of the apoptotic response than *Mlh1*$^{-/-}$ mice (p =<0.04 MWU) and this suggests loss of Mbd4 to be more important to the apoptotic response to these agents than Mlh1.

Given the wider range and greater dependency for Mbd4 in apoptosis within the gut than Mlh1, this strongly suggests Mbd4 may play a role outside of MMR mediated apoptosis, possibly by direct signalling. Additionally, γ-IR induced apoptosis showed dependence for Mbd4 but not Mlh1, again strengthening reports that γ-IR-induced death is independent of the MMR response (Sansom and Clarke 2002, Meyers *et al* 2004).

Studies in *Mbd4*$^{-/-}$ MEFs conducted soon after my investigations found MMR components to be down regulated at the protein level and when treated with cytotoxic regimes, found similar Mbd4 dependency for the direct signalling of apoptosis and a delay in the kinetics of p53 induction (Cortellino *et al* 2003). However, there may be some level of redundancy for MMR genes in signalling apoptosis. G:T mismatches can occur by mis-incorporation of G into the newly synthesised strand and not from CpG deamination. In this situation, removal of Thymidine by MBD4 would be potentially mutagenic, but recognition and removal by other MMR mechanisms such as those involving Mlh1 would correct the lesion. It therefore seems likely that cross talk between MMR, BER and Mbd4 mechanisms exists to cover a wide range of repair and apoptotic functions.

Mbd4 plays a dual role in repair and direct signalling to apoptotic effectors and this may be in part linked to its suggested interactions with FADD, which was found to sequester Mbd4 in the nucleus with Mlh1. This converse role for Mbd4 in the inhibition of receptor mediated death is suggested to due to its nuclear localization and is possibly cell type dependent (Screaton *et al* 2003).

3.4.6 Relevance to tumourigenesis and conclusions

- I have shown that Mbd4 is essential to the immediate and intermediate apoptotic response in the intestine following exposure to a variety of DNA damaging agents.

- Mbd4 plays a role in initiating apoptosis in addition to its MMR dependent role.

- This finding is underlined by the increased clonogenic survival following 5FU (and Cisplatin) treatment.

- Therefore Mbd4 status can determine long term survival *in vivo* but only to specific types of damage (see Sansom *et al* 2003c see Appendix).

Mbd4 has recently been shown to play an essential role in reducing the mutability of 5 methyl CpG sites along the genome (Millar *et al* 2002), and this deficiency of Mbd4 clearly leads to accelerated tumourigenesis on the Apc^{MIN} background (Millar *et al* 2002). However when $Mbd4^{-/-}$ mice were crossed to a MMR deficient background, no additional mutation level or acceleration of tumourigenesis was observed compared to singly mutant $Mlh1^{-/-}$ and $Msh2^{-/-}$ mice (Sansom *et al* 2004 b).

Loss of Mbd4 and consequently its function in MMR independent apoptosis may contribute to the accelerated tumourigenesis described above. This outlines a role for Mbd4 as an intestinal tumour suppressor gene, and indicates that MBD4 status may also play an important role in 5FU drug resistance. It has also been recently reported that MBD4 mediates transcriptional repression by its histone deacteylase activities, similar to the other members of the MBD family. This finding implicates further tumour suppressor functions for Mbd4 through epigenetic regulation (Kondo *et al* 2005).

Chapter 4. Investigating the intestinal apoptotic response in *Dapk*$^{-/-}$ mice

4.1.1 DAPK structure and function

DAPK (Death associated protein kinase) has a large multi subunit structure 1431 amino acids long with a serine/threonine kinase catalytic unit at the N-terminus (figure 4.1). The protein contains 11 subunits and the C terminal domain contains a death domain motif homologous to those found in P55, TNFRs, CD95/FasR, DR35, FADD/ MORT1, RIP, TRADD and RAID. This domain is critical for the death inducing effects of DAPK (Levy-strump and Kimchi 1998).

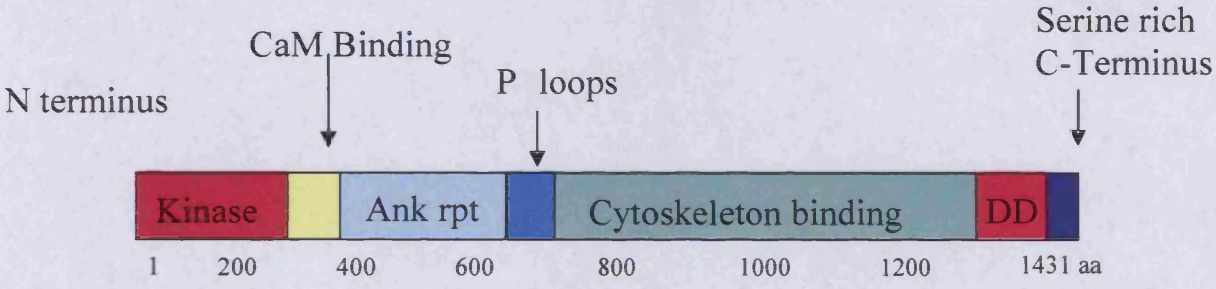

Figure 4.1– Schematic of DAPK functional domains. DAPK mediates cell death through several functional domains including a Serine/Threonine kinase domain and cytoskeleton binding site involved in membrane blebbing. The CaM (Calmodulin) domain and serine rich c-terminal tail act as regulatory domains. Additional subunits: Ank rpt = Ankyrin repeats, DD = Death domain, P-loop = nucleotide interacting phosphate binding loops (adapted from Cohen *et al* 1997).

The pro-apoptotic activity of DAPK depends on the cellular location, death domain interactions and catalytic activity of the protein (Shohat *et al* 2001). Several levels of regulation ensure that the protein is activated only after death signals are received (Shohat *et al* 2001). Firstly, kinase activity is regulated by a Ca2+/Calmodulin (CaM) domain (Cohen *et al* 1999) and binding of Calcium to this domain relieves the inhibition on the adjacent kinase domain (Raveh and Kimchi 2001). The sensitivity of DAPK to intracellular calcium levels may serve to activate the death signal in response to subtle alterations in calcium levels (Shohat *et al* 2001).

Secondly, post-translational modification has also been shown to be important in DAPK regulation via prenylation and phosphorylation. Inhibition by auto and trans-phosphorylation of serine 308 within the calmodulin binding domain stabilizes Calmodulin binding and hence represses DAPK activity in response to apoptotic stimuli (Shohat *et al* 2001). Finally, Jin *et al* identified a Dapk isoform *in vitro* which displayed cell survival properties and protected against apoptosis via and extra length of C-terminus residues (Jin *et al* 2001). Subsequently, this serine rich tail was found to inhibit DAPK *in trans* and negatively regulate the death promoting properties of the protein. Deletion of this domain increased the death inducing abilities of the protein (Shohat *et al* 2001).

Adjacent to the CaM binding domain is a series of eight ankryin repeats, 2 nucleotide interacting phosphate binding loop P- loop motifs and a cytoskeleton binding domain. Ankyrin repeats are capable of many protein interactions including cell cycle regulators, transcription factors, and tumour suppressor genes (Sedgwick and Smerdon 1999) and these repeats may interact with as yet unknown downstream effectors of DAPK.

Although DAPK localizes to the cytoskeleton, it does contain a nuclear localization signal within the kinase domain suggesting loaclization to be key to correct function (Kögel *et al* 2001). Furthermore, ZIP kinase is phosphorylated and activated by DAPK to amplify the death-promoting signal (Shani *et al* 2004) and this function depends on translocation from the nucleus to cytoplasm (Shani *et al* 2004). MBD4 may also play some part in these death signalling pathways, as ZIP kinase has been shown to bind and shuttle MBD4 from the nucleus to the cytoplasm (Catherine Millar unpublished observation).

4.1.2 DAPK induces membrane blebbing

DAPK is localized to the cytoskeleton in association with the actin stress fibres via its ankyrin repeats and plays a part in the disruption and rearrangement of the cytoskeleton in response to the death signal (Bialik *et al* 2004). Membrane blebbing is a common feature of cell death and the DAPK family are integral to this process.

Myosin light chain (MLC) phosphorylation and cleavage has been suggested to be essential for membrane blebbing (Mills *et al* 1998) and both DAPK and ZIP kinase are known to phosphorylate MLC in a similar way to MLCK (myosin light chain kinase) when correctly localized (Velentza *et al* 2001, Niiro and Ikebe 2001, Bialik *et al* 2004). ZIP kinase is phosphorylated and activated by DAPK to amplify the death-promoting signal (Shani *et al* 2004) and this function depends on translocation from the nucleus to cytoplasm (Shani *et al* 2004).

The action of membrane blebbing causes loss of adhesion and matrix detachment induced cell death termed 'Anoikis'. DAPK inhibits matrix induced survival signalling via MLC cleavage (Kögel *et al* 2001) and inactivation of integrins, consequently blocking matrix survival cues and inducing death (Wang *et al* 2002). DAPK pro-apoptotic activity is also stimulated by the dependence receptor UNC5H2 in the absence of the survival ligand netrin-1 and as a result induces p53 activity and apoptosis (Llambi *et al* 2005). The effector function of DAPK in membrane blebbing provides some clues as to how external death signals are mediated to induce cytoplasmic changes (Cohen *et al* 1997).

DAPK and DRP-1 have also been associated with the process of Autophagy ('self-eating') and therefore may be critical to stress induced cell death (Inbal *et al* 2002). Furthermore DAPK function within membrane blebbing and autophagy is independent of caspase activity, confirming a multifunctional role for DAPK in caspase dependent and independent signalling (Inbal *et al* 2002). These multiple roles for DAPK in detachment based cell death and membrane blebbing may prevent malignant transformation, attesting to a role for DAPK as a tumour suppressor gene (Gozuacik and Kimchi 2004).

4.1.3 DAPK induced cell death

As DAPK mediates both extrinsic and intrinsic death signals, it may act as a convergence point between several apoptotic pathways (Levy-strumpf and Kimchi 1998). Indeed the role of DAPK in mediating ceramide induced death in neuronal cells involves recruitment of SAPK/JNK, FAS/APO-1, Caspase and p53 cell death pathways (Shohat *et al* 2001).

DAPK has been identified as a mediator of caspase dependent death signalling as a result of appropriate death signals (Raveh and kimchi 2001, Jang *et al* 2002) and DAPK mitochondrial function can be blocked by inhibitors of caspases such as Crma and p35 in addition to Bcl-2 expression. This response was not blocked by mutations in FADD/MORT1, therefore outlining a role for DAPK downstream of receptor/caspase 8 signals and upstream of mitochondrial cytochrome C release (Cohen *et al* 1999).

Oncogenic signalling by c-Myc and E2F-1 produces hyperproliferative signals which up-regulate DAPK transcripts in a negative feedback loop that suppress oncogene expression and prevent inappropriate transformation of cells (figure 4.2 Raveh *et al* 2001, Qi *et al* 2004). This mechanism is dependent on p53 status and expression of both genes has been linked to improved 5FU induced apoptosis in CRC patients (Arango *et al* 2001). DAPK has been shown to regulate p53 via $P19^{ARF}$ upregulation, which stabilizes and activates p53 by sequestering MDM2 (Raveh *et al* 2001, Kögel *et al* 2001).

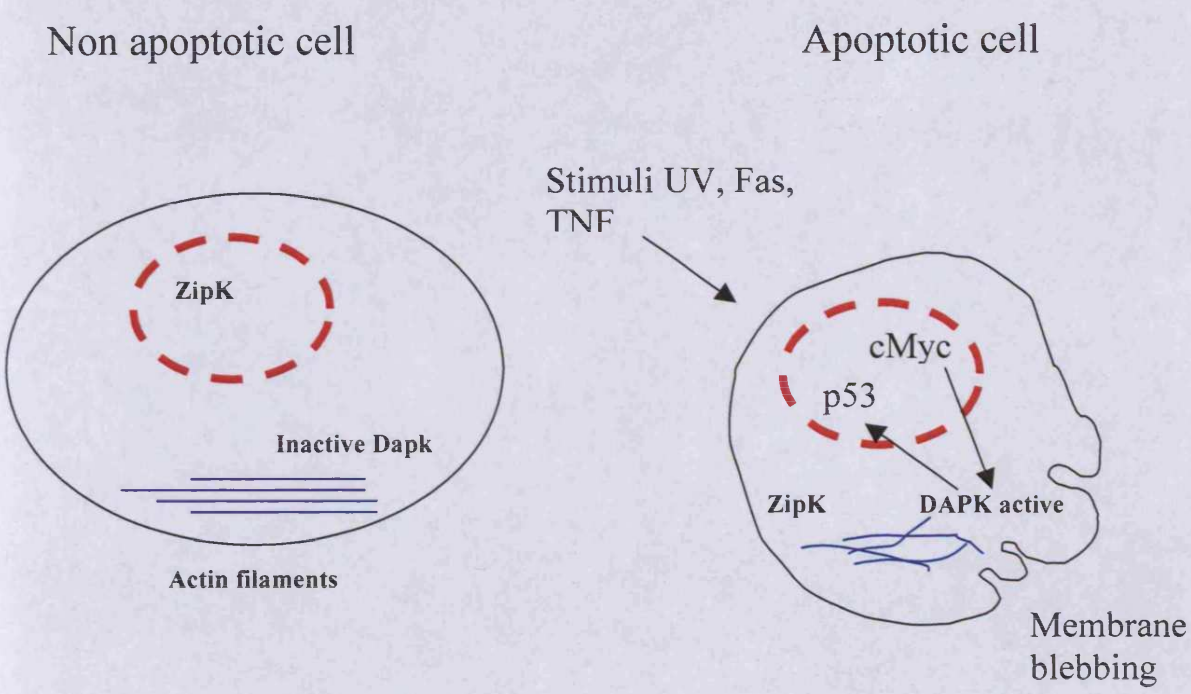

Figure 4.2 - DAPK death signalling within normal and apoptotic cell types. Death inducing stimuli activate DAPK pro-apoptotic activities, remodelling cytoplasmic actin stress fibres and resulting in membrane blebbing characteristic of apoptosis (adapted from Raveh *et al* 2001).

The DAPK dependent mechanism channelling p53 towards apoptosis instead of cell cycle arrest remains unknown and DAPK may contribute towards the apoptotic response by signalling p53 dependent and independent events (Figure 4.2, Raveh *et al* 2001, Raveh and kimchi 2001). A positive feedback loop was recently identified whereby p53 binds and up-regulates the *DAPK* sequence. In turn, DAPK then stabilizes and activates p53 to induce apoptosis by an unknown mechanism (Martoriati *et al* 2005). Additionally DAPK has recently been implicated in sequestering ERK and inhibiting its survival functions. Bidirectional phosphorylation between ERK and DAPK results in activated DAPK whilst retaining ERK in the cytoplasm (Chen *et al* 2005).

4.1.4 DAPK and cancer

Down regulation of DAPK is commonly found in sporadic cancers including Burkitts lymphoma, B cell malignancies and thyroid lymphoma (Kissil *et al* 1997, Nakatsuka *et al* 2000, Katzenellenbogen *et al* 1999, Esteller *et al* 1999), non small cell lung carcinoma (Tang *et al* 2000), multiple myelomas (Ng *et al* 2001), Uterine and Ovarian carcinomas (Bai *et al* 2004), Gastric carcinomas (Kim *et al* 2003) and CRCs

(Satoh *et al* 2002). *DAPK* maps to the chromosomal region 9q34.1, which has been shown to be prone to translocations and LOH in human leukaemia and bladder carcinomas (Chan *et al* 2002). Screening has also identified loss of heterozgosity at this region in breast, lung and colorectal cancers (Raveh and Kimchi 2001, Toyooka *et al* 2003), with an associated high level of *DAPK* promoter methylation in these tissues (Raveh *et al* 2001).

Hypermethylation of the *DAPK* promoter is far more common than somatic mutation (Bialik and Kimchi 2004) and promoter hypermethylation was frequently observed in lung cancers, lymphomas, head and neck cancers and colon cancers (Esteller *et al* 2001). DAPK expression could be restored in many of these cancer cell lines by adding the known demethylation agent 5aza2deoxycytidine (Bialik and Kimchi 2004). Hypermethylation of the *DAPK* promoter was also found in early stage lung lesions, which led to the hypothesis that loss was an early event in tumour progression (Pulling *et al* 2004). In addition, hypermethylation of the *DAPK* promoter has been linked to CRCs and may contribute to neoplastic progression in the intestine as a result of activating K-Ras mutations (Nagasaka *et al* 2004, Dong *et al* 2005).

The loss of DAPK has been associated with an invasive phenotype particularly in pituitary and head and neck tumours (Sanchez-Cespedes *et al* 2000, Esteller *et al* 2001). Selection against positive mediators of cell death is an advantage to the progression of tumourigenesis and indeed loss of DAPK has been shown to predispose to increased tumour metastasis and decreased sensitivity to death inducing signals (Kissil and Kimchi 1998). DAPK has therefore been implicated as a metastatic suppressor (Tang *et al* 2000) but also has other tumour suppressor gene functions in its ability to mediate anoikis, p53 dependent apoptosis and down-regulate oncogenes (Raveh *et al* 2001). These factors provide a link between loss of apoptosis and metastatic progression (Ng *et al* 2001, Inbal *et al* 1997).

The data linking loss of DAPK with impaired cell death and cancer progression has identified DAPK as a tumour suppressor gene and a novel therapeutic target. Use of demethylating drugs such as Zebularine to halt cancer progression is currently under investigation, but specific gene targeting still remains a problem (Bialik and Kimchi 2004). Also, given the role of DAPK in early neuronal cell death, small molecule

inhibitors of DAPK have been developed for treatment of acute brain injury (Velentza *et al* 2003).

4.1.5 Mouse models of DAPK loss

Previous work has shown that cultured hippocampal neurons from *Dapk*$^{-/-}$ MEFs show decreased apoptotic response to ceramide induced cell death (Pelled *et al* 2002). Dapk$^{-/-}$ retinal ganglion cells also showed impaired apoptotic response to glutamate treatment (Schori *et al* 2002), highlighting the importance of Dapk in the development of these tissues.

DAPK kinase mutant mice generated by gene targeting and display decreased renal tubular cell apoptosis and renal fibrosis (Yukawa *et al* 2005). Additionally, reactivation of DAPK in intravenously injected highly metastatic cells suppressed their ability to form lung metastasis and restored apoptotic sensitivity (Bialik and Kimchi 2004).

4.2 Aim

Increased DAPK expression has been shown to be associated with several pro-apoptotic effector processes such as: PARP cleavage, chromatin condensation, membrane blebbing and therefore is integral to mediating the apoptotic response (Cohen *et al* 1999). Loss of DAPK may contribute to tumourigenesis by loss of the immediate apoptotic response and by loss of control of cell adhesion and detachment based mechanisms (Bialik and Kimchi 2004).

Based on the evidence of a significant role for DAPK in mediating both DNA damage and cytokine induced cell death *in vitro*, I decided to assess the *in vivo* contribution of DAPK to the apoptotic response in the murine small intestine following treatment with DNA damage inducing agents (such as those used in chapter 3) and also to the endogenous death inducing Fas ligand. To achieve this, I made use of mice constitutively null for DAPK,which are viable, fertile and show no overt phenotype or predisposition to tumourigenesis (Kimchi unpublished observation).

4.3 Results

4.3.1 Investigating the apoptotic dependency for Dapk following DNA damage

Studies were initiated to observe if loss of DAPK inhibited the immediate apoptotic response to cytotoxic agents such as 5FU, Cisplatin and γ-ionising radiation (γ-IR). *Dapk*$^{-/-}$ mice were dosed with DNA damaging agents as previously described (chapter 2.3, 3.3) and tissue harvested at the maximal apoptotic response time of 6 hours. At least 3 mice of each genotype (*Dapk*$^{-/-}$ and *Dapk*$^{+/+}$) were treated per agent and apoptosis scored per 50 half crypts.

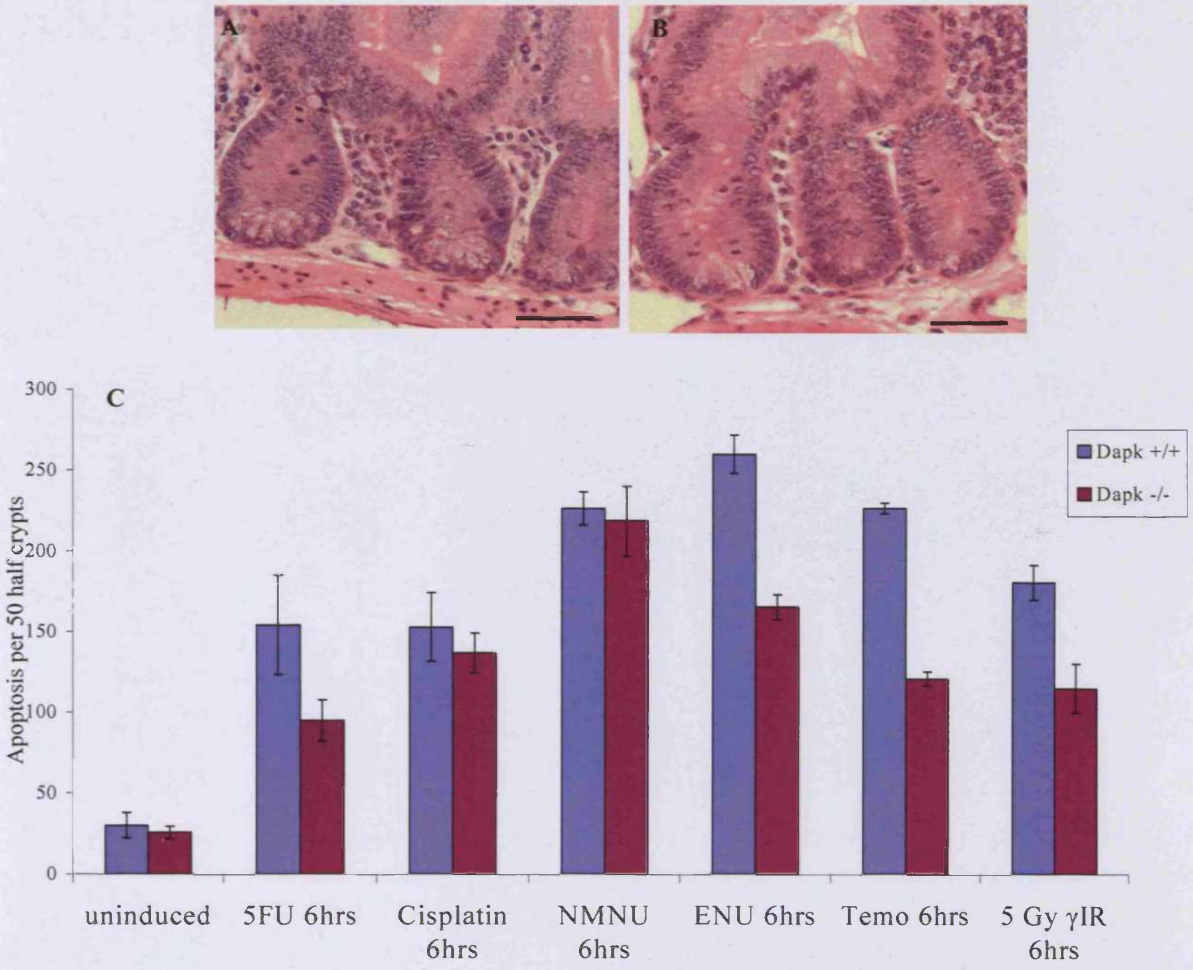

Figure 4.3– H&E histology from: **A,** *Dapk*$^{+/+}$ **B,** *Dapk*$^{-/-}$ mice (scale bars = 50μm) **C,** Scoring of apoptosis in the murine small intestine following exposure to 1x400mg/kg 5FU, 10mg/kg Cisplatin, 50mg/kg NMNU, 50mg/kg ENU, 100mg/kg Temozolomide and 5Gy γ-IR. *Dapk*$^{+/+}$ = Blue bars, *Dapk*$^{-/-}$ = burgundy bars. (5FU 6hrs: N=9, 5Gy γ-IR: *Dapk*$^{+/+}$ N=6, *Dapk*$^{-/-}$ N=5. All other agents N=3 for both genotypes, error bars = SEM).

No difference was observed between *Dapk*$^{-/-}$ and *Dapk*$^{+/+}$ genotypes in untreated tissue (figure 4.3A-B). The apoptotic response to cytotoxic treatments in the intestine in figure 4.3 shows a clear dependency for Dapk with the following agents 6 hours after dosing: 5FU (p=0.01 MWU), ENU (p=0.04 MWU), Temozolomide (p=0.04 MWU) and finally 5Gy γ-IR (p=0.01 MWU). There is no significant reduction at 6 hours with Cisplatin or NMNU (p=>0.05 MWU), suggesting that Dapk mediated induction of apoptosis is lesion dependent at 6 hours.

I next decided to investigate whether the dependency for Dapk mediated apoptosis observed in figure 4.3C extended to a later time point of 24 hours, to observe if Dapk loss significantly altered the kinetics of the drug response.

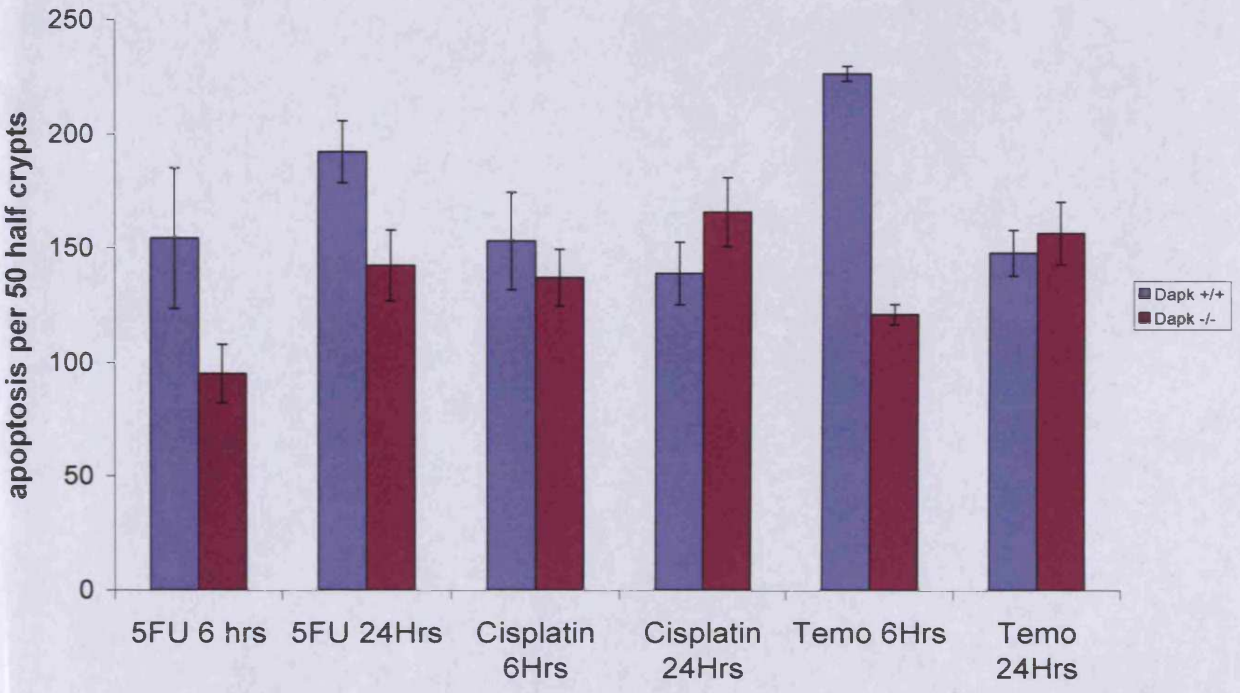

Figure 4.4– Scoring of apoptosis 6 and 24 Hrs after dosing with 1x400mg/kg 5FU 6hrs, 2x400mg/kg 5FU 24hrs, 10mg/kg Cisplatin and 100mg/kg Temozolomide. *Dapk*$^{+/+}$ = Blue bars, *Dapk*$^{-/-}$ = burgundy bars. (5FU 6hrs: *Dapk*$^{+/+}$ N=9, *Dapk*$^{-/-}$ N=9. 24 hrs 5FU: *Dapk*$^{+/+}$ N=7, *Dapk*$^{-/-}$ N=5. Cisplatin 24Hrs: both N=6. All others N=6 (error bars = SEM).

Figure 4.4 shows the delayed effects of apoptosis induction in Dapk null animals compared to that of the 6 hour response in figure 4.3. The apoptotic dependency for Dapk is retained 24 hours following 5FU dosing (p=0.02 MWU). There is no change in the Dapk-independent Cisplatin response (p=>0.05 MWU), and the reduced response to Temozolomide in Dapk null mice at 6 hours is restored to that of *Dapk*$^{+/+}$control mice (p=>0.05 MWU).

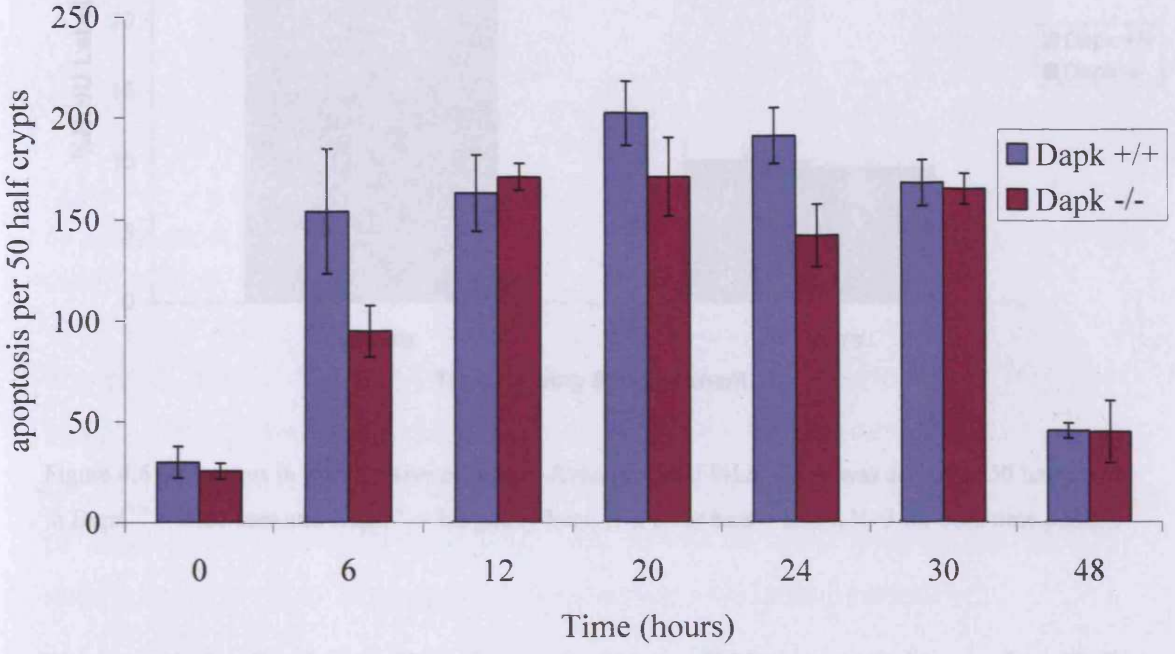

Figure 4.5 – Apoptosis timecourse following 2x400mg/kg 5FU treatment. *Dapk*$^{+/+}$ = Blue bars, *Dapk*$^{-/-}$ = burgundy bars. (6hrs: N=9 both genotypes, 24 hrs: *Dapk*$^{+/+}$ N=7, *Dapk*$^{-/-}$ N=5, all other time points N=3, error bars = SEM).

Figure 4.5 details the kinetics of the apoptotic response to 5FU treatment in *Dapk*$^{+/+}$and *Dapk*$^{-/-}$ mice by observing the apoptotic response over an extended timecourse. There is no significant difference between genotypes at the time points between 6 and 24 hours (12 and 20 hours). This result is unexpected considering the suppressed apoptosis in *Dapk*$^{-/-}$ mice either side (6hours: p=0.01 MWU, 24 hours: p=0.02 MWU). However timecourse data from *Dapk*$^{+/+}$control mice reflects that observed for control mice treated with 5FU in chapter 3 (figure 3.2), with a maximal apoptotic response at 20 hours and a return towards basal level at 48 hours, suggesting controls to be reliable and 5FU kinetics in *Dapk*$^{-/-}$ mice to be complex.

To address the accompanying changes in proliferative response following 5FU dosing, mice were injected with BrdU 2 hours prior to harvesting and %labelling scored at 6 and 24 hours post 5FU treatment.

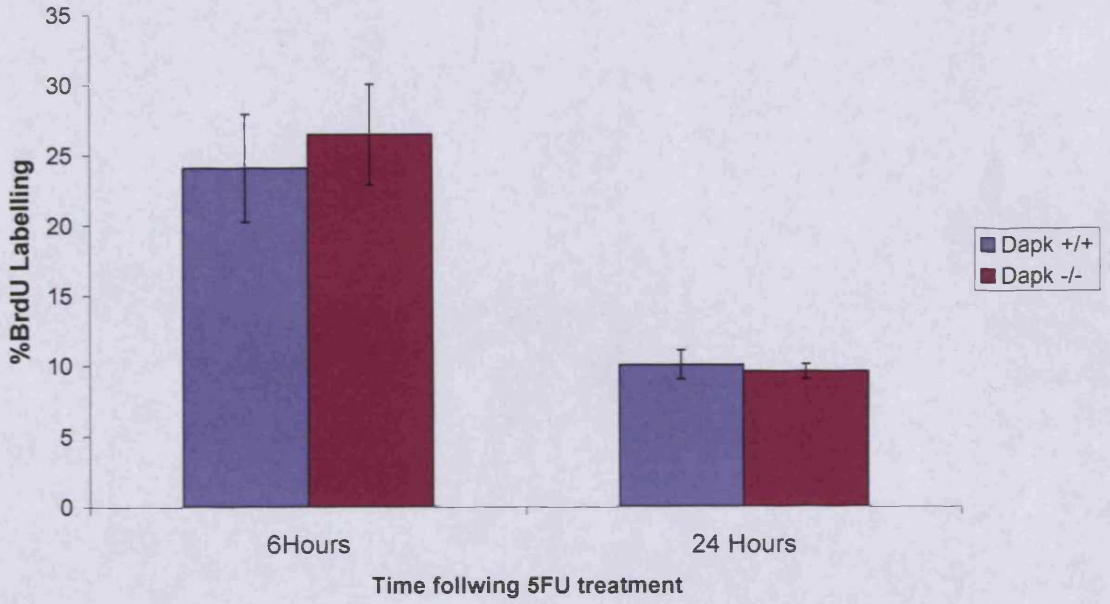

Figure 4.6 – Changes in proliferative response. Average BrdU %Labelling was scored in 50 half crypts in *Dapk*$^{+/+}$ = Blue bars and *Dapk* $^{-/-}$ = burgundy bars. (All error bars = SEM, N=3 for both time points).

Figure 4.6 details the proliferative response to 5FU treatment by scoring BrdU incorporation during S-phase. 5FU treatment targets transit cells in the crypt and as a result a drop in proliferative capacity is often observed following 5FU treatment. Figure 4.6 follows this pattern with a decrease in BrdU %labelling by 24 hours, however no difference was observed between genotypes at either 6 or 24 hours following 5FU dosing (P=>0.05 MWU).

I also studied the effects of loss of Dapk on induction of apoptosis by 5 Gy γ-IR over an extended time period to establish if Dapk loss impacted upon the initial p53-dependent apoptotic response to γ-IR, or the later stage secondary p53-independent apoptotic waves (Clarke *et al* 1997, Merritt *et al* 1997).

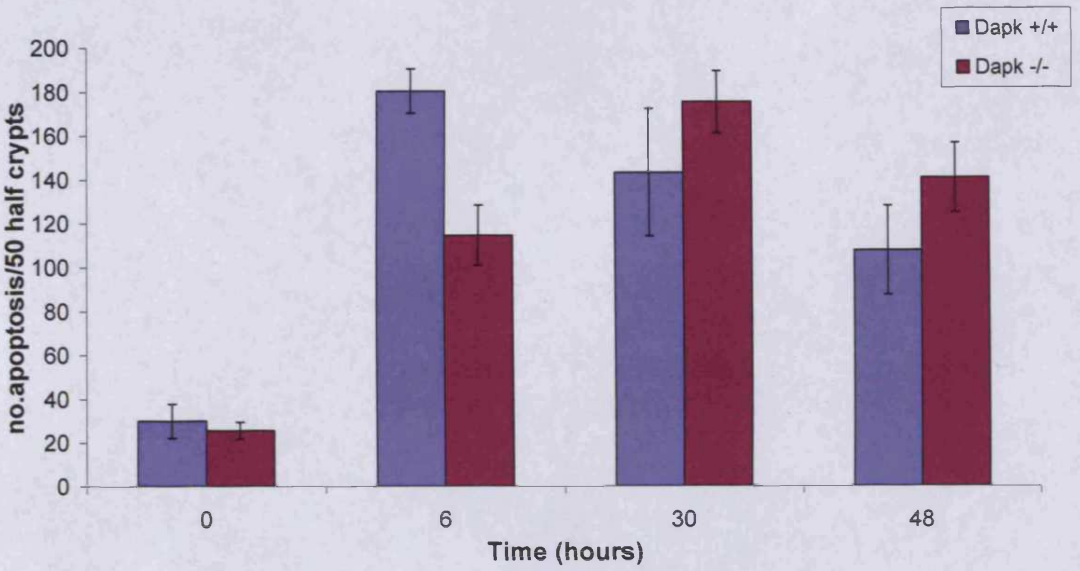

Figure 4.7– Apoptosis time course following 5Gy γ-irradiation. *Dapk*$^{+/+}$ = Blue bars, *Dapk*$^{-/-}$ = burgundy bars. (6 Hrs: *Dapk*$^{+/+}$ N=6, *Dapk*$^{-/-}$ N=5, all other points N=3. Error bars = SEM except 30Hrs *Dapk*$^{-/-}$ = range).

Figure 4.7 details the effects of Dapk loss on the apoptotic response to 5Gy γ-IR. Results indicate that the suppression of apoptosis observed in *Dapk*$^{-/-}$ mice at 6 hours ($p=0.01$) does not persist at 30 hours or later time points ($p=<0.05$), indicating the loss of Dapk has immediate but not long term effects on apoptosis and that the p53-independent late wave of apoptosis is not dependent on Dapk function.

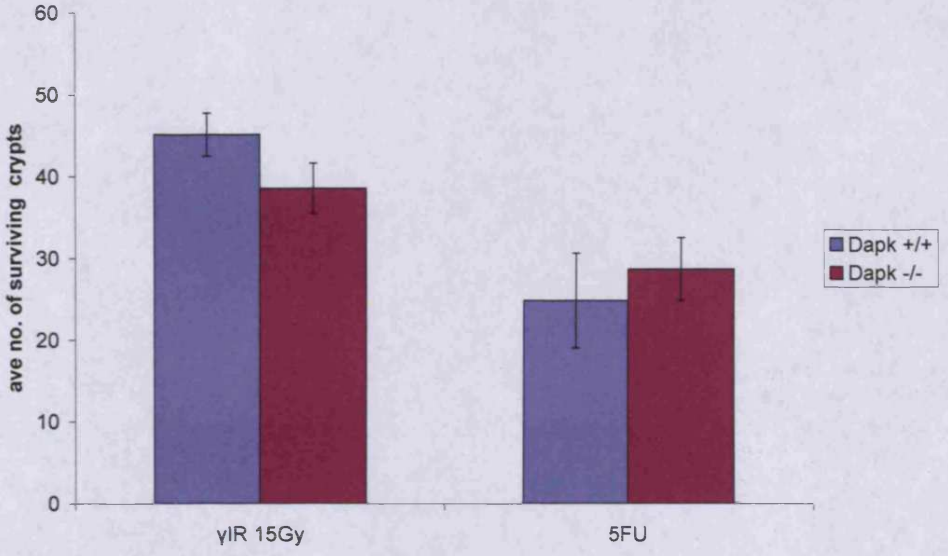

Figure 4.8 – Clonogenic microcolony assay for crypt survival. *Dapk*$^{+/+}$ = Blue bars, *Dapk*$^{-/-}$ = burgundy bars. (15Gy γ-IR: N=6, 1x400mg/kg 5FU:N=3. All error bars = SEM).

Clonogenic survival was investigated to establish if the suppression of apoptosis seen with 5FU or γ-IR translated into an increased survival rate. Figure 4.8 shows that there is no significant difference in clonogenic survival between *Dapk*$^{+/+}$and *Dapk*$^{-/-}$ mice 72hours following administration of 1x400mg/kg 5FU or 15Gy γ-IR as scored by the clonogenic microcolony assay (p=>0.1 MWU for both agents). This indicates the initial decrease in apoptotic response in Dapk null mice is insufficient to lead to inappropriate crypt survival.

4.3.2 Investigating the apoptotic dependency for Dapk following Fas Treatment

Previously, *in vitro* studies have shown reliance for DAPK in mediating the cell death response to endogenous signals such as Fas ligand, TGF-β, TNF and IFN-γ, with expression of DAPK anti-sense RNA protecting cells from Fas induced cell death (Cohen *et al* 1999, Jang *et al* 2002). Mutations of genes involved in the Fas pathway may give selective advantage to cells to escape and survive the death response (Shin *et al* 2002). Following my finding that Dapk could mediate the apoptotic response to DNA damage inducing agents, I decided to look at the *in vivo* role for Dapk in Fas-induced apoptosis by injecting 10μg/kg of anti-Fas/Apo1 agonistic antibody. Tissues were harvested 6 hours later and histologically scored for apoptosis in the Spleen, liver and intestine, all of which show sensitivity to Fas-induced apoptosis (Screaton *et al* 2003).

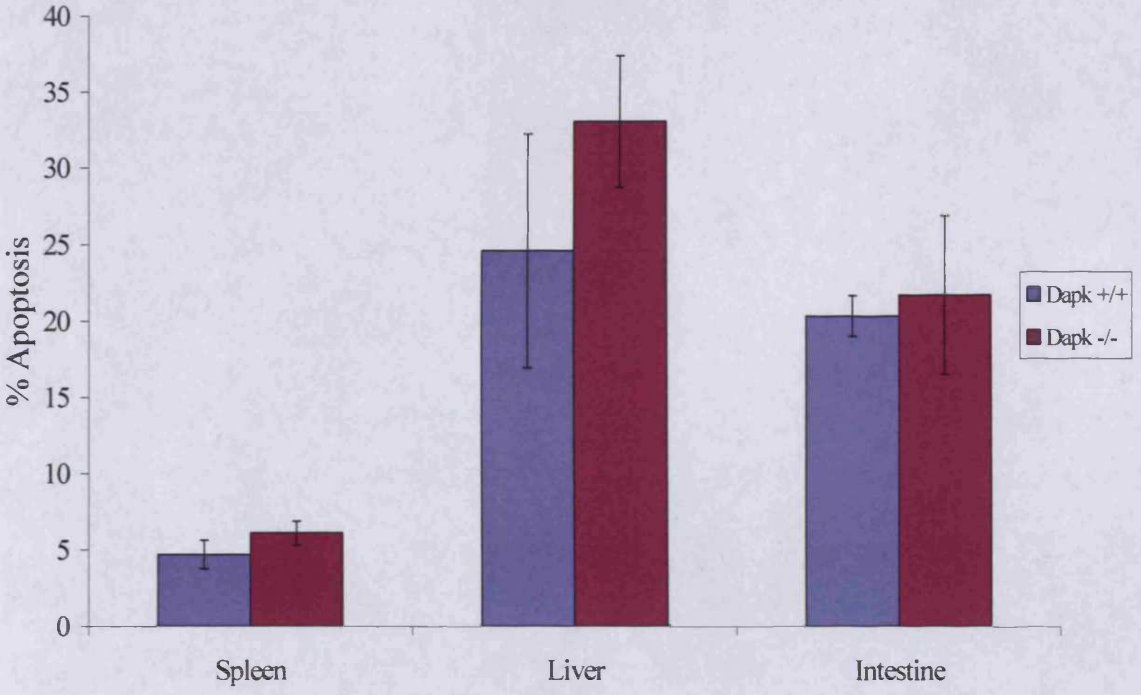

Figure 4.9– Apoptosis scoring in Spleen, Liver and Intestinal crypt cells following 1x i.p. injection of 10µg/kg Fas ligand. *Dapk*$^{+/+}$ = Blue bars, *Dapk*$^{-/-}$ = burgundy bars. (All error bars = SEM, N=3).

Figure 4.9 shows that the levels of apoptosis were elevated in response to Fas treatment in all 3 tissues (Screaton *et al* 2003), but that no change was seen between *Dapk*$^{+/+}$ and *Dapk* $^{-/-}$ genotpyes in the intestine, spleen and liver samples (p=>0.05 MWU). Slightly higher induction of apoptosis in the gut in is seen than that previously reported by Screaton *et al* 2003, although this may reflect differences in the backgrounds of mice.

4.3.3 P21 and p53 analysis

The reduction in apoptosis in *Dapk* $^{-/-}$ mice from figures 4.3C- 4.4 shows a clear dependency for Dapk in response to a subset of agents. P21 is up-regulated by p53 in response to damage and p53 plays a major role in mediating the apoptotic response following DNA damage (Brugarolas *et al* 1995). To try and identify a possible mechanism through which Dapk may mediate cell death in the intestine, I analysed histological sections for p53 and p21 protein levels by IHC.

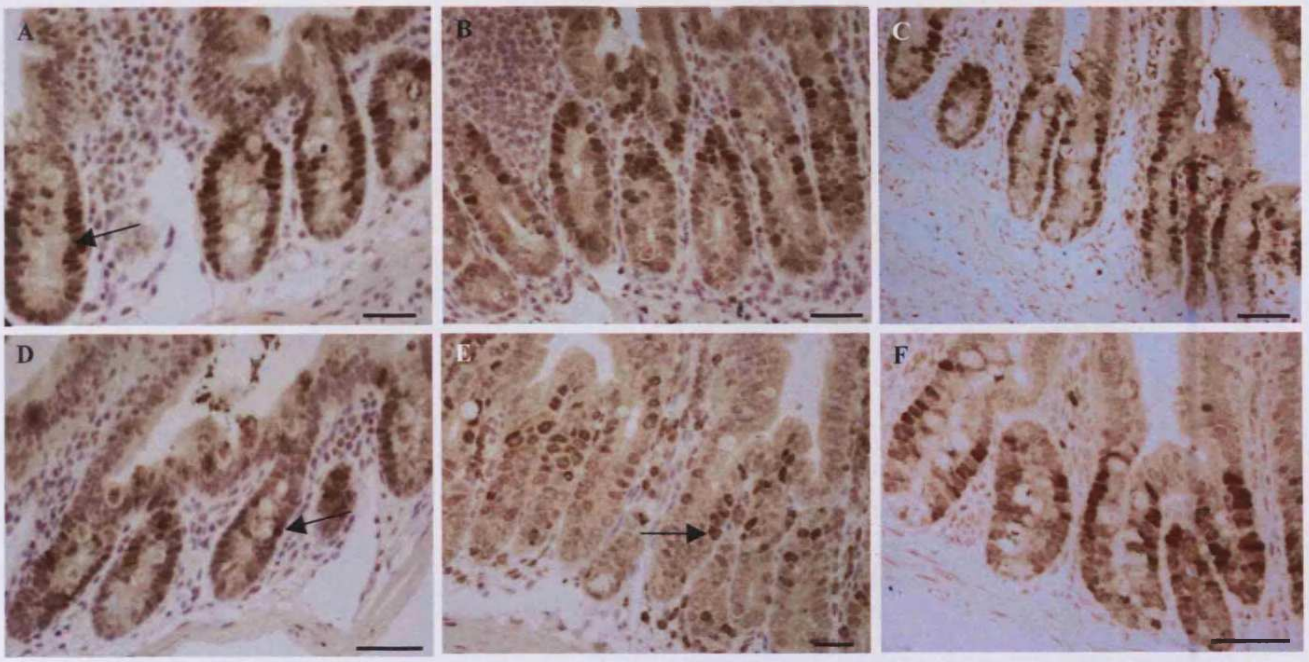

Figure 4.10 – Immunohistochemistry staining for p21. **A,** *Dapk*$^{+/+}$ **B,** *Dapk*$^{-/-}$ IHC staining 6Hrs following 1x 400mg/kg 5FU **C,** *Dapk*$^{+/+}$ **D,** *Dapk*$^{-/-}$ IHC staining 24Hrs following 10mg/kg Cisplatin **E,** *Dapk*$^{+/+}$ **F,** *Dapk*$^{-/-}$ IHC staining 6Hrs following 5Gy γ-IR. (Arrows denote positive staining, all scale bars= 50μm)

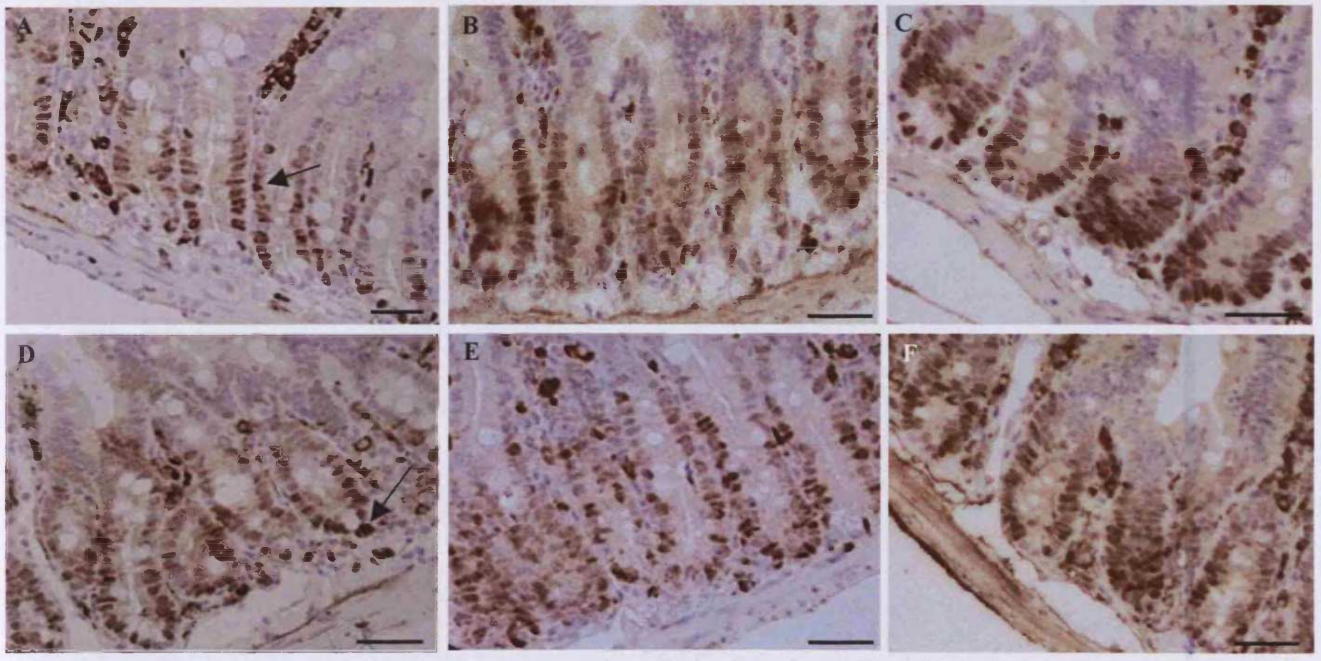

Figure 4.11 – Immunohistochemistry staining for p53. **A,** *Dapk*$^{+/+}$ **B,** *Dapk*$^{-/-}$ IHC staining 6Hrs following 400mg/kg 5FU **C,** *Dapk*$^{+/+}$ **D,** *Dapk*$^{-/-}$ IHC staining 24Hrs following 10mg/kg Cisplatin **E,** *Dapk*$^{+/+}$ **F,** *Dapk*$^{-/-}$ IHC staining 6Hrs following 5Gy γ-IR. (Arrows denote positive staining, all scale bars= 50μm)

Figure 4.10 outlines IHC patterns of staining for p21. No dramatic reduction in staining is seen in *Dapk*$^{-/-}$ mice compared to *Dapk*$^{+/+}$ controls for either 5FU (4.10 **A, D**), Cisplatin (4.10 **B, E**) or 5Gy γ-IR (4.10 **C, F**). Figure 4.10 **B** suggests that there may be down regulation of p21 in the Dapk null in response to 5FU and that this differs to other agents such as Cisplatin (figure 4.10 **B, E**) where no Dapk apoptotic dependency was seen at 6 hours (figure 4.3). In addition, γ-IR treated samples show similar p21 positives between genotypes although *Dapk*$^{-/-}$ mice displayed reduced apoptosis at 6 hours in response to this agent.

Figure 4.11 IHC staining for p53 fails to highlight any marked differences between genotypes for any of the cytotoxic agents used, which suggests loss of Dapk may not affect p53 protein levels.

4.3.4 Western blot analysis

IHC staining from figures 4.10-4.11 gave an indication that Dapk may mediate apoptosis by induction of p21 and that this mechanism may be reduced in *Dapk* $^{-/-}$ mice in response to 5FU. I therefore used a quantitative method such as western blot analysis of whole gut tissue extract to quantify any differences in p21 and p53 induction in *Dapk* $^{-/-}$ mice, and to determine whether this varied between cytotoxic agents. I compared protein samples from one agent that showed a Dapk dependency for apoptosis (5FU) and one agent that displayed no requirement for Dapk (Cisplatin).

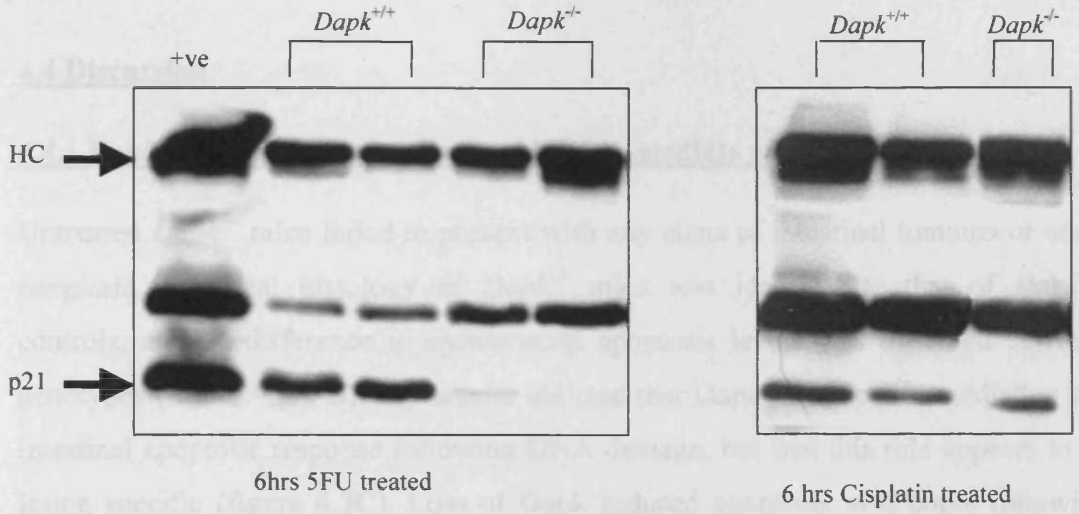

Figure 4.12 - Western blot analysis of p21 protein levels from whole tissue extracts of murine small intestine 6 hours following treatment with either 1x400mg/kg 5FU or 10mg/kg Cisplatin. HC = 60Kda mouse heavy chain IgG to mouse monoclonal antibody used as loading control between samples. 30µg protein loaded for each sample.

Figure 4.12 reveals that 5FU treated samples show significant reduction in p21 in *Dapk* $^{-/-}$ samples compared to *Dapk* $^{+/+}$ controls. This reduction in p21 is not observed in Cisplatin treated *Dapk*$^{-/-}$ samples, strengthening the data from IHC (figure 4.10) that Dapk may induce apoptosis by up-regulation of p21. Western blot analysis for p53 levels was inconclusive due to technical antibody problems and therefore I cannot rule out changes in p53 protein levels.

4.4 Discussion

4.4.1 Dapk is essential for mediation of the immediate apoptotic response

Untreated *Dapk*$^{-/-}$ mice failed to present with any signs of intestinal tumours or other neoplasia. Intestinal histology of *Dapk*$^{-/-}$ mice was identical to that of *Dapk*$^{+/+}$ controls, and no difference in spontaneous apoptosis levels was observed between genotypes (figure 4.3A-B). My results indicate that Dapk is critical in mediating the intestinal apoptotic response following DNA damage, but that this role appears to be lesion specific (figure 4.3C). Loss of Dapk reduced apoptosis at 6 hours following treatment with 5FU, Temozolomide, γ-IR and ENU. Dapk was found to be redundant in the apoptotic response to NMNU and Cisplatin treatment. Cisplatin damage has been shown to signal death via the Caspase 9 response pathway (Mueller *et al* 2003). This may circumvent a role for DAPK in Cisplatin-induced apoptosis as DAPK has been linked to Caspase 8 and mitochondrial mediated death (Cohen *et al* 1999). This may explain the normal levels of Cisplatin induced apoptosis observed in *Dapk*$^{-/-}$ mice in figure 4.3C and 4.4.

Interestingly, Temozolomide, ENU and NMNU give relatively similar ratios of the cytotoxic O6MeG adduct, however the dependency for Dapk in response to these agents differs with Temozolomide and ENU showing reduced apoptosis in *Dapk*$^{-/-}$ mice, and NMNU showing no change (figure 4.3C). Given the many other types of lesion produced from each drug, subtle changes in lesion ratios may initiate different cell death pathways and recruit different apoptotic complexes. Additionally DAPK could be redundant is some of these complexes.

4.4.2 Dapk and the late apoptotic response

As with Mbd4 deficiency (chapter 3), the apoptotic response to cytotoxic agents is not completely eliminated in Dapk null animals. This suggests that there may be some degree of overlap between signalling pathways in the absence of genes such as *Mbd4* and *Dapk*. Indeed p53 and MMR genes such as *Mlh1* have been shown to be involved in signalling damage from all these agents (Clarke *et al* 1994, Pritchard *et al* 1998, Toft *et al* 1999)(Chapter 3). Therefore DAPK loss and decreased immediate apoptosis may not affect the later time points of the death response. In support of this, the

reduced apoptotic levels seen with Temozolomide (figure 4.3C) do not persist 24 hours post-treatment (figure 4.4), and similarly the difference in γ-IR induced apoptosis was restored at the 30 hour time point during the γ-IR timecourse (figure 4.7). This implies that normal induction of the secondary p53-independent apoptotic wave during the response to γ-IR treatment (Clarke *et al* 1997, Merritt *et al* 1997) is sufficient to compensate for Dapk loss after the immediate death response. This late wave is also known to be independent of MMR status (Sansom and Clarke 2002) and induction of other p53 gene family members such as p73 has been suggested to play a compensatory role in the late intestinal apoptotic response, in response to cisplatin treatment (section 3.1.4, Gong *et al* 1999, Shimudaira *et al* 2003). Hence the compensatory mechanism observed at 30 hours in Dapk null mice may be due to p73 activation.

4.4.3 Dapk is required for mediating 5FU induced apoptosis

The involvement of Dapk in mediating the 5FU induced apoptotic response appears to be far more intricate than other agents. As mentioned above, the Temozlomide and γ-IR treated *Dapk*$^{-/-}$ mice show wild type levels of cell death by 24 hours, and 5FU is the only agent in which the apoptotic deficiency in Dapk null mice persists at 24 hours (figure 4.4). However, when investigating the kinetics of this response over an extended timecourse (figure 4.5), it is clear that the role of Dapk in 5FU induced apoptosis is complicated, as the 12 and 20 hour time points show no Dapk dependency. This unexpected pattern may be attributed to complex kinetics of the 5FU response, or may simply reflect low sample numbers (N=3) at these time points when compared to high sample sets at 6 and 24 hours (N=9 and 6 respectively).

BrdU incorporation during this timecourse was measured at 6 and 24 hours to assess changes in the proliferative response. The results from figure 4.6 indicate that loss of Dapk does not affect the levels of proliferation during 5FU cytotoxic damage, and suggests that loss of Dapk may not effect long-term survival in the same way that loss of Mbd4 does (chapter 3). Clonogenic survival assays show that the reduced apoptosis seen in *Dapk*$^{-/-}$ mice in response to γ-IR and 5FU does not bear any effect on the long-term survival of crypts following DNA damage (figure 4.8), a phenomenon reported for several other agents and gene deficiencies (Pritchard *et al* 1998, Sansom and

Clarke 2002)(chapter 3.4.4). Interestingly $p53^{-/-}$ mice also showed no difference in clonogenic survival following similar doses of γ-IR (Merrit *et al* 1997), suggesting that loss of Dapk confers no long-term survival advantage to such cells.

4.4.4 Dapk does not mediate Fas induced apoptosis *in vivo*

Previous reports regarding DAPK and endogenous cytokine induced cell death have greatly contributed to the pro-apoptotic function assigned to DAPK i*n vitro*. My results indicate that Dapk does not mediate Fas induced apoptosis *in vivo* (figure 4.9). Although there is some uncertainty about the kinetics of the delivery of Fas ligand by injection, as Fas is very rapidly induced endogenously, the 6 hour time point does produce elevated apoptosis levels in these tissues and appears sufficient to reject a Dapk dependency for Fas induced death *in vivo*.

This result was unexpected, but there may be several reasons for this finding. Although Fas intrinsic death signalling has been shown to induce both Caspase 8 and 9 dependent pathways (Sun *et al* 1999), DAPK function has only been implicated in the Caspase 8 death pathway (Cohen *et al* 1999), suggesting levels of redundancy or compensation in the Fas response may explain the apparent lack of Dapk dependency for Fas-induced death *in vivo*. Furthermore positive feedback loops that function via Caspase 9 to upregulate receptor mediated death pathways during Fas stimulation may amplify the death response and negate the affects of Dapk loss (Sun *et al* 1999). Additionally many i*n vitro* studies were performed on immortalised cells lines, and my data indicates there are discrepancies between *in vitro* Dapk interactions and the *in vivo* functions. Part of this failure to confirm *in vitro* interactions may be due to the role of DAPK in adhesion and anoikis induced death (Kögel *et al* 2001, Wang *et al* 2002). As yet this cannot be reproduced for intestinal cells in culture and compensatory changes in cell communication networks in $Dapk^{-/-}$ mice may have arisen during development given the constitutive nature of the Dapk knockout mouse.

Finally, the presence of both pro and anti-apoptotic splice variants of DAPK (Jin *et al* 2001 and the finding that expression of antisense DAPK in HeLa cells made cells more sensitive to IFN-γ /TNF induced cell death (Jin *et al* 2003), indicates that

DAPK may play dual roles in survival and cell death depending on stimulus, cellular location and binding partners, although this has yet to be proven *in vivo*. Indeed endogenous ceramide induced apoptosis has been shown to be DAPK dependent in cultured neuronal hippocampus cells (Pelled *et al* 2002), although preliminary experiments injecting C6-ceramide into *Dapk*$^{-/-}$ and control mice failed to induce apoptosis in the intestine.

4.4.5 Dapk mediates p21-induced cell death

The mechanism by which DAPK signals apoptosis is unknown, however my initial experiments suggest an alteration in p21 levels as a possible mechanism (figure 4.10 and 4.12). Figure 4.10 indicates that decreased p21 induction may be responsible for the suppressed apoptotic response to 5FU observed in *Dapk*$^{-/-}$ mice (figure 4.3C), although it is clear that loss of Dapk does not completely abrogate the apoptotic response to 5FU as apoptosis levels are still raised above uninduced samples (figure 4.3C) and p21 IHC positives are still visible on *Dapk* $^{-/-}$ sections (figure 4.10D).

The presence of normal p21 staining in Cisplatin treated *Dapk* $^{-/-}$ mice (figure 4.10 E) suggests that p21 is activated normally in Dapk null mice in response to this agent, and indeed figure 4.3C confirms apoptosis levels to be similar to controls ($p=>0.05$ MWU). IHC for p21 from γ-IR treated mice suggests no difference between genotypes and although there is a dependency for Dapk in γ-IR induced apoptosis (figure 4.3C), this does not appear to be due to lack of p21 (figure 4.10 F). This data adds to the observation that DAPK mediation of DNA damage induced apoptosis is lesion dependent and may have different mechanisms of action depending on cytotoxic insult. It is unlikely that Dapk directly interaction with p21 due to its cytoplasmic localization (Kögel *et al* 2001).

Loss of p21 leads to increased apoptosis after treatment with DNA damaging agents, and is often associated with cancer formation, particularly brain tumours (Makin and Hickman 2000). Recently it was found that p21 deficient mice show reduced apoptosis in colon epithelial cells and were predisposed to formation of ACF – an initiating step in intestinal tumourigenesis. This outlines a role for p21 in apoptosis, albeit in a lesion dependent fashion and as an intestinal tumour suppressor gene

(Poole *et al* 2004). This finding may be relevant to the loss of DAPK reported in CRCs (Raveh *et al* 2001, Nagasaka *et al* 2004, Dong *et al* 2005).

P21 is not required for oncogenic p53-dependent apoptosis (Attardi *et al* 1996), however it is reported to be induced by p53 in response DNA damaging agents (Macleood *et al* 1995), such as those investigated with the *Dapk* $^{-/-}$ mice. The DAPK family have been implicated in regulating the p53 pathway via ZIP kinase interactions with MDM2 and by stabilizing and promoting p21 activity *in vivo*. These interactions may provide a link to the unknown mechanism by which DAPK channels p53 toward apoptosis by p19arf interaction (Raveh *et al* 2001, Burch *et al* 2004). The immediate γ-IR induced death response in the intestine is known to be dependent on p53 at early time points such as 6 hours, and the reduced apoptotic response in *Dapk* $^{-/-}$ mice at this time point may reflect lower levels of p53 activation, as p53 null mice show similar decreased apoptosis in response to γ-IR at this time point (Clarke *et al* 1997). However, Figure 4.11 IHC indicates that p53 is still up-regulated in *Dapk*$^{-/-}$ mice treated with 5FU, Cisplatin and γ-IR.

P21 may also be up-regulated independently of p53 through TGF-β and Smad4 signalling to induce cell cycle arrest. This process also activates Caspase cascades and mitochondrial cytochrome C release and recently DAPK has been found to be upregulated by Smad4 (Jang *et al* 2002). Initial western blots of total p53 protein levels in *Dapk*$^{-/-}$ samples were inconclusive, although Dapk may alter phospohorylation and activity of p53 post-translationally (Burch *et al* 2004). Furthermore, p21 upregulation may be post-translationally (Macleod *et al* 1995) and independent of p53 status, perhaps by the recently identified TGFβ-DAPK interaction (Jang *et al* 2002). Therefore DAPK may be responsible for post-translational phosphorylation and stabilization of p53, thereby inducing p21 promoter binding, or subtly changing the ratio of p53:p21 and as a consequence affecting the dependency for Dapk in the apoptotic response to each agent.

4.5 Chapter summary and conclusions

- Dapk contributes to the initial apoptotic response in the intestine. However, this is highly lesion dependent in a similar manner to Mbd4.

- Dapk may signal apoptosis via p21 activation, although it is unclear whether this is dependent or independent of p53.

- This role in mediating apoptosis fails to predict a clonogenic response *in vivo*.

Dapk is not the first gene to show variable apoptotic dependency to cytotoxic agents in the intestine, as p53 null mice show similar lesion dependent results and are not predisposed to spontaneous intestinal tumourigenesis (Sansom and Clarke 2002). These observations suggest that apoptotic gene dependency and damage response in the intestine is complex, highly tissue specific and may have layers of redundancy, some of which may be mediated by other members of the DAPK family.

The clear presence of a delayed Dapk independent apoptotic mechanism may explain the failure for initial apoptotic defects to translate into clonogenic changes. Crossing *Dapk* mutant mice to create doubly null mutants for genes such as *p53* and the MMR gene *Mlh1* may help to identify further Dapk signalling pathways. These crosses in addition to the Apc^{MIN} background may also discern a role for Dapk loss in accelerating tumourigenesis.

Chapter 5. Investigation of the immediate consequences of Lkb1 loss in the murine small intestine

5.1 Introduction

LKB1 (STK11) mediates several key signalling pathways including: cell cycle arrest, AMPK energy cascades, mTOR mediated growth inhibition, Wnt signalling, Polarity and apoptosis (previously discussed further in chapter 1.5.2- 1.5.6). These major roles in cellular metabolism and homeostasis have implicated LKB1 as a 'master kinase (Lizcano *et al* 2004).

Recent data has provided several indications that correct LKB1 function may protect against intestinal tumourigenesis. For example, Wnt signalling is activated during development in intestinal progenitor cells and in many colorectal cancers. Additionally, nuclear accumulation of β-Catenin has been reported in a subset of PJS polyps (Miyaki *et al* 2000), suggesting loss of LKB1 function may alter Wnt signalling within the intestine and hence predispose to intestinal tumourigenesis in a similar way to APC. Identification of LIP (LKB1 interacting protein), which shuttles LKB1 from the nucleus to the cytoplasm to participate in regulation of TGF-β signalling in complex with Smad4 (Smith *et al* 2001), has added a further intestinal homeostasis pathway to those already linked to LKB1, and also raises the importance of localization regulation to different LKB1 functions.

5.2 AIM

Given the involvement of LKB1 in Wnt and TGF-β signalling, in conjunction with polarity and adhesion roles, it appears LKB1 may be critical in regulating intestinal homeostasis. However, the increasing volumes of *in vi*tro data on novel LKB1 binding partners, activators and substrates have yet to be confirmed *in vivo* and the relevance of these studies is still unclear, as is the contribution of LKB1 loss to tumourigenesis.

Previous analysis of constitutive knockout mice for *Lkb1* has been severely restricted by embryonic lethality at E9.5 (see section 1.5.7) (Jishage *et al* 2002, Ylikorkala *et al* 2001), although heterozygotes are viable and develop phenotypes similar to those patients with PJS (Miyoshi *et al.* 2002, Bardeesy *et al.* 2002).

To define the role played by *Lkb1* in normal intestinal epithelium, I used an elegant inducible Cre-Lox strategy to synchronously delete *Lkb1* from 100% of the small intestine of the adult mouse (as scored by the Rosa26 reporter locus Sorriano *et al* 1999). This approach relies on Cre recombinase driven induction of the Cyp1A transgene in the base of the intestinal crypt following exposure to a suitable inducing agent such as β-napthoflavone (see section 1.11.5). This approach will be used to assess the immediate early phenotypic consequences of Lkb1 loss in the murine small intestine, with an aim to outline a function for this tumour suppressor gene in the intestine. Previous studies using a similar system in the $Apc^{fl/fl}$ mice (Sansom *et al* 2004a), suggests that analysis of tissue homeostasis and cell lineage changes over a short term time course of 3, 4, and 6 days, will provide an insight into the role of Lkb1 in the intestine.

5.3 Results of Immediate Phenotype

5.3.1 High level Cre-mediated recombination

Mice bearing a Lox-P flanked *Lkb1* allele were generated (figure 1A, Sakamoto *et al* 2005) and exposed to four daily i.p injections of β-napthoflavone. Repeated exposure to high dose (80mg/kg) β-napthoflavone (BNF) results in near 100% deletion of loxP flanked alleles within the intestinal epithelium (Ireland *et al* 2004, Sansom *et al* 2004a).

This regime resulted in high levels of recombination within the small intestine of *Lkb1*$^{fl/fl}$ mice as evidenced by recombination at the surrogate Rosa 26R reporter locus (Soriano *et al* 1999) (figure 5.1B-C). Recombination of the LoxP flanked stop cassette in the Rosa26 transgene, allows expression of β-galactosidase and subsequent blue staining of recombined cells (see 2.4.2). BNF targets recombination in the intestinal stem cell, which then repopulates the entire crypt- villus axis with blue recombined cells over approximately 5 days (figure 5.1D). Mice were evaluated for signs of illness and sacrificed at appropriate time points depending on the severity of the phenotype.

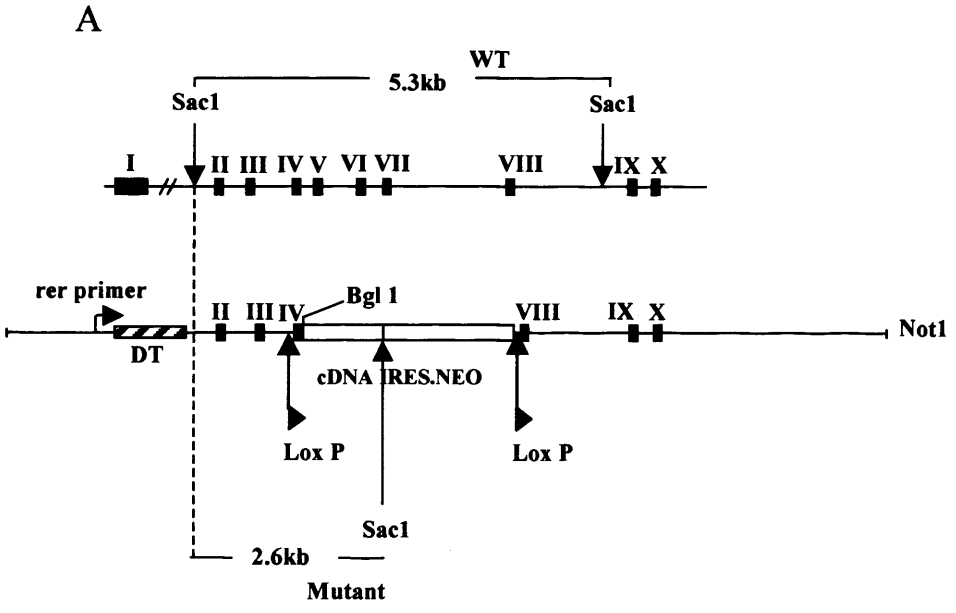

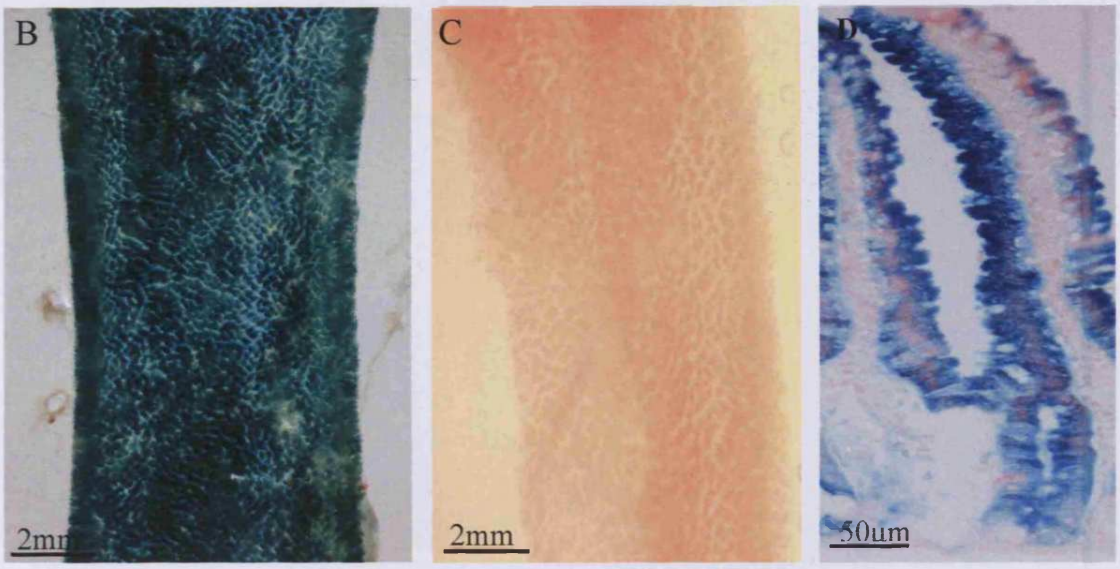

Figure 5.1– Injection with 80mg/kg β-napthoflavone gives 100% deletion of LKB1 in the murine small intestine. **A,** Targeting construct for *Lkb1* transgene, exons 4-8 are replaced by cDNA IRES neo cassette. **B,** Wholemount Lacz staining of $Lkb1^{fl/fl}$ Cre+ gut following 4 daily injections of 80mg/kg β-napthoflavone showing 100% recombination by cre. **C,** $Lkb1^{fl/fl}$ Cre- control. **D,** LacZ histological section from $Lkb1^{fl/fl}$ mouse, blue cells migrate fully to the tip of villus by day 6.

5.3.2 Changes in crypt morphology

Following exposure to BNF, Haematoxylin and Eosin staining of quick fixed gut roles revealed rapid disruption of the crypt/villus architecture in the $Lkb1^{fl/fl}$ compared to $Lkb1^{+/+}$ sections (see Figure 5.2A-H). Histological changes were evident from day 3 in $Lkb1^{fl/fl}$ mice (figure 5.2E), with a small increase in goblet cell number and the appearance of apoptotic and mitotic figures within the crypt. Goblet cell number and size became progressively more noticeable by day 6 (figure 5.2G), with an accompanying increase in crypt size. By day 13 (figure 5.2H), crypts in $Lkb1^{fl/fl}$ mice were grossly overpopulated with dysplastic goblet cells and enterocyte number appeared to be in decline. The base of such crypts showed loss of integrity and mice were sacrificed at this time point due to clear signs of morbidity.

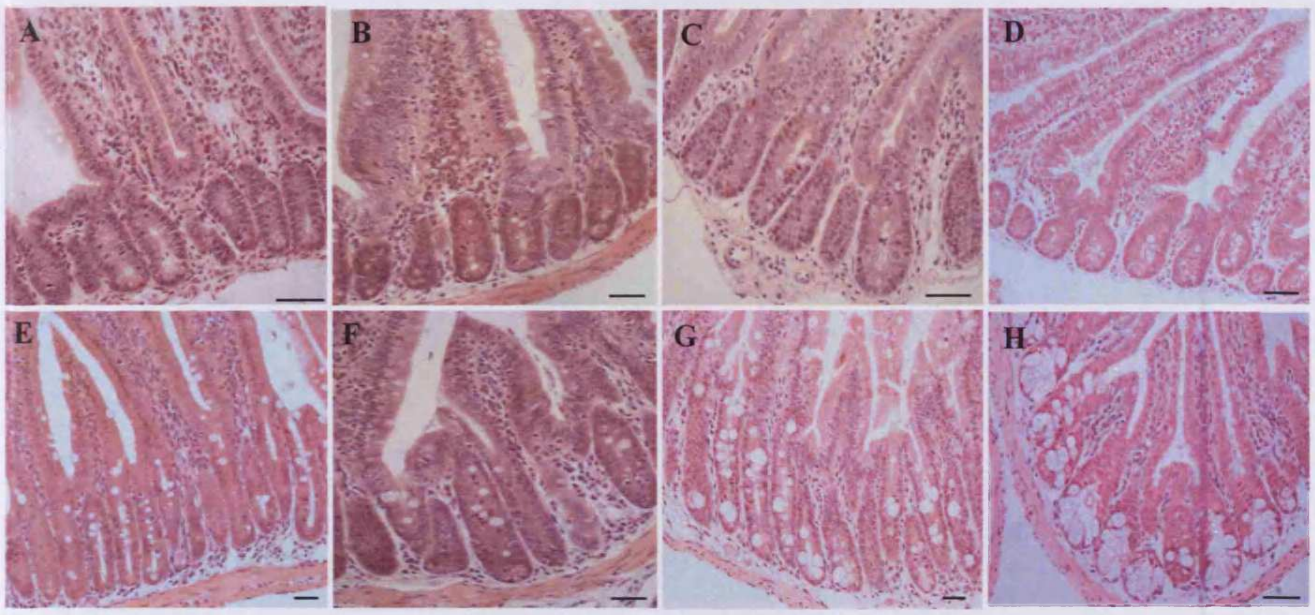

Figure 5.2 - Haematoxylin and Eosin stained sections showing histological changes following loss of *Lkb1*. **A, B, C, D,** *Lkb1*$^{+/+}$ Cre+ mice at day 3, 4, 6, and 13 respectively and **E, F, G, H,** *Lkb1* $^{fl/fl}$ Cre+ mice at day 3, 4, 6, and 13 respectively following recombination with 80mg/kg β-napthoflavone. Disruption of homeostasis is clearly seen from day 3 onwards, and crypt-villus structure is severely perturbed by day 13 (Scale bars = 50μm).

5.3.3 Changes in cellularity

Tissue homeostasis maintains the balance between proliferation and apoptosis and is critical to achieve correct gut function and maintain cell number of the crypt/villus axis. Figure 5.3 shows that at day six, the average number of cells per crypt had increased from 21.9 (+/-0.53sem) cells in *Lkb1*$^{+/+}$ control tissues to 31.3 (+/-1.1sem) cells in recombined *Lkb1*$^{fl/fl}$ tissues (p=0.007 MWU test). Villus cellularity was unchanged at this time point (69.4 (+/-3.6) and 67.2 (+/-12.5) cells respectively). At day thirteen, the mean number of crypt cells in *Lkb1*$^{fl/fl}$ mice was reduced approximate to control levels (*Lkb1*$^{+/+}$, 20.6; *Lkb1*$^{fl/fl}$, 18.2). Mean villus cellularity was also reduced, from 68.7 to 46.0 cells per villus structure in the *Lkb1*$^{fl/fl}$ recombined tissue ($p<0.05$ MWU test).

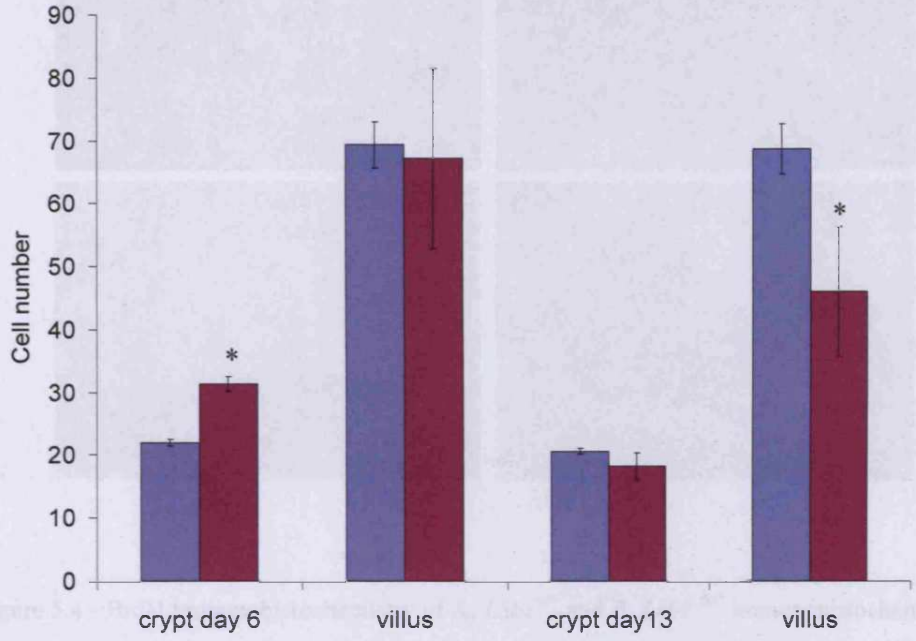

Figure 5.3 - Graph showing changes in epithelial cell number from day 6 to day 13 in both the crypt and villus. $Lkb1^{+/+}$ = blue bars, $Lkb1^{fl/fl}$ = burgundy bars. (Day 6 crypt N=7, All other values N=3, Error bars show SEM * shows significant differences, p=<0.05 by MWU).

5.3.4 Proliferative changes

Given the disruption to intestinal homeostasis observed from figures 5.2-5.3, changes in crypt proliferation were investigated using Bromodeoxyuridine (BrdU) incorporation into S phase. Lkb1 null mice show increased proliferative capacity compared to control mice measured according to BrdU incorporation 2 hours prior to harvesting tissue (figure 5.4B). This increased BrdU staining is retained at day 13, at which point crypt/villus architecture is highly disrupted and mice show signs of morbidity (figure 5.4D).

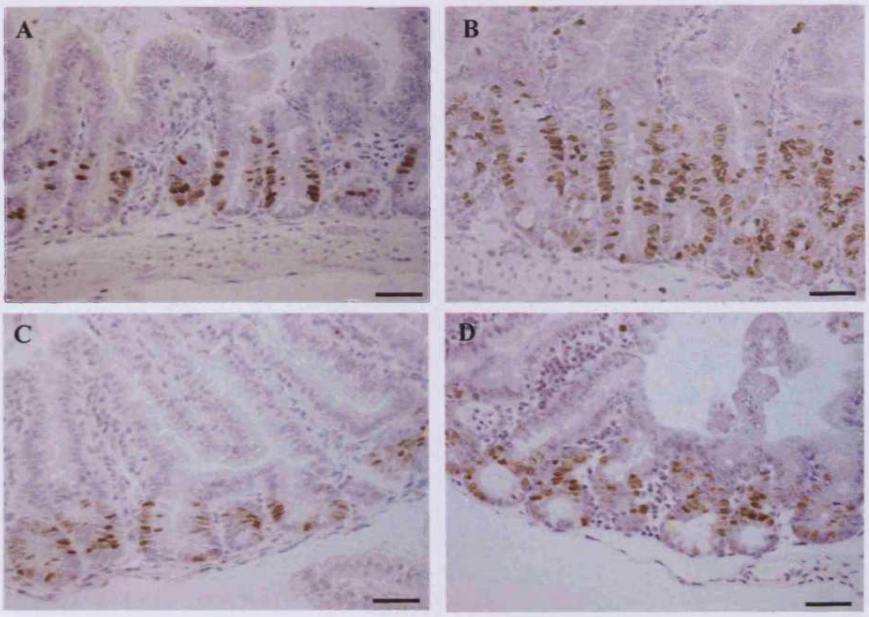

Figure 5.4 - BrdU Immunohistochemistry of **A,** *Lkb1*$^{+/+}$ and **B,** *Lkb1* $^{fl/fl}$ immunohistochemistry staining for BrdU following injection 2 hours prior to harvesting gut tissue at day 6 and **C,** *Lkb1*$^{+/+}$ **D,** *Lkb1* $^{fl/fl}$ 2 hour BrdU staining at day 13 showing retention of proliferative capacity (scale bars = 50μm).

BrdU labelling was further scored as a percentage of the total size of the crypt (% labelling index) to allow for the increase in crypt cellularity noted in Lkb1 deficient mice in figure 5.3. The differences observed in epithelial cell number were indeed reflected in BrdU labelling index at day 6 (*Lkb1*$^{+/+}$, 27.0% (+/-0.57sem); *Lkb1* $^{fl/fl}$, 37.9%(+/-1.4sem), $p<0.05$ MWU, Figure 5.5A), and in the relative size of the proliferative zone (figure 5B), which demonstrates that *Lkb1* $^{fl/fl}$ mice show more BrdU positive cells over a greater area than that of the control animals. Comparative evaluation of proliferative zone location within the crypt revealed a shift upwards in the Lkb1 null proliferative zone relative to the size of the crypt at day 6 (figure 5.5C). For example, *Lkb1*$^{+/+}$ control animals achieve 50 % of their total BrdU positives (cumulative frequency) at a lower position in the crypt than *Lkb1* $^{fl/fl}$ animals (*Lkb1*$^{+/+}$= cell position 5.5, *Lkb1* $^{fl/fl}$ = cell position 12.5 up from the base of the crypt). These results also correlated with changes in Mcm2 staining (figure 5.5D-E), with *Lkb1* $^{fl/fl}$ animals showing an expansion in the number of replication permissive cells in both the enterocytes and goblet cells lineages.

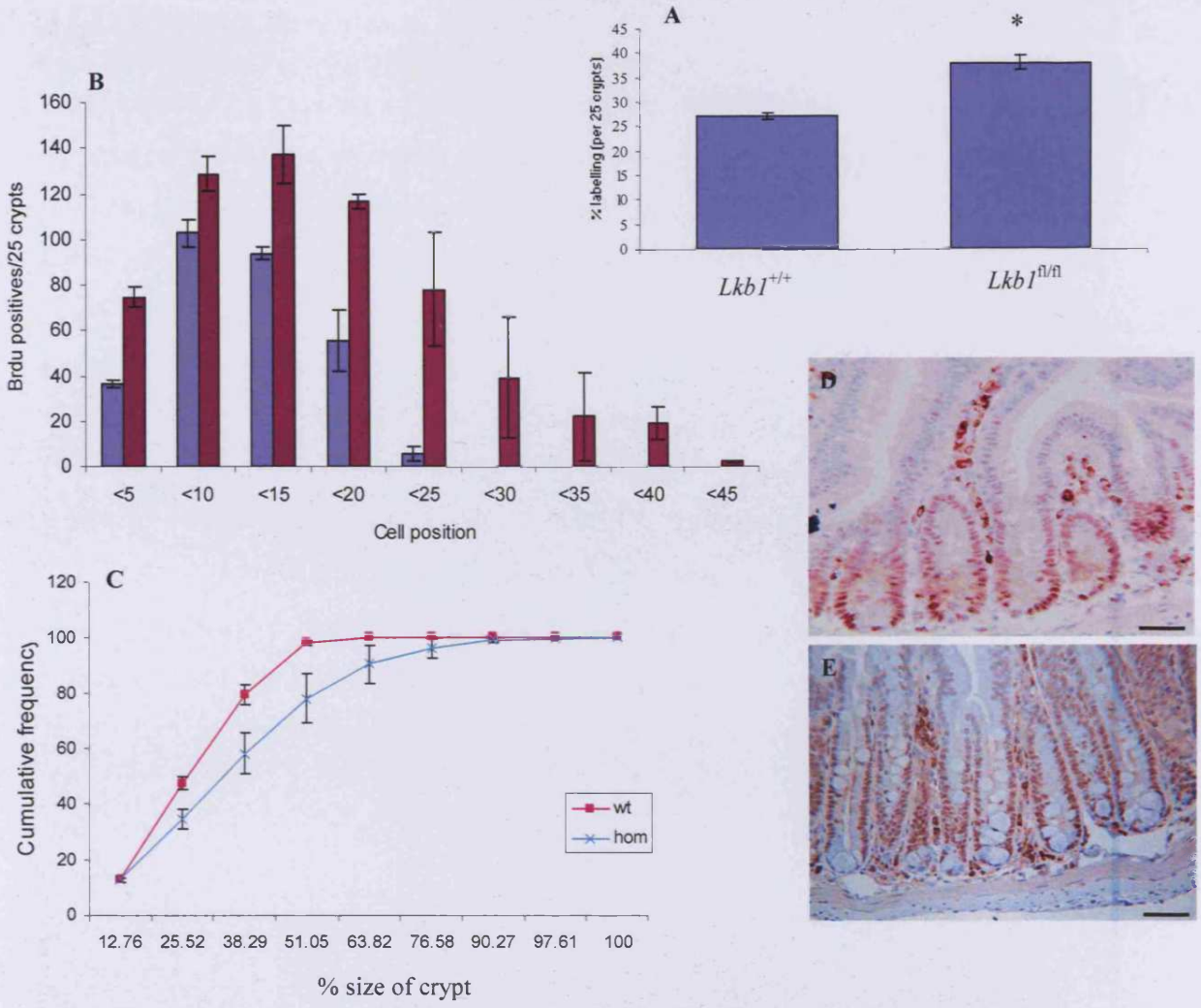

Figure 5.5- **A,** Graph of BrdU labelling as a percentage of the crypt size. **B,** Histogram showing distribution of BrdU positives within crypts of *Lkb1*$^{+/+}$ Cre^{+} mice (Blue bars) and *Lkb1*$^{fl/fl}$ Cre^{+} mice (burgundy bars). *Lkb1*$^{fl/fl}$ mice show expanded proliferative zone compared to *Lkb1*$^{+/+}$ controls. Graph of BrdU labelling as a percentage of the crypt size **C,** Graph comparing relative positioning of proliferative zone within the crypt between *Lkb1*$^{+/+}$ (pink line) and *Lkb1*$^{fl/fl}$ (blue line) mice. (N=3 for all values, error bars = SEM). **E,** *Lkb1*$^{+/+}$ **F,** *Lkb1*$^{fl/fl}$ Cre^{+} immunohistochemistry staining for Mcm2 marker of replicative capacity (scale bars = 50μm).

5.3.5 Changes in spontaneous apoptosis

Previous chapters have assessed the contributions of tumour suppressor gene loss to the apoptotic response following cytotoxic agents. In this chapter I will be assessing the contributions of Lkb1 to normal tissue homeostasis and therefore investigating levels of spontaneous or uninduced apoptosis. Spontaneous apoptosis within the crypt/villus structure helps to maintain correct cell number in a balance with proliferative control of the crypt. Figure 5.6 highlights the uninduced apoptotic changes within *Lkb1* deficient mice. Elevated basal levels of apoptosis are seen within Lkb1 null crypts both at day 6 ($Lkb1^{+/+}$, 2.8% (+/-0.57sem); $Lkb1^{fl/fl}$, 5.1% (+/-0.56sem) $p<0.05$ MWU), and at day 13 ($Lkb1^{+/+}$, 1.4% (+/-0.35sem); $Lkb1^{fl/fl}$, 4.7% (+/-0.92sem), $p =<0.05$ MWU), and similarly in the villus at both time points (day 6 $Lkb1^{+/+}$, 1.4% (+/-0.29sem); $Lkb1^{fl/fl}$, 2.69% (+/-0.58sem) (day 13 $Lkb1^{+/+}$, 1.1%(+/-0.18sem); $Lkb1^{fl/fl}$, 2.5%(+/-0.54sem) $p=<0.05$ MWU).

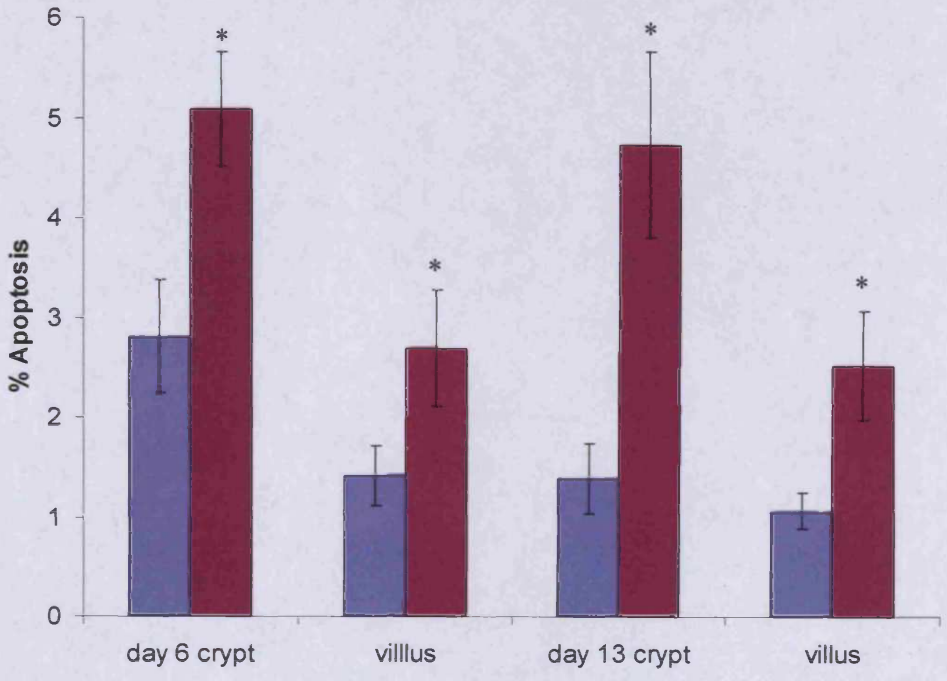

Figure 5.6– Graph showing changes in spontaneous apoptosis 6 and 13 days following injection with 80mg/kg β-napthoflavone (Blue bars = $Lkb1^{+/+}$, burgundy bars = $Lkb1^{fl/fl}$ (N=3, * denotes significant differences, error bars = SEM).

Given the reported interactions of LKB1 with cell cycle arrest and apoptosis and the increase in basal apoptosis detailed in figure 5.6, I decided to investigate the involvement of p53 and p21 activity in the apoptotic response via protein immunohistochemistry.

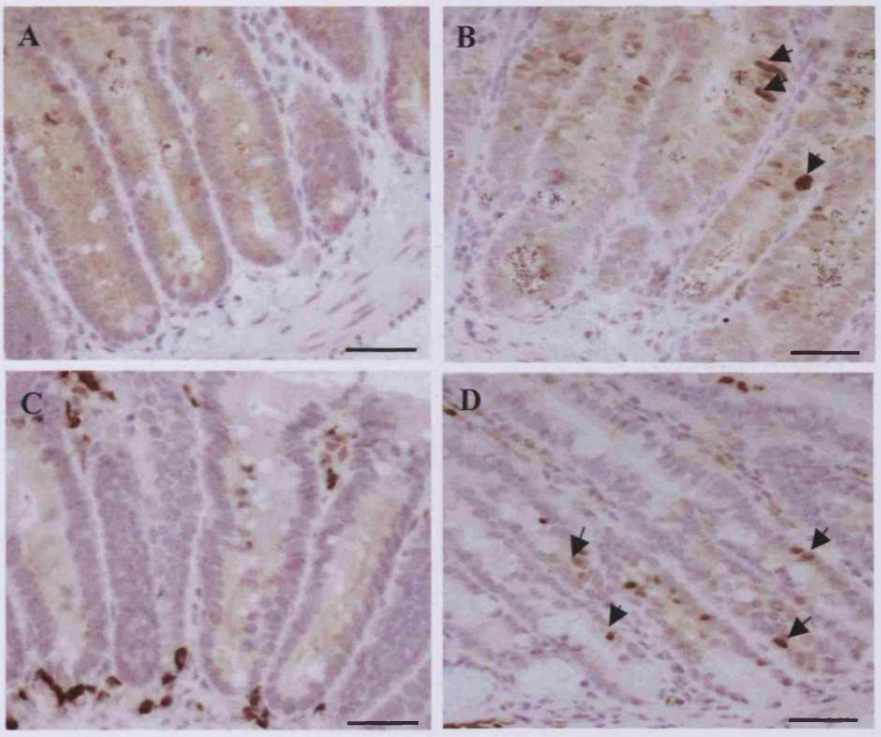

Figure 5.7- Immunohistochemistry staining for **A**, *Lkb1*$^{+/+}$ and **B**, *Lkb1* $^{fl/fl}$ p21 **C**, *Lkb1*$^{+/+}$and **D**, *Lkb1*$^{fl/fl}$ p53 positive staining day 6 following recombination with 80mg/kg β-napthoflavone (arrows denote brown positive cells with large nuclear volume, scale bars = 50μm).

Figure 5.7 shows increases in levels of spontaneous p53 and p21 staining in *Lkb1*$^{fl/fl}$ mice. Positive staining nuclei for both these proteins are rarely seen in wild type animals unless challenged by cytotoxic agents (see chapters 3 and 4) and given that β-napthoflavone injection may raise levels of spontaneous apoptosis, *Lkb1*$^{+/+}$controls (figure 5.7A, C) show very little positive staining when compared to *Lkb1* $^{fl/fl}$ samples (figure 5.7 B, D). Additionally, p21 positive cells in figure 5.7 B appear to have a large nuclear volume (p21+ve = 59.6μm (+/-13.8SD), p21 –ve = 21.37μm (+/-5.1SD) which is associated with cells undergoing G1 cell cycle arrest.

One approach to track the fate of proliferating cells is to score the increase in numbers of BrdU positive cells 24 hours after exposure, an increase that predominantly reflects retention of BrdU in daughter cells. If *Lkb1* deficiency sensitizes cycling cells to death (Bardessy *et al* 2002), this increase is predicted to be reduced relative to controls. To address this, I used mice at day 6 following recombination, and compared total BrdU positives scored from incorporation at 2hr and 24hrs prior to harvesting.

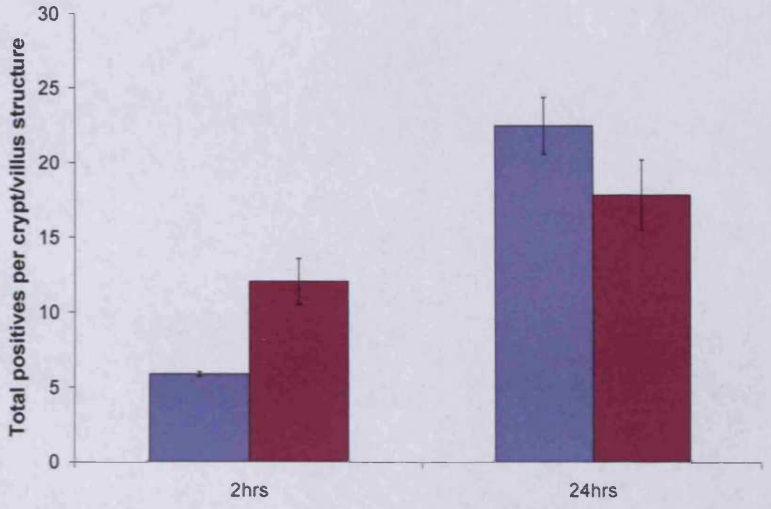

Figure 5.8 –Graph comparing total remaining BrdU positives from 2 to 24 hours. Lkb1 loss increases death within cycling cells (blue bars = $Lkb1^{+/+}$, burgundy bars = $Lkb1^{fl/fl}$, N=3, error bars = SEM).

Figure 5.8 indicates that Lkb1 loss increases death within cycling cells. Indeed over a 24 hour period the mean number of BrdU labelled cells in $Lkb1^{+/+}$controls (Blue bars) increased by 380% from 11.8 to 45.0 positives per crypt/villus structure. Comparable figures in the $Lkb1^{fl/fl}$ recombined tissues (burgundy bars) shows an increase of only 148%, from 24.1 to 35.7 positives per crypt/villus structure.

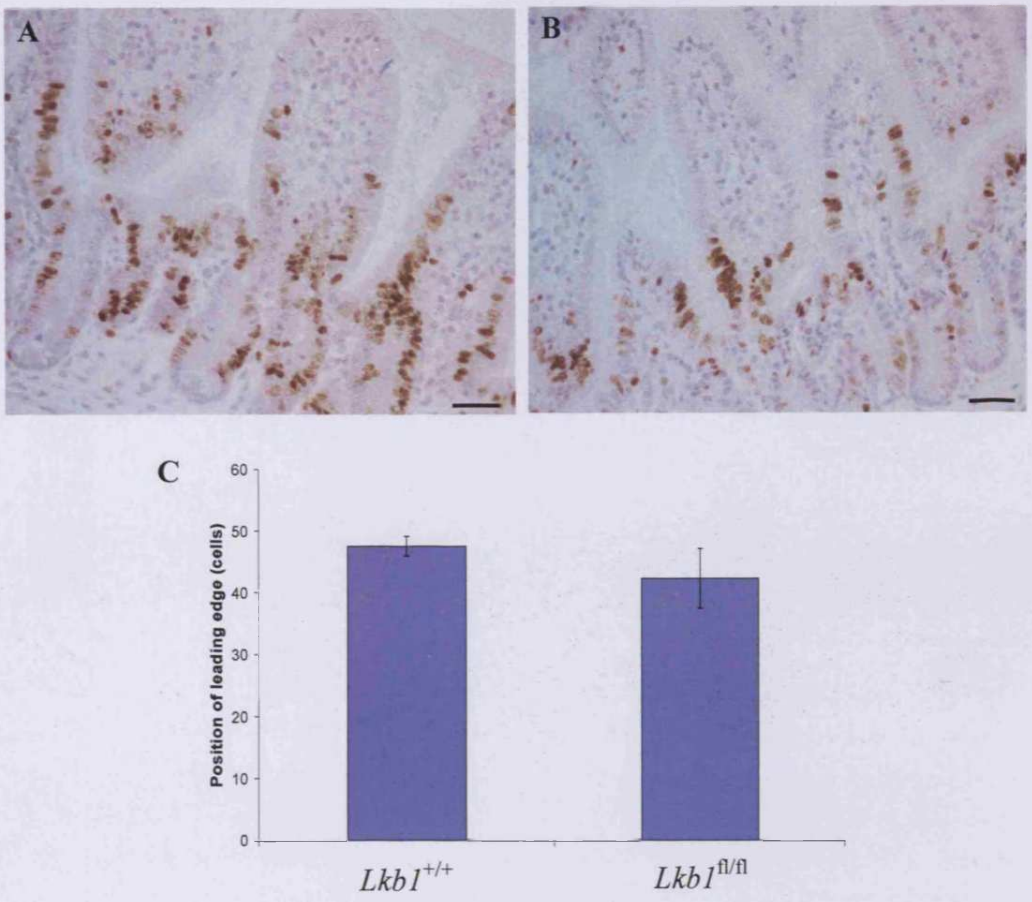

Figure 5.9 – Lkb1 loss does not affect migration **A,** *Lkb1*$^{+/+}$and **B,** *Lkb1*$^{fl/fl}$ immunohistochemistry staining for BrdU 24 hours prior to harvesting at day 6 recombination (scale bars = 50μm). **C,** Graph showing distance migrated by BrdU positive leading edge cells in 24 hours (N=3, error bars = SEM).

When comparing the distance migrated up the crypt-villus axis over a 24 hour period, I found no significant difference between genotypes when comparing the number of cells migrated by the leading edge of the BrdU staining (figure 5.9 A-C, *Lkb1*$^{+/+}$, 47 cells (+/-1.98sem); *Lkb1*$^{fl/fl}$, 43 cells (+/-4.83sem) migrated p =>0.05 MWU). This suggests overall cell migration is unaffected by Lkb1 loss.

5.3.6 Changes in differentiation

Following the increases seen in proliferation and apoptosis and given the dramatic phenotype evidenced in figure 5.2, I next looked at changes in differentiation of the 4 main intestinal cell lineages: goblet, enteroendocrine, paneth and enterocyte cells.

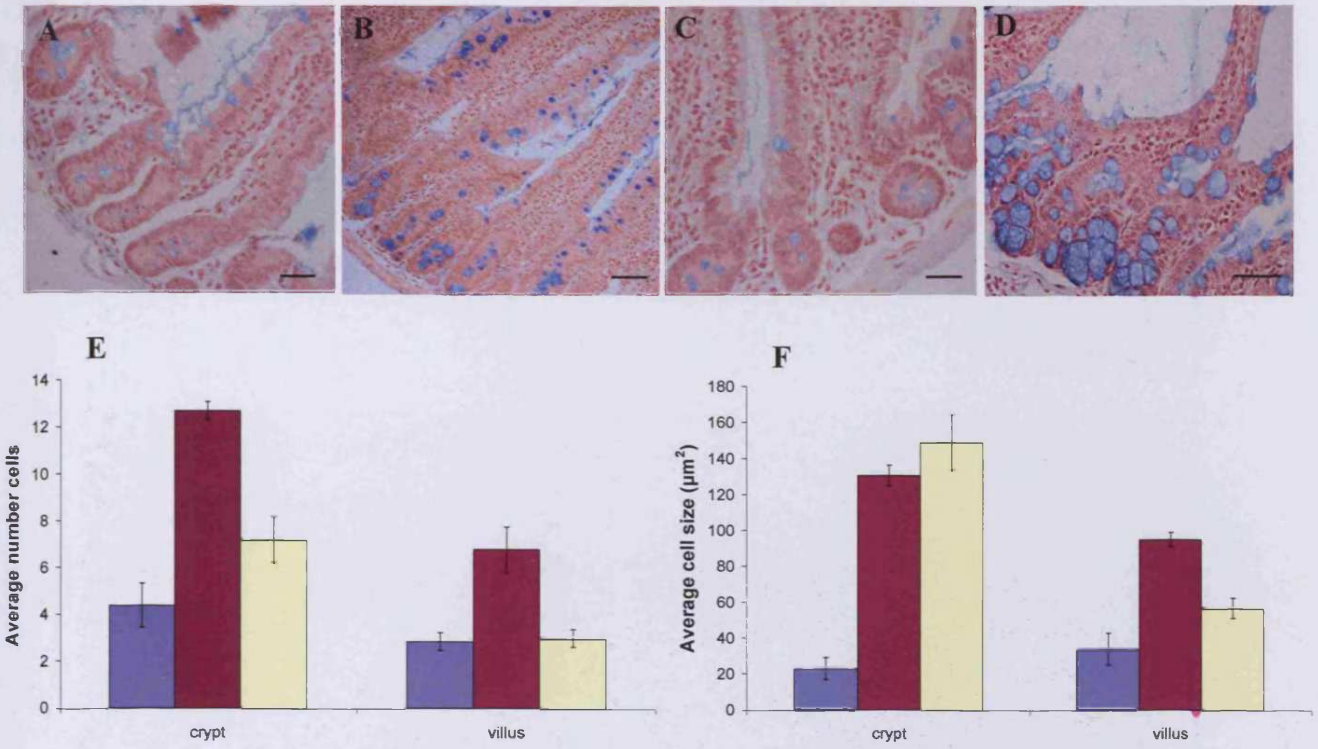

Figure 5.10 - *Lkb1* null mice show massive expansion of secretory cell lineages. **A**, $Lkb1^{+/+}$ and **B**, $Lkb1^{fl/fl}$ Cre^{+} histology samples stained with Alcian blue highlighting goblet cell lineage expansion at day 6 and **C**, $Lkb1^{+/+}$ **D**, $Lkb1^{fl/fl}$ Cre^{+} at day 13 following injection with 80mg/kg β-Napthoflavone (scale bars =50µm). **E**, Graph comparing $Lkb1^{+/+}$ mice (blue bars) and $Lkb1^{fl/fl}$ mice (Burgundy bars day 6), (yellow bars day 13) average goblet cell number per crypt or villus structure. **F**, Graph comparing $Lkb1^{+/+}$ mice (blue bars) and $Lkb1^{fl/fl}$ mice (Burgundy bars day 6), (yellow bars day 13) average cell size in μm^2. (N=3, 25 crypts per animal were counted, error bars = SEM, p=<0.05 MWU for all values).

Alcian blue staining for goblet cells progressively increased in both cell number and cell size in Lkb1 deficient mice compared to $Lkb1^{+/+}$controls (Figure 5.10 A-D). At day 6, controls showed a mean of 4.3 goblet cells per crypt (+/-0.8sem), with an average area of 23μm^2 (+/-6.2sem), and comparable values for $Lkb1^{fl/fl}$ recombined tissue were 12.7 cells (+/-0.3sem) and 130.7μm^2 (+/-5.7sem) respectively (p=<0.05 MWU). Similar increases were also seen in the villus cell populations ($Lkb1^{+/+}$, 2.8 cells (+/-0.3sem) and 33.8μm^2 (+/-8.1sem) ; $Lkb1^{fl/fl}$, 6.8 cells(+/-0.9sem) and 94.9μm^2 (+/-3.9sem) respectively).

Using the combined Alcian blue / Periodic Schiffs staining gives an indication of the distribution of acidic and neutral mucins within the intestine. This is usually determined by the position of the various types of mucin secreting goblet cells and varies upon maturity and differentiation of the cell type. Acidic mucins (blue) are generally located at the base of the crypt and neutral mucins (magenta) further up the villus.

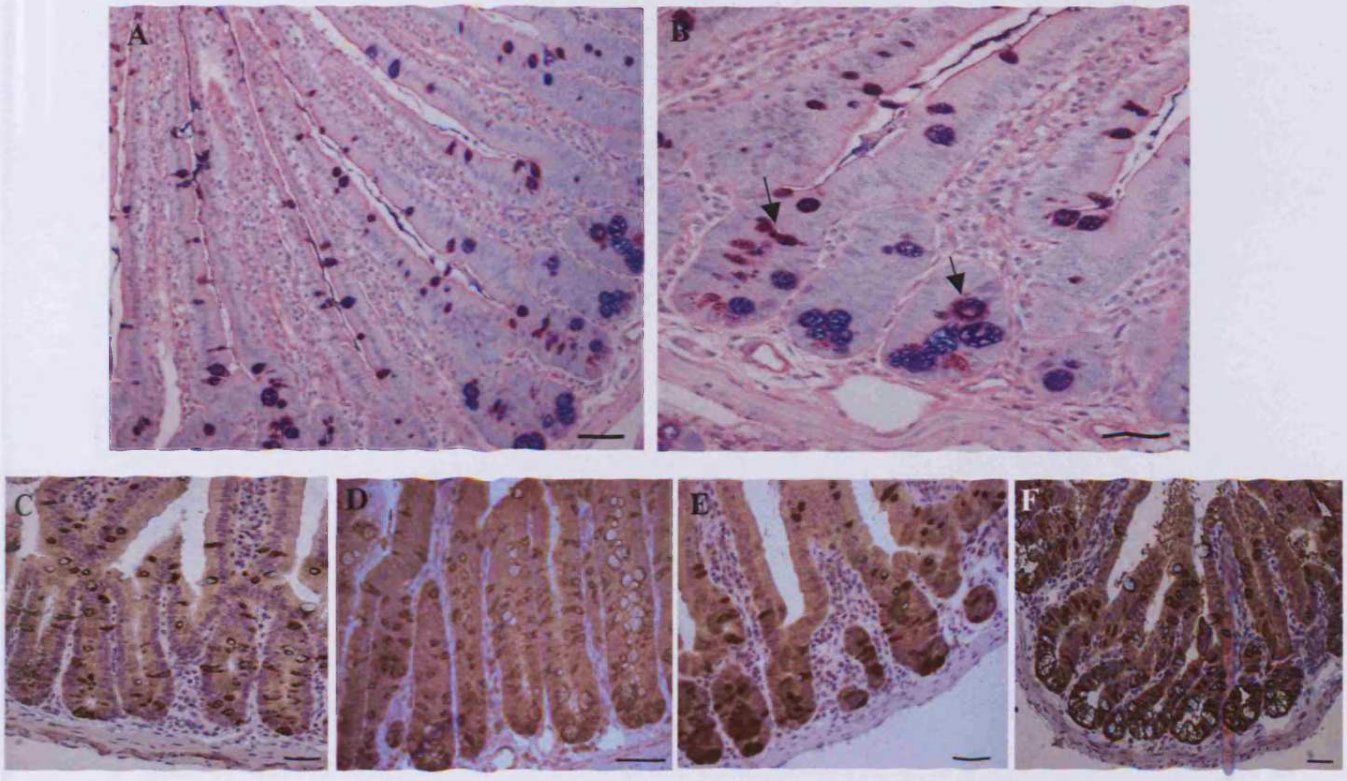

Figure 5.11 - Loss of Lkb1 results in overproduction and mislocalization of mucin types. **A,** Combined Alcian blue and Periodic acid/Schiffs staining for acidic (blue) and neutral (magenta) mucins in *Lkb1* $^{fl/fl}$ murine small intestine. **B,** Close view histology, arrows point to neutral mucins mislocalized to the crypt. Muc2 staining reveals aberrant mucin production in secretory lineages at day 6 **C,** *Lkb1*$^{+/+}$ and **D,** *Lkb1*$^{fl/fl}$ Cre^{+} and at day 13 **E,** *Lkb1*$^{+/+}$ **F,** *Lkb1*$^{fl/fl}$ Cre^{+} (brown staining denotes Muc2 positives, pale blue staining represents Alcian blue positives, all scale bars = 50μm). Muc2 staining carried out by DJ Winton

Figure 5.11 A-B shows some deregulation of mucin distribution with both blue and magenta staining in the base of the crypt and along the villus.

Muc2 is an intestinal marker of mature goblet cells. Goblet cells are most commonly localized to the non- proliferating differentiated villus region of the intestine. However figure 5.11 C-F reveals grossly distended Muc2 staining throughout the whole crypt-villus structure of *Lkb1*$^{fl/fl}$ animals (Figure 5.11 C-F). In addition, Muc2 expression was found to overlie Alcian blue staining in both goblet and paneth cells.

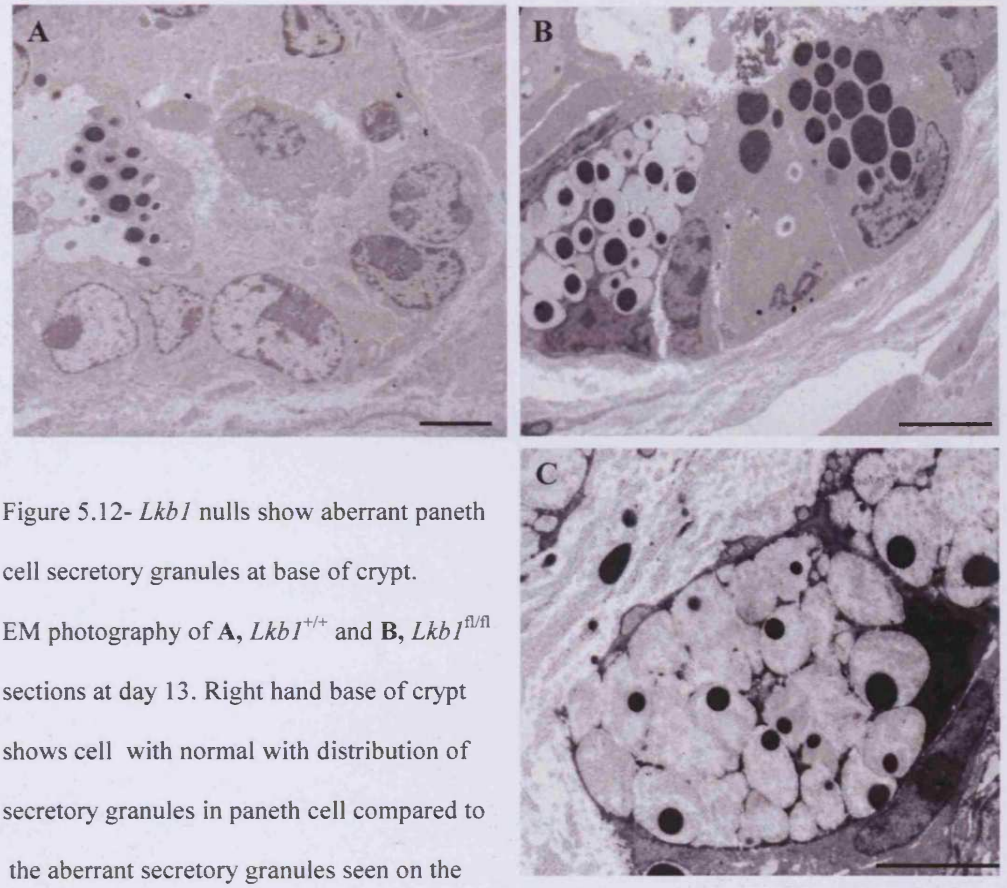

Figure 5.12- *Lkb1* nulls show aberrant paneth cell secretory granules at base of crypt. EM photography of **A,** *Lkb1*$^{+/+}$ and **B,** *Lkb1*$^{fl/fl}$ sections at day 13. Right hand base of crypt shows cell with normal with distribution of secretory granules in paneth cell compared to the aberrant secretory granules seen on the left of the picture. **C,** close up of aberrant granule in *Lkb1*$^{fl/fl}$ (scale bars = 5 μm).

Upon closer EM analysis, *Lkb1* $^{fl/fl}$ crypts displayed goblet cells with aberrant secretory granules more characteristic of paneth cells, in addition to paneth cells distended with mucin (figure 5.12A-C). Further histological analysis (figure 5.13) revealed paneth cell mislocalization up the crypt with many cells some distance from the usual residence at the base of the crypt (Figure 5.13A-B). Furthermore, paneth cell lysozyme granule secretion was found to be aberrantly localized and granules show signs of mucin blockage in *Lkb1* null mice (Figure 5.13 C-D).

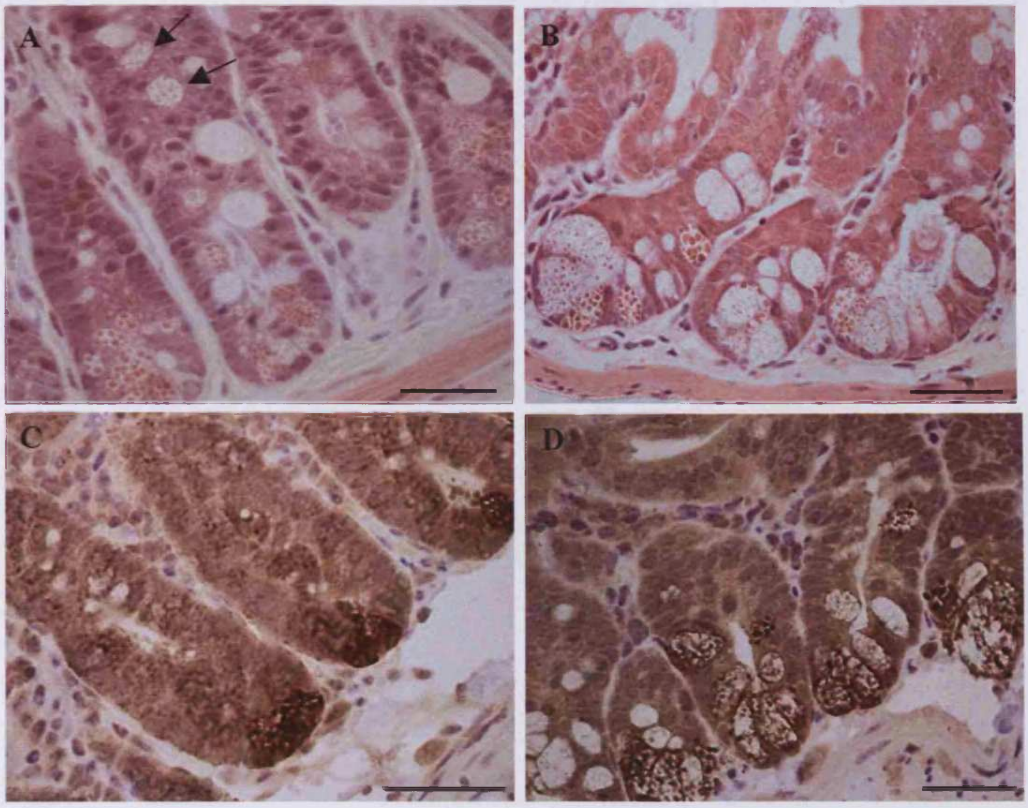

Figure 5.13 - Loss of *Lkb1* produces aberrant and mislocalized paneth cells. **A,** $Lkb1^{fl/fl}$ Cre^{+} 6 days and **B,** 13 days following recombination, arrow demonstrates mislocalized paneth cells mid way up the crypt. **C,** $Lkb1^{+/+}$ and **D**, $Lkb1^{fl/fl}$ Lysozyme staining of paneth cells, showing upward migration and distended granule secretion (scale bars = 50μm). (lysozyme staining carried out by DJ Winton).

In addition to secretory goblet and paneth cells, I investigated disruption of the neuropeptide secreting enteroendocrine cell lineage using Grimelius silver nitrate staining (figure 5.14 A-B). The proportion of positive stained enteroendocrine cells increased within both the crypt and the villus, although this difference only became significant at day 13 in conjunction with the loss of the enterocyte cell lineage. Thus, at day 6 the proportion of enteroendocrine cells within $Lkb1^{+/+}$ crypts was 2.2% (+/-0.4sem) and in the villus was 1.0% (+/-0.2sem). This is compared with values of 2.4%(+/-0.3sem) and 1.1% (+/-0.15sem) respectively in $Lkb1^{fl/fl}$ recombined tissues. At day 13, control values were 2.3%(+/-0.23sem) and 0.4% (+/-0.11sem) respectively, compared to recombined values of 4.2%(+/-0.6sem) and 1.3%(+/-0.23sem) ($p=<0.05$ MWU) (figure 5.14C).

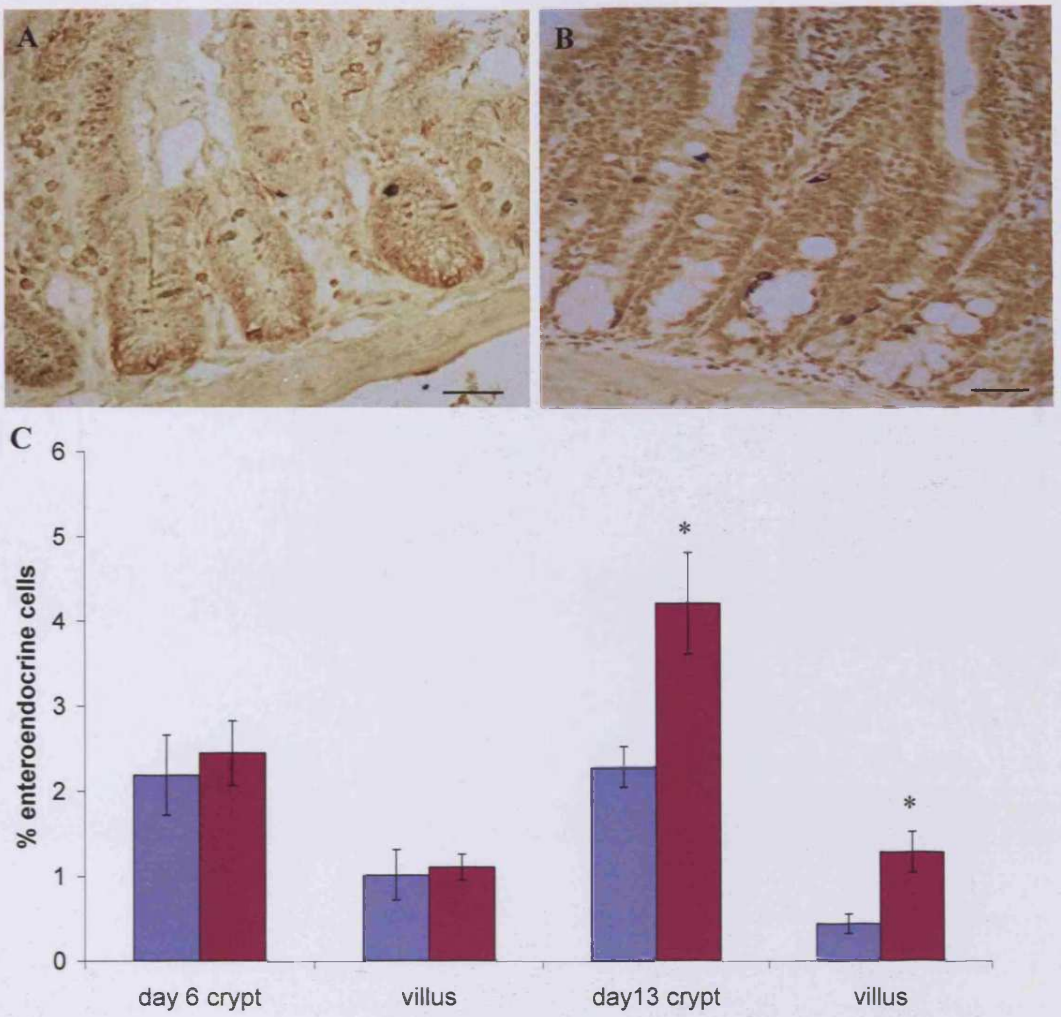

Figure 5.14 - Enteroendocrine cell number increases at day 13. **A,** Day 13 *Lkb1*$^{+/+}$ grimelius staining for enteroendocrine cells **B,** *Lkb1*$^{fl/fl}$ (positive cells stain black, scale bars = 50μm). **C,** Graph showing significant increases (*) in enteroendocrine cells at day 13 in *Lkb1*$^{fl/fl}$ mice. Blue bars = *Lkb1*$^{+/+}$, burgundy bars = *Lkb1*$^{fl/fl}$ (N=3, p=<0.05 MWU).

5.3.5 Epithelial cell Polarity

Given the recent findings that LKB1 plays a crucial role in formation of apical brush borders, I undertook EM analysis of the *Lkb1*$^{fl/fl}$ intestinal epithelium to look for any changes in Basolateral to Apical cell polarity in addition to presence of brush borders (microvilli described in figure 1.4). Brush borders were determined by EM analysis and by the presence of villin staining – a cytoskeletal associated marker present only in the brush border forming differentiated cells of the villus.

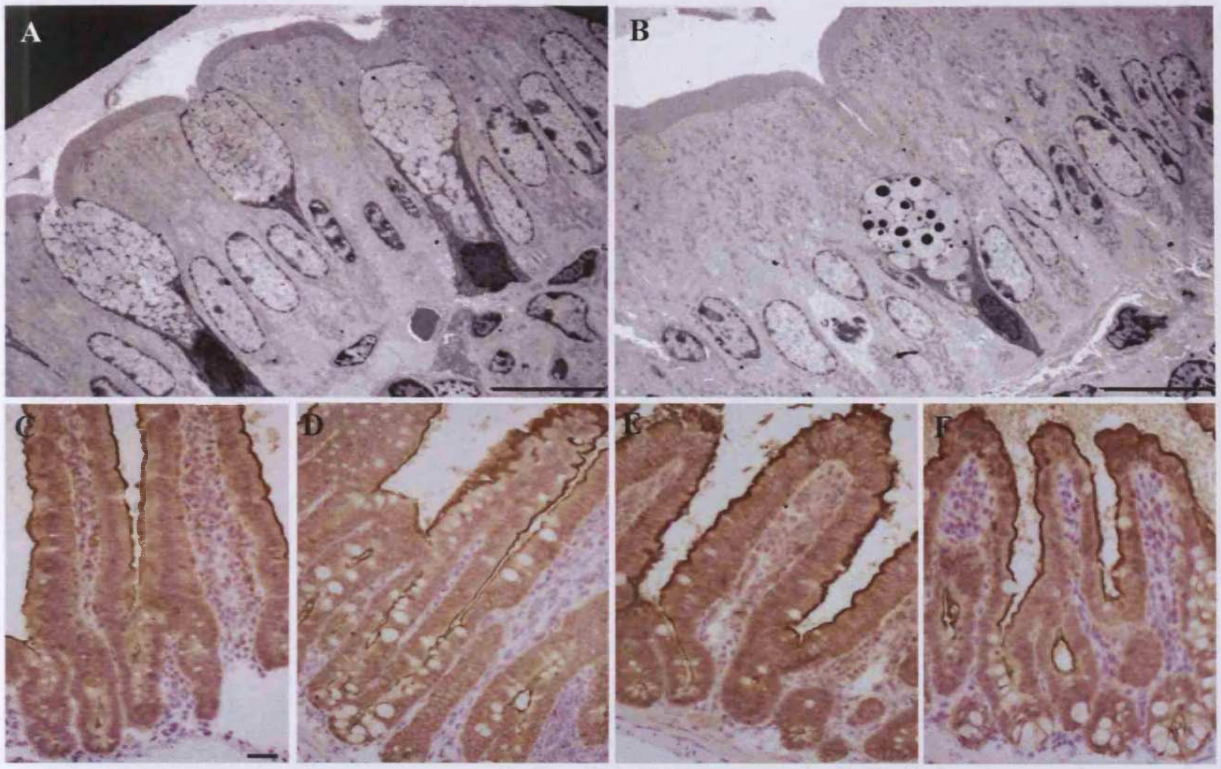

Figure 5.15 - **A,** EM picture of *Lkb1*$^{+/+}$ and **B,** *Lkb1*$^{fl/fl}$ Cre^{+} intestinal villus epithelium displaying normal apical polarity and presence of brush border (scale bars = 10μm). **C,** *Lkb1*$^{+/+}$ and **D,** *Lkb1*$^{fl/fl}$ Cre^{+} histological sections were stained using villin as a marker of cytoskeletal and villus organisation at day 6 and **E,** *Lkb1*$^{+/+}$ **F,** *Lkb1*$^{fl/fl}$ at day 13 following Cre mediated recombination (Scale bars = 50 μm). (Villin staining carried out by DJ Winton).

Upon examination of EM photography (figure 5.15 A-B), I observed no changes in polarity 6 days following *Lkb1* loss, with retention of both correct basolateral polarity and brush borders. Furthermore, the pattern of Villin expression is unperturbed in all samples, again supporting the presence of the brush border along the villus axis following loss of *Lkb1* function (figure 5.15 C-F).

5.4 Discussion

5.4.1 Lkb1 loss results in disrupted crypt cellularity and aberrant proliferation

Initial results show that 4 daily injections of BNF were sufficient to achieve 100% recombination in the murine small intestine (figure 5.4B). Histological analysis of Lacz staining revealed blue cells colonising the entire crypt-villus structure by day 6, therefore indicating that floxing has occurred in the stem cell region and repopulated the entire crypt-villus structure. In addition, crypt/villus repopulation shows apparent normal migration at day 6 in the *Lkb1*$^{fl/fl}$ mice, unlike the *Apc*$^{fl/fl}$ AHCre model which displays aberrant 'packing' of blue recombined cells at the crypt villus junction and perturbed migration (Sansom *et al* 2004a).

Several distinct morphological changes are observed in the *Lkb1* homozygote by day 6 (Figure 5.2). First, crypt cellularity is increased from 22 to 31 cells in the *Lkb1*$^{fl/fl}$ mouse (Figure 5.3). In part this increase in crypt size can be attributed to the increased proliferative burst observed in figures 5.4-5.5. Figures 5.4-5 reveal BrdU incorporation into S phase is increased in the Lkb1 knockout at day 6 (*Lkb1*$^{+/+}$, 27.0%; *Lkb1* $^{fl/fl}$, 37.9%, p=<0.05 MWU, Figure 5.5A). This phenotype confirms a role for Lkb1 in cell cycle control (as previously reported by Tiainen *et al* 1999, Marignani *et al* 2001). In addition, the proliferative zone in *Lkb1*$^{fl/fl}$ mice was clearly expanded to cover a greater area of the crypt than the usual mid-upper third of the crypt area, with BrdU positive cells throughout the entire crypt length (figure 5.5 B). The amplification zone is also relocated higher in the crypt compared to *Lkb1*$^{+/+}$controls (Figure 5.5C). Regulation of proliferation in the crypt is not purely cell-autonomous, with distinct separation of amplification and differentiation zones observed along the crypt-villus axis (Sancho *et al* 2004). Mcm2 staining gives a measure of replicative ability, and should therefore also overlie the amplification zone. Recent collaboration has shown the Lkb1 null to exhibit increased staining for Mcm2 (figure 5.5D-E), and of note is the lack of distinct amplification zone, which overlaps with areas key to the differentiation process. In this scenario terminally differentiated cells such as the goblet cell lineage are seen to stain positive for Mcm2 (figure 5.5 E).

5.4.2 *Lkb1*$^{fl/fl}$ cells are sensitized to Apoptosis

Proliferative bursts are often accompanied by compensatory increases in the apoptotic programme. Previous reports show expression of LKB1 in epithelial cells and the stem cell region, and as a result it has been proposed that hamatomatous polyps arise from a dysregulation of the apoptotic response and/or proliferative alterations (Sancho *et al* 2004)

Clearly the initial increases in crypt size at day 6 (figure 5.3) fail to persist through to day 13 where *Lkb1*$^{+/+}$ and *Lkb1*$^{fl/fl}$ mice show no significant differences in enterocyte cell number in the crypt region (figure 5.3). However, *Lkb1*$^{fl/fl}$ mice show a significant reduction in villus length and enterocyte cell number by day 13, perhaps suggesting over compensation of an apoptotic mechanism or alternatively targeted deletion of *Lkb1* floxed cells. Figure 5.6 confirms that significant increases in apoptosis are detected in both crypt and villus of *Lkb1*$^{fl/fl}$ at both time points compared to similarly dosed control mice ($p=<0.05$ MWU). Deregulation of the apoptotic programme in the absence of *Lkb1* is not entirely unexpected, although contrasting reports have linked LKB1 to p53-dependent apoptosis (Karuman *et al* 2001) whereas *Lkb1*$^{-/-}$ MEFs are reported to be extremely sensitive to cell death (Bardeesy *et al* 2002). One role proposed for LKB1 is in mediating protection from stress at times of high energy demand, including deregulated proliferation (Shaw *et al* 2004a). Certainly oncogenic transformation of cells is highly energy consuming, and death promoting p53 activation was considered a by-product of Ras stimulated Lkb1 null MEFs (Morin and Huot 2004). Increases in cellular AMP levels resulted in *Lkb1*$^{-/-}$ cells undergoing apoptosis due to changes in the balance of stress signalling molecules. C-Jun and P38 were both found to be activated in *Lkb1*$^{-/-}$ MEFs and ERK and AKT survival signals were not, hence tipping the balance in favour of cell death (Shaw *et al* 2004a).

In conjunction with Lkb1 loss, β-Napthoflavone metabolism may cause an additive stress to floxed cells and predispose to apoptosis. Further characterisation of the immediate apoptotic response and analysis of apoptosis within long term knockouts may shed light on the lasting effects of Lkb1 loss.

Figures 5.8 and 5.9 investigate the issue of cell death or fate by following BrdU labelled cells as they migrate up the villus in 24 hrs. As briefly mentioned in figure 5.8, *Lkb1*$^{-/-}$ mice show a net decrease of labelled daughter cells from 2 to 24hrs of BrdU labelling when compared to *Lkb1*$^{+/+}$ controls (*Lkb1*$^{+/+}$= 380% increase from 11.8 to 45.0 per crypt/villus structure, *Lkb1*$^{fl/fl}$ = 148%, from 24.1 to 35.7 per crypt/villus). Clearly Lkb1 recombined proliferative cells seen at 2hrs in the crypt are being deleted as they migrate up through the crypt villus junction and along the villus. This gives a decreased enterocyte cell population by day 13 as detailed in figure 5.3. As the migration pattern of the Lkb1 homozygote reflects that seen in the *Lkb1*$^{+/+}$ control (figure 5.9), the differences observed in the expansion and relocation of the amplification zone appear to exert little influence on the migration of labelled daughter cells. Together these data indicate that *Lkb1* deficiency elevates cell death within cycling cells, perhaps in an attempt to delete aberrant cells from the system.

As LKB1 has direct interactions with p53 (Ferrandes *et al* 2005, Karuman *et al* 2001), immunohistochemistry was performed against p21 and p53 following loss of Lkb1. Figure 5.7 confirms that both p53 and p21 are upregulated as a result of Lkb1 loss. This is contrary to expectation from previous reports implicating LKB1 in mediating p53 dependant apoptosis. However, LKB1 has been shown to induce arrest via p21 (Shen *et al* 2002), and over expression of LKB1 lead to G1 arrest in Hela cells but not apoptosis (Tianen *et al* 1999). Thereby suggesting a backseat for LKB1-P53 binding activity, in favour of an important role in cell cycle arrest. Indeed LKB1 is seen to induce apoptosis only with functional p53, and may not act to activate p53 alone, thereby requiring additional signals for complex activation (Tianen *et al* 1999).

As suggested above, LKB1 may only be required for a subset of p53 dependent apoptosis and levels of redundancy or tissue specificity may exist as with many other genes involved in the cell death programme. Differential LKB1 induced sensitivity to apoptosis has been reported in a number of cell types, with AMPK activation mediating both anti and pro apoptotic effects in a cell specific manner (Marigani 2005). Alterations in large cellular macromolecules such as long chain polyunsaturated fatty acids in the membrane can cause damage and reactive stress to a cell, leading to activation of the death response (Zhou *et al* 2001). Given the input of

LKB1 into the metabolic pathway, loss of metabolic control may give rise to many of the stresses that sensitize to death.

Hsp90 and Cdc37 stabilize LKB1 and protect it from proteosome degradation. Additionally Hsp90 is also commonly involved in the stress signalling response and Hsp90 with Cdc37 stabilizes LKB1 and protects it from proteosome degradation in the response to cellular energy crisis. Elevated apoptosis has been reported in mouse knockout models for *Hsp90*, creating an interesting link between LKB1 mediated AMPK activation and Hsp90 protection (Boudeau *et al* 2003, Marignani *et al* 2001).

Both AMPK and TSC2 activation prevent overgrowth and protect against death when energy sources are low. Not surprisingly the death response is elevated when either are dysfunctional (Luo *et al* 2005). As LKB1 lies upstream of both AMPK and TSC2, lack of input to either arms of the pathway may contribute to increased apoptosis. In terms of cancer cell therapy, AMPK reactivation may be of benefit to induce apoptosis in tumour cells sensitive to mTOR, fatty acid synthesis or p21 activation.

It is also of note to mention that in previous constitutive mouse models of Lkb1 loss, heterozygote mice exhibiting hepatocellular carcinomas (HCCs) display increased apoptosis as a result of inhibition of TGF-β signalling (Nakau *et al* 2002). Furthermore, given that apoptosis levels are usually decreased in late stage malignancies such as HCC, PJS patients predisposition to further malignancies may be a reflection of an additional genetic lesion altering the apoptotic response rather than an initiating event. Further investigation of the possible molecular mechanisms underlying the Lkb1 null phenotype will be further discussed in chapter 6.

Subsets of PJS polyps have shown decreased LKB1 staining and reduced apoptosis. COX2 may increase apoptosis in addition to changes in increasing angiogenesis, ECM adhesion and remodelling. *Cox2* induction by oncogenic Ras in *Lkb1*$^{+/-}$ heterozygote mice increased adhesion and decreased apoptosis within the intestine, suggesting that without additional oncogenic stimulus, the increases in apoptosis detailed above may not reflect Cox2 involvement but as mentioned previously an overwhelming energy crisis facing the cells (Rossi *et al* 2002). Given the

inconsistency in genetic disruptions within hamartomas, it appears more likely that COX2 activation may be a later stage change and is not directly linked to LKB1 signalling.

From my data collected on loss of Lkb1 and apoptosis *in vivo*, it seems a likely scenario that the increases in apoptosis may reflect the immediate consequences of Lkb1 loss, and indeed the dramatic overgrowth of certain cell populations provides an extra stress upon the normal crypt population, leading to increased levels of apoptosis. This situation provides an apparent defence mechanism by which to eliminate inappropriately stressed or aberrant cells.

5.4.3 Changes in differentiation and cell lineage

The net outcome of these dramatic changes to intestinal homeostasis is a switch in the differentiation programme to the goblet/paneth cell secretory lineage. My investigations revealed goblet cells were severely deregulated both in size, frequency and position (figure 5.10-5.11). The aberrant goblet cells were grossly dysplastic, aberrantly staining positive for proliferative markers such as Mcm2 (figures 5.5D-E), and secreting vast quantities of mucins compared to the wild type animals (figure 5.10, 5.12). Indeed hyperdifferentiation and overproduction of mucin are common features of benign hamartomas characteristic of PJS (Hemminki *et al* 1997, Sancho *et al* 2004), and inappropriately dividing differentiated cell types have been reported in many intestinal neoplasias (Wong *et al* 2000).

Mucin production also depends on positional cues along the crypt villus axis, and is mostly seen in the non-proliferating villus region. Here however (see figure 5.5D-E, 5.10-5.11), grossly dysplastic hyperdifferentiated goblet cells are seen throughout the whole structure including the proliferative crypt region, suggesting perturbed positional signalling. The *Lkb1*$^{fl/fl}$ mouse shows a proliferative zone that spans from the base of the crypt up to position 35 (figure 5.5B). This expansion of proliferation and subsequent overlap of the differentiation zone may explain the aberrant differentiation and localisation of the secretory lineages.

The PAS assay (figure 5.11A-B) also reveals dysregulation of maturation within the goblet cell lineage. Acidic mucins normally secreted at the base of the crypt are distributed aberrantly along the villus and in contrast neutral mucins normally detected in the villus, are apparent in the crypt base. This suggests failure to differentiate into appropriate goblet cell sub groups. Milano *et al* report intestinal goblet cell metaplasia and an associated switch in mucin production from sialomucin to sulphomucins in rats following treatment with a γ-secretase inhibitor- usually associated with Alzheimers treatment. This switch to less neutral mucin types is considered to predict increased cancer risk (Milano *et al* 2004). Clearly the increased inappropriate differentiation has given rise to an overwhelming population of apoptosis resistant goblet cells displaying aberrant patterns of localization, secretion and cell size.

The majority of lineages migrate upwards along the crypt -villus axis where they are shed into the lumen or undergo apoptosis within a 3-5day period. Migration patterns in *Lkb1*$^{-/-}$ nulls appear unperturbed, as confirmed by Rosa26R lacz cell repopulation and migration (figure 5.1 D) and BrdU pulse labelling following 24 hours (figure 5.9C, p =>0.05 MWU). I did however observe frequent mislocalization of Paneth cells (figure 5.13 A-D). In contrast to other cell populations, paneth cells once differentiated migrate downwards to their position at the base of the crypt (Potten *et al* 1997). Correct localisation of paneth cells along the crypt- villus axis is controlled by expression of Eph/Ephrin gradients, which are downstream targets of Wnt signalling. Disruption of these gradients results in intermingling of the proliferative and differentiated cell populations, as reported by Batlle *et al* who report similar mislocalization of paneth cells in EphB3$^{-/-}$ mice (Batlle *et al* 2002). Details recently published of the Apc knockout mouse (Sansom *et al* 2004a), confirm aberrant cell proliferation, migration and differentiation of the intestine in addition to a similar phenotype of mislocalized paneth cells (Sansom *et al* 2004a). The mislocalization phenotype in Lkb1 null mice may suggest alterations in Wnt signalling, which will be discussed further in molecular mechanisms of chapter 6.

Figure 5.14 gives an insight into the changes to the enteroendocrine cell lineage of hormone secreting cells. Although *Lkb1*$^{fl/fl}$ animals display increased enteroendocrine cell population, this only becomes significant when enterocyte cells succumb to apoptosis and cell number within the crypt and villus dies down at day 13 (figure 5.14C *Lkb1*$^{+/+}$ 2.3% crypt and 0.4% villus, *Lkb1*$^{fl/fl}$ 4.2%crypt and 1.3% villus, p=<0.05 MWU). Enteroendocrine cells are usually located in the villus of wild type mice and in very low levels within the crypt. Again the *Lkb1*$^{fl/fl}$ mouse shows aberrant localization of enteroendocrine cells and increased numbers of cells are localized to the crypt region.

5.4.4 Failure of terminal differentiation

The processes behind lineage commitment are still relatively unknown, although it has been suggested that multiple intermediate progenitors could lead to one or more intestinal cell types. Muc2 is found highly expressed in goblet cells, in addition to factors such as ITF (intestinal trefoil factor) – also a mucin producing differentiation factor (Velich *et al* 2002). Mice lacking Muc2 and hence goblet cells are predisposed to undifferentiated adenoma type tumours (Velcich *et al* 2002). These proteins are considered to be highly restricted to goblet cell lineages. Figure 5.11 C-F however confirms that cells located in the paneth cell compartment at the base of the crypt show positive staining for Muc2. This may reflect failure of terminal differentiation between the secretory cell lineages. The loss of zonal distinction within the *Lkb1*$^{fl/fl}$ mice gives rise to a population of terminally differentiated cell types proliferating in inappropriate areas and a less distinct separation of cell types, where I find both goblet and paneth cells producing lysozyme and Muc2 staining (figure 5.11-13). Indeed EM analysis describes goblet cells with aberrant secretory granules more characteristic of paneth cells, in addition to paneth cells distended with mucin (Figure 5.12). Furthermore, lysozyme positive cells were observed away from the base of the crypt (figures 5.13C-D). Signalling alterations in these immature progenitors may explain the propagation of committed cell lineages seen here in my model. Lkb1 may act as a cell fate determinant at a critical point of intermediate progenitors.

5.4.5 Lkb1 and Polarity

Loss of polarity may induce cell overgrowth and differentiation by loss of junctional contacts, plasma membrane markers and cytoskeletal reorganisation (Sancho *et al* 2004). Polarity and neoplastic transformation are linked via loss of control of cell proliferation and are commonly found in more invasive and aggressive cancer cell types.

Previous reports have identified found mutations in the kinase region of the protein abolishing the metabolic functions of LKB1. A recent report shows missense mutation in the c terminal tail region of LKB1 interferes with its polarity inducing functions without affecting kinase activity. The tumour suppressor properties of LKB1 in PJS and hamartoma formation may be due to mutations in this regulatory C-terminal tail and polarity alterations rather than the kinase domain and metabolic functions, as PJS patients rarely present with any metabolic disorders (Forcet *et al* 2005).

Given the multiple links between LKB1 and polarity including: PAR4 homology (Martin and St Johnston 2003) and intestinal brush border formation, a loss of polarity or impaired asymmetric stem cell division has been suggested to explain the disorganised tissues seen in PJS hamartomas (Sancho *et al* 2004). Another possible explanation for the observed Lkb1 phenotype relies on the fact that stem cell activity controls proliferation, transit amplifying zone, lineage commitment, terminal differentiation and cell death (reviewed Radtke and Clevers 2005). Indeed many of the alterations in the observed Lkb1 null phenotype correlate with the immediate early stage loss of LKB1 in the stem cell.

Although LKB1 has been linked to spontaneous brush border formation, essential information regarding maintenance of intestinal polarity is at present lacking, as is loss of polarity in PJS polyps, which ultimately display a differentiated cell type normally polarised. The EM studies in figure 5.15A-B clearly show basolateral polarity is maintained following Lkb1 deletion in the murine intestinal epithelium. Villin expression has been positively linked to PI3K signalling and it is thought that E cadherin and cell-to-cell contacts activate PI3K cascades, resulting in brush border formation and cytoskeleton reorganisation (see figure 1.4, Laprise *et al* 2002). Indeed

Villin staining appears unperturbed in this model (figure 5.15C-F) and therefore this reaffirms that brush border and actin organisation are not altered during Lkb1 loss *in vivo*. LKB1 loss in terminally differentiated secretory cell lineages may have little effect on polarity as these cells have already established brush border formation. Therefore loss of Lkb1 in the adult mouse may present a very different situation from that of embryonic loss. My data suggests that Lkb1 does not participate in the maintenance of cellular polarity in the adult mouse, although its role in formation of brush boarders during development cannot be discounted (Baas *et al* 2004). Investigation of polarity using *in utero* floxing of the Lkb1 transgene in addition to studies in the constitutive knockout heterozygote mice may help to shed light on the role of LKB1 in intestinal polarity.

As loss of LKB1 in the proliferative enterocyte lineage sensitizes cells to death, those cells that acquire a secondary genetic mutation targeting either the apoptotic response or loss of polarity present a much greater threat of persistence and could be the driving force behind hamartoma formation or progression to malignancy. The role of LKB1 in tumourigenesis will be discussed further in chapters 6 and 7.

5.5 Chapter summary and conclusions

- *Lkb1* is absolutely required for normal differentiation within the adult murine intestine.

- Loss of Lkb1 drives proliferation within the absorptive enterocyte lineages, but this is unsustainable and leads to the rapid decline of enterocytes via cell death.

- These results therefore substantiate reports that LKB1 functions to inhibit cell proliferation both directly (Tiainen *et al* 1999, Marignani *et al* 2001) and through its role in cellular energy control (Hawley *et al* 2003).

- Deficiency of *Lkb1* also drives proliferation within the secretory lineages. In contrast to enterocytes, these cells tolerate *Lkb1* deficiency and indeed proliferate in the absence of *Lkb1*.

- Polarity and brush boarders are maintained within Lkb1 null epithelial cells.

The resultant crypt population shows an expansion of differentiated cells with aberrant secretary functions. This drive toward the secretory intestinal lineages rather than the adsorptive enterocyte lineages may prime tissue for overgrowth and increased secretions observed in hamartoma formation.

I have therefore been able to demonstrate the immediate effects of *Lkb1* loss on the intestinal crypt: effects that are conflicting but lead to the selective survival and growth of the secretory cell lineage. Chapters 6 and 7 will investigate the underlying molecular mechanisms of LKB1 in intestinal homeostasis and tumourigenesis and determine whether the inappropriate survival of these aberrant cells predisposes to hamartoma formation.

Chapter 6. Analysis of molecular mechanisms following Lkb1 loss

6.1 Introduction

6.1.1 Affymetrix array strategy

The introduction of DNA microarray analysis using oligonucleotides or CDNA fragments immobilised on a solid state chip have provided an invaluable tool for investigating expression patterns, effector pathways and identifying novel targets for new therapies in normal and tumour cell types.

Affymetrix produce high-density oligonucleotide expression gene chips through a process of photolithography and combinational chemistry, which simultaneously generates combinations of probes. The extracted, amplified and labelled cDNA from each sample is hybridised to the oligonucleotide array and the amount of label detected from target RNA transcripts is used as a measure of gene expression. Quantitative hybridization analysis using standardised control probes is then employed to validate samples for any variation in binding efficiency.

6.2 Aim

Loss of LKB1 leads to changes in both proliferation and cell fate signal; ultimately resulting in the production of a population of terminally differentiated proliferating cell types with aberrant secretary functions (chapter 5). I therefore decided to examine the possible underlying molecular mechanisms of the intestinal changes associated with *Lkb1* loss and disrupted crypt-villus architecture. LKB1 has previously been implicated in a number of pathways (see chapter 1.5.1-1.5.6), and characterisation of the molecular interactions of LKB1 *in vivo* will be critical to determining its function as a tumour suppressor gene and contribution to PJS. I will investigate signalling pathways implicated in Lkb1 function such as Wnt, AMPK and mTOR, by western blot, immunohistochemistry and microarray analysis to determine whether those reports from *in vitro* studies bear any relevance to my *in vivo* mouse model.

6.3 Results

The Affymetrix MOE430 2.0 murine genome chip (46,000 genes) was used to assess transcriptome changes in intestinal samples from *Lkb1*$^{+/+}$AHCre+ (control) and *Lkb1*$^{fl/fl}$ AHC+ mice at day 4 following recombination with 80mg/kg β-napthoflavone. This time point was chosen as it precedes the onset of the major intestinal phenotype described in chapter 5, and hence transcriptome changes will reflect those pathways driving the phenotype.

Affymetrix data retrieved from the 46,000 gene set was arranged in terms of signal value (the intensity of the spot, the higher the value the higher the expression), PMA value (present (low p value), marginal, or absent (high p value), and finally the corresponding p value to indicate the significance of the signal value.

6.3.1 Fold change

Fold change was calculated by dividing averaged raw signal value from *Lkb1*$^{+/+}$ and *Lkb1*$^{fl/fl}$ mice (N=6 and N=5 respectively). T-test pairwise statistical comparison between groups was added to show gene changes with high significance. Genes with a fold change of 2 or above were considered strong candidates and Table 6.1 A –B shows the top up and down regulated genes (minus unknown proteins or ESTs). This shows that there are less than 100 genes showing up or down regulation greater than 2 fold and many of these are judged not significant (p=>0.05) according to T-test values. Table 6.1B also confirms that Lkb1 is down regulated approximately 4 fold (p=0.011 Ttest).

6.1A – upregulated genes

Descriptions	foldchange	ttest	Accession no.
G protein-coupled receptor 61	7.714286	0.08705	gb:AW493195
POZ 56 protein mRNA,	5.882609	0.096061	gb:AF290198.1
Aqp6 aquaporin 6	5.818605	0.075792	gb:AI956846
achaete-scute complex homolog-like 1 (Drosophila) (Ascl1),	5.355789	0.096088	gb:NM_008553.1
a disintegrin and metalloprotease domain 18 (Adam18)	5.2	0.077254	gb:NM_010084.1
integrin binding sialoprotein (Ibsp),	4.996721	0.048676	gb:NM_008318.1
Foxo1 forkhead box O1	4.767273	0.06611	gb:AW121569
keratin complex 1, acidic, gene 13 (Krt1-13),	4.583415	0.076989	gb:NM_010662.1
Similar to ERGL protein; ERGIC-53-like protein	4.4	0.099388	gb:BC020188.1
tumour necrosis factor (Tnf),	4.085393	0.064941	gb:NM_013693.1
UDP-Gal:betaGlcNAc (B3galt5),	4.077876	0.069442	gb:NM_033149.1
nicotinic acetylcholine receptor beta4 subunit (Chrnb4)	4.029474	0.021862	gb:AF492840.1
claudin 16 (Cldn16),	3.80339	0.017291	gb:NM_053241.1
PDZ LIGAND OF NEURONAL NITRIC OXIDE SYNTHASE,	3.667742	0.090959	gb:AK018149.1
(C4.4a-pending)	3.634069	0.055121	gb:NM_133743.1
Tdgf1 /UG_TITLE=teratocarcinoma-derived growth factor	3.62	0.03815	gb:AV294613
leukocyte cell derived chemotaxin 1 (Lect1),	3.568831	0.098719	gb:NM_010701.1
X-linked lymphocyte-regulated 5 (Xlr5),	3.453659	0.094037	gb:NM_031493.1
interphotoreceptor matrix proteoglycan 1,	3.394521	0.071275	gb:BC022970.1
S100 calcium binding protein A8 (calgranulin A) (S100a8)	3.358333	0.086765	gb:NM_013650.1
Adcyap1 adenylate cyclase activating polypeptide 1	3.353571	0.077821	gb:AI323434
Bmp1 bone morphogenetic protein 1	3.346875	0.027002	gb:BG248060
solute carrier family 4 (anion exchanger), member 1,	3.227907	0.0807	gb:AK010967.1
similar to SERINE 2 ULTRA HIGH SULFUR PROTEIN	3.212903	0.044769	gb:AK020699.1
transmembrane, cochlear expressed 1 (Tmc1)	3.204969	0.093704	gb:NM_028953.1
FXYD domain-containing ion transport regulator 2 (Fxyd2)	3.184	0.039737	gb:NM_052824.1
acetylcholinesterase (Ache),	3.176	0.025147	gb:NM_009599.1
receptor-associated protein of the synapse, 43 kDa (Rapsn),	3.152	0.095865	gb:NM_009023.1
ATX1 (antioxidant protein 1) homolog 1 (yeast) (Atox1)	3.145865	0.089411	gb:NM_009720.1
protocadherin beta 6 (Pcdhb6),	3.1344	0.023495	gb:NM_053131.1
Moloney sarcoma oncogene (Mos),	3.133981	0.097542	gb:NM_020021.1
prolactin-like protein I (Prlpi)	3.105405	0.089802	gb:NM_013766.1
Mouse histidase locus histidine ammonia-lyase	3.10303	0.019337	gb:L07645.1
Bicd2 bicaudal D homolog 2	3.079121	0.098797	gb:BI250512
Lifr /DEF=Mouse mRNA for soluble D-factorLIF receptor	3.050382	0.06743	gb:D17444.1
rjs (rjs) mRNA, rjs-p6H allele	3.032911	0.041614	gb:AF061532.1
SIMILAR TO BOVINE SCP2 (STEROL CARRIER PROTEIN 2)	3.008696	0.049955	gb:AK005847.1
tweety homolog 2 (Drosophila) (Ttyh2)	2.996319	0.065303	gb:NM_053273.1
solute carrier family 4 (anion exchanger), member 3 (Slc4a3)	2.993072	0.032269	gb:NM_009208.1
signal transducing adaptor molecule 2	2.955254	0.02695	gb:AK017668.1
Trim17 /UG_TITLE=tripartite motif protein 17	2.936364	0.018863	gb:AI385992
Ids /UG_TITLE=iduronate 2-sulfatase	2.909091	0.095604	gb:X75636.1
similar to GAMMA CRYSTALLIN E,	2.908978	0.009891	gb:AK013953.1
protocadherin beta 14 (Pcdhb14)	2.902703	0.097265	gb:NM_053139.1
homeo box D11 (Hoxd11),	2.845161	0.037662	gb:NM_008273.1
Pla2g2f /UG_TITLE=phospholipase A2, group IIF	2.832492	0.091341	gb:AV228827
guanine nucleotide binding protein, alpha transducing 1,	2.806957	0.076034	gb:BC022793.1
growth arrest specific 1 (Gas1)	2.769133	0.096032	gb:NM_008086.1

Weakly similar to sox-4 protein (M.musculus)	2.763871	0.091664	gb:BQ180104
sperm tail associated protein (Stap-pending)	2.72	0.021695	gb:NM_019938.1
Hsf2bp heat shock transcription factor 2 binding protein	2.69037	0.093986	gb:AW550693
Edn1=endothelin-1	2.686047	0.093117	gb:D43775.1
Pdyn /DEF=Mus musculus prodynorphin	2.68289	0.07737	gb:AF026537.1
Rps19 ribosomal protein S19	2.672269	0.069196	gb:AI594148
Klra18 / lectin-related NK cell receptor LY49R	2.669318	0.076046	gb:AF288377.1
drebrin A2,	2.65	0.086872	gb:AB064321.1
Moderately similar to pot. ORF VI (H.sapiens)	2.60107	0.0866	gb:BG067746
Mef2a Similar to MADS box transcription enhancer factor 2	2.590728	0.038354	gb:BC019116.1
cholinergic receptor, nicotinic, alpha polypeptide 7 (Chrna7)	2.590654	0.05695	gb:NM_007390.1
(metargidin) (Adam15)	2.588957	0.006746	gb:NM_009614.1
Sema3a secreted, (semaphorin) 3A	2.569727	0.078841	gb:BB124175
:related to ZINC FINGER PROTEIN FEZ,	2.542234	0.019199	gb:AK014242.1
Weakly similar to FYB_MOUSE FYN-BINDING PROTEIN	2.540468	0.058401	gb:AI561611
LIM homeobox protein 3 (Lhx3)	2.5	0.051943	gb:NM_010711.1
TIE1 MOUSE TYROSINE-PROTEIN KINASE RECEPTOR TIE-1	2.47156	0.040747	gb:AV319076
Syn2 synapsin II	2.471006	0.052496	gb:BM936504
high-glycinetyrosine protein type I E5 (LOC170939)	2.468354	0.08237	gb:NM_133359.1
Slc21a2 solute carrier family 21 (prostaglandin transporter	2.385366	0.034452	gb:BI108501
hyaluronan synthase1 (Has1)	2.381581	0.072545	gb:NM_008215.1
Elavl2 =ELAV (embryonic lethal, abnormal vision, Drosophila)-like 2	2.37733	0.06265	gb:BG069102
Highly similar to T43275 neurabin - rat (R.norvegicus)	2.376	0.097244	gb:BB748939
chloride channel 4-2,	2.361753	0.08554	gb:AK016058.1
POL2 MOUSE RETROVIRUS-RELATED POL POLYPROTEIN	2.360221	0.068027	gb:BB283455
steroid sulfatase (Sts)	2.333835	0.08742	gb:NM_009293.1
triggering receptor expressed on myeloid cells 2c (Trem2c-pending)	2.330704	0.094492	gb:NM_021410.1
nephrosis 2 homolog, podocin (human) (Nphs2)	2.315285	0.03469	gb:NM_130456.1
ectodysplasin-A isoform Ta A (Ta)	2.30137	0.079816	gb:AF016629.1
transcriptional regulating protein 132, isoform 2; rapa-2; rapa-1	2.292225	0.092191	gb:BB409198
implantation serine protease 1 (Isp1-pending)	2.287006	0.06402	gb:NM_053259.1
meprin 1 alpha (Mep1a)	2.280399	0.084748	gb:NM_008585.1
Forkhead box B2 (Foxb2)	2.266171	0.085671	gb:NM_008023.1
Ftp-1	2.226765	0.03217	gb:D88187.1
mesogenin 1 (Msgn1),	2.210101	0.052091	gb:NM_019544.1
similar to PROLACTIN-LIKE PROTEIN-CALPHA PRECURSOR	2.19759	0.079619	gb:AK005485.1
Highly similar to ANF MOUSE ATRIAL NATRIURETIC FACTOR	2.171228	0.056812	gb:BM122009
Brp14 brain protein 14	2.167401	0.096855	gb:BB428900
naked cuticle 1 homolog (Drosophila) (Nkd1)	2.162824	0.086068	gb:NM_027280.1
Clasp2-pending CLIP associating protein 2	2.161024	0.071055	gb:BM221361
cytochrome P450, 46 (cholesterol 24-hydroxylase) (Cyp46)	2.160206	0.051704	gb:NM_010010.1
protocadherin 15 (Pcdh15)	2.157558	0.087649	gb:NM_023115.1
Pask PAS domain containing serinethreonine kinase	2.065544	0.087495	gb:BB729869
B4galt6 UDP-Gal:betaGlcNAc	2.05469	0.089945	gb:BG068243
cholinergic receptor, nicotinic, delta polypeptide (Chrnd)	2.049642	0.086917	gb:NM_021600.1
forkhead box P3 (Foxp3)	2.04	0.053003	gb:NM_054039.1
Ndn necdin	2.026756	0.072751	gb:AV124445
Npas2=neuronal PAS domain protein 2	2.018605	0.070404	gb:BG070037
Mlsn1 melastatin 1	2.002174	0.095961	gb:BB772425
CA1C MOUSE COLLAGEN ALPHA 1(XII) CHAIN PRECURSOR	2	0.028	gb:BB704902
Homolog to COCKAYNE SYNDROME WD-REPEAT PROTEIN	1.984275	0.094476	gb:AK013216.1
stefin A3 (Stfa3)	1.982367	0.064696	gb:NM_025288.1
H6 homeo box 1 (Hmx1)	1.981132	0.055234	gb:NM_010445.1
Ddr1discoidin domain receptor family, member 1	1.98	0.062878	gb:BB378700

6.1B- Down regulated genes

	Descriptions	Fold change	ttest	Accession number
	melanoma-derived leucine zipper, extra-nuclear factor (Mlze)	12.2425	0.088025	gb:NM_031378.1
	hornerin	9.275362	0.088149	gb:AY027660.1
	Fhl4 our and a half LIM domains 4	7.058458	0.009947	gb:AV047468
	plasminogen (Plg),	5.935374	0.058171	gb:NM_008877.1
	sulfotransferase, hydroxysteroid preferring 2 (Sth2)	5.568783	0.045836	gb:NM_009286.1
	CEA-related cell adhesion molecule 10 (Ceacam10)	5.093599	0.082551	gb:NM_007675.1
	CEA-related cell adhesion molecule 10 (Ceacam10)	4.984531	0.095909	gb:NM_007675.1
	myelodysplasiamyeloid leukemia factor 1 (Mlf1)	4.695946	0.086948	gb:AF100171.1
	stromal antigen 3 (Stag3)	4.591611	0.050901	gb:NM_016964.1
	Igf2bp3 /UG_insulin-like growth factor 2, binding protein 3	4.427861	0.02794	gb:AW681763
	N-myc protein	4.034392	0.015879	gb:M36277.1
*	**Peutz-Jeghers syndrome kinase LKB1 (Lkb1)**	**4.01211**	**0.011046**	**gb:AF145287.1**
	H2-D1 histocompatibility 2, D region locus 1	3.994662	0.064676	gb:X00246.1
	Emx2 /empty spiracles homolog 2 (Drosophila)	3.992248	0.072154	gb:BG072869
	neuropilin and tolloid like-1	3.955556	0.053308	gb:AV346211
	homeo box C5 (Hoxc5),	3.907658	0.034042	gb:NM_008271.1
	homolog to LYSOZYME C PRECURSOR	3.896714	0.065946	gb:AK020538.1
	C-type lectin-like receptor 2 (Clec2-pending)	3.835859	0.045719	gb:NM_019985.1
	immunoglobulin kappa chain variable 4 (V4)	3.814465	0.009009	gb:AK012310.1
	inwardly-rectifying K+ channel protein (mb-IRK3)	3.570833	0.072062	gb:U11075.1
	Klkb1 kallikrein B, plasma 1	3.558897	0.048504	gb:BC026555.1
	Rnf17 RING finger protein Mmip-2	3.538961	0.019567	gb:AF190166.1
	similar to ZNT3 MOUSE ZINC TRANSPORTER 3	3.500882	0.077877	gb:BB433667
	pituitary specific transcription factor 1 (Pit1)	3.488372	0.060101	gb:NM_008849.1
	cysteine and tyrosine-rich protein 1 (Cyyr1)	3.441278	0.016097	gb:AF442733.1
	Col9a3 procollagen, type IX, alpha 3	3.42803	0.055995	gb:BG074456
	large conductance ca dependant K ion channel B4	3.403614	0.063072	gb:AK016591.1
	EIB (Serpinb1b)	3.383085	0.052713	gb:AF426025.1
	Myh8 myosin, heavy polypeptide 8,	3.376068	0.048438	gb:BB011213
	prostaglandin F receptor (Ptgfr)	3.353994	0.076618	gb:NM_008966.1
	Oprl kappa3 related opioid receptor isoform A	3.255208	0.083394	gb:AF043276.1
	Vesl-1L,	3.254258	0.034281	gb:AB019479.1
	mscd6 precursor (Cd6)	3.22601	0.019158	gb:U12434.1
	hematopoietic-specific IL-2 deubiquitinating enzyme (DUB-2)	3.215884	0.05309	gb:U70369.1
	Bcat1 =branched chain aminotransferase 1, cytosolic	3.200837	0.095892	gb:X17502.1
	Cyp2j9 cytochrome P450 CYP2J9	3.188299	0.030516	gb:AF336850.1
	Gpr85, G protein-coupled receptor 85,	3.18306	0.079112	gb:BC026975.1
	cathepsin 8 (Cts8),	3.157895	0.054531	gb:NM_019541.1
	BAI2 human brain specific angiogenesis inhibitor 2	3.153846	0.095998	gb:BB351248
	Bcl11a /B-cell CLLlymphoma 11A (zinc finger protein)	3.130885	0.082756	gb:BB772866
	ATPase, H+K+ transporting, beta polypeptide, (Atp4b)	3.089189	0.02142	gb:NM_009724.1
	Neu2 neuraminidase 2	3.071161	0.057145	gb:AK009828.1
	nter alpha-trypsin inhibitor, heavy chain 4	3.066667	0.088649	gb:AK004893.1
	Ptdss2 phosphatidylserine synthase 2	3.05313	0.037477	gb:AI596401
	PHEMX (Phemx)	3.034188	0.031694	gb:AF175771.1
	Similar to immunoglobulin heavy chain 1 (serumIgG2a)	2.944139	0.054397	gb:BC018535.1
	Cox8a cytochrome c oxidase, subunit VIIIa	2.940141	0.062333	gb:AI604777
	similar to collagen alpha 1(II) chain precursor	2.87037	0.04963	gb:BB251623

Iroquois related homeobox 4 (Drosophila) (Irx4)	2.830189	0.078308	gb:NM_018885.1
guanine nucleotide binding protein (G protein), gamma 5,	2.794872	0.077837	gb:BC010725.1
TRKB mouse BDNFNT-3 growth factor receptor	2.774823	0.099239	gb:BB456963
insulin-like growth factor binding protein 1 (Igfbp1)	2.743902	0.040555	gb:NM_008341.1
cathepsin J (Ctsj)	2.742165	0.072061	gb:NM_012007.1
Pbx4 pre-B-cell leukemia transcription factor 4	2.664042	0.06912	gb:BE951484
inter-alpha trypsin inhibitor, heavy chain 2 (Itih2)	2.649306	0.023092	gb:NM_010582.1
kidney androgen regulated protein (Kap)	2.647059	0.064729	gb:NM_010594.1
Nfic nuclear factor IC	2.644033	0.057939	gb:BF785921
Csng casein gamma	2.622549	0.032322	gb:AI463693
Slc21a10 solute carrier family 21, member 10	2.599638	0.089768	gb:AB037192.1
activation-inducible lymphocyte immunomediatory molecule AILIM	2.586207	0.090688	gb:AB023132.1
(Mc7-pending)	2.578348	0.098556	gb:NM_020267.1
Cmkbr5 MIP-1 alpha receptor 2	2.577839	0.04344	gb:X94151.1
Lhx9 LIM homeobox protein 9	2.576087	0.034931	gb:AK013209.1
Ly-6I.1 (Ly-6I)	2.530353	0.068989	gb:AF232024.1
leukotriene C4 synthase (Ltc4s)	2.47134	0.078144	gb:NM_008521.1
Oprm / opioid receptor isoform MOR-1Ia	2.46633	0.05702	gb:AF260307.1
cytochrome P450, 1a1, aromatic compound inducible (Cyp1a1)	2.443968	0.071529	gb:NM_009992.1
MSim	2.414906	0.084509	gb:D63383.1
Zfp94 zinc finger protein 94,	2.408815	0.057568	gb:BC005437.1
Uba52 /ubiquitin A-52 residue ribosomal protein fusion product 1	2.38568	0.089455	gb:AV098730
pre-pro-proteinase 3 (Prtn3)	2.362403	0.015724	gb:U97073.1
(osteoprotegerin) (Tnfrsf11b)	2.361769	0.026406	gb:NM_008764.1
Gabt1 (GABA-A) transporter 1	2.34375	0.046625	gb:M92378.1
semaphorin C	2.314815	0.079334	gb:X85992.1
Lmbr1 /UG_limb region 1	2.295387	0.026334	gb:BG070844
kallikrein 26 (Klk26)	2.262693	0.036239	gb:NM_010644.1
Masp1 mannan-binding lectin serine protease 1	2.253599	0.034433	gb:BB732340
anti-human CD20 antibody 1F5 kappa light chain	2.248325	0.097643	gb:AY058906.1
Syngr1 synaptogyrin 1	2.227273	0.027933	gb:BI696936
Tnfrsf9 tnf receptor superfamily, member 9	2.225275	0.074553	gb:BC028507.1
Phkg skeletal muscle phosphorylase kinase, gamma subunit	2.195122	0.012953	gb:J03293.1
homolog to KALLIKREIN 5 PRECURSOR	2.191092	0.072135	gb:AK003996.1
neural cell adhesion molecule 2 (Ncam2)	2.184909	0.075677	gb:NM_010954.1
sodium channel, voltage-gated, type I, alpha polypeptide (Scn1a)	2.154321	0.075431	gb:NM_018733.1
Siat7c sialyltransferase 7	2.151709	0.072923	gb:BQ176193
pre-B lymphocyte gene 2 (Vpreb2)	2.144608	0.049006	gb:NM_016983.1
calbindin-D9K (Calb3)	2.128475	0.040306	gb:NM_009789.1
Scya27 small inducible cytokine A27	2.112933	0.050412	gb:BE198116
Samsn1 SAM domain, SH3 domain and nuclear localisation signals	2.112211	0.038055	gb:AK015008.1
Y box protein 2 (Ybx2),	2.107046	0.068201	gb:NM_016875.1
distal-less homeobox 5 (Dlx5)	2.088079	0.060358	gb:NM_010056.1
diacylglycerol O-acyltransferase 2-like 1 (Dgat2l1)	2.018547	0.075453	gb:NM_026713.1
RANKL 2 receptor activator of NF-kB ligand 2	1.989796	0.030283	gb:AB032771.1
keratin associated protein 8-2 (Krtap8-2)	1.988225	0.073444	gb:NM_010676.1
cystatin F (leukocystatin) (Cst7)	1.983369	0.071996	gb:NM_009977.1
glutamate transporter	1.979167	0.046452	gb:BB357585
steroid 5 alpha-reductase 2 (Srd5a2)	1.974576	0.065064	gb:NM_053188.1

Table 6.1 -Fold change charts calculated from raw signal values from day 4 samples. **A,** Top most up-regulated genes ordered by fold change **B,** Top most down-regulated genes ordered by fold change. Genes with p=<0.05(ttest) show significant difference between control *Lkb1*$^{+/+}$ and *Lkb1*$^{fl/fl}$ groups (N=6 and N=5 respectively). LKB1 is indicated in 6.1B in bold (*).

6.3.2 Ranked products

The fold change analysis in table 6.1 was performed on raw signal data from Affymetrix array chips, as normalised data is scaled and looses the correct ratios. However raw signal values do not account for variations between chips and hybridization efficiency and therefore data requires normalisation of the signal value, either by housekeeping genes or by global normalisation. I used the MaxD programme to filter out PMA columns and select genes with 2 or more samples with a p value of <0.1. This process filters and reduces the number of genes to be analysed. Data is then transformed and normalised using the Global Geometric Mean (GGM) method. The GGM normalises data by dividing the signal intensity for each probe set by the mean value for the chip to account for background or noise variation. Signal values are then logged using Natural log (Log_e), and are centred around the mean signal value, which is set to zero. Hence those genes above the mean show up-regulation and those below show down-regulation.

In addition to raw fold change values, ranked product is another method of pairwise comparison between the *Lkb1*$^{+/+}$ and *Lkb1*$^{fl/fl}$ samples (Table 6.2). The ranked product is a value calculated by ranking genes in order of largest fold change between each possible combination of control and mutant samples rather than an average fold change of the control vs. mutant groups. For *Lkb1*$^{+/+}$ N=6 and *Lkb1*$^{fl/fl}$ N=5, there are 30 possible combinations of samples and therefore 30 rank columns. Total Rank product for each gene is then calculated by the sum of its position in all 30 rank lists. GGM normalised and centred data from MaxD is used as the input for ranked product and a T-test is included for significance. Table 6.2 details the top 100 up and down regulated genes according to this method. Although several genes appear in both tables 6.1 and 6.2, however Lkb1 does not appear in the rank product list suggesting sample variation for this gene.

6.2A – Up regulated ranked products from GGM

gene	product	ttest	gene
inhibitory_receptor_NKR-P1D	2.1E+106	0.088685	gb:AF342896.1
cytochrome_P450,_1a1(Cyp1a1),	8.7E+107	0.026831	gb:NM_009992
homeobox_protein_zhx-1	1E+108	0.008044	gb:AV298304
G_protein-coupled_receptor_61	1.5E+108	0.041061	gb:AW493195
LMA1_MOUSE_laminin a1 chain precursor	1.1E+109	0.009345	gb:BB483642
H13_histocompatibility_13	1.3E+109	0.072804	gb:BQ175993
Rps19ribosomal_protein_S19	5E+109	0.010054	gb:AI594148
Histidase_locus_histidine_ammonia-lyase	5.3E+109	0.006329	gb:L07645.1
Aqp6_aquaporin_6	6.5E+109	0.026618	gb:AI956846
ALCOHOL_DEHYDROGENASE_CLASS_IV_	1.1E+110	0.085716	gb:AK007397.1
interphotoreceptor_matrix_proteoglycan_1	1.3E+110	0.034042	gb:BC022970.1
(Pcdhb6) protocadherin_beta_6_	1.6E+110	0.013088	gb:NM_053131
H-2Ealpha major histocompatibility_complex_H-2E	2.1E+110	0.069913	gb:U13648.1
Gpr73_G_protein-coupled_receptor_73	2.5E+110	0.011358	gb:BB037474
(Chrnb4)_nicotinic_acetylcholine_receptor_beta4	2.9E+110	0.009639	gb:AF492840.1
melanoma-derived_leucine_zipper,_extra-nuclear_factor_(Mlze),	1.6E+111	0.052687	gb:NM_031378
VITELLOGENIC_CARBOXYPEPTIDASE-LIKE_PROTEIN,	1.6E+111	0.084322	gb:AK017087.1
immunoglobulin_lambda_chain,_variable_1	3E+111	0.06814	gb:AK008145.1
Hsf2bp_/heat_shock_transcription_factor_2_binding_protein	3.6E+111	0.062549	gb:AW550693
ORF_VI_(H.sapiens)	4.2E+111	0.017202	gb:BG067746
Nik_related_kinase_/	4.7E+111	0.011442	gb:AK012873.1
Aco2_aconitase_2,_mitochondrial_	5.1E+111	0.083081	gb:AA034553
transcriptional_regulating_protein_132 rapa-2;_rapa-1	1.4E+112	0.027467	gb:BB409198
Nptx2__neuronal_pentraxin_2	2.6E+112	0.085099	gb:BC026054.1
Spi2_serine_protease_inhibitor_2_	4.7E+112	0.032988	gb:BF234005
Il2ra_interleukin_2_receptor,_alpha_chain_	7.1E+112	0.073812	gb:AF054581.1
Integrin_binding_sialoprotein_(Ibsp)	7.2E+112	0.034492	gb:NM_008318
reverse_transcriptase_	8.4E+112	0.079094	gb:BB167026
contactin_6_(Cntn6),	1.5E+113	0.094038	gb:NM_017383
B3galt5__UDP-Gal:betaGlcNAc	2.5E+113	0.086179	gb:NM_033149
Lifr_/D soluble_D-factorLIF_receptor,_	2.7E+113	0.01794	gb:D17444.1
NADH_dehydrogenase_(ubiquinone)_1,(Ndufc1)	2.8E+113	0.056008	gb:NM_025523
neuronal_pentraxin_2_(Nptx2)	2.9E+113	0.072729	gb:NM_016789
protein_kinase,_lysine_deficient_1	4.8E+113	0.094944	gb:BG176150
(Atox1) ATX1_(antioxidant_protein_1,_yeast)_homolog_1	5E+113	0.013728	gb:NM_009720
zinc_finger_protein_98_(Zfp98)	5.1E+113	0.035386	gb:NM_016793
Fzd4 frizzled_homolog_4_(Drosophila)	5.2E+113	0.098137	gb:BF783030
Ttyh1_tweety_homolog_1_(Drosophila)	1E+114	0.065194	gb:BB335591
Lama4_/laminin,_alpha_4_	1.5E+114	0.032653	gb:BB053010
Ndufb5_/,_NADH_dehydrogenase_(ubiquinone)_1_	1.7E+114	0.077863	gb:BC025155.1
Igk-V28_anti-Pseudomonas_aeruginosa_lipid-A_of_lipopolysaccharide,	1.7E+114	0.07092	gb:U25103.1
Arginase_type_II_(Arg2)	2.4E+114	0.062683	gb:NM_009705
ANF_mouse atrial natriuretic factor precursors	2.9E+114	0.067124	gb:BM122009
Dbi_/diazepam_binding_inhibitor	3.5E+114	0.089205	gb:AV007315

Gabra6 (GABA-A) receptor,subunit alpha 6	4E+114	0.035744	gb:NM_008068.1
Pcna / proliferating cell nuclear antigen	4.3E+114	0.092251	gb:BC010343.1
Foxp3 /forkhead box P3	5.9E+114	0.017442	gb:NM_054039.1
Granule cell antiserum pos 8	6.7E+114	0.080669	gb:AK021073.1
H3f3a /H3 histone, family 3A	7E+114	0.057471	gb:BI111967
Pdha1 pyruvate dehydrogenase E1 alpha 1	7.3E+114	0.083531	gb:BF681901
L1 cell adhesion molecule	8.1E+114	0.012599	gb:BB202655
Vamp3 vesicle-associated membrane protein 3	8.2E+114	0.02496	gb:BB552111
Bmp1 bone morphogenetic protein 1	9.2E+114	0.000595	gb:BG248060
prodynorphin	1.2E+115	0.068291	gb:AF026537.1
gap junction membrane channel beta 4 (Gjb4),	1.3E+115	0.080628	gb:NM_008127.1
Surp module containing protein	1.3E+115	0.038012	gb:AK017525.1
desmocollin 1 (Dsc1)	1.5E+115	0.020988	gb:NM_013504.1
Stap-pending	1.6E+115	0.016977	gb:NM_019938.1
carbonic anhydrase 4 (Car4),	1.8E+115	0.04811	gb:NM_007607.1
TMS2 (EPITHELIASIN)	1.9E+115	0.058962	gb:BB524685
ERGL protein; ERGIC-53-like protein	2.4E+115	0.09544	gb:BC020188.1
Vti1b-pending	4.1E+115	0.012789	gb:AV002218
NADH dehydrogenase (ubiquinone) 1Ndufc1)	4.2E+115	0.043813	gb:NM_025523.1
INTESTINAL MUCIN-LIKE PROTEIN (MLP)	4.2E+115	0.041544	gb:AK008250.1
TYROSINE-PROTEIN KINASE JAK3	4.4E+115	0.011619	gb:BI500065
Trem2c-pending)	5.1E+115	0.092693	gb:NM_021410.1
IG LAMBDA-2 CHAIN C REGION	5.5E+115	0.062061	gb:AK008551.1
transcription factor AP-2, alpha	6.6E+115	0.093253	gb:AK017409.1
anti-human CD37 antibody WR17	7.5E+115	0.088075	gb:AY058908.1
tumour necrosis factor (Tnf)	8.5E+115	0.014356	gb:NM_013693.1
Cox7a2l /cytochrome c oxidase subunit VIIa	1E+116	0.066926	gb:AK009614.1
protocadherin beta 22 (Pcdhb22)	1.1E+116	0.03328	gb:NM_053147.1
Fh1 Similar to Fumarate hydratase	1.1E+116	0.068522	gb:BC006048.1
acetylcholinesterase (Ache), m	1.7E+116	0.008683	gb:NM_009599.1
Oxct Mus musculus 3-oxoacid CoA transferase	1.7E+116	0.08731	gb:NM_024188.1
ATX1 (antioxidant protein 1) homolog 1	2.1E+116	0.079172	gb:NM_009720.1
Igk-V28 /immunoglobulin kappa chain variable 28	2.2E+116	0.092888	gb:M35669.1
X-box binding protein 1 (Xbp1)	2.3E+116	0.087027	gb:NM_013842.2
secreted modular calcium binding protein 1 (Smoc1)	2.4E+116	0.071562	gb:NM_022316.1
nephrosis 2 homolog, podocin Nphs2),	2.6E+116	0.036905	gb:NM_130456.1
zinc finger protein 278,	2.8E+116	0.065835	gb:BM208058
heat shock 27kD protein 3 (Hspb3)	2.8E+116	0.012588	gb:NM_019960.1
hydroxyacyl-Coenzyme A	3.1E+116	0.086425	gb:BG866501
Acetyl-Co A acetyltransferase 1	3.2E+116	0.029052	gb:BG070487
forkhead box B2 (Foxb2	3.3E+116	0.006654	gb:NM_008023.1
Asml3a-pending)	3.6E+116	0.021616	gb:NM_020561.1
TSC22-related inducible leucine zipper 1b (Tilz1b)	4E+116	0.085813	gb:AF201285.1
anti-DNA immunoglobulin light chain IgG,	4.2E+116	0.049034	gb:U55641.1
3-KETOACYL-COA THIOLASE	6.5E+116	0.027271	gb:AK002555.1
ornithine transcarbamylase (Otc)	8.2E+116	0.018826	gb:NM_008769.1
Jun N-terminal kinase binding protein 1	9.4E+116	0.043832	gb:AK016792.1
Gabra1 (GABA-A) receptor, subunit alpha 1	9.7E+116	0.01149	gb:BQ268470
sphingomyelin phosphodiesterase 3	1.2E+117	0.019203	gb:BB615725
Hnrpk heterogeneous nuclear ribonucleoprotein K	1.2E+117	0.050259	gb:BB722680
Ttyh1 tweety homolog 1	1.2E+117	0.057587	gb:BB040598
Mouse myosin heavy chain	1.2E+117	0.048724	gb:M74753.1
leukemia associated gene protein (Mllt1)	1.3E+117	0.063785	gb:AF312858.1
Ptp4a2 / protein tyrosine phosphatase 4a2	1.6E+117	0.065019	gb:BE134116

6.2B - Down regulated ranked products from GGM

gene	product	ttest	Accession no.
Moderately similar to T17280 hypothetical protein	9.15E+129	0.0277855	gb:BG075083
Map3k14 mitogen-activated protein kinase kinase kinase 14	8.0755E+129	0.0246907	gb:BG072756
Plxnc1 plexin C1	7.3523E+129	0.0693287	gb:BG092693
DIMETHYLGLYCINE DEHYDROGENASE PRECURSOR	6.5417E+129	0.053924	gb:BG069459
pituitary specific transcription factor 1 (Pit1),	6.3681E+129	0.0057661	gb:NM 008849.1
guanine nucleotide binding protein (G protein), gamma 5,	6.3221E+129	0.0387153	gb:BC010725.1
neuropilin and tolloid like-1	4.9515E+129	0.0160108	gb:AV346211
Traf1Tnf receptor-associated factor 1	4.335E+129	0.0693859	gb:BG064103
forkhead box C1 (Foxc1)	4.02E+129	0.0703185	gb:NM 008592.1
inter-alpha trypsin inhibitor, heavy chain 2 (Itih2)	3.8516E+129	0.0089376	gb:NM 010582.1
Neu1 neuraminidase 1	3.7391E+129	0.0642769	gb:AI649303
Weakly similar to JAK3 MOUSE TYROSINE-PROTEIN KINASE JAK3	3.6416E+129	0.0527004	gb:AU022979
f-box only protein 16 (Fbxo16)	3.4062E+129	0.0881637	gb:NM 015795.1
clone:4932442J20:glycoprotein m6b, full insert sequence.	2.9963E+129	0.0273513	gb:AK016567.1
Nfic nuclear factor IC	2.8801E+129	0.0460187	gb:BF785921
G protein-coupled receptor 85, clone MGC:38964	2.8433E+129	0.0066044	gb:BC026975.1
RAD52 homolog, (S. cerevisiae) (Rad52)	2.5989E+129	0.0939775	gb:NM 011236.1
poliovirus receptor-related 1 (Pvrl1)	2.5387E+129	0.0608825	gb:NM 021424.1
Lorsdh lysine oxoglutarate reductase, saccharopine dehydrogenase	2.3697E+129	0.0913172	gb:BF687395
SAM domain, SH3 domain and nuclear localisation signals, 1,	2.3051E+129	0.0399173	gb:AK015008.1
NFI-B protein, clone NFI-B6.	2.2587E+129	0.0886298	gb:D90176.1
Rnf32 ring finger protein 32	2.2518E+129	0.0260152	gb:AW018385
Csng casein gamma	2.0945E+129	0.0681033	gb:AI463693
dexamethasone induced product	2.0861E+129	0.000879	gb:D44443.1
Weakly similar to FXC1 MOUSE FORKHEAD BOX PROTEIN C1	1.995E+129	0.0439788	gb:AV295543
RING finger protein Mmip-2	1.9501E+129	0.0135257	gb:AF190166.1
Klf9 Kruppel-like factor 9	1.9242E+129	0.014113	gb:BB327336
blue opsin	1.7022E+129	0.0472489	gb:AF190670.1
serine (or cysteine) proteinase inhibitor, clade C (antithrombin)	1.6448E+129	0.0974133	gb:BC019447.1
anaplastic lymphoma kinase (Alk)	1.3526E+129	0.0340504	gb:NM 007439.1
Klf9 Kruppel-like factor 9	1.3331E+129	0.0064829	gb:AI267126
gamma-parvin, clone MGC:18790	1.3291E+129	0.0942431	gb:BC011200.1
Cd28 CD28 antigen	1.2558E+129	0.0550767	gb:AV313615
aldo-keto reductase family 1, member D1 (delta 4-3-ketosteroid-5-beta-reductas	1.1673E+129	0.0348562	gb:BC018333.1
Tpp2 tripeptidyl peptidase II	1.1568E+129	0.0459872	gb:BB484264
Figf c-fos induced growth factor	1.0548E+129	0.0173178	gb:BB359521
Weakly similar to TYROSINE-PROTEIN KINASE JAK3	1.0462E+129	0.0189682	gb:BB461203
Il7r interleukin 7 receptor	1.0453E+129	0.0597377	gb:AI573431
Igsf4 immunoglobulin superfamily, member 4	1.0423E+129	0.0562726	gb:BF148825
protocadherin beta 13 (Pcdhb13)	1.0298E+129	0.0635343	gb:NM 053138.1
TATA box binding protein (Tbp)-associated factor, RNA polymerase I, A (Ta	1.0068E+129	0.0197657	gb:NM 021466.1
ELL MOUSE RNA POLYMERASE II ELONGATION FACTOR ELL	1.0041E+129	0.0512688	gb:BI660702
A35041 ryanodine receptor type 1, skeletal muscle	9.6638E+128	0.0931339	gb:BG793713
coagulation factor V (F5)	9.3274E+128	0.078354	gb:NM 007976.1
nuclear DNA-binding protein, clone MGC:5983	9.2694E+128	0.0400819	gb:BC005436.1
Trim 8 tripartite motif protein 8	8.7246E+128	0.0680718	gb:BB620112
N-myc protein	7.9635E+128	0.013439	gb:M36277.1
Igf2bp3 insulin-like growth factor 2, binding protein 3	7.7795E+128	0.007094	gb:AW681763
Mus musculus Burkitt lymphoma receptor 1 (Blr1)	7.6946E+128	0.072968	gb:NM 007551.1

Burkitt_lymphoma_receptor_1_(Blr1)	7.6946E+128	0.07296804	gb:NM_007551.1
Kruppel-type_zinc-finger_protein_ZIM3-like	7.2533E+128	0.09676004	gb:AF365932.1
seminal_vesicle_secretion_3_(Svs3)	7.2291E+128	0.0371703	gb:NM_021363.1
Similar_to_medium-chain_S-acyl_fatty_acid_synthetase	7.163E+128	0.08333443	gb:BC025001.1
Weakly_similar_to_TYROSINE-PROTEIN_KINASE_JAK3_(M.musculus)	7.0467E+128	0.08389813	gb:BM207275
clone:2700056O10:block_of_proliferation_1,_full_insert_sequence	7.0116E+128	0.02462923	gb:AV128350
stanniocalcin_(Stc2)_mRNA	6.9684E+128	0.09735387	gb:AF031035.1
BCR_downstream_signaling_1_(Brdg1-pending)	6.9268E+128	0.07097313	gb:NM_019992.1
Weakly_similar_to_ZF37_MOUSE_ZINC_FINGER_PROTEIN_37	6.9255E+128	0.09741268	gb:AV377052
Idb4_inhibitor_of_DNA_binding_4	6.8975E+128	0.05578935	gb:BB306828
clone:2010001L06:G_protein-coupled_receptor_68	6.2796E+128	0.09952722	gb:AK008013.1
putative_protein_p243_which_interacts_with_transcription_factor_Sp1	6.045E+128	0.09717868	gb:BB540053
ATP-binding_cassette,_sub-family_C_(CFTRMRP),_member_9	5.8207E+128	0.03257225	gb:AK019938.1
homolog_to_PUTATIVE_DIMETHYLADENOSINE_TRANSFERASE	5.7783E+128	0.08946855	gb:AK015145.1
Similar_to_myeloid_cell_nuclear_differentiation_antigen	5.596E+128	0.08263414	gb:BE685969
cytochrome_P450_CYP2J9_mRNA,_	5.1341E+128	0.01229848	gb:AF336850.1
Lyst_lysosomal_trafficking_regulator	5.0937E+128	0.04288591	gb:BB463428
fetal_liver_zinc_finger_1_(Fliz1-pending)	5.0376E+128	0.0410481	gb:NM_020594.1
clone:1110031N17:homolog_to_RAB-LIKE_PROTEIN_2A,_	5.0155E+128	0.04742787	gb:AK004012.1
(P4ha2)_procollagen-proline,_2-oxoglutarate_4-dioxygenase_(proline_4-hydroxy	4.9719E+128	0.0474468	gb:NM_011031.1
chemokine_(C-C)_receptor_2_(Cmkbr2)	4.7414E+128	0.02209202	gb:NM_009915.1
nth_(endonuclease_III)-like_1_(E.coli)_(Nthl1)	4.0077E+128	0.06001066	gb:NM_008743.1
PHEMX_(Phemx)_mRNA	3.9545E+128	0.0216872	gb:AF175771.1
Moderately_similar_to_leucine-rich_repeat-containing_F-box_protein_FBL3a	3.9278E+128	0.07592361	gb:BE946365
glucocorticoid_receptor_interacting_protein_GRIP1	3.9246E+128	0.05945245	gb:BB701723
OL-protocadherin_isoform_(Pcadh10)	3.6367E+128	0.09611282	gb:AF334801.1
SKAP55_homologue;_Src-associated_adaptor_protein	3.6264E+128	0.0355054	gb:BG075562
T-cell_receptor_zeta_gene_locus_(TCRiota)	3.5517E+128	0.05864736	gb:X84237.1
cyclin-dependent_kinase-like_2_(CDC2-related_kinase)_(Cdkl2)	3.3911E+128	0.03004602	gb:NM_016912.1
Mus_musculus_parvin,_gamma_(Parvg)	3.3418E+128	0.09274885	gb:NM_022321.1
Gdm1_glycerol_phosphate_dehydrogenase_1,_mitochondrial	3.1841E+128	0.07130016	gb:BB251875
Arl6ip6_DP-ribosylation-like_factor_6_interacting_protein_6	3.088E+128	0.00273118	gb:BB837198
CABI_RAT_CALCINEURIN-BINDING_PROTEIN_CABIN_1_(R.norvegicus)	2.9831E+128	0.07133863	gb:BM199891
spermatogenesis_associated_factor_(Spaf)	2.9487E+128	0.05657793	gb:NM_021343.1
zinc_metallopeptidase_(Adamts10)	2.8909E+128	0.00225426	gb:BG064835
esterase_22_(Es22)	2.8401E+128	0.04990442	gb:NM_133660.1
Bloom_syndrome_homolog_(human)_(Blm)	2.8149E+128	0.0267804	gb:NM_007550.1
crystallin,_zeta,_clone_MGC:6074	2.6842E+128	0.05270564	gb:BC003800.1
overexpressed_and_amplified_in_teratocarcinoma_cell_line_ECA39	2.6169E+128	0.05194757	gb:X17502.1
Mouse_neonatal_mandibla_mRNA_for_amelogenin	2.5413E+128	0.04211263	gb:D31769.1
Weakly_similar_to_KERATIN,_TYPE_I_CUTICULAR_HA3_	2.5139E+128	0.00199975	gb:AI845957
clone:4930447P09:dynamin_2,_full_insert_sequence.	2.4625E+128	0.05139918	gb:AK015410.1
Cd84_CD84_antigen	2.4612E+128	0.04153091	gb:BM212728
Weakly_similar_to_nuclear_protein_95_	2.3948E+128	0.08353105	gb:BB292098
Axl_/UG_TITLE=AXL_receptor_tyrosine_kinase	2.3718E+128	0.09068081	gb:BB498381

Table 6.2 – Total Rank product tables for **A,** top 100 most up-regulated genes **B,** top 100 most Down-regulated genes. (P=<0.05 is significant, N=6 and N=5 for $Lkb1^{+/+}$ and $Lkb1^{fl/fl}$ samples respectively). Lists ordered by Rank product.

6.3.3 SAM analysis

A further alternative method is Statistical Analysis of Microarray (SAM), which produces a ranked list of up and down regulated candidate genes. SAM analysis ranks the significance of the changes observed following MaxD filtering and GGM normalisation and also controls the expected number of false positives (Tusher *et al* 2001).

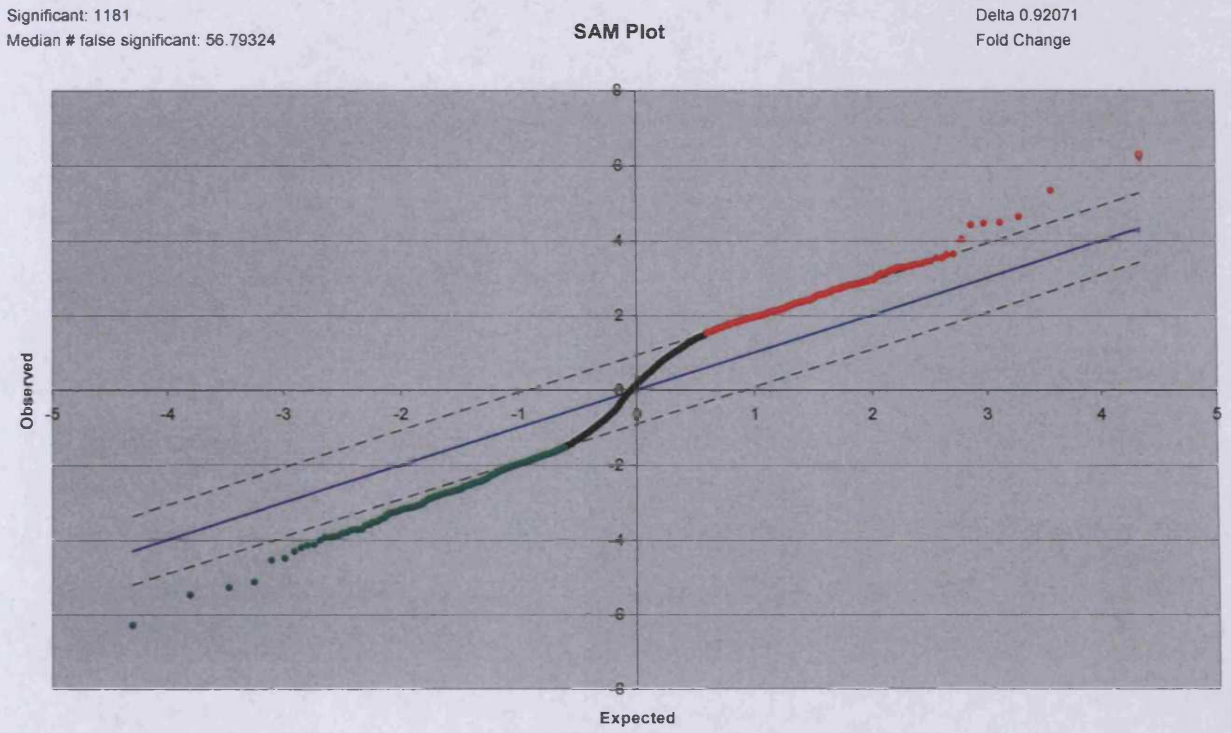

Figure 6.3 – SAM plot of significant genes from day 4 microarray analysis. Genes plotted in red denote up-regulated candidates whereas those in green are down-regulated. (N=6 vs N=5 for $Lkb1^{+/+}$ and $Lkb1^{fl/fl}$ samples respectively).

SAM analysis from figure 6.3 calls 1181 significant genes when using a false discovery rate (FDR) of 4.8% (a FDR of around 5% is considered adequate, using a FDR of 4.8% subsequently calls 56.79 genes as false positives). SAM called 607 significant upregulated genes and 574 significantly down regulated genes, although there is no fold change value assigned to these changes.

6.4A- SAM generated significant up-regulated genes

Continued

Gene Name	Ndn_/=necdin
tumor_necrosis_factor_(Tnf)	**Atoh1__atonal_homolog_1_(Drosophila),**
Impg1_interphotoreceptor_matrix_proteoglycan_1	Spi16_/serine_proteinase_inhibitor_mBM17
zinc_finger_protein_98_(Zfp98),	protocadherin_beta_6_(Pcdhb6)
Slc21a2_solute_carrier_family_21_(prostaglandin_transporter)	L1_cell_adhesion_molecule_
sema3A__semaphorin_3A,	ets-related_transcription_factor
nicotinic_acetylcholine_receptor_beta4_subunit_(Chrnb4)	Tle3_/transducin-like_enhancer_of_split_3,
G_protein-coupled_receptor_61;	Col15a1_collagen,_
Bmp1_bone_morphogenetic_protein_1	Rap1ga1_Rap1,_GTPase-activating_protein_1_
prostate_specific_ets_transcription_factor_(Pse-pending),_	Fcnb_ficolin_B_
Hpd_4-hydroxyphenylpyruvic_acid_dioxygenase,	Ndn necdin
T-cell_death_associated_gene_(Tdag)	Bmp2_bone_morphogenetic_protein_2
Aqp6_aquaporin_6	Cnnm3_cyclin_M3
Drag1_Rho-_and_Arf-GTPase_activating_protein_1	CCAATenhancer_binding_protein_(CEBP),_beta_(Cebpb),
oxytocin_(Oxt),	Hmgn2_high_mobility_group_nucleosomal_binding_domain_2
Dtx3_deltex_3_homolog	Slc21a2_solute_carrier_family_21_(prostaglandin_transporter)
Brp14_brain_protein_14_	Lasp1_=LIM_and_SH3_protein_1
Clasp2-pending_/	Tuba2_tubulin,_alpha_2
haptoglobin_(Hp),	ATX1_(antioxidant_protein_1)_homolog_1_(yeast)_(Atox1)
claudin_2_(Cldn2),	Fgfr1_ibroblast_growth_factor_receptor_1_
(metargidin)_(Adam15),	cystic_fibrosis_transmembrane_conductance_regulator_homolog
INTESTINAL_MUCIN-LIKE_PROTEIN_(MLP)	heat_shock_27kD_protein_3_(Hspb3)
SRY-box_containing_gene_18_(Sox18),	Hal__histidase_locus_histidine_ammonia-lyase
Wars_tryptophanyl-tRNA_synthetase	cholinergic_receptor,_nicotinic,_alpha_polypeptide_7_(Chrna7)
3-oxoacid_CoA_transferase_2_(Oxct2),	Ggcx_gamma-glutamyl_carboxylase
Fibroblast_growth_factor_21_(Fgf21),	LMA1_MOUSE_LAMININ_ALPHA-1_CHAIN
FXYD_domain-containing_ion_transport_regulator_3_(Fxyd3)	forkhead_box_P3_(Foxp3),
Poliovirus_sensitivity_(Pvs),	(ADAMTS-1),
solute_carrier_family_2,_member_10_(Slc2a10),	Gabra1__(GABA-A)_receptor,
Ttyh1_tweety_homolog_1_	nuclear_receptor_coactivator_3_(Ncoa3)
solute_carrier_family_4__member_3_(Slc4a3)	soluble_D-factorLIF_receptor,
Pla2g2fphospholipase_A2,_group_IIF	sideroflexin_3_(Sfxn3),
integrin_binding_sialoprotein_(Ibsp)	similar_JAK3_
ATP-dependent_RNA_helicase	solute_carrier_family_21_member_2_(Slc21a2),_
_PBX1B_homeobox_protein	ferredoxin_reductase_(Fdxr),
_disabled_homolog_2_(Drosophila)_(Dab2),	Tm9sf2_transmembrane_9_superfamily_member_2
Peg3_paternally_expressed_3	SMAF1
cation-chloride_cotransporter_9_(CCC9)	Acetylcholinesterase_(Ache),
GPI-anchored_metastasis-associated_protein_homolog_(C4.4a-pending)	naked_cuticle_1_homolog_(Drosophila)_(Nkd1)
Gpr73_protein-coupled_receptor_73	Notch_gene_homolog_3,_(Drosophila)_(Notch3)
natriuretic_peptide_receptor_3_(Npr3)	inhibitor_of_DNA_binding_3_(Idb3)
Paxip1_PAX_interacting protein_1	septin_3_(Sept3)
Atf5_/activating_transcription_factor_5-beta	Npas2_neuronal_PAS_domain_protein_2
IGnTB_beta-1,6-N-acetylglucosaminyltransferase_B	zinc_finger_protein_385_(Zfp385)
Neurexin_1-alpha_(Neurexin_I-alpha)	YY1_transcription_factor_(Yy1),
Asns_asparagine_synthetase	Rho_GTPase_activating_protein_1,
tripartite_motif_protein_8_(Trim8)	forkhead_box_B2_(Foxb2)
Ephb2_Nuk_receptor_tyrosine_kinase	Ttyh1_tweety_homolog_1
signal_transducing_adaptor_molecule_2	Glns_/glutamate-ammonia_ligase
Osbp2_oxysterol_binding_protein_2	growth_arrest_specific_1_(Gas1)

6.4B- SAM generated significant down-regulated genes

Gene Name	Continued
Bdkrb2_bradykinin_receptor,_beta_2	regulator_of_G-protein_signalling_10_(Rgs10)
Fhl4_four_and_a_half_LIM_domains_4	Rnf32_ring_finger_protein_32
Ncf1_p47phox,	cysteine_dioxygenase_1,_cytosolic_(Cdo1),
CEA-related_cell_adhesion_molecule_10_(Ceacam10),	Klf9_Kruppel-like_factor_9
small_nuclear_ribonucleoprotein_N_(Snrpn),	NADH_dehydrogenase_(ubiquinone)_1,_(Ndufc1)
Sth2_sulfotransferase,_hydroxysteroid_preferring_2	Yamaguchi_sarcoma_viral_(v-yes-1)_oncogene_homolog#
FMS-like_tyrosine_kinase_3_(Flt3),	plasminogen_(Plg),
CEA-related_cell_adhesion_molecule_10_(Ceacam10)	chemokine_(C-C)_receptor_2_(Cmkbr2),
pituitary_specific_transcription_factor_1_(Pit1)	Pthlh_parathyroid_hormone-like_peptide
N-myc	cyclin-dependent_kinase-like_2_(CDC2-related_kinase)_(Cdkl2),
inversin_(Invs),	fucosyltransferase_8_(Fut8),
acyl-Coenzyme_A_oxidase_3,_pristanoyl_(Acox3)	lymphocyte_antigen_86_(Ly86),
Arl6ip6_DP-ribosylation-like_factor_6_interacting_protein_6	T-cell_receptor_gamma,_variable_4_(Tcrg-V4),
Drr3_developmentally_regulated_repeat_element-containing_transcript_3	Nap1l1_nucleosome_assembly_protein_1-like_1
mscd6_precursor_(Cd6)	Bpgm__2,3-bisphosphoglycerate_mutase,_
lyn_B_protein_tyrosine_kinase_(lynB)	Pea15_phosphoprotein_enriched_in_astrocytes_15_
coagulation_factor_II_(thrombin)_receptor-like_2_(F2rl2)	fragile_X_mental_retardation_gene_1,_autosomal_homolog_(Fxr1h)
vacuolar_protein_sorting_16_(Vps16),	alcohol_dehydrogenase_5_(Adh5
anti-human_CD20_antibody_1F5_kappa_light_chain_	peroxisome_proliferator_activated_receptor_gamma_(Pparg),
Tcea3	calbindin-D9K_(Calb3)
zinc_metallopeptidase_(Adamts10)	gbpyruvate_dehydrogenase_kinase,_isoenzyme_1,
Gpr85_/G_protein-coupled_receptor_85	Uros uroporphyrinogen_III_synthase_
Lck-interacting_transmembrane_adaptor_protein	ornithine_transcarbamylase_(Otc)
hepatocellular_carcinoma-associated_antigen_59,_	Oct2.4_transcription_factor.
* **Peutz-Jeghers_syndrome_kinase_LKB1**	PHEMX_(Phemx)
Cyp2j9__cytochrome_P450_CYP2J9	tnf (ligand)_superfamily,_member_13b_(Tnfsf13b),
_inter-alpha_trypsin_inhibitor,_heavy_chain_2_(Itih2)	Nfic_/nuclear_factor_IC_
Gdm1_glycerol_phosphate_dehydrogenase_1	Cyp40_/cytochrome_P450,_40_
Sla_src-like_adaptor_protein	Samsn1_SAM_domain,_SH3_domain_and_nuclear_localization_signals,_1
_small_nuclear_ribonucleoprotein_N_(Snrpn)	immunoglobulin-associated_alpha_(Iga)
lymphoid-restricted_membrane_protein_(Lrmp)	hydroxysteroid_11-beta_dehydrogenase_1_(Hsd11b1)
haplotype_t_axonemal_dynein_heavy_chain_8_long_form_(Dnahc8)	proteoglycan,_secretory_granule_(Prg)
neuropilin_and_tolloid_like-1	Stxbp3_syntaxin_binding_protein_3
RING_finger_protein_Mmip-2	RNA_for_high_mobility_group_2_protein
(proline_4-hydroxylase),_alpha_II_polypeptide_(P4ha2),	CC_chemokine_receptor_10A_(Ccr10)
myeloperoxidase(Mpo),	Nqo1_NAD(P)H_dehydrogenase,_quinone_1
homeo_box_C5_(Hoxc5)	melanoma_antigen_recognized_by_T_cells_2,_
f-box_only_protein_16_(Fbxo16),	carbonic_anhydrase_5b,_mitochondrial_(Car5b)
Src-associated_adaptor_protein_(	carbonic_anhydrase_4_(Car4)
Igf2bp3_insulin-like_growth_factor_2,_binding_protein_3	D5Buc24e_
BarH-like_1_(Drosophila)_(Barhl1)	Cbp_cytohesin_binding_protein
guanine_nucleotide_binding_protein_(G_protein),_gamma_5,_	Cdc42_cell_division_cycle_42_homolog
signal_transducer_and_activator_of_transcription_4_(Stat4)	Axl_=AXL_receptor_tyrosine_kinase
C-type_lectin-like_receptor_2_(Clec2-pending)	cathepsin_E_(Ctse),
Cyyr1_cysteine_and_tyrosine-rich_protein_1	Snrpn_/small_nuclear_ribonucleoprotein_N
Twg-pending_twisted_gastrulation_protein	Ntan1_N-terminal_Asn_amidase_
P4ha1__(proline_4-hydroxylase)	Cnn3_calponin_3,_acidic
guanine_nucleotide_binding_protein_gamma_4_subunit_(Gng4),	
dihydropyrimidinase-like_4_(Dpysl4),	
melanoma-derived_leucine_zipper,_extra-nuclear_factor_(Mlze)	
SNRPN_upstream_reading_frame_(Snurf)	

Table 6.4 –SAM output data from combined SAM methods **A,** Top 100 most significant up-regulated genes **B,** Top 100 most significant down-regulated genes. (N=6 vs N=5 for *Lkb1*$^{+/+}$ and *Lkb1*$^{fl/fl}$ samples respectively). LKB1 is indicated in 4B in bold (*).

Originally SAM analysis was performed on MaxD normalised data sorted by T-test for significance. Genes with a P value of <0.1 were filtered then inputted to SAM. However, this data must be interpreted with caution as inputting prefiltered data into SAM will affect the degree of noise in the system and generate inaccurate FDRs. Therefore SAM analysis should be performed on the entire MaxD output of normalised, centred data and unfiltered data. However, the MOE430_2.0 gene chips generate a very large data set of 46,000 genes, which is incompatible with SAM analysis. Dividing the data set in half produced very high FDRs and few significant genes, however comparison of the tables produced by this method with those generated from filtered data revealed very little difference in the top genes called. Table 6.4 outlines those genes called by SAM analysis to be most significantly changed between the 2 genotypes by both methods. Again several genes that were identified from tables 6.1 and 6.2 appear in the SAM lists, including LKB1, which appears on the down regulated list (table 6.4B) as the 26th most significantly down regulated gene.

6.3.4 Clustering analysis

Cluster analysis investigates expression patterns of gene sets and may identify genes that are similarly regulated. I used Hierarchical clustering to define the distance (Euclidean) between the gene profiles from each sample and to order genes in terms of greatest similarity (Mcshane *et al* 2002). The output is a large tree of patterns of interest, which may be followed to reveal gene cascades and molecular events involved in feedback loops or knock on mechanisms. I entered normalised, centred, T-test ranked array data to Epiclust software primarily to observe reliability and quality of samples.

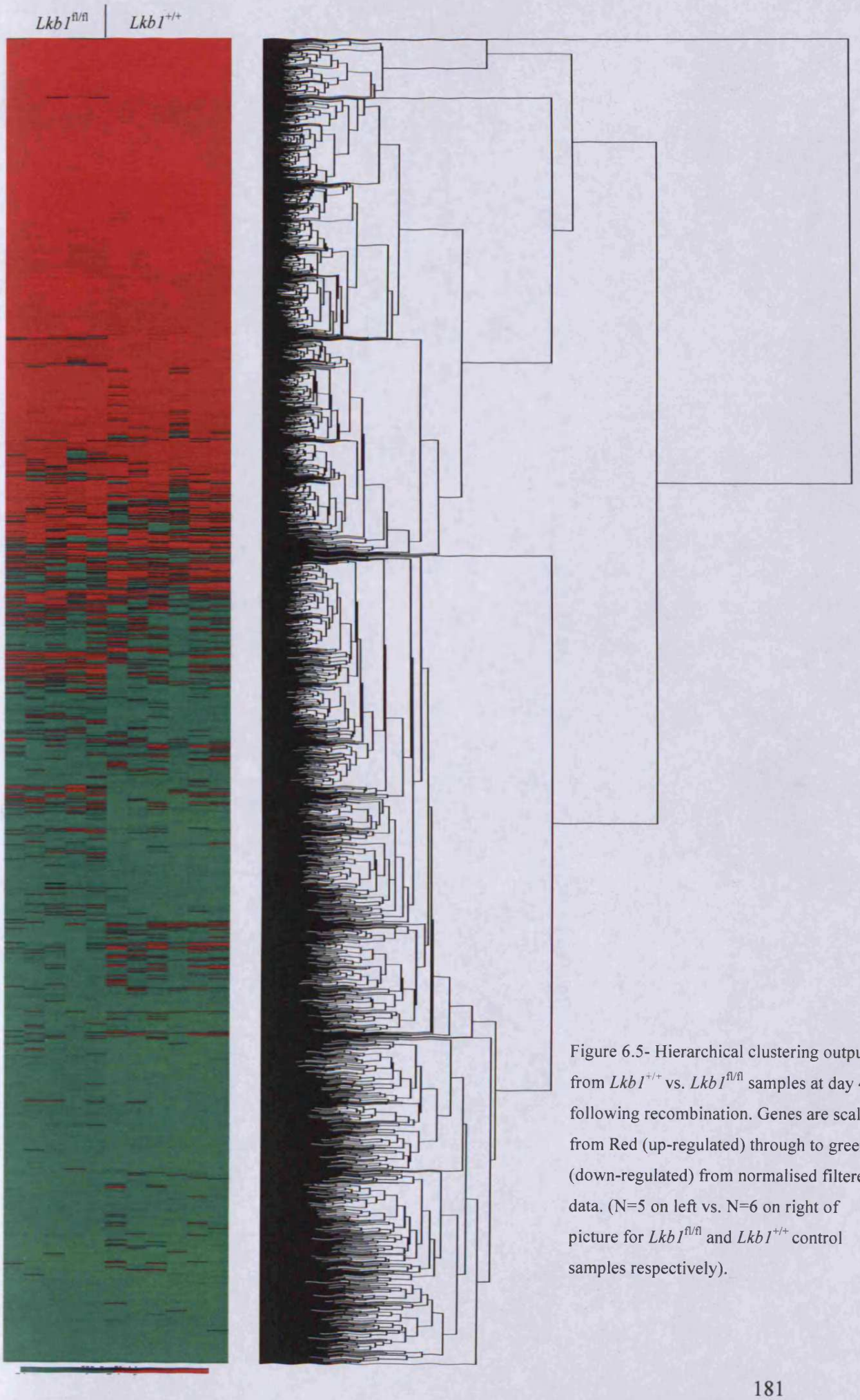

Figure 6.5- Hierarchical clustering output from *Lkb1*$^{+/+}$ vs. *Lkb1*$^{fl/fl}$ samples at day 4 following recombination. Genes are scaled from Red (up-regulated) through to green (down-regulated) from normalised filtered data. (N=5 on left vs. N=6 on right of picture for *Lkb1*$^{fl/fl}$ and *Lkb1*$^{+/+}$ control samples respectively).

Visual inspection of the clustering analysis shown in figure 6.5 suggests that the quality of the samples was high as no individual samples displayed strikingly different patterns of expression.

6.3.5 Generation of Candidate gene lists

An overall list of genes of interest (Table 6.6) was generated by combining array data from all the above lists (Fold change (Table 6.1), Rank product (Table 6.2) and SAM (Table 6.4), all of which methods alone show various shortcomings. Together these lists contained genes that frequently appeared in more than one of the top 100 lists. These genes were considered strong candidate genes to further pursue and validate and were arranged in order of largest fold change from raw data (Table 6.6). Additionally those genes that were not implicated by the microarray analysis methods but that were of considerable interest to the Lkb1 system were also marked as candidates for investigation. The relevance of these candidates will be discussed further in the section 6.4.

6.6A – Candidate up-regulated genes

gene	accession no	fold change	ttest	name	function
Adn	**gb:NM_013459**	**13.62**	**0.1622**	**adipsin**	**Adipocyte differentiation/Immune**
Hp	gb:NM_017370	11.09	0.1162	haptoglobin	Heme binding /differentiation /immune/ adipocyte
Gpr61	gb:AW493195	7.714	0.087	G protein-coupled receptor 61	G-protein signal transduction
POZ56	gb:AF290198	5.883	0.0961	POZ 56 protein	Protein binding
Aqp6	**gb:AI956846**	**5.819**	**0.0758**	**aquaporin 6**	**secretory ion channel/Immune/ Adipocyte regulation**
ADAM18	gb:NM_010084	5.2	0.0773	a disintegrin and metalloprotease domain 18	Adhesion/ecm remodelling
Npas2/MOP4	gb:NM_008719	5.084	0.077	neuronal PAS domain protein 2	bHLH Transcription factor/ circadian behaviour
Ibsp	gb:NM_008318	4.997	0.0487	integrin binding sialoprotein	Adhesion/integrin signalling/
fzd3	gb:NM_021458	4.129	0.1614	Frizzled homolog 3	Gprot/Ras/ Growth/Adhesion/Wnt
TNF	**gb:NM_013693**	**4.085**	**0.0649**	**tumour necrosis factor**	**Inflammation/Cell death /differentiation/ proliferation**
B3galt5	gb:NM_033149	4.078	0.0694	UDP-Gal:betaGlcNAc	Carbohydrate metabolism
Chrnb4	gb:AF492840	4.029	0.0219	nicotinic acetylcholine receptor beta4 subunit	Ion channel/ nAchR
Zfp98	gb:NM_016793	3.868	0.1419	zinc finger protein 98	Growth/ differentiation/ p38/ERK
Kcne1/ISK/MINK	gb:NM_008424	3.804	0.3688	potassium voltage-gated channel1	ATPase/Cl^- secretory/cAMP
Ttyh1	gb:BB560071	3.749	0.0653	tweety homolog 1	Iron transport/ Cation transport
IL2 R α/CD25	gb:AF054581	3.671	0.1313	interleukin 2 receptor, alpha chain	differentiation/inflammation/ proliferation/JAK-STAT
C4.4a pending	gb:NM_133743	3.634	0.0551	GPI-anchored metastasis-associated protein homolog	Metastasis/ecm remodelling
Lect1/ChM-1	gb:NM_010701	3.569	0.0987	leukocyte cell derived chemotaxin 1	Growth/ proteoglycan synthesis/inhibits angiogenesis
Impg1	gb:BC022970	3.395	0.0713	interphotoreceptor matrix proteoglycan 1	Adhesion/survival
S100a8	gb:NM_013650	3.358	0.0868	calgranulin A	Ca2+ binding/ immune/inflammation
Bmp1	**gb:BG248060**	**3.347**	**0.027**	**bone morphogenetic protein 1**	**patterning/organogenesis/differentiation**
Pcdhb6	gb:NM_053131	3.134	0.0235	protocadherin beta 6	Polarity/Ca2+/Adhesion/Wnt
Lifr	gb:D17444	3.05	0.0674	soluble D-factorLIF receptor	Immune/ hormone/differentiation
Ttyh2	gb:NM_053273	2.996	0.0653	tweety homolog 2	unknown
Cldn2	**gb:NM_016675**	**2.864**	**0.0173**	**Claudin 2**	**Cell adhesion-Tight junction/ TNF/ Cdx2/ differentiation**
Pla2g2f	gb:AV228827	2.832	0.0913	phospholipase A2, group IIF	Lipid catabolism/Ca2+ binding/
Slc2a10	gb:NM_130451	2.806	0.2254	solute carrier family 2 ,10	Ion /Glucose transport
Cntn6	gb:NM_017383	2.746	0.1121	contactin 6	Notch ligand/ progenitor differentiation
Pdyn	gb:AF026537	2.683	0.0774	prodynorphin	Glucose signalling/ secretion/immune/stress
Rps19	gb:AI594148	2.672	0.0692	ribosomal protein S19	Protein synthesis/ribosome/differentiation
NOS2	gb:AF065921	2.576	0.1728	nitric oxide synthase 2	Immune/ stress/ TNF induced /TJ adhesion
Adam 15/MDC15	gb:NM_009614	2.575	0.0175	metargidin	TNF cleavage/ secretory/ adhesion/ ecm remodelling
Sema 3A/SemD	**gb:BB124175**	**2.554**	**0.0788**	**secreted, (semaphorin) 3A**	**Angiogenesis/ vascular remodelling/ growth/p38/MAPK/motility**

Gcap8	gb:AK021073	2.391	0.1471	Granule cell antiserum pos 8	unknown
Slc21a2	gb:BI108501	2.382	0.0725	solute carrier family 21 member 2	Solute transport/prostaglandin transport/
Has1	gb:NM_008215	2.377	0.0627	hyaluronan synthase1	Growth/transformation
Lama 4	gb:BB053010	2.358	0.1228	laminin, alpha 4	Cell adhesion/ecm remodelling/angiogenesis
Foxb2/Fkh4	**gb:NM_008023**	**2.264**	**0.0287**	**forkhead box B2**	**Transcription factor/development**
Atf5	gb:AF375476	2.162	0.1085	activating transcription factor 5-beta	Transcription/ development/ differentiation
Nkd	gb:NM_027280	2.161	0.0711	naked cuticle 1 homolog (Drosophila)	Zn binding/ Wnt antagonist/cell fate/polarity
Dsc1	gb:NM_013504	2.077	0.1211	desmocollin 1	Cell adhesion/differentiation/protease
ADAM-TS 10/Znmp	gb:BB193444	2.072	0.4034	A disintegrin and metalloproteinase with thrombospondin motifs 10	ECM remodelling /integrin signalling
foxp3	gb:NM_054039	2.04	0.0597	forkhead box P3	T cell Immune response/TGFβ induced/ Transcription/ development/
Ndn	gb:AV124445	2.024	0.0321	necdin	Differentiation/TGFβ induced/Transcription
Gpr73	gb:BB037474	2.007	0.1562	G protein-coupled receptor 73	Angiogenesis/Proliferation/migration/
Hes 3	**gb:NM_008237**	**2.007**	**0.2552**	**hairy and enhancer of split3**	**Differentiation inhibition /Stemness/ Notch**
Ngn3	**gb:NM_009719**	**2.002**	**0.1845**	**neurogenin 3**	**Endocrine Cell fate/ Notch/ differentiation**
MLP	gb:AK008250	1.708	0.0374	Intestinal mucin-like protein	Unknown
Atoh1/ Math1	**gb:BC010820**	**1.529**	**0.3116**	**atonal homolog 1 (Drosophila)**	**DNA binding/Differentiation – secretory/ transcription/Notch**
Sox18	gb:NM_009236	1.478	0.1588	SRY-box containing gene18	Transcription/development
Bmp2	gb:AV239587	1.382	0.5185	bone morphogenetic protein 2	Differentiation/ Growth/pro-apoptosis/ Development/cell fate/ TGFβ signalling
Notch 3	**gb:NM_008716**	**1.363**	**0.2996**	**Notch gene homolog 3**	**Development/ inhibition of differentiation/**
Oxt	gb:NM_011025	1.281	0.4243	oxytocin	Blood pressure/stress/hormone/
L1cam	gb:BB132473	1.28	0.5347	L1 cell adhesion molecule	Neural growth/ adhesion/ motility/ proliferation/ differentiation
Hes1	**gb:BC018375**	**1.028**	**0.9334**	**hairy and enhancer of split 1**	**Differentiation inhibition /Stemness/Notch/ Math1 inhibition**

6.6B– Candidate down-regulated genes

gene	accession no	fold change	ttest	name	function
Mlze	gb:NM_031378	12.24	0.088	melanoma-derived leucine zipper, extra-nuclear factor	Oncogenic/c-myc
Hornerin	gb:AY027660	9.27	0.088	hornerin	Ca2+binding/cornification
Fhl4	gb:AV047468	7.05	0.009	four and a half LIM domains 4	CREB activator/
Plg	gb:NM_008877	5.93	0.058	plasminogen	Apoptosis/coagulation/Ca2+binding/ angiogenesis inhibition/ regeneration
Siat7c	gb:NM_011372	5.54	0.220	sialyltransferase 7	Glycosylation/
Ceacam 10	**gb:NM_007675**	**5.09**	**0.082**	**CEA-related cell adhesion molecule 10**	**Adhesion/ transcription/ embryogenesis/ development**
Igf2bp3	gb:AW681763	4.42	0.027	insulin-like growth factor 2, binding protein 3	RNA synthesis/metabolism/ differentiation inhibition
CKII	**AK011501**	**4.19**	**0.126**	**Casein kinase 2 alpha1**	**Wnt signalling/ ATPase/ phosphorylation/ Adhesion/ oncogenic**
N-myc	gb:M36277	4.032	0.015	N-myc protein	Oncogenic/ cell cycle/ transcription/
LKB1/ STK11	**gb:AF145287**	**4.01**	**0.011**	**Peutz-Jeghers syndrome kinase/ Ser/Thr kinase 11**	**AMPK stress cascade/ cell cycle/cell death/ polarity/ Wnt?**
Neto1	gb:AV346211	3.95	0.053	neuropilin and tolloid like-1	Cell adhesion/motility/ development/
Hoxc5	gb:NM_008271	3.90	0.034	homeo box C5	transcription factor/ development/ adhesion
Klkb1	gb:BC026555	3.55	0.048	kallikrein B, plasma 1	Inflammatory/proteolysis/ bradykinin release
Rnf17	gb:AF190166	3.53	0.019	RING finger protein Mmip-2	Ubiquitination
Pit1	gb:NM_008849	3.48	0.060	pituitary specific transcription factor 1	Transcription/ development/ cell cycle/ growth hormones
Car4	**gb:NM_007607**	**3.22**	**0.112**	**carbonic anhydrase 4 (Car4)**	**Differentitation/ polarity/ ion transport/ anti-apoptosis**
Cd6	gb:U12434	3.22	0.019	mscd6 precursor	Cell adhesion/ lymphocyte antigen
Cts8	gb:NM_019541	3.15	0.054	cathepsin 8	Proteolysis/ placenta growth
Phemx	gb:AF175771	3.03	0.031	Pan hematopoietic expression	Differentiation/ embryogenesis
Snrpn	gb:NM_013670	2.85	0.152	small nuclear ribonucleoprotein N	Spliceosome complex/ maternally imprinted/
Nog	**gb:NM_008711**	**2.78**	**0.156**	**noggin**	**Development /BMP inhibitor/ growth**
Klf9	gb:BB327336	2.74	0.112	Kruppel-like factor 9	Transcription/ growth
stat4	gb:NM_011487	2.51	0.114	signal transducer and activator of transcription 4	Proliferation/ immune/ transcription/ differentiation
Parvg	gb:BC011200	2.50	0.174	gamma-parvin	Actin binding/ adhesion/cytoskeletal organisation/
Gabt1	gb:M92378	2.34	0.046	gamma-aminobutyric acid (GABA-A) transporter 1	Solute- Na transport/ neurotransmitter/
Invs	gb:NM_010569	2.31	0.104	inversin	Transcritption/ Development/ symmetry/ cell cycle/ Adhesion
Semac	**gb:X85992**	**2.31**	**0.079**	**semaphorin C/4b**	**Differentiation/ development**
Klk26	gb:NM_010644	2.26	0.036	kallikrein 26	Proteolysis/ growth factor binding
Calb3/S 100g	gb:NM_009789	2.12	0.040	calbindin-D9K	Ca2+ binding/ hormone regulated/ growth
Car5b	gb:NM_019513	2.00	0.112	carbonic anhydrase 5b, mitochondrial	Zn binding/ metabolism
Arl6ip6	gb:BB837198	1.98	0.143	DP-ribosylation-like factor 6	Ras family/ differentiation inhibition/

				interacting protein 6	membrane trafficking/
OB-Rs	**gb:U58862**	**1.98**	**0.123**	**leptin receptor short form**	**Metabolism/ hormonal regulator/ STAT/ enterocyte absorption**
Plxnc1	**gb:BG092693**	**1.93**	**0.228**	**plexin C1**	**Development/semaphorin receptor / integrin signalling/ angiogenesis/**
Gng4	gb:NM_010317	1.70	0.212	guanine nucleotide binding protein gamma 4 subunit	G-protein coupled transduction/
Klf7	gb:AF338369	1.69	0.365	Kruppel-like factor 7	Transcritption/ growth factor/
Bdkrb2	gb:NM_009747	1.53	0.493	bradykinin receptor, beta 2	G-protein coupled/ PIP3/Ca2+/ ERK
Pten	**gb:AA214868**	**1.48**	**0.382**	**phosphatase and tensin homolog**	**Ppase activity/ PI3K regulation/ cell cycle/ pro-apoptosis /migration/ development**
Acox3	gb:NM_030721	1.46	0.332	acyl-Coenzyme A oxidase 3, pristanoyl	Fatty acid oxidation/ electron transport
Cdkl2	gb:NM_016912	1.37	0.387	cyclin-dependent kinase-like 2 (CDC2-related kinase)	Kinase activity/development/ ATP binding
Cdx2	gb:NM_007673	1.04	0.900	caudal type homeo box 2	Transcription factor/ development/ cell fate/ differentiation/adhesion

Table 6.6 – Lists of Candidate genes compiled from Fold change, GGM rank product, SAM analysis and other genes of interest. **A,** Up-regulated chosen candidate genes **B,** Down-regulated candidate genes of interest. Those genes of particular interest to LKB1 signalling were highlighted in bold type.

6.3.6 qRT-PCR validation of target genes

Microarray data is a powerful tool to identify target genes from a knockout system, however these candidate genes must be confirmed and validated by means of qRT-PCR, immunohistochemistry or western blotting. To confirm targets picked from Table 6.6, I employed quantitative RT-PCR analysis of gene expression levels in cDNA samples from day 4 $Lkb1^{+/+}$ and $Lkb1^{fl/fl}$ mice (N=5 for $Lkb1^{fl/fl}$ mutant mice and N=6 for $Lkb1^{+/+}$controls). This technique relies on incorporation of Sybr green labelled nucleotides into the PCR product to assess changes in fold change of a gene of interest when compared to a control or housekeeping gene for normalisation. In my experiments β-actin gave consistent signal values from array data and was chosen as the normalising house keeping gene.

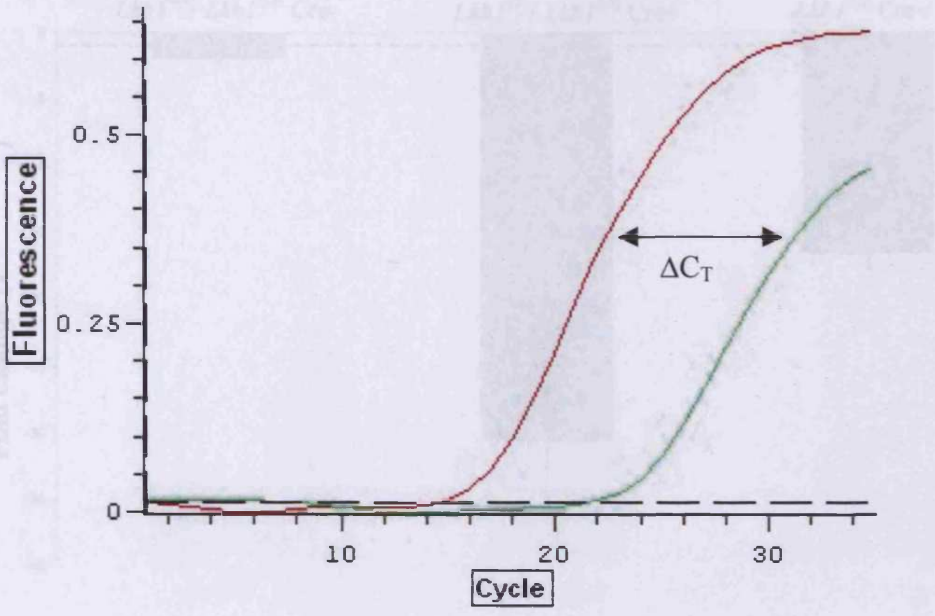

Figure 6.7– qRT-PCR light cycle graph for *Math1* PCR. Red line denotes fluor absorbance of *Lkb1*$^{fl/fl}$ sample for Math1, Green line denotes *Lkb1*$^{fl/fl}$ sample for β-actin housekeeping gene, and dotted line denotes noise band or threshold value). ΔC_T is the value at which the amount of product reaches a fixed threshold determined from a log-linear plot of PCR signal versus cycle number.

Figure 6.7 details the qRT-PCR output for the gene *Math1*. The cycle number is plotted against C_T value (threshold fluorescence value), showing log portion of the amplification process. Livak and Schmittgen recently described a method of analysing relative fold changes from qRT-PCR with the equation $2^{-\Delta\Delta C}{}_T$. The equation $2^{-\Delta\Delta C}{}_T$ is a conversion of the exponential data to a linear form and directly measures fold change in gene expression and is normalised to an endogenous housekeeping gene and relative to a wild type control.

$$\Delta\Delta C_T = (C_{T\ \text{target gene}} - C_{T\ \text{actin}})_{\text{mutant}} - (C_{T\ \text{target gene}} - C_{T\ \text{actin}})_{\text{wt}}$$

β-actin triplicates and gene x triplicates were averaged for each sample prior to ΔC_T calculation as reactions were performed in separate wells and variance was calculated using $\Delta\Delta C_T$ plus or minus standard error of the mean (considering each animal to be a separate experiment) (Livak and Schmittgen 2001).

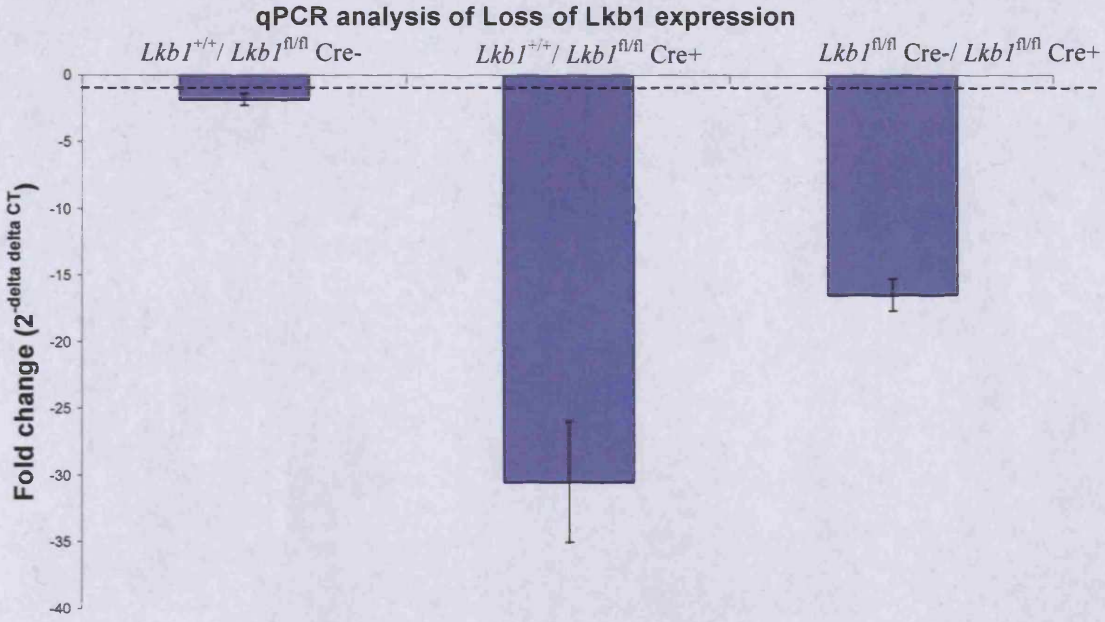

Figure 6.8– Graph of Lkb1 fold change (measured by $2^{-\Delta\Delta C}{}_T$) between *Lkb1*$^{+/+}$ Cre+, *Lkb1* $^{fl/fl}$ Cre+ and *Lkb1* $^{fl/fl}$ Cre- genotypes, N=6,7,10 respectively (error bars = SD, $2^{-\Delta\Delta C}{}_T$ calculated according to GAPDH housekeeping gene (dashed line). Work by Boris Shorning.

Figure 6.8 outlines the fold changes observed 4 days following intestinal loss of *Lkb1* using 80mg/kg β-Napthoflavone. Originally when *Lkb1*$^{+/+}$samples were compared to *Lkb1*$^{fl/fl}$ Cre+ mice, a 30.5 (+/-4.53 SD) fold decrease in transcript was observed (figure 6.8). Following the finding that the *Lkb1* floxed transgene may be a hypomorph (see chapter 7, Sakamoto *et al* 2005), *Lkb1*$^{+/+}$ and *Lkb* $^{fl/fl}$ Cre- mice were compared for loss of *Lkb1* transcript. Figure 6.8 shows that *Lkb1* $^{fl/fl}$ Cre- mice have a 1.85 (+/-0.44 SD) fold reduction in *Lkb1* mRNA compared to *Lkb1*$^{+/+}$ animals. Furthermore, when fold change was calculated between *Lkb1*$^{fl/fl}$ Cre+ and *Lkb1*$^{fl/fl}$ Cre- mice the reduction was 16.5 fold (+/-1.2 SD). Results confirm a significant level of knockdown of *Lkb1* within the intestine by day 4. Using whole tissue RNA extract it is not possible to show 100% deletion or knockdown by qRT-PCR or southern blot and a good Lkb1 antibody has yet to be developed.

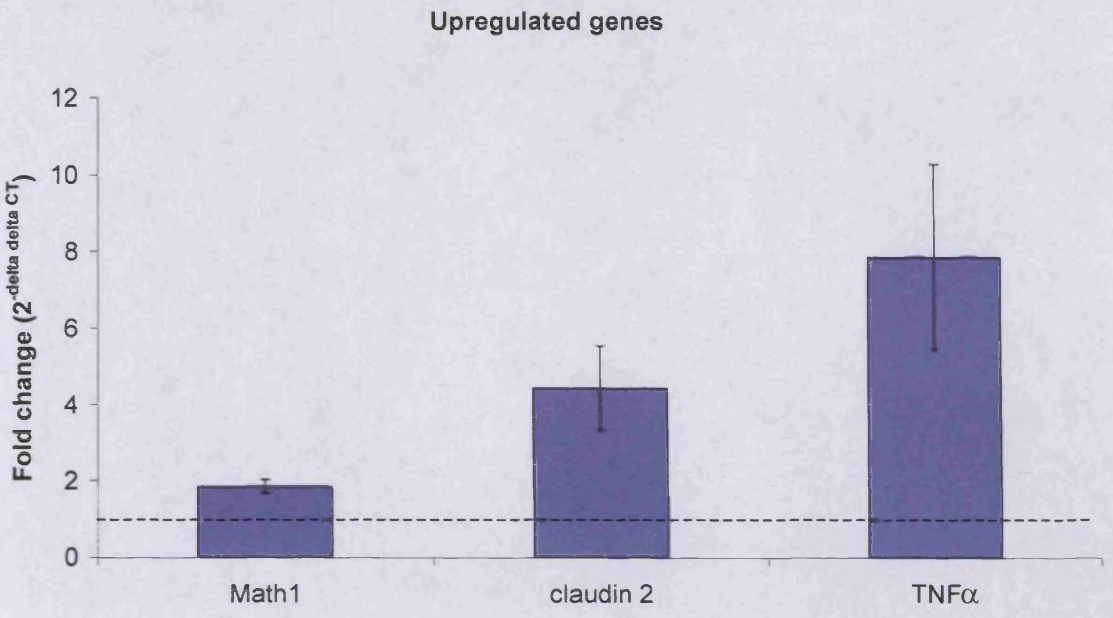

Figure 6.9 Graph confirming fold change (measured by $2^{-\Delta\Delta C}{}_T$) of upregulated targets from array data. (*Lkb1*$^{+/+}$; N=6, *Lkb1*$^{fl/fl}$ Cre+ N=5, error bars =SEM), dashed line indicates *Lkb1*$^{+/+}$ threshold level against β-actin housekeeping gene.

An inspection of Table 6.6 suggested a series of genes for preliminary qRT-PCRs to confirm up-regulated genes from the array. Math1, Claudin2 and TNFα showed increases in fold change compared to *Lkb1*$^{+/+}$ mice of: 1.85 (+/- 0.17sem), 4.42 (+/- 1.09 sem) and 7.85 (+/- 2.41 sem) respectively (figure 6.9). When these values are compared to data obtained from fold change from the array (Table 6.6A: Math1 = 1.52 (p= 0.31), Claudin2 = 2.86 (p=0.01) and TNFα = 4.08 (p=0.06)), we find actual transcript levels to be higher than predicted from the array. I also investigated qRT-PCR for BMP1 and Adipsin expression but found changes insignificant because of large sample variation.

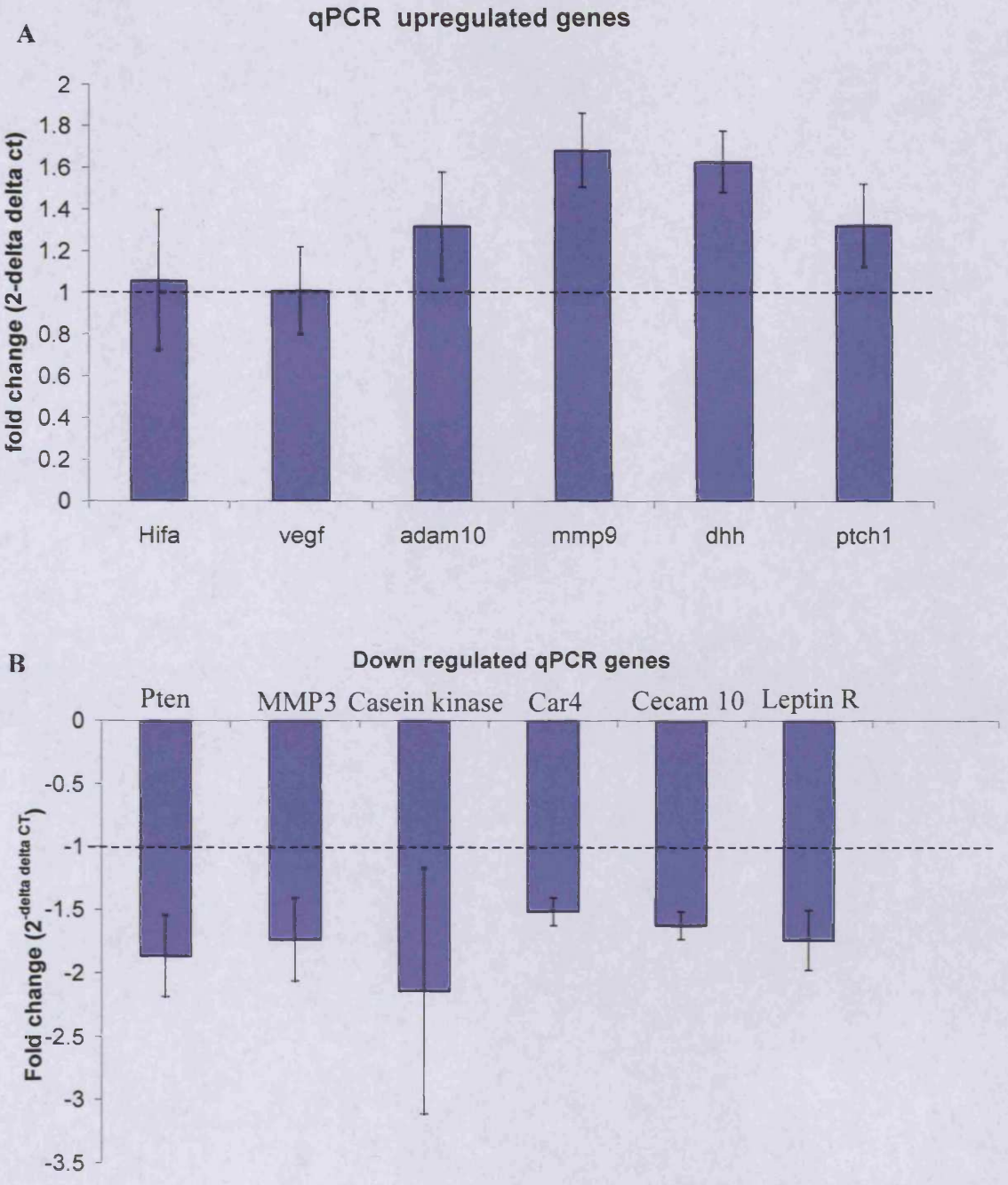

Figure 6.10 – Graph investigating fold change (measured by $2^{-\Delta\Delta C}{}_T$) of genes of interest and array targets. **A,** qPCR results of up-regulated genes involved in angiogenesis and matrix remodelling **B,** qPCR results of down regulated genes of interest. (*Lkb1*$^{+/+}$ Cre+; N=6, *Lkb1* $^{fl/fl}$ Cre+; N=5, error bars =sem), dashed line indicates *Lkb1*$^{+/+}$ Cre+; threshold level against GAPDH housekeeping gene. qRT-PCR work kindly performed by **A,** Dylan Edwards (Norwich university) and **B,** Boris Shorning (Cardiff university).

Matrix metalloproteinases (MMPs) are involved in the remodelling and degradation of the extracellular matrix (ECM), and changes in adhesion and matrix remodelling proteins such as the MMPs are commonly late stage changes in tumourigenesis (Lijnen 2004). Analysis by Boris Shorning (Cardiff University) and Dylan Edwards (MMP laboratory, Norwich university) investigated several of these genes of interest from array data (Table 6.6) and also a general screen for MMP related transcript changes. Figure 6.10A shows that HIFα and VEGF (angiogenesis regulators) were unchanged from *Lkb1*$^{+/+}$controls and similar data was obtained from my array data analysis. Minor changes were observed in matrix remodelling genes such as *Mmp9, Mmp3* and *Adam10* (fold changes: +1.68, -1.73, and +1.3 respectively), and these values were similar to those from my array data (+1.7, +1.05 and +2.07 respectively). Additionally *Casein kinase*, *Car4, Cecam10* and LeptinR were confirmed to be down regulated (2.1, 1.5, 1.6, 1.7 fold respectively figure 6.10B), although less so than indicated from the array (4.1, 5.09, 3.2 and 1.98 fold respectively Table 6.6B).

11A

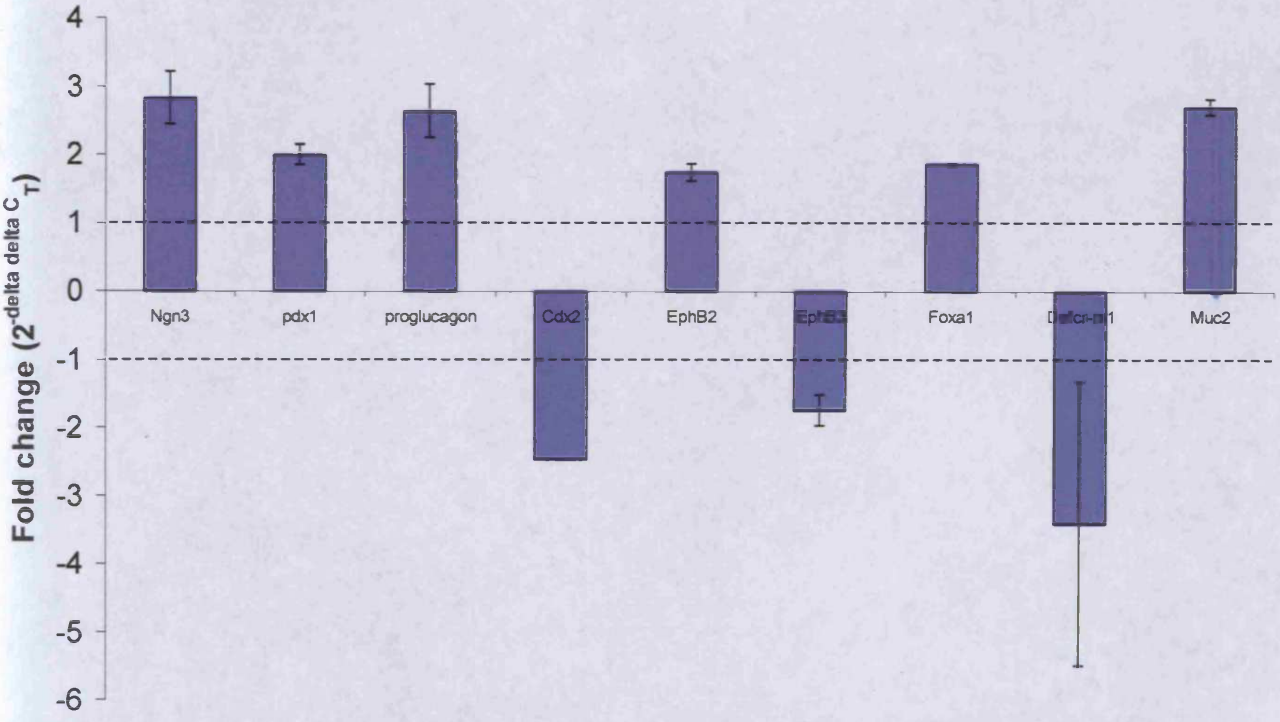

11B

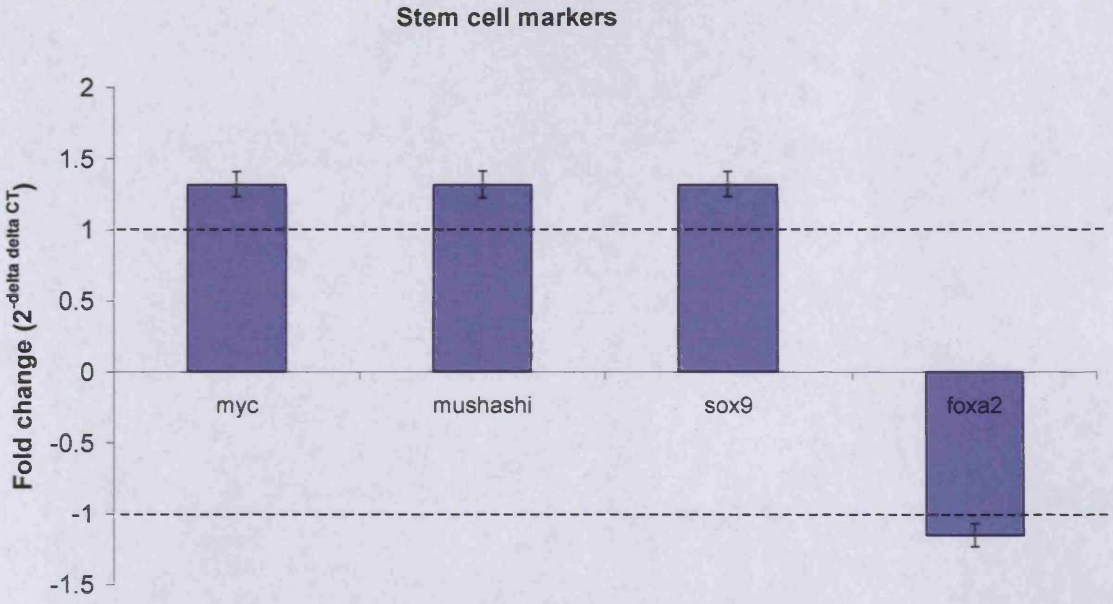

Figure 6.11 –qPCR fold changes from day 4 samples (measured by $2^{-\Delta\Delta C}{}_T$) **A,** Genes of interest relating to observed intestinal phenotype **B,** Stem cell associated genes (control = *Lkb1* $^{fl/fl}$ Cre- N=3, *Lkb1* $^{fl/fl}$ Cre+ N=3, error bars =SD, dashed line indicates control threshold level against GAPDH housekeeping gene). (qPCR performed by Boris Shorning).

Figure 6.11 indicates some of the genes of interest in the Lkb1 null mouse currently being investigated. Changes in differentiation markers such as Ngn3, Cdx2, Pdx1, proglucagon and Foxa1 were prominent from figure 6.11A. In addition, Eph expression and Defcr-rs1 reflected the aberrant paneth cell phenotype and Muc2 (marker of mature goblet cells) was also confirmed to be upregulated.

LKB1 has been shown to regulate AGS-3, a receptor independent activator of G-protein involved in asymmetric cell division and polarity by positioning of the mitotic spindle (Blumer *et al* 2003). This has given rise to the speculation that LKB1 may maintain correct stem cell division or polarity (Baas *et al* 2004). Figure 6.11B shows that transcripts for genes such as *c-Myc, Sox9 Foxa2,* and *Mushashi*, which are potential candidates for stem cell markers in the intestine (Potten *et al* 2003, Blache *et al* 2004, Wan *et al* 2004), are only weakly modified in response to Lkb1 loss.

6.3.7 Immunohistochemical validation of array targets

Although qRT-PCR analysis of Math1 transcripts in figure 6.9 confirmed array data values of 1.86 (+/-0.174) fold up-regulation, this does not indicate the effects at the protein level, if any, of increased Math1 mRNA. Therefore I investigated immunohistochemistry (IHC) of Math1 protein expression. Figure 6.12 shows a clear increase in Math1 positive cells in *Lkb1*$^{fl/fl}$ mice at day 4 and day 6 following recombination with 80mg/kg β-Napthoflavone. When positives were scored as a percentage of the crypt size, *Lkb1*$^{fl/fl}$ mice showed significant increased positives (*Lkb1*$^{+/+}$= 2.2% (+/-0.134), *Lkb1*$^{fl/fl}$ = 5.64% (+/-0.696) p= 0.0259 MWU).

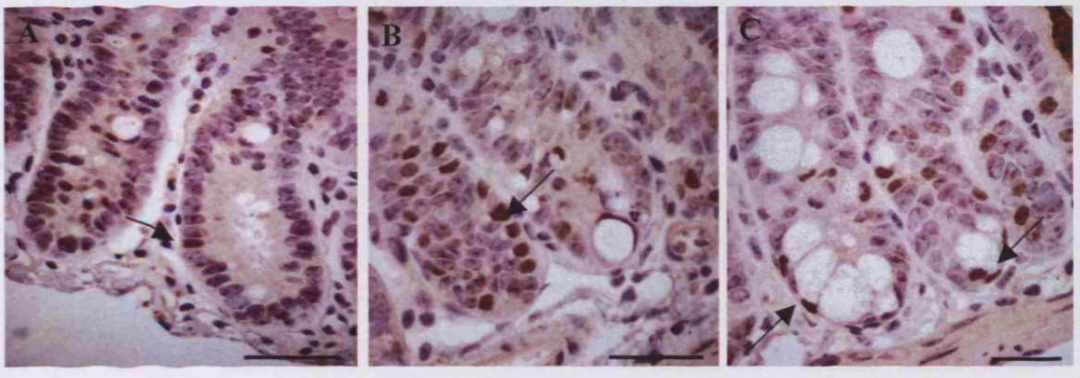

Figure 6.12 - Immunohistochemistry staining for Math1 secretory lineage transcription factor. Sections from **A**, *Lkb1*$^{+/+}$ **B**, *Lkb1* $^{fl/fl}$ mice at day 4 **C**, *Lkb1* $^{fl/fl}$ mouse at day 6 following recombination with 80mg/kg β-napthoflavone. (Arrows denote positive cells, scale bars=50μm).

Given the range of possible Lkb1 interactions discussed in section 1.5, I analysed *Lkb1*$^{fl/fl}$ sections for IHC changes in mTOR, and Wnt signalling. These signalling pathways were not obviously altered from the array data, however subtle changes in genes such as Pten, the MMPs or stem cell markers (figures 6.10-11) may suggest deregulation of these pathways, both of which may underlie the phenotype described in chapter 5.

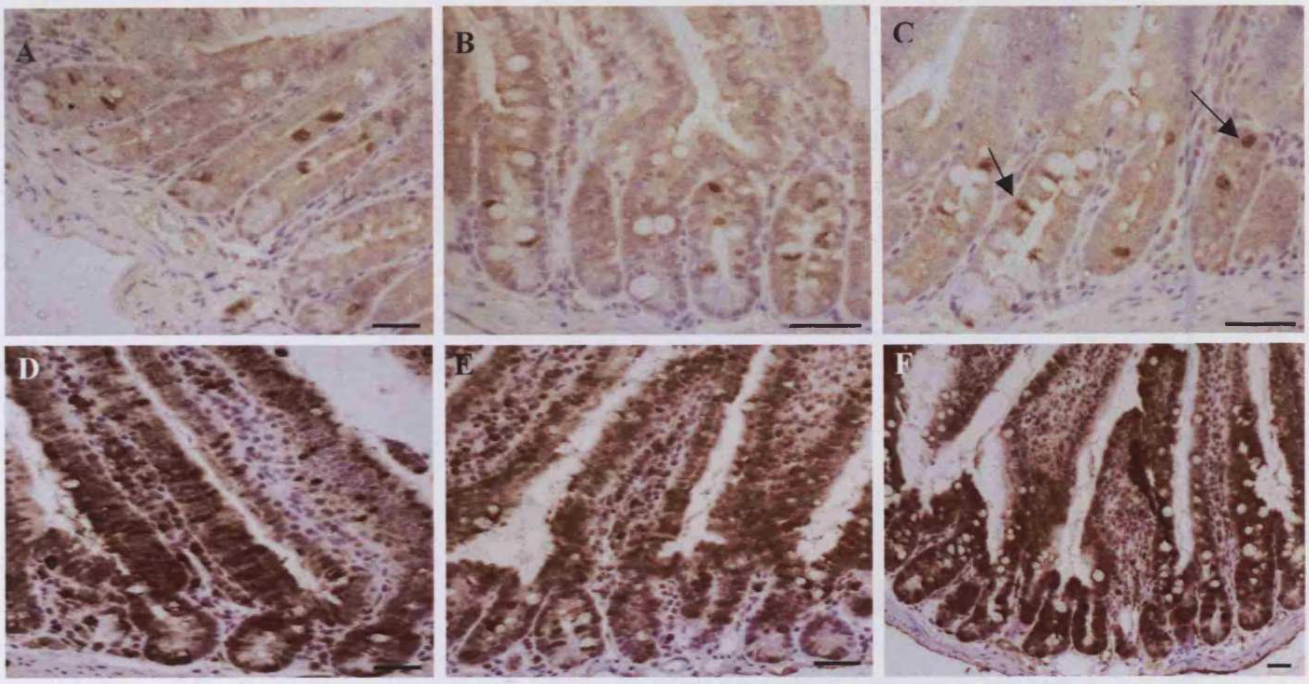

Figure 6.13 – Immunohistochemistry staining of possible Lkb1 effector proteins. Immunohistochemistry staining for activated phosphor-mTOR **A,** *Lkb1*$^{+/+}$ **B,** *Lkb1* $^{fl/fl}$ Day 6 following recombination **C,** *Lkb1* $^{fl/fl}$ 5 months following low level recombination with β-napthoflavone (arrows denote similar staining in crypts of both aberrant and Wt appearance. Immunohistochemistry staining for S6 ribosomal protein in **D,** *Lkb1*$^{+/+}$ **E,** *Lkb1* $^{fl/fl}$ mice day 4 **F,** *Lkb1* $^{fl/fl}$ mice day 6 following recombination (all scale bars =50μm).

Figure 6.13 A-C illustrates that there are no marked changes in phospho-mTOR protein levels by IHC, with percentage positives in crypts unchanged (*Lkb1*$^{+/+}$ =2.16% +/-0.96, *Lkb1*$^{fl/fl}$ = 2.45%+/-0.419 p=0.5959 MWU). Figure 13C shows phospho-mTOR IHC in a long-term low level recombined *Lkb1*$^{fl/fl}$ mouse (0.8mg/kg β-Napthoflavone), with histologically normal and aberrant crypts displaying similar mTOR staining.

S6K is a downstream effector of mTOR and AKT signalling and is up-regulated by survival signalling. S6 ribosomal protein phosphorylation is considered to be a good readout of this activated pathway. Figure 6.13 D-E demonstrates that cytoplasmic staining for S6 appears equal to control samples following Lkb1 loss and there are no signs of upregulation of S6 ribosomal protein at day 4. However, day 6 staining in *Lkb1*$^{fl/fl}$ animals does appear darker in area (figure 6.13 F).

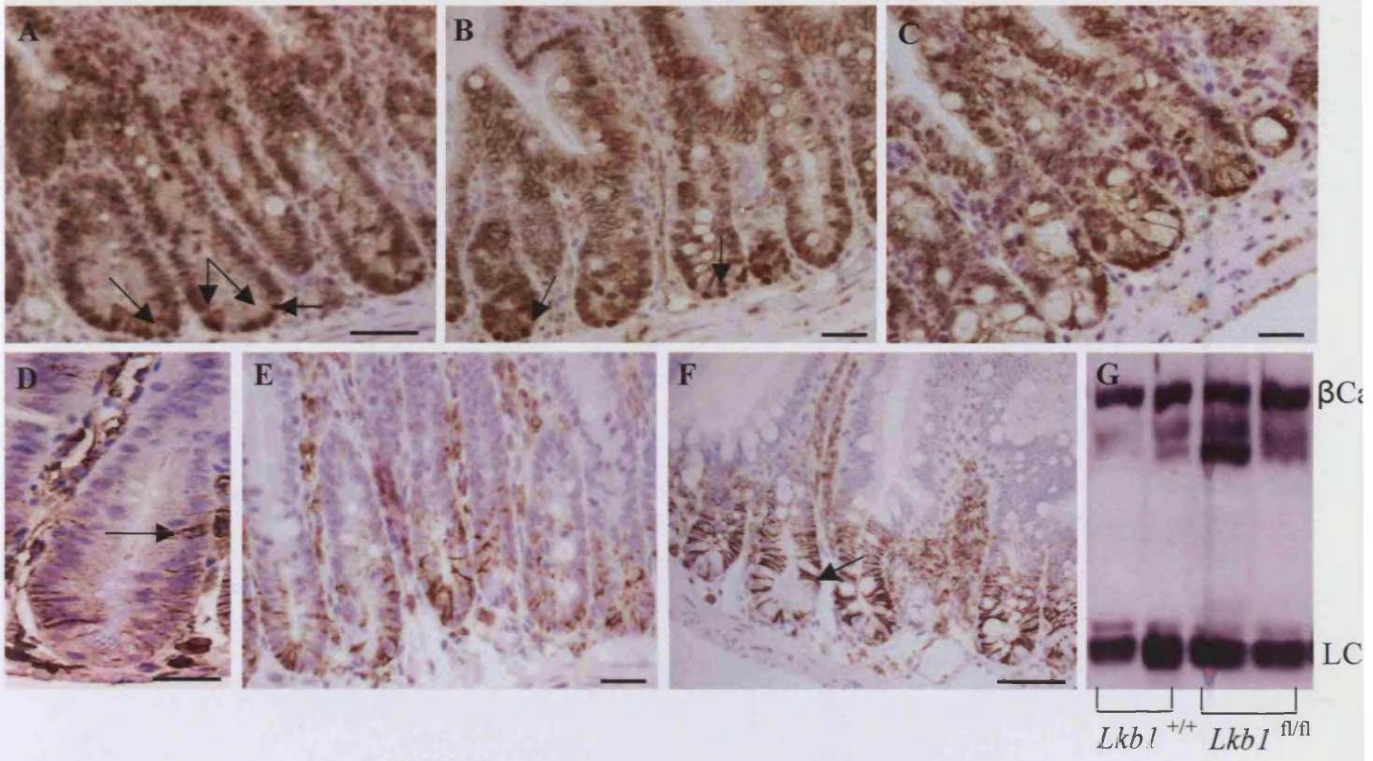

Figure 6.14 – Immunohistochemistry staining of Lkb1 effector proteins. Immunohistochemistry staining for nuclear β-Catenin **A,** *Lkb1*$^{+/+}$ **B,** *Lkb1* $^{fl/fl}$ day 4 **C,** *Lkb1* $^{fl/fl}$ day 6 following recombination. (arrows denote nuclear activated β-Catenin). Immunohistochemistry staining for CD44 **D,** *Lkb1*$^{+/+}$ (scale bar = 20μm) **E,** *Lkb1* $^{fl/fl}$ day 4 **F,** *Lkb1* $^{fl/fl}$ day 6 following recombination with 80mg/kg β-napthoflavone (arrow denotes basolateral staining) (all other scale bars = 50μm). **G,** Western blot analysis of total β-Catenin from day 4 recombined *Lkb1* $^{+/+}$ and *Lkb1* $^{fl/fl}$ whole tissue extract. LC= Light chain loading control.

Figure 6.14 outlines IHC for β-Catenin and CD44, both involved in Wnt signalling. Initial results from IHC staining for nuclear β-Catenin (activated Wnt) show no increase in nuclear catenin at the base of crypts between genotypes (Figure 6.14A-C). CD44 is another Wnt target that is up-regulated by β-Catenin and again *Lkb1* $^{fl/fl}$ mice show similar basolateral staining to *Lkb1*$^{+/+}$ controls (figure 6.14D-F). However, as was observed with S6 protein staining at day 6, levels of CD44 appear stronger at day 6 (figure 6.14F). Overall figures 13 and 14 confirm array data and qRT-PCR analysis with no significant changes in mTOR or Wnt signalling associated with the immediate Lkb1 loss in the intestine at day 4.

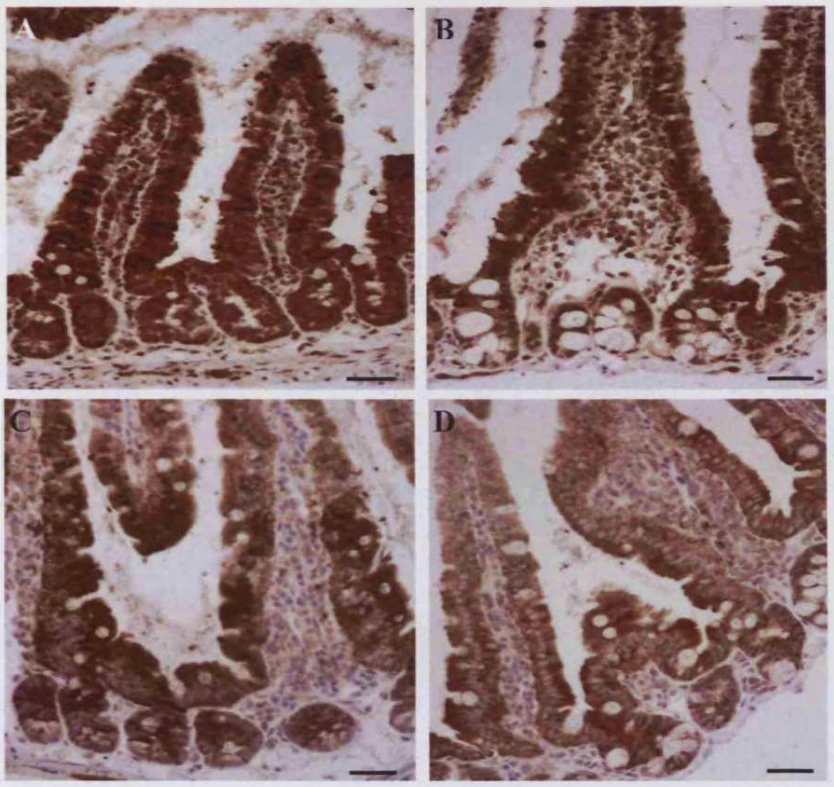

Figure 6.15– Immunohistochemistry staining of *Lkb1* $^{fl/fl}$ tissue. Phospho-Akt immunohistochemistry of **A,** *Lkb1* $^{+/+}$ **B,** *Lkb1* $^{fl/fl}$ sections 6 days following recombination with β-napthoflavone. **C,** *Lkb1* $^{+/+}$ **D,** *Lkb1* $^{fl/fl}$ Phospho-GSK-3 immunohistochemistry 6 days following recombination with β-napthoflavone. (scale bars = 50μm).

Finally, figure 6.15 details IHC of phospho-AKT as another readout of the PI3K/mTOR survival pathway, and GSK-3 is phosphorylated and inactivated by p-AKT. Figure 17 shows no gross changes in IHC in either protein in *Lkb1* $^{fl/fl}$ mice 6 days following recombination when compared to *Lkb1* $^{+/+}$ controls.

6.4 Discussion

6.4.1 Data Quality

During the course of the array analysis I found each type of analysis (Fold change, Rank product, SAM (Tables 6.1, 2 and 4 respectively) to have their own limitations. The variation in the signal values from the chips meant that once data was normalised and filtered by MaxD, many genes associated with Lkb1 signalling were screened out as insignificant. Also when analysing the raw data by fold change, many of the large fold changes were found to be insignificant when T-test pairwise analysis was performed, reflecting some variation for these genes between samples. This was in part alleviated by use of the Rank product test, which ranks genes in order of their fold change ratio between each possible sample combination rather than as a whole group average, giving genes a ranking from normalised, scaled and centred data, although no actual fold change value.

SAM analysis (Figure 6.3, Table 6.4) produced lists with several similar genes to those identified by fold change and rank product, including Lkb1. However using the unfiltered data set, SAM returned very high FDRs and few genes, highlighting the limitations of SAM with a large gene chip set or small sample number. To further investigate the reliability of the array data I performed clustering analysis (figure 5) on filtered data and confirmed samples to be of good quality and showing similar trends of gene expression between chips.

Alone each method of analysis contains flaws and limitations, however taken together, those genes that frequently appeared at the top of lists were considered strong candidate genes, and the majority of my preliminary work to validate array data has again confirmed the array results to be largely reliable. However, some inconsistencies were observed, for example, figure 6.10A detailing qRT-PCR data for angiogenesis and matrix remodelling genes finds differences in Dhh and Ptch1, which I find unchanged from my array data. Also *Lkb1* was called by the array as 4 fold down regulated (p=0.01) in Table 6.1B, however qRT-PCR revealed this to be an underestimate with true reduction in *Lkb1* found to be 32 fold down regulated (figure 6.8). The array therefore showed clear reduction in Lkb1 transcripts in *Lkb1* $^{fl/fl}$ mice

following recombination, but was unable to show complete knockdown of Lkb1 due to the use of whole gut RNA extract, containing mesenchymal/endothelial tissue which is unrecombined. Work is currently underway to produce high quality intestinal RNA from laser captured epithelial cells only. These inconsistencies highlight the importance of validation of array targets by q-RT-PCR and also at the protein level, preferably by IHC to observe changes in protein level and localization.

6.4.2 Lkb1 loss induces alterations in differentiation

One of the most noticeable trends from the candidate list (table 6.6) was the alteration of several cell differentiation markers. Table 6.6A implicated the upregulation of: *BMP1, TNF, Lifr, Zfp98, Adipsin, Ndn, Atf5, Nn3, Math1/Atohl* and Rps19 in addition to down regulated *Cdx2, Car4, noggin, Pten* (table 6.6 B), all of which are known to play roles in cell differentiation.

Notch signalling is critical in regulating cell fate, cell-to-cell communication and spatial patterning during development and homeostasis. Recent communications by Van Es *et al* 2005a have implicated disruption of intestinal Notch signalling as a mechanism behind altered differentiation states similar to that observed in the $Lkb1^{fl/fl}$ mouse (see Chapter 5). The over production of mature goblet cells and the secretory lineage was correlated to high expression of Math1 – a basic helix-loop-helix (bHLH) transcription factor negatively regulated by Notch signalling.

Math1 expression in goblet cells is repressed by Hes1; a notch driven transcription factor. $Hes1^{-/-}$ mice show increases in goblet cells, mucin secretion and Math1 staining in addition to fewer absorptive cells (Jensen *et al* 2000). This phenotype closely resembles that of *Lkb-1* deficiency in the crypt and provides an attractive potential link between Notch deregulation and intestinal neoplasia. Indeed, IHC analysis in figure 6.12 shows that the number of Math1 positive cells is significantly increased in Lkb1 null mice compared to controls ($Lkb1^{+/+}$= 2.2%(+/-0.134), $Lkb1^{fl/fl}$ = 5.64% (+/-0.696), p=<0.05 MWU). This increase is again confirmed by qRT-PCR, which showed a 1.8 (+/-0.1 sem) fold up-regulation of Math1 in the recombined tissues (figure 6.9). Furthermore, SAM analysis (Table 6.4A) called Math1/Atoh1 as significantly up-regulated between $Lkb1^{+/+}$and $Lkb1^{fl/fl}$ genotypes.

Interestingly when mouse models of Alzeimers were treated with γ-secretase inhibitors (known to cleave Notch intracellular domains), a similar intestinal phenotype of increased goblet cells was noted (Wong *et al* 2004). Milano *et al* also report similar goblet cell metaplasia, increased crypt apoptosis, and stunted villus length using γ-secretase inhibitors and suggest this goblet cell phenotype to be a direct result of altered Notch and *Math1* up-regulation (Milano *et al* 2004). This process may also be hormonally regulated by Adipsin secretion and my array data correlates with observations by Searfoss *et al* 2003, with increased Adipsin and Math1 expression and down-regulation of Ngn3, Alcohol dehydrogenase and EphB2 (Table 6.6).

Although Hes1 deficiency has been reported to confer a similar phenotype to the *Lkb1*$^{fl/fl}$ mice, down regulation of *Hes1* was not observed in my array data or by qRT-PCR (personal communication Boris Shorning). However, *Hes5* was found to be down-regulated in a Notch knockout mouse model (personal communication DJ Winton), and some members of the *Hes* gene family may antagonise *Hes1* function in a tissue specific manner, for example *Hes6* is known to antagonise *Hes1* expression in prostate cells (Hu *et al* 2002). This may explain the unusual finding that *Hes3* and *Notch 3* are up-regulated from array data (Table 6.6A), and imply negative feedback loops in the Notch system. Yang *et al* show that Hes1 and Notch receptor levels are surprisingly unchanged in Math1 knockout mice, and suggest up-regulated Math1 as a product of subtle changes in the balance of notch components controlling cell fate (Yang *et al* 2001) (figure 6.16). Many questions remain about sequential cell fate decisions and characterisation of the intestinal pathway to date is outlined in figure 6.16.

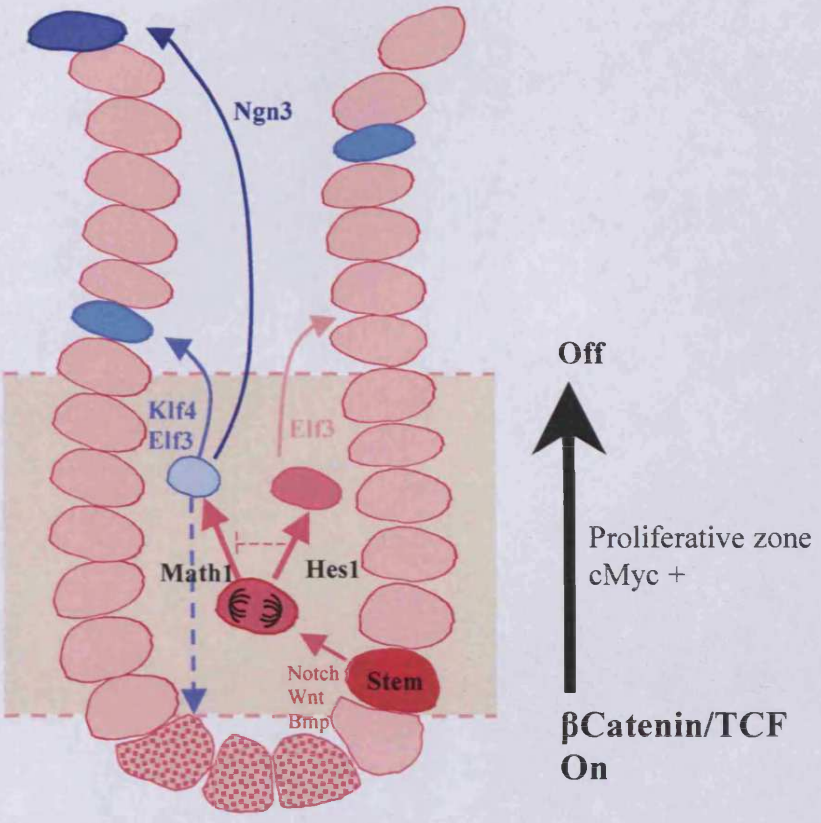

Figure 6.16 – Schematic diagram of intestinal cell fate processes. Stem cells at the base of the crypt (red) produce intermediate progenitor cells (dark pink) sensitive to notch signalling. Transcription factors Math1 and Hes1 give rise to secretory (blue) and absorptive (pale pink) cell lineages respectively. Cells migrate out of the c-Myc+ proliferative zone away from activated Wnt and further transcriptional changes specify the terminal cell phenotype.

Neurogenin 3 (Ngn3) is a cell fate transcription factor in the pancreas and small intestine (Schonhoff *et al* 2004). Ngn3 expression is also associated with the secretory cell lineage and is negatively regulated by Notch induced Hes1. Mice deficient for Neurogenin 3 lack enteroendocrine cells (Jenny *et al* 2002). Figure 6.11A confirms that Lkb1 loss results in up-regulation of Ngn3 (2.8 fold (+/-0.38) sem), however this may be of limited relevance as Ngn3 signalling is downstream of Math1 and therefore may reflect a secondary consequence of Math1 overexpression. Furthermore, only a small increase in neuroendocrine cells was observed in Lkb1 null animals and this only became significant when enterocyte cell number declined at day 13 (see chapter 5, figure 5.14).

Pdx1 provides an opposite role to Ngn3 in differentiation, and was originally identified as a cell fate factor in the pancreas. Pdx1 is highly expressed in precursor Enteroendocrine cells and can transform immature enterocytes into neuroendocrine cells (Yamada 2001). Surprisingly loss of Lkb1 resulted in up regulation of *Pdx1* (figure 6.11 A). This may reflect the mixture of cell types in the extract, or deregulation of ratios of progenitor cells. Further array analysis of laser micro dissected secretory versus absorptive cell types would be needed to determine these differences.

Notch ligand expression is mostly localized to the mesenchyme underlying the intestinal epithelium. However transcriptional targets of Notch such as Hes1 and Math1 are localised to the epithelium (Schroder and Gossler 2002). Deletion of Lkb1 in my model occurs solely in the epithelial tissue and may well disrupt the epithelial interpretation of autocrine and paracrine underlying Notch signalling or effectors such as Math1.

Intestinal specific differentiation genes

The intestinal cell maturation process is relatively uncharacterised due to difficulties in culturing intestinal epithelial cells. However work by Velich *et al* investigating intestinal differentiation by gene expression analysis found expression patterns between secretory cells to be very similar. Thereby suggesting that differentiation in the gut is regulated by sequential recruitment of the same gene set common to all cell lineages in varying amounts and as a result of contact inhibition (Velich *et al* 2005). Lkb1 may alter the subtle balance of gene sets, and does show evidence of chromatin remodelling and transcription factor capabilities (Marignani *et al* 2001).

Muc2 is known to be a Math1 driven marker of mature goblet cells and figure 6.11A confirms up-regulation of Muc2 (2.7+/-0.11SD) by qRT-PCR in $Lkb1^{fl/fl}$ mice. Muc2 is also expressed in conjunction with the cell cycle inhibitors p21, p27 and suppression of Cyclin D1 (Leow *et al* 2004). Inhibition of TGFβ/BMP signalling and β-Catenin/c-Myc expression also mark disruption of the proliferative capacity of a

cell and the differentiation process as cells migrate up the crypt-villus axis (Velich *et al* 2005) (figure 6.16).

Interestingly p21 and p27, both heavily implicated in intestinal differentiation have no intestinal phenotype in knockout mouse models, implying some levels of redundancy (Sancho *et al* 2003). My previous results from chapter 5 demonstrated p21 to be up-regulated in Lkb1 null mice by IHC (see chapter 5 figure 5.7), although mRNA levels appear unchanged suggesting post-translational modification. Induction of p21 in the Lkb1 null environment may either reflect stress-induced arrest in enterocyte cells or exit from the cell cycle and differentiation in the secretory cell lineage. Indeed Math1 was found to co-localize with Ki67 in secretory progenitors and mark progression of the differentiation process (Yang *et al* 2001).

Cdx2 expression correlates with increased Muc2 levels and hence is also an intestinal differentiation factor (Brabletz *et al* 2004). *CDX2* mutations were investigated in PJS and JPS patients following the observation that *Cdx2*$^{+/-}$ mutant mice developed similar well-differentiated hamartomatous polyps. However no correlation was found between CDX2 and LKB1 mutations (Woodford-Richens *et al* 2001). Post-translational modifications to this gene and its effectors may be crucial in tumour formation (Lynch and Silberg 2002) and progression of well differentiated tumour types such as a hamartomas to a less differentiated lesion such as an adenocarcinoma is commonly associated Cdx2 loss (Brabletz *et al* 2004).

Initially array data (Table 6.6B) found very little change in *Cdx2* expression between genotypes (1.04 fold). However given the importance of *Cdx2* for intestinal differentiation, qRT-PCR analysis was performed and found to be 2.46 (+/-0.001SD) fold down regulated (figure 6.11A). This is unexpected given the increase in Muc2, although inhibition of Cdx2 by PI3K and TNFα signalling has been reported (Kim *et al* 2002) and this may correlate with my array data with up-regulated TNFα (figure 6.9) and the decline of the enterocyte lineage.

6.4.3 Alterations in Wnt signalling

Wnt signalling is predominantly activated in the stem cell compartment and is suggested to maintain an undifferentiated cell state (figure 6.16). The recent finding that Hath1 (the human ortholog of Math1) is down-regulated in aggressive colonic cancer cell lines by activated Wnt signalling (Leow *et al* 2004), may implicate Lkb1 in the positive regulation of Wnt and the maintenance of 'stemness' in the cancer cell environment (Leow *et al* 2004). However conversely, Wnt signalling has been implicated in the up-regulation of Math1, following the observation that Dkk1 (inhibitor of Wnt) represses Math1 levels and that Tcf4 null mice still retained goblet cells (Pinto *et al* 2003). In support of this, Ireland *et al* 2004 demonstrated that the β-Catenin knockout mouse lead to goblet cell depletion, and work on the Apc knockout mouse showed similar loss of differentiation within crypts (Sansom *et al* 2004a).

These inconsistencies may suggest one of the complicated negative feedback loops in Wnt signalling, or the broad nature of Wnt inhibition by Dkk1. Previous array analysis of LKB1 null HeLa cells found GSK3 inactivation, β-catenin up-regulation and activated Wnt in addition to Dkk1 up-regulation, again suggesting a negative feedback theory (Lin Marq *et al* 2005). No significant differences were observed in the major Wnt associated components such as Apc, β-catenin, CD44, Gsk-3, Cyclin D1 or c-Myc from day 4 array analysis or IHC (nuclear β-catenin figure 6.14A-C, G, CD44 figure 6.14D-F, p-GSK3 figure 6.15C-D). However, my array data did show changes in some lesser-known Wnt inhibitors: Nkd, CKII, Sema3A and positive regulators Fzd3 and Pcdhb6 (Table 6. 6).

Another possibility is that the LKB1 kinase domain inhibits Wnt irrespective of β-Catenin activity by inhibition of CD44, Cyclin D1, and Eph/Ephrins (Lin Marq *et al* 2005). The IHC staining from figure 6.14 D-F shows CD44 to show normal expression patterns at day 4 following Lkb1 loss, suggesting CD44 mediated Wnt activity is not the underlying mechanism behind the observed phenotype at this time. However CD44 staining at day 6 (figure 6.14F) is stronger suggesting CD44 may be upregulated as a secondary event at a later time point.

The mislocalization of paneth cells described in *Lkb1*$^{fl/fl}$ mice in chapter 5 may reflect disrupted Ephrin/Eph gradients as a result of disrupted Wnt signalling and may cause altered differentiation by inappropriate positional cues (Wong *et al* 2000). Initial data from figure 6.11A demonstrates reciprocal changes in EphB2 and EphB3 expression (+1.74(+/-0.1 SD) and -1.74 (+/-0.2 SD) respectively), although protein levels are still to be confirmed. Chapter 5 also discusses loss of Lkb1 and paneth cell maturity/granule secretion, which is supported by qRT-PCR values for the paneth cell specific defensin related gene Defcr-rs1 (Lin *et al* 1992), showing a 3.4 (+/-2) fold decrease (figure 6.11A).

6.4.4 Alterations in Stem cell signalling

Biallelic loss of LKB1 has been implicated in the formation of malignancy due to loss of polarity or impaired asymmetric division of the stem cell population (Baas *et al* 2004). The immediate phenotype from chapter 5 and the cell fate changes detailed above make aberrant stem cell signalling a potential mechanism for the phenotype.

Interaction of Notch, Wnt, BMP/TGF-β signalling pathways in the crypt niche controls proliferation, cell fate and migration. Notch signalling interacts with Wnt signals from the stem cell to provide a proliferation-differentiation switch at the base of the crypt (Jensen *et al* 2000). Wnt and Notch signalling show some overlap in expression in the stem cell compartment and cell fate appears to be determined by consecutive binary decisions (Wong *et al* 2004).

The Forkhead or winged helix family are transcription factors also associated with 'Stemness' and Wnt regulation possibly via mesenchymal interactions. Loss of fork head factors in mice results in hyperproliferation, decreased villus length and goblet cell hyperplasia (Kaestner *et al* 1997). Figure 6.11 B shows that qRT-PCR values for stem cell markers such as Mushashi- 1, Foxa2, Sox9 and c-Myc (Potten *et al* 2003), show very little increase in *Lkb1*$^{fl/fl}$ animals, despite array data from Table 6.6A reporting Foxa2 up 2.26 fold (p=0.028). Although no large changes in stem cell markers were seen, Proglucagon expression (encoding endocrine GLP-1 and 2) was 2.6(+/-0.39SD) fold upregulated by qRT-PCR (figure 6.11A), and is reported to be regulated by Foxa2 and TCF-4 (Yi *et al* 2005). This up-regulation of hormonal

signalling may affect many processes in the gut such as adsorption, cell fate, and positioning cues. Additionally, Sox 9 activity is known to repress Cdx2, Muc2 and hence differentiation in the intestine (Blache *et al* 2004). Although it is unclear from my results whether the small change in Sox 9 expression is sufficient to down regulate Cdx2.

Recent work suggests that BMP/TGFβ signalling in the mesenchymal cells surrounding the crypt base may play a role in controlling stem cell division and renewal, providing a specification/differentiation counter balance to Wnt signalling in the stem cell niche (He *et al* 2004, Leedham *et al* 2005). Up-regulation of BMP1 consistently appeared in array data lists from tables 6.1-6.6 (3.34 fold p=0.02), although due to large variation between samples qRT-PCR results did not validate the array. Furthermore, Noggin (BMP antagonist) expression was down-regulated 2.78 fold (p=0.1) (Table 6.6B), adding to the suggestion that loss of Lkb1 and alterations in BMP signalling may contribute to inhibition of stem cell renewal, loss of 'stemness' and impaired asymmetric division resulting in the decline of certain progenitor cell types such as the absorptive cell lineage (Baas *et al* 2004). In conjunction with reports of hyperproliferation, crypt overgrowth and mucinous cell type in diseases such as JPS and Smad4/BMP1 mouse models (Sancho *et al* 2004), the Lkb1 interaction in the BMP/ TGFβ pathway is an attractive hypothesis for deregulated stem cell signalling, and the increased differentiation drive observed in Lkb1 null animals.

Each stem cell gives rise to long-lived progenitor daughter cells of either absorptive or secretory lineage (Stappenbeck *et al* 2003). As discussed in chapter 5, multiple intermediate progenitors could lead to one or more differentiated cell type (Bjerknes and Cheng 1999), which may be influenced by altered Notch, Wnt or BMP/TGFβ signalling (Sancho *et al* 2003). These uncommitted progenitor daughter cells also reside between the paneth cell population at the base of the crypt compartment, making both cell types subject to Wnt signals. However, paneth cells are non-proliferative, differentiated cell types therefore suggesting that some cells may be capable of selectively reading Wnt (Sancho *et al* 2003). Furthermore Van Es *et al* have recently confirmed a separate paneth cell gene programme dependant on TCF4 signalling rather than a stem cell/progenitor cell phenotype (Van Es *et al* 2005b).

Further characterisation of this alternative Wnt pathway in paneth cells or progenitors is needed to determine if Lkb1 is involved. Given the location of progenitor cells within the base of the crypt, autocrine and paracrine signalling may influence their final differentiation state (Van de Wetering *et al* 2002).

6.4.5 TNFα signalling

TNFα signalling and cytokine induction has been shown to induce p38/MAPK pathways of differentiation and apoptosis in addition to integrin/BMP signalling, angiogenesis and is frequently associated with malignancy and inflammatory diseases (Hehlgans and Pfeffer 2005). TNFα was up-regulated in several of my array lists (Tables 6.1-6) 4.08 fold (p=0.06), and was confirmed as 7.8(+/-2.4 sem) fold up-regulated by qRT-PCR (figure 6.9). Furthermore, many of the genes up-regulated from the array may be as a secondary result of TNFα activation (e.g. MMPs, adhesion genes, differentiation genes, inflammatory and immune response genes, proliferative genes). Goblet cell differentiation via Muc2 and TFF3 expression is also mediated by TNFα /STAT induced stimulation of cytokines (Blanchard *et al* 2004).

Increases in Cl^- secretions are seen to inhibit the barrier functions of the gut in response to NOS2 (Velich *et al* 2005). *Nos2* was up-regulated from the array (Table 6B) and can signal Tight junction alterations via Claudins, Ca^{2+} channel signalling, JAK/STAT pathway activation, TNFα induced apoptosis and IL2Rα inflammatory responses.

6.4.6 Alterations in Survival and Death pathways

PI3K, PKB/AKT survival signalling protects against apoptosis, and can promote the formation of new blood vessels (angiogenesis) via VEGF expression (Laprise *et al* 2002). HIF (hypoxia inducible factor) mediates increased vascularization through VEGF signalling in an attempt to bring further nutrients to cells during times of stress (Morin and Huot 2004). LKB1 may function to up-regulate the PI3K pathway during embryogenesis as Lkb1 constitutively null mice were embryonic lethal as a result of aberrant VEGF signalling (Ylikorhala *et al* 2001). Additionally HIF and VEGF are

found up regulated in all hamartomatous cancer syndromes (Brugarolas and Kaelin 2004). My array data does not suggest any direct changes in phospho-Akt (figure 6.15A-B IHC) or in Vegf transcript levels (qRT-PCR analysis figure 6.12 A). Indeed studies in *Lkb1*$^{-/-}$ Mefs also fail to show any change in Vegf levels (Brugarolas and Kaelin 2004). Plasminogen (Plg) and Ceacam 10 were both found to be down regulated from my array (Table 6.6B, 5.93 and 5.09 fold respectively) and down regulation of these genes is associated with increased angiogenesis and matrix remodelling (Lijnen 2004).

Data from chapter 5 indicates high levels of apoptosis in Lkb1 deficient cells (figure 5.6) and IHC staining linked P21 and p53 upregulation to this process (figure 5.7). However, the mechanism of enterocyte sensitivity to cell death is still unclear, and array data of whole tissue extract failed to identify any specific death inducing pathways. One possibility is the involvement of the stress induced p38/ERK pathway, which pauses growth during stress and balances the decision between life or death. The pathway relies on cell:cell contact and Anoikis (detachment induced death) for activation and cell death (Morin and Huot 2004). Interaction of LKB1 with AGS3, reported by Blumer *et al* 2003, provides a link mediated by Rac/Cdc42 and PI3K to activation of the p38 pro-apoptotic pathway (Shaw *et al* 2004a) and enterocyte cells may be primed for execution of this pathway.

Expression of the pro-apoptotic Ceacam family members is frequently lost in adenomas and carcinomas (Nittka *et al* 2004). Ceacam 10 was frequently called as down regulated in *Lkb1*$^{fl/fl}$ mice from the array data (Table 6.1B, 4B, 6B) and qRT-PCR confirmed down regulation at 1.6 fold (+/- 0.1SD)(figure 6.10B). This data contrasts with the overall increase in apoptosis but may simply reflect the differential responses of intestinal cell types to Lkb1 loss.

6.4.7 Changes in Adhesion and polarity related genes

The mounting evidence for changes in differentiation control may be as a result of altered adhesion or cell communications. When finalising Table 6.6 of candidate genes, many adhesion related genes were altered including: Aquaporin 6, matrix remodelling genes:*Adam18, Adam15, MMP3, MMP9, Cathepsin 8*, angiogenesis and

motility genes: *Laminin 4, Sema3A, Plexin C, Netol, Gpr73, Plg, Lectl,* Polarity genes: *Claudin2, Desmocollinl, Nkd, Nos2* and many more (see Table 6.6A-B).

The MMP and Plasminogen (Plg) systems work together to proteolytically remodel the ECM. Initially array data indicated some up-regulation of MMP related genes (Table 6.6A), However qRT-PCR results show only minor differences in Adam10 (+1.3+/-0.15), Mmp9 (+1.6+/-0.1) and Mmp3 (-1.7+/-0.3) (Figure 6.10). Down regulation of MMP precursor processing enzymes such as kallikrein and Cathepsin proteases was observed from array data in Table 6.6B (Klkb1 3.55 (p=0.04), Klk26 2.26 (p=0.036), Ctsp8 3.15 (p=0.05), suggesting an indirect remodelling role for Lkb1.

Aquaporins are endothelial water channel proteins highly expressed in proliferating microvessels that increase cell membrane water permeability. They are often over expressed in several cancer cell types and *AQP1* null mice show reduced tumour growth, decreased vascularity and necrosis, suggesting a key role in cell migration (Saadoun *et al* 2005). Aquaporin 6 was often high ranking in up-regulated charts (5.8 fold p=0.07) (Table 6.6B), although this has not been validated by qRT-PCR. Aquaporin 1 has also been shown to play a role in fat adsorption in the intestine (Velich *et al* 2005), and this may be linked to increased Adipsin levels. LKB1 may be involved in regulating these polarised water channels and late stage disruption of LKB1 function following classical tumour initiation may contribute to metastatic progression.

Loss of proliferative capacity, correct polarity and tight junction (TJ) remodelling plays an important role in intestinal differentiation (Velich *et al* 2005). Tight junctions provide a paracellular barrier to control the movement of ions and solutes in epithelial cells. Claudin2 is a major component of TJs and up-regulation is associated with reorganisation of adhesion and differentiating cells (Escaffit *et al* 2005). qRT-PCR from figure 6.9 shows that Claudin2 is up-regulated (4.42,+/-0.958 sem) in $Lkb1^{fl/fl}$ mice. Disruption of TJs has also been reported in $Tsc2^{+/-}$ heterozygote mice, which are also predisposed to hamartoma formation (Hardie 2004).

E cadherins link catenins to the cytoskeleton in adheren junctions and extracellular calcium signals induce loss of these contacts and subsequent rounding of cells characteristic of migratory cells (Morin and Huot 2004). LKB1 belongs to a family of Ca/CaM dependant kinases (Marignani 2005), is a Par4 homologue (St Johnson and Martin 2003), and hence may act as a switch that activates Ca^{2+} adhesion pathways in the cytoplasm whilst inhibiting Wnt and β-Catenin signalling in the nucleus (Lin Marq *et al* 2005). It is possible that the mutations in β-Catenin associated with PJS (Miyaki *et al* 2000) are related to failures in the adheren junction function of catenin and polarity rather than activating Wnt. Inhibition of cadherins has been shown to cause hyperproliferation, aberrant differentiation, increase migration, loss of differentiation, polarization, increased apoptosis and also Crohns disease (an inflammatory bowel condition) (Laprise *et al* 2002). Many of these changes are seen in the immediate phenotype of the *Lkb1*$^{fl/fl}$ mouse (chapter 5) and reflected in some of the adhesion related genes listed above.

6.4.8 AMPK and mTOR signalling

No differences were observed in AMPK, TSC2 and mTOR signalling as a result of Lkb1 loss. As Lkb1 has been identified as a key activator of AMPK by phosphorylation, it is possible that array analysis of transcriptome changes would not yield results for AMPK changes. Another possibility is that AMPK mediates reduction of mRNAs as a result of stress signalling in a subset of cells independently of Lkb1 (Marigani 2005).

Figure 6.13 A-B shows that *Lkb1*$^{fl/fl}$ samples have similar numbers of mTOR positives to that of controls (*Lkb1*$^{+/+}$ =2.16% (+/-0.96 sem), *Lkb1*$^{fl/fl}$ =2.45% (+/-0.419 sem) p=0.5959). Furthermore, figure 6.13D-E shows that S6 ribosomal protein (used as readout of activated mTOR) remained unchanged 4 days following Lkb1 loss. The failure to see S6K increases in Lkb1 nulls may reflect the ongoing energy crisis within mutant cells, as during times of stress and low cellular energy, mTOR signalling is suppressed (Ohanna *et al* 2005). Activation of mTOR by LKB1 may only become important in transformed tissues and not in the normal cell population.

Finally, hamartomas associated with Lkb1 loss may arise as a result of changes or defects in adhesion signalling leading to altered differentiation states, all of which are upstream of Wnt, AMPK, mTOR and Notch signalling, and may explain the lack of substantial evidence for alterations in these pathways.

6.5 Chapter summary

- Array analysis showed the increased secretory phenotype in $Lkb1^{fl/fl}$ mice to arise from compromised Notch signalling resulting in increased *Math1* expression.

- Additionally, changes in adhesion signalling may underlie the differentiation and cell death changes observed in chapter 5.

- The role of Lkb1 in proliferative and cellular energy control is independent of mTOR and Wnt.

The precise interactions or hierarchy of Wnt, Notch and BMP signalling in the intestine is still unclear (Reya and Clevers 2005). Subtle changes in stem cell environment, Notch effectors, cell positioning, and Wnt components leading to the expansion of the secretory cell lineage were hard to detect using microarray analysis, although it is clear that Lkb1 provides cross talk between all these pathways, and hence plays a pivotal role in mediating intestinal signalling and cell fate decisions in the crypt microenvironment.

Many of the interactions suggested for LKB1 function *in vivo* have been carried out on $Lkb1^{-/-}$ MEFs, and the relevance of these interactions to mouse models or to the human disease is still unknown. Jansen *et al* raise the observation that other than hamartomatous polyps TS, PJS and Cowdens have few similarities, suggesting underlying gene functions to be non-overlapping. In addition, several groups fail to report intestinal phenotypes in Pten knockout mice, Cowdens disease, Tuberous sclerosis, or AMPK knockout mouse models. Additionally the lack of metabolic dysfunction in PJS patients presents evidence that the *in vivo* data for LKB1 substrates is at best incomplete (Jansen *et al* 2005 in press).

Chapter 7. Long term consequences of Lkb1 loss and tumourigenesis

7.1 Introduction

Following the previous limited study in constitutive LKB1 knockout models, a combination of rare LOH of the wild type allele and epigenetic silencing of LKB1 has helped to shape the current hypothesis toward haploinsufficiency as a prerequisite to polyp formation (Miyoshi *et al* 2002, Nakau *et al* 2002). However, the lack of consistent data regarding haploinsufficiency and the previous inability to detect the genetic accumulation of mutations suggests that LKB1 does not follow conventional methods of tumourigenesis.

LKB1 expression in PJS polyps has also been reported as heterogeneous, even within polyps from same patient. This strongly suggests that a further hit is required for hamartoma formation and that LKB1 loss primes this progression. Indeed a whole host of additional mutations such as *KRAS, APC, β-Catenin,* and *P53*, all known to be linked to malignancy, have been identified in polyps from PJS patients (Miyaki *et al* 2000, Back *et al* 1999).

Investigations previously described in section 1.5.1 regarding LOH, genetic analysis of LKB1 status and the malignant potential of hamartomas have left a number of questions unanswered. Firstly, whether haploinsufficiency is truly required for hamartoma predisposition irrespective of a second hit at the LKB1 locus. Secondly the contribution of homozygosity to tumourigenesis, and finally, given that the tumours isolated from PJS patients and $Lkb1^{+/fl}$ mice contain multiple genetic lesions at relatively late stage time points, the precise role of LKB1 in progression of intestinal tumourigenesis is yet to be elucidated.

7.2 AIM

This chapter will aim to further investigate the long- term effects of homozygote loss of Lkb1 in the murine small intestine following the findings from chapters 5 and 6 that Lkb1 plays a crucial role in mediating intestinal homeostasis, in particular differentiation. I will determine whether the aberrant crypt structures observed following immediate loss of Lkb1 are retained over long periods and whether *Lkb1*$^{fl/fl}$ AHCre+ mice are predisposed to hamartoma formation. Additionally I will address the role of haploinsufficiency and tumourigenesis using *Lkb1* $^{fl/+}$AHCre+ heterozygote mice. Finally, I will compare the *Lkb1*^{fl} AHCre conditional allele with previous constitutive heterozygotes for Lkb1 by using the Deleter Cre transgene to constitutively delete Lkb1 in all tissues from embryogenesis.

7.3 Results

7.3.1 Long term persistence of recombined cells

As previously described in chapter 5, high penetrance deletion of *Lkb1* was not compatible with long-term tumourigenesis studies due to the severity of the phenotype at day13 even when dosed with 1 x 80mg/kg β-Napthoflavone. Therefore, lower frequency recombination was employed to assess the contribution of *Lkb1* loss to tumourigenesis.

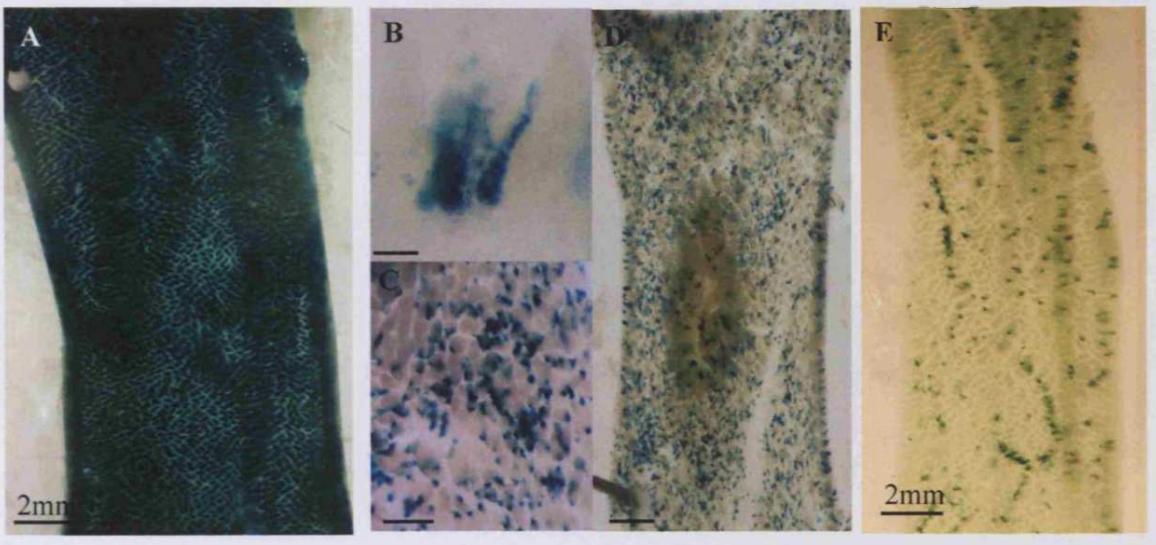

Figure 7.1- Whole mount Lacz recombination analysis of long-term *Lkb1* $^{fl/fl}$ mice **A,** Intestinal whole mount LacZ staining of *Lkb1* $^{fl/+}$ AHCre+ mouse age 18 months following 4x80mg/kg injection of β-Napthoflavone. **B, C, D,** *Lkb1* $^{fl/fl}$ day 13 following recombination with 1x80mg/kg β-Napthoflavone dosing showing mosaic floxing of approx 30-40% (Scale bars = 50μm, 400μm and 2mm respectively) **E,** Wholemount Mosaic floxing (approx 10 %) of *Lkb1* $^{fl/fl}$ 5 months following 1xi.p. injection of low dose 0.8mg/kg β Napthoflavone.

Lkb1 $^{fl/fl}$ mice were crossed to mice carrying the Rosa26 reporter allele and figure 7.1 details patterns of LacZ staining in response to various intestinal floxing regimes. Panel A confirms that recombined cells are retained for long periods, as heterozygote cohorts left to age for 18 months clearly display the high level blue staining following 4x80mg/kg β-Napthoflavone. Panels B-D investigate levels of blue following a lower

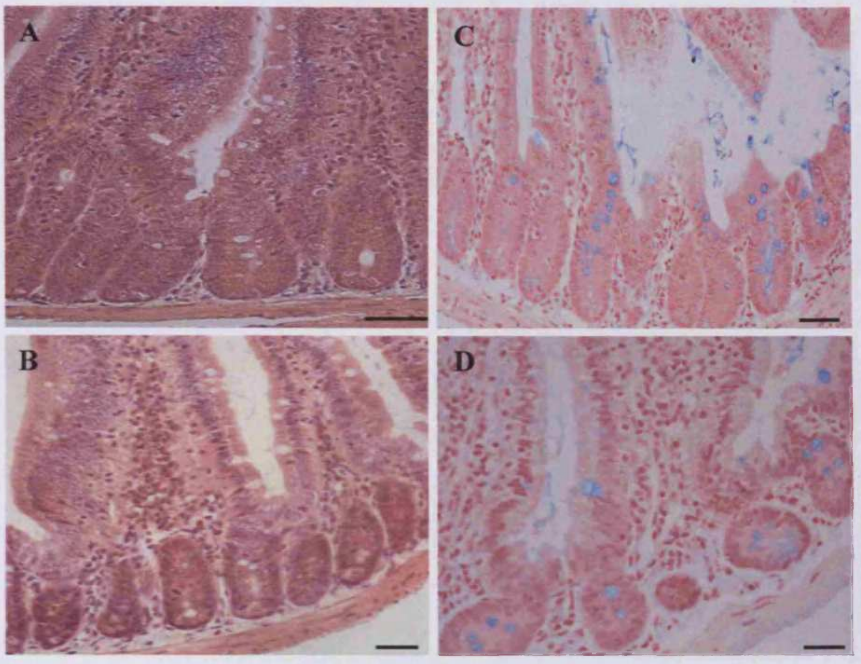

Figure 7.2. *Lkb1*$^{+/fl}$ AHCre+ mice show no intestinal phenotypes. H&E stained histology of murine intestine day 6 following recombination with 4x 80mg/kg β-Napthoflavone. **A,** *Lkb1*$^{fl/+}$ Cre+ **B,** *Lkb1*$^{+/+}$ Cre+ control samples. **C,** *Lkb1*$^{fl/+}$ Cre+ **D,** *Lkb1*$^{+/+}$ Cre+ Alcian blue staining for goblet cells (scale bars = 50μm).

Figure 7.2 demonstrates that *Lkb1*$^{fl/+}$AHCre+ mice show no significant phenotype when compared to *Lkb1*$^{+/+}$ Cre+ histology at day 6 following recombination with high dose 4x 80mg/kg β-Napthoflavone. These mice displayed 100% floxing as evidenced by retention of blue clones (as detailed in figure 7.1 A), although no intestinal tumourigenesis phenotype or changes in alcian blue staining were observed when compared to *Lkb1*$^{+/+}$ Cre+ control mice at 22 months (figure 7.2 A-D).

7.3.3 Effects of homozygote Lkb1 loss in AHCre mice

To address the relevance of homozygous deletion of Lkb1 to tumourigenesis, two *Lkb1*$^{fl/fl}$ mice were fed and 2 injected with low dose 0.8mg/kg β-Napthoflavone and closely monitored for disease over time. *Lkb1*$^{+/fl}$ mice were used as a control and fed at high dose 80mg/kg β-Napthoflavone to compare whether there is a difference in predisposition to hamartoma formation between total heterozygote loss and low-level homozygote Lkb1 loss.

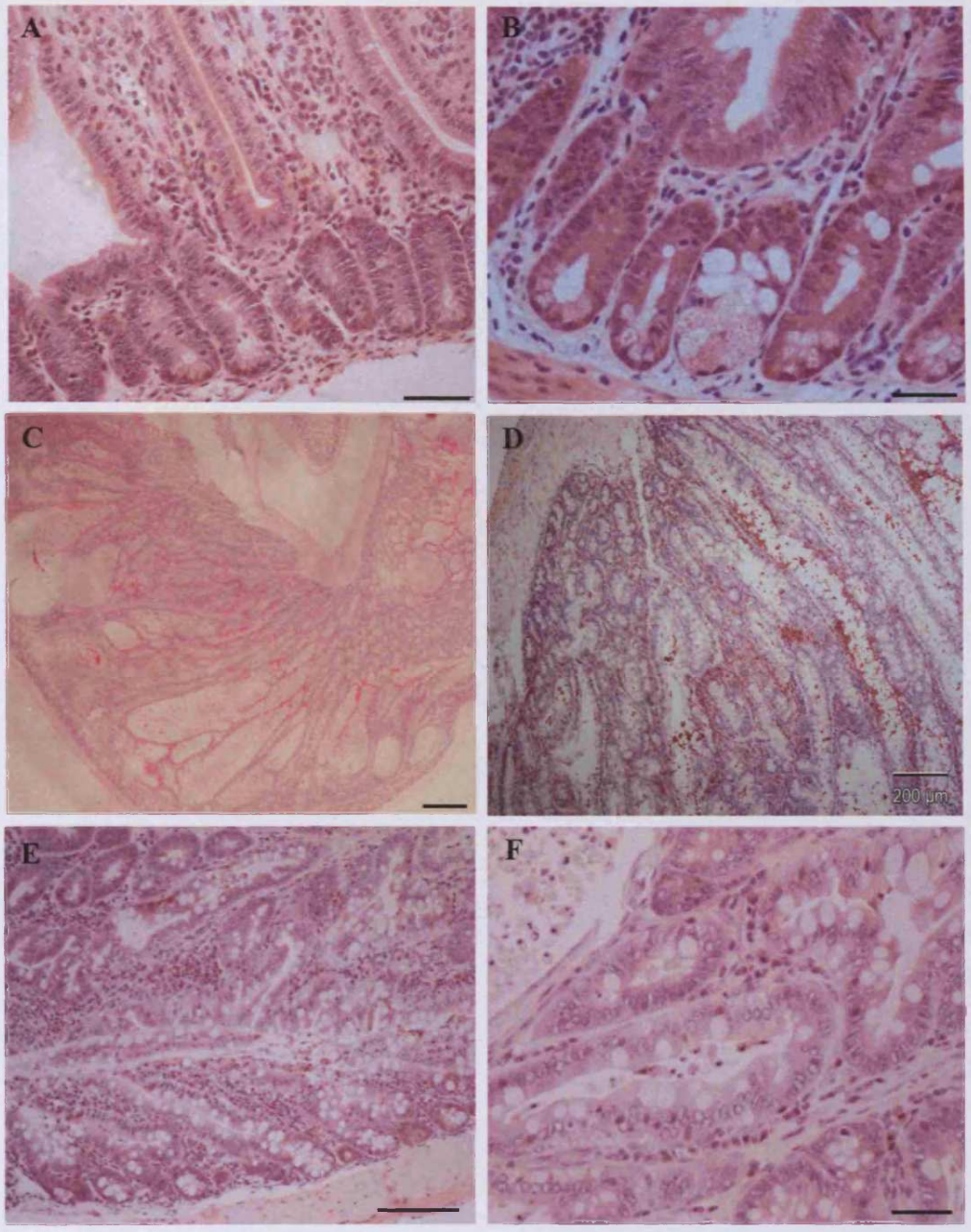

Figure 7.3. Low-level aberrant *Lkb1*$^{-/-}$ crypts show long-term persistence. **A,** *Lkb1*$^{+/+}$ and **B,** *Lkb1* $^{fl/fl}$ H&E staining 6 months following 1 injection of 0.8mg/kg β-Napthoflavone (scale bars = 50µm). **C, D,** H&E section of distal intestinal hamartoma from *Lkb1*$^{fl/fl}$ mouse 6 months following low dose feeding regime of 0.8mg/kg β-Napthoflavone (scale bars = 300 µm and 200 µm respectively). **D, E,** High power sections of distal hamartoma histology from *Lkb1*$^{fl/fl}$ mouse (scale bar = 100µm and 50 µm respectively).

Lkb1$^{+/fl}$ control mice failed to develop any intestinal or other phenotypes by 6 months, even at high dose 80mg/kg recombination, with histology identical to that of *Lkb1*$^{+/+}$ control mice. *Lkb1*$^{fl/fl}$ mice displayed symptoms of disease within 5-6 months and H&E analysis of histology from all 4 mice revealed that the low level floxing detailed in figure 7.1D resulted in infrequent aberrant crypts that were clearly stable and retained 6 months following *Lkb1* deletion (figure 7.3 A-B). These crypts closely resembled the appearance of hypermucinous crypts at day 13. I also identified infrequent highly mucinous hamartomas in a single *Lkb1*$^{fl/fl}$ mouse, localized to the distal end of the small intestine at this time point (figure 7.3 C-F). Mice displayed weight loss prior to morbidity at 5-6 months, which may have been due to intestinal obstruction by the hamartoma.

7.3.4 Deleter Cre and constitutive Lkb1 heterozygosity

The failure of conditional *Lkb1*$^{fl/+}$AHCre+ mice to present with intestinal phenotypes was somewhat unexpected, therefore I decided to compare the conditional *Lkb1*^{fl} AHCre+ transgene with a model constitutively heterozygote for *Lkb1,* to test that the targeted floxed allele was indeed a true null allele.

Deleter Cre mice express Cre recombinase in all tissues (including germline) driven by the human cytomegalovirus minimal promoter. The Del Cre is transmitted on the X chromosome and expression is active early in embryogenesis in all cell types (Schwenk *et al* 1995). Deleter Cre + mice were crossed to the *Lkb1*^{fl} transgene and the resultant offspring were constitutive *Lkb1*$^{+/fl}$ heterozygotes. Cohorts of 13 *Lkb1*$^{+/fl}$ DelCre+ and 9 *Lkb1*$^{+/+}$ DelCre+ were left to age and observed for signs of morbidity. Mice surviving to 18-24 months of age were harvested and analysed for neoplastic phenotypes, particularly hamartoma formation in the intestine.

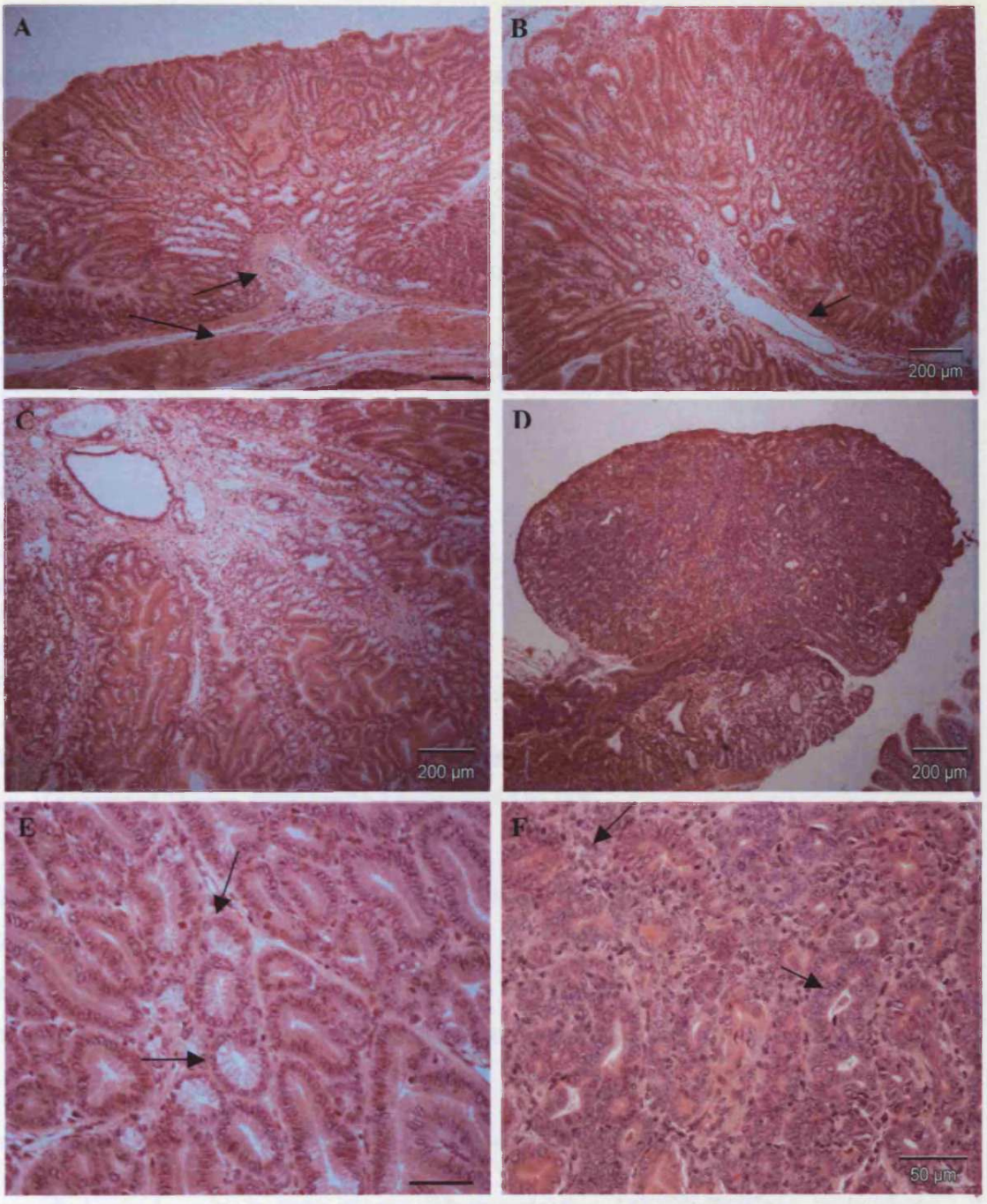

Figure 7.4 - *Lkb1*$^{+/fl}$ DelCre+ mice succumb to intestinal hamartoma formation at late stages of life. Proximal hamartomatous polyps from: **A, B,** *Lkb1*$^{+/fl}$DelCre+ aged 18 and 22 months respectively (arrows note polyp protrusion of sub mucosa and smooth muscle layer of stalk formation, scale bars = 200µm). **C,** closer view of frond-like overgrowth and differentiated mucinous cells types in hamartoma of *Lkb1*$^{+/fl}$ DelCre+ mouse, **D,** Proximal intestinal adenomatous polyp from *Apc* $^{fl/+}$ mouse at 14 months of age. **E,** Close view histology of well differentiated, organised secretory cells (arrows) in *Lkb1*$^{+/fl}$ hamartoma (scale bar = 50µm), compared to **F,** Close view adenoma histology from *Apc* $^{fl/+}$ mouse, (arrows denote undifferentiated cell type and disorganised structure).

Mice heterozygote for *Lkb1* in the deleter colony frequently developed proximal hamartomas. Figure 7.4 outlines histological characteristics of hamartomas compared to intestinal adenomas commonly found in the *Apc* $^{fl/+}$ mouse. Hamartomatous polyps were identified in most *Lkb1*$^{+/fl}$ DelCre+ mice at relatively late time points (average age 19.5 months) see table 7.1.

Phenotype	Frequency observed
Intestinal hamartoma	10
Stomach hamartoma	1
Invasive Peyer's patches	10
Enlarged Peyer's patches/ lymphoid aggregate	14
Colon polyp	2
Lymphoma	5
Kidney	5
Liver steatosis	5
Osteosarcoma	2

Table 7.1–Phenotypic changes associated with *Lkb1*$^{+/fl}$ DelCre+ status during long-term tumourigenesis studies of a cohort of 22 mice, mean age 19.5 months (+/-2.45 SD).

Fishers exact t test was performed on tumour incidence at a given time point between AHCre and DelCre colonies. Comparison of the mean onset showed a significant difference ($p=<0.001$) between the onset of phenotype between genotypes of the AHCre and Del Cre mice in susceptibility to hamartoma formation.

7.3.5 *Lkb1*$^{+/fl}$ DelCre+ mice display aberrant lymph activity

Histopathological analysis from figure 7.5 reveals that *Lkb1*$^{+/fl}$ DelCre+ mice show aberrant Peyer's patch histology in addition to hamartoma formation. Intestinal lymph tissue appears hyperplasic (figure 7.5B) and frequently protruded through the muscle wall, covered by only a single layer of mesothelial cells (figure 7.5 C-D). Invasive Peyer's patches are monomorphic and maybe low grade marginal or mantle zone lymphomas of the intestine. Infiltration into other organs such as that seen in figure 7.5E occurs rarely and is slight in *Lkb1*$^{+/fl}$ DelCre+ mice compared with sporadic lymphomas observed in *Lkb1*$^{+/+}$ DelCre+ control mice of the same age (figure 7.5 F).. Table 7.1 overviews the major phenotypes observed in the DelCre colony.

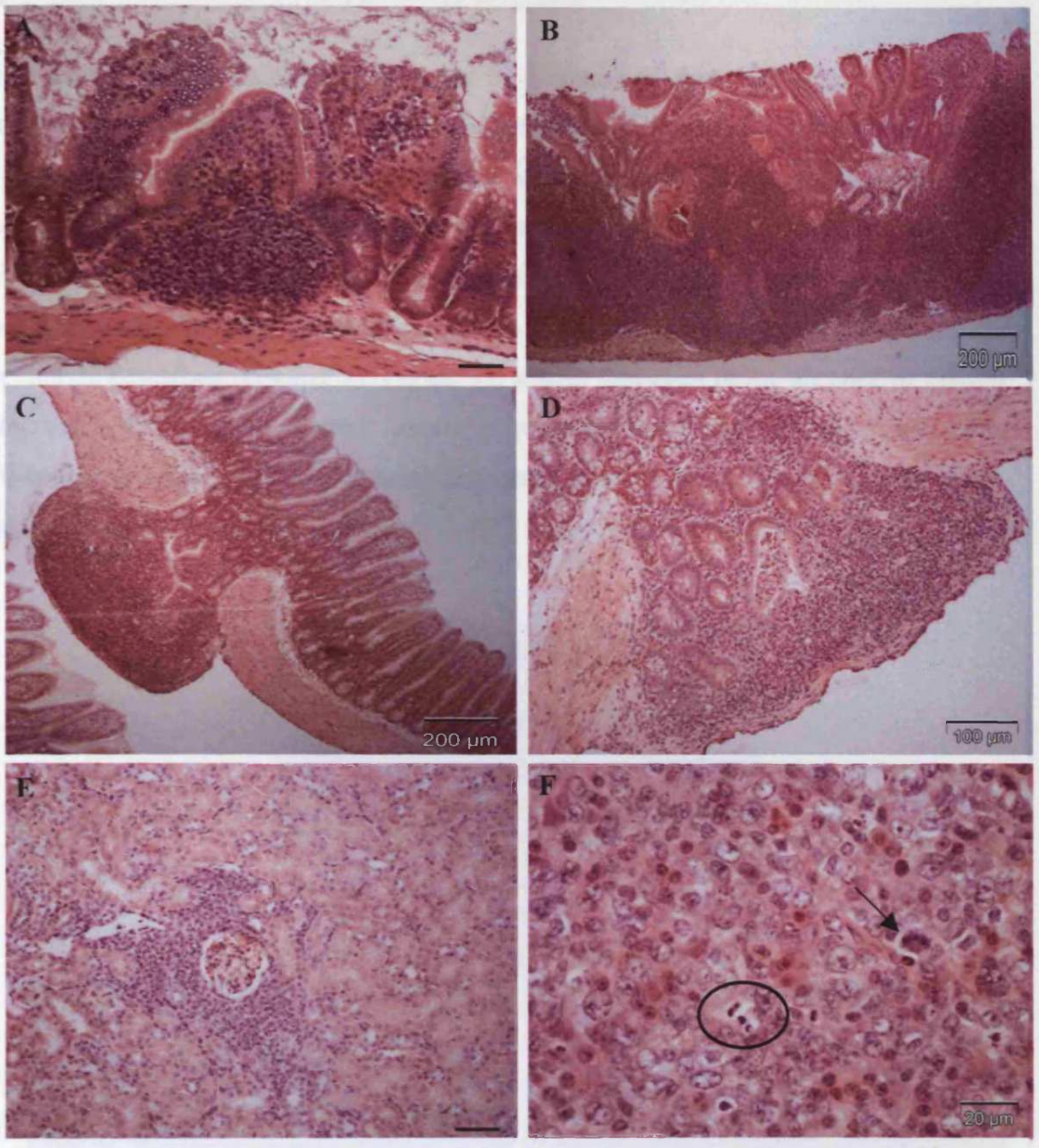

Figure 7.5 – H&E histology reveals *Lkb1*$^{+/fl}$ DelCre+ mice show an additional susceptibility to lymphomatous polyposis and invasion of the basement membrane. **A,** H&E section of normal gut Peyer's patch in *Lkb1*$^{+/fl}$ AHCre+ mouse at 18 months of age following 4x i.p 80mg/kg β-napthoflavone (scale bar= 50µm). **B**, Aberrant enlarged Peyer's patch from *Lkb1*$^{+/fl}$ DelCre+ mouse at 20 months of age **C, D,** Invasion of basement membrane by Peyer's patch in *Lkb1*$^{+/fl}$ DelCre+ mice. **E,** Kidney infiltrate in *Lkb1*$^{+/+}$ DelCre+ control mouse with lymphoma (scale bar= 50µm). **F,** Close view histology of lymphoma from *Lkb1*$^{+/+}$ DelCre+ mouse, classically characterised by high mitosis and 'starry sky' apoptosis (arrow denotes mitosis, circle highlights apoptotic bodies).

7.3.6 Lkb1 null mice are susceptible to infection

In previous studies detailed in chapter 5, I observed that Lkb1 null mice were particularly susceptible to infection, in particular severe cases of giardosis were noted in 70% of animals 6 and 13 days following recombination. To exclude the possibility that the immediate phenotypes observed in chapter 5 were a result of immune dysfunction and infectious pathogens, the *Lkb1*^{fl} transgene was rederived into specified pathogen free isolators and the immediate phenotype characterised as previously described (chapter 5). Figure 7.6 shows that even in the absence of giardia infection, *Lkb1*$^{fl/fl}$ mice display identical phenotypes of aberrant secretory cells, mislocalized paneth cells and diminished enterocytes to that described at day 13 in chapter 5 (figure 7.6 A-C).

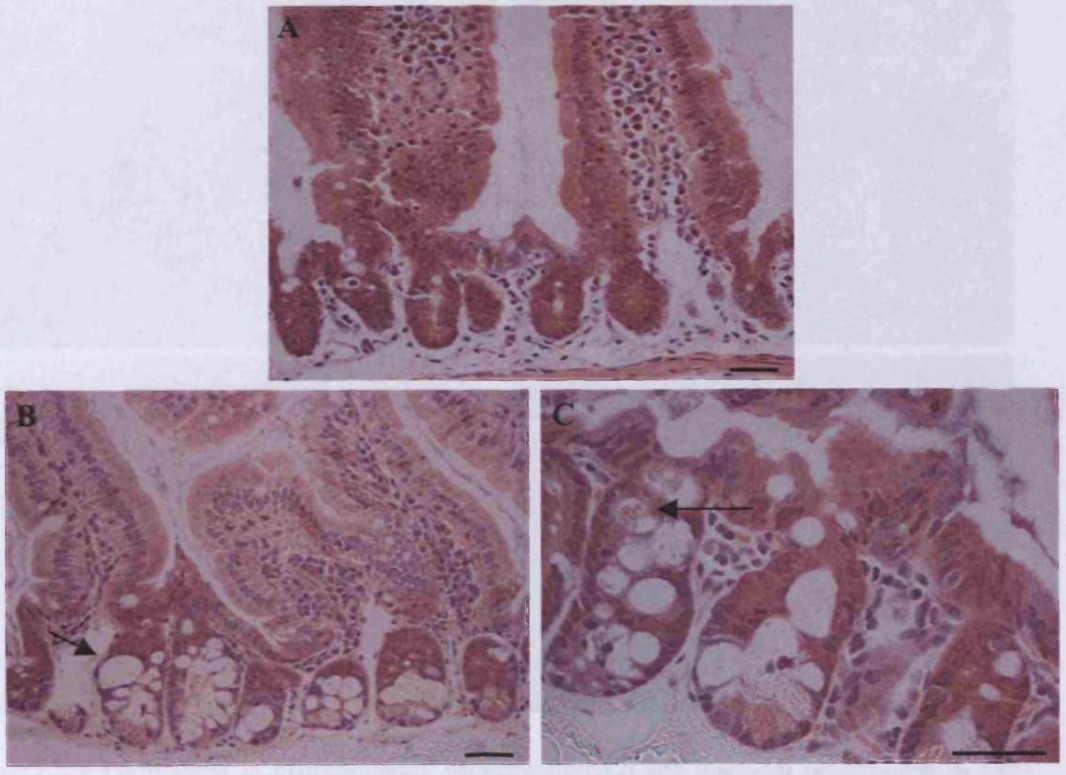

Figure 7.6 – H&E histological sections of rederived *Lkb1*^{fl} AHCre colony. **A**, *Lkb1*$^{+/+}$ AHCre+ **B, C**, *Lkb1*$^{fl/fl}$ AHCre+ sections 13 days following recombination with 1x i.p injection 80mg/kg β-napthoflavone (arrows denote aberrant goblet and paneth cells, scale bars = 50μm).

7.3.7 Localization dependent differences in hamartomas

Previous studies of hamartoma development in constitutive heterozygote Lkb1$^{+/-}$mice, report polyps to be glandular in nature and more commonly localized to the pyloric region of the stomach rather than the small intestine (Miyoshi *et al* 2002, Bardeesy *et al* 2002). Figure 7.7 shows a difference in the morphology of polyps occurring in the small intestine compared to those of the glandular stomach region. Stromal outgrowth and stalk formation are commonly observed in intestinal polyps, as are dysplastic blocked crypt structures (figure 7.7 A-B). Histopathology of stomach hamartomas from within the same mouse shows significantly different glandular structures (figure 7.7 C-D). Proximal hamartomas were most common in *Lkb1*$^{+/fl}$ DelCre+ mice, although stomach and colonic polyps were infrequently observed (table 7.1).

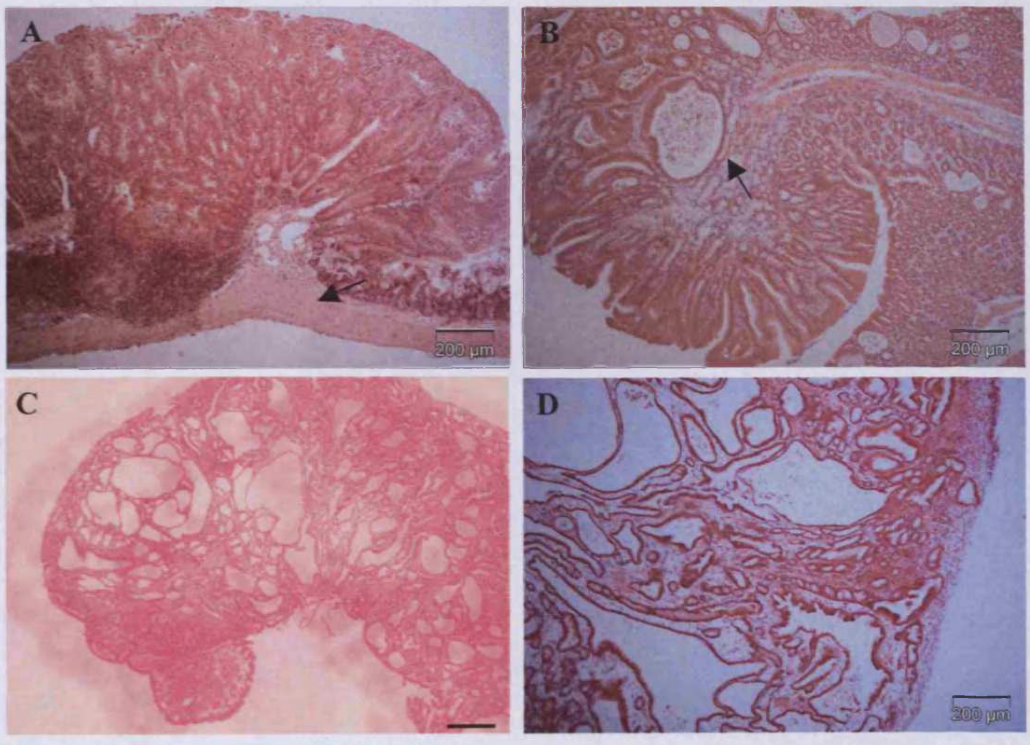

Figure 7.7 – Differences in histopathology between stomach and intestinal hamartomas **A,** *Lkb1*$^{+/fl}$ DelCre+ small intestinal hamartoma located 20cm from distal end. Arrow denotes stromal stalk and overgrowth of crypt structures. **B,** *Lkb1*$^{+/fl}$ DelCre+ hamartoma of the gastro duodenal junction (arrow denotes blocked crypt structures). **C,** Wholemount picture of *Lkb1*$^{+/fl}$DelCre+ glandular stomach hamartoma (scale bar = 400µm). **D,** Close view histology of *Lkb1*$^{+/fl}$ DelCre+ stomach hamartoma with large open secretory structures. (all other scale bars = 200µm).

7.3.8 *Lkb1* deficient hamartomas have limited malignant potential

Hamartomas are highly differentiated in nature and cells predominantly retain correct polarity (Bosman 1999). Figure 7.8 illustrates *Lkb1* deficient hamartomas maintain polarity even at late stages in $Lkb1^{+/fl}$ DelCre+ mice (figure 7.8A-B) compared to $Apc^{+/fl}$ adenomas, which display loss of polarity, irregular nuclear volumes and a predominantly undifferentiated cell type (figure 7.8 C-D).

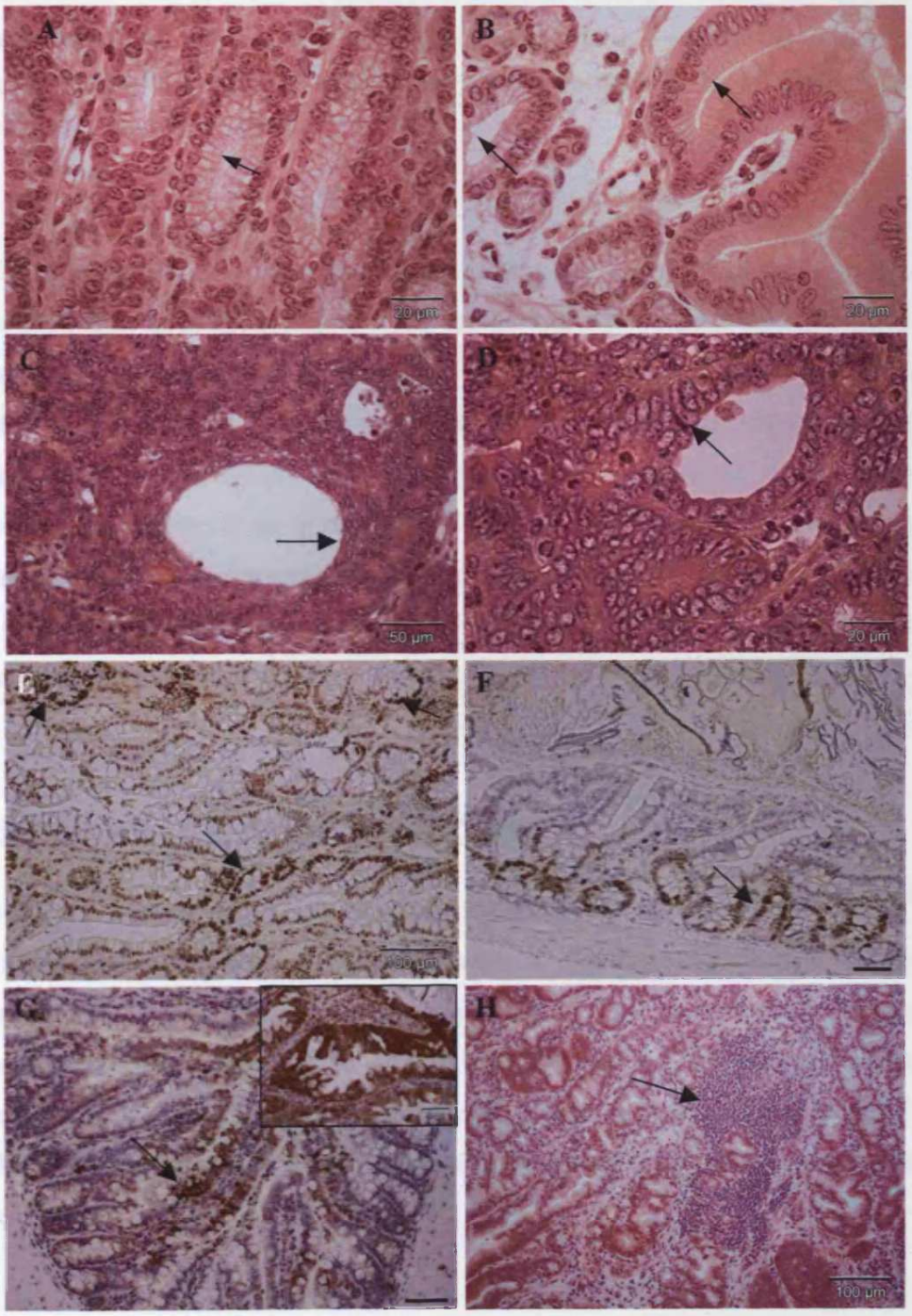

Figure 7.8 – Polarity is retained in hamartomas from *Lkb1*$^{+/fl}$ DelCre+ mice. **A, B,** H&E staining of proximal hamartoma from *Lkb1*$^{+/fl}$DelCre+ at 18 months (arrows denote correctly polarised predominantly secretory cell types). **C,** *Apc*$^{+/fl}$ proximal adenomatous polyp at 14 months showing epithelial loss of polarity (arrows denote aberrant stacking of cells). **D,** Close view of adenoma from *Apc*$^{+/fl}$ mouse (arrow denotes polarity loss, irregular nuclear volumes and predominantly undifferentiated cell types.) **E,** Ki-67 immunohistochemistry of *Lkb1*$^{fl/fl}$ intestinal hamartoma at 5 months, showing aberrant proliferative capacity of cells in disorganised tissue (scale bar = 100μm) and **F,** in relatively normal areas of the polyp (scale bar =50μm) **G,** Phospho-S6K (Ser240/244) immunohistochemistry of *Lkb1*$^{fl/fl}$ hamartoma at 5 months showing infrequent staining in villus like structures within the polyp (scale bar = 50μm), **Inset** - close view detailing occasional strong upregulation of cytoplasmic S6K within aberrant crypt structures. **H,** *Lkb1*$^{+/fl}$ DelCre+ hamartoma showing lesion of undifferentiated cells.

Ki-67 immunohistochemistry marks the replicative capacity of cells, and is often associated with neoplasias. Figure 7.8E shows that proliferative activity can be found in areas of aberrant epithelial structure within the polyp, but also that expression is limited to the crypt region in areas of the polyp that retain relatively normal crypt-villus architecture (figure 7.8F). Furthermore, S6 ribosomal protein previously described in chapter 6 as a readout of activated mTOR, is found upregulated in isolated pockets of hamartoma tissue (figure 8G). Polyps appear largely differentiated and polarised, although some patches of heterogeneity, or possible adenoma precursor lesions are rarely observed (figure 7.8H).

7 3.9 Hypomorphic nature of the *Lkb1* ^{fl} allele

Analysis of my Lkb1 colony revealed deficiency in the number of *Lkb1*$^{fl/fl}$ mice produced from heterozygote matings, with a significant difference between the expected and observed genotypes of mice (Chi squared, p =<0.001). Furthermore, unpublished data from Dario Alessi (University of Dundee) assessing the hypomorphic nature of the *Lkb1*^{fl} transgene, revealed that the unrecombined *Lkb1*^{fl} allele shows very low expression in skeletal muscle, liver and testis tissues, with male mice proving sterile.

In collaboration with Dario Alessi, we show that the phosphorylation assays used for LKB1 activity show considerable reduction of Lkb1 in the homozygote sample (472) in both liver and gut, however the hypomorphic nature of the allele in $Lkb1^{+/+}$ and $Lkb1^{+/fl}$ heterozygote samples is unclear as this assay produced no consistent data for each genotype and high variation between samples (Figure 7.9).

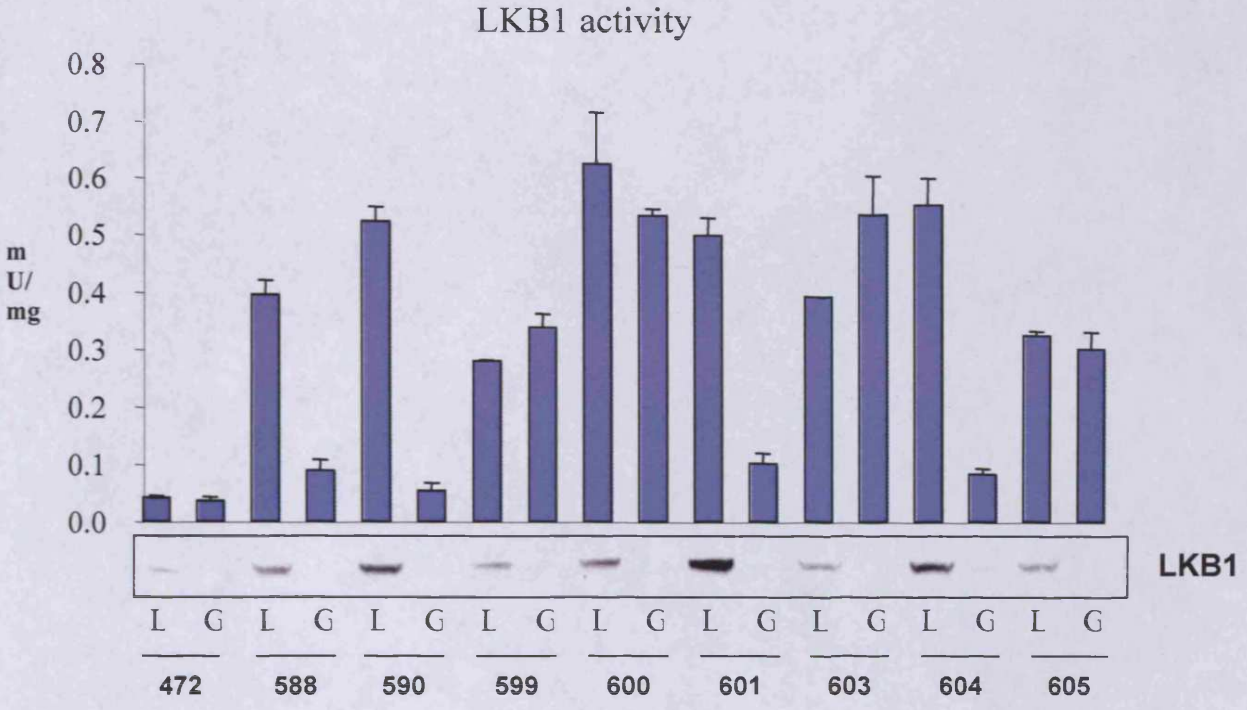

Figure 7.9 – Kinase activity assay and western blot analysis for Lkb1 in $Lkb1^{+/+}$, $Lkb1^{fl/fl}$ and $Lkb1^{+/fl}$ Cre negative mice. Panel below shows western blot analysis for Lkb1 protein level in Liver (L) or gut (G) samples (588, 590, 600, 601, 604 = $Lkb1^{+/+}$, 599, 603, 605 = $Lkb1^{+/fl}$ and 472 = $Lkb1^{fl/fl}$).

7.3.10 *In utero* floxing and Lkb1 loss during development

Constitutive loss of Lkb1 results in mice dying at E9.5 prior to gastrulation and the ability to flox out Lkb1 after this time point but during development may be of interest to determine if homozygote mice develop further malignant phenotypes.

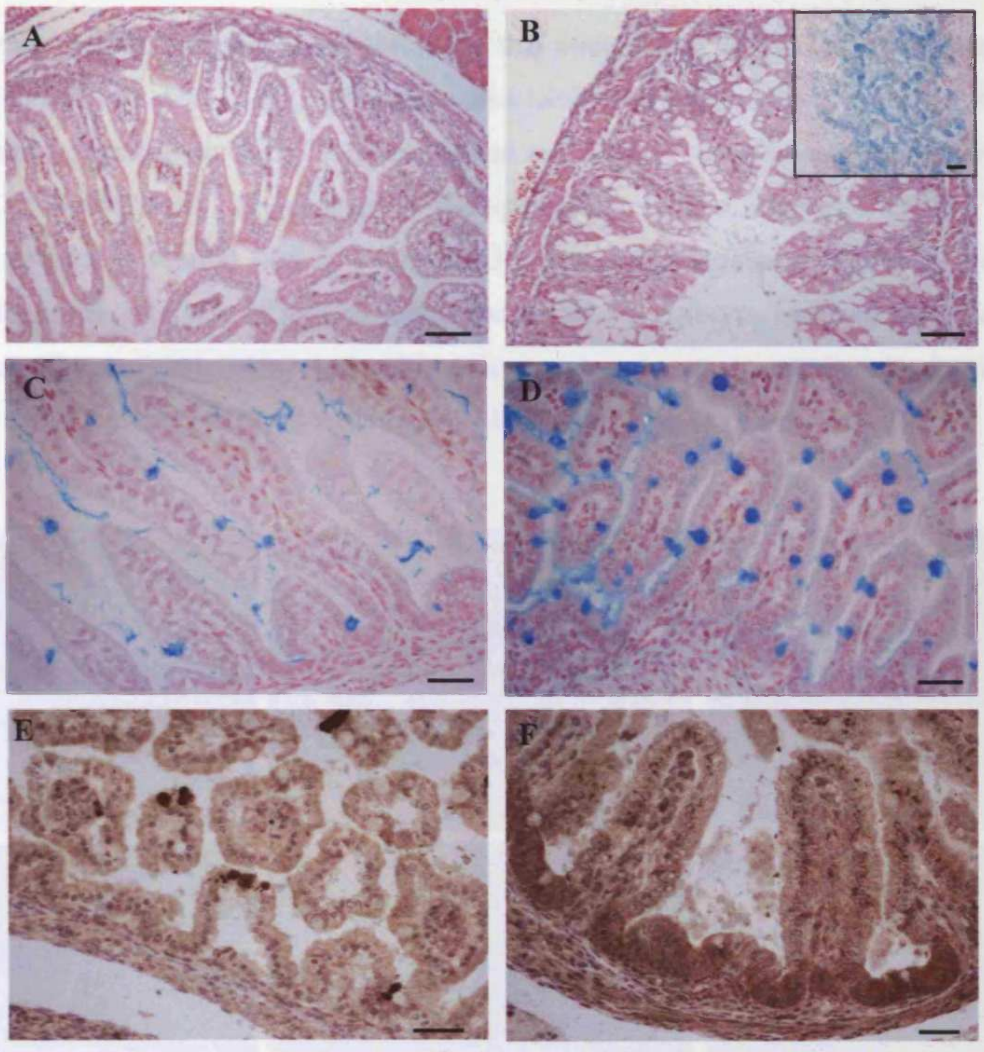

Figure 7.10 – *Lkb1*$^{fl/fl}$ embryos at day E18.5 shows similar increased secretory lineage as in adult following *in utero* floxing. **A,** *Lkb1*$^{+/+}$ and **B,** *Lkb1*$^{fl/fl}$ H&E staining of day E18.5 embryos following 3x *in utero* injections of 80mg/kg β-napthoflavone at E10.5, inset - Lacz staining of *Lkb1*$^{fl/fl}$ *in utero* gut recombination (scale bar = 100μm). **C,** *Lkb1*$^{+/+}$ and **D,** *Lkb1*$^{fl/fl}$ day E18.5 alcian blue histological staining for goblet cells. **E,** *Lkb1*$^{+/+}$ **F,** *Lkb1*$^{fl/fl}$ day E18.5 caspase 3 staining for apoptosis (all other scale bars =50μm).

Initial experiments have shown that 3x i.p injections of 80mg/kg β-napthoflavone at E10.5 are sufficient to induce recombination in embryos by passing across the placenta. Lacz staining of *in utero* floxed tissue confirms that the protocol is sufficient for a high level of floxing within the embryonic intestine (figure 7.10B inset).

An aberrant goblet cell phenotype similar to that observed in adult $Lkb1^{fl/fl}$ mice can clearly be seen at day E18.5, with large mucinous secretory cells dominating the epithelium compared to $Lkb1^{+/fl}$ heterozygote and $Lkb1^{+/+}$ control embryos (figure 7.10A-D). Additionally, an increase in the apoptotic response compared to $Lkb1^{+/+}$ control samples is seen at E18.5 by caspase 3 immunohistochemistry (figure 7.10 E-F). Furthermore, analysis of several major tissues within embryos revealed increased apoptosis (figure 7.11). Most noticeable was the absence of clear trabeculae in the lung of $Lkb1^{fl/fl}$ mice compared with that of $Lkb1^{+/+}$ litter mates (figure 7.11 C-D).

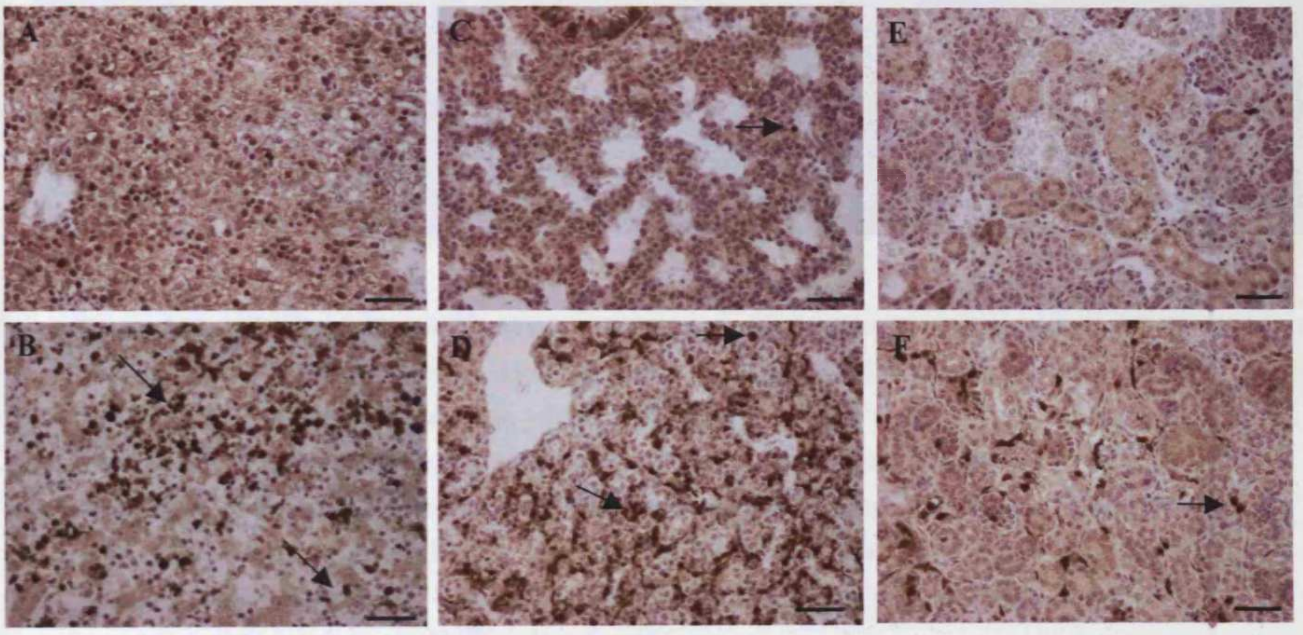

Figure 7.11- *In utero* floxing of intestine from day E10.5 results in widespread apoptosis in *Lkb1* null tissues. Caspase 3 immunohistochemistry of day E18.5 embryos; **A**, $Lkb1^{+/+}$ **B**, $Lkb1^{fl/fl}$ embryonic liver **C**, $Lkb1^{+/+}$ **D**, $Lkb1^{fl/fl}$ embryonic lung **E**, $Lkb1^{+/+}$ **F**, $Lkb1^{fl/fl}$ embryonic kidney (all scale bars = 50μm, arrows denote caspase 3 positive cells).

7.3.11 GU phenotypes

LKB1 is highly expressed in the testis (Luukko *et al* 1999), and somatic mutation is further seen in sporadic testicular cancers as well as PJS patients (Ylikorkala *et al* 1999). The AHCre $Apc^{fl/fl}$ mouse shows a low level of Cre mediated recombination in the testis and is consequently sterile, I therefore investigated the effects of *Lkb1* loss on the mouse Genitourinary (GU) tract.

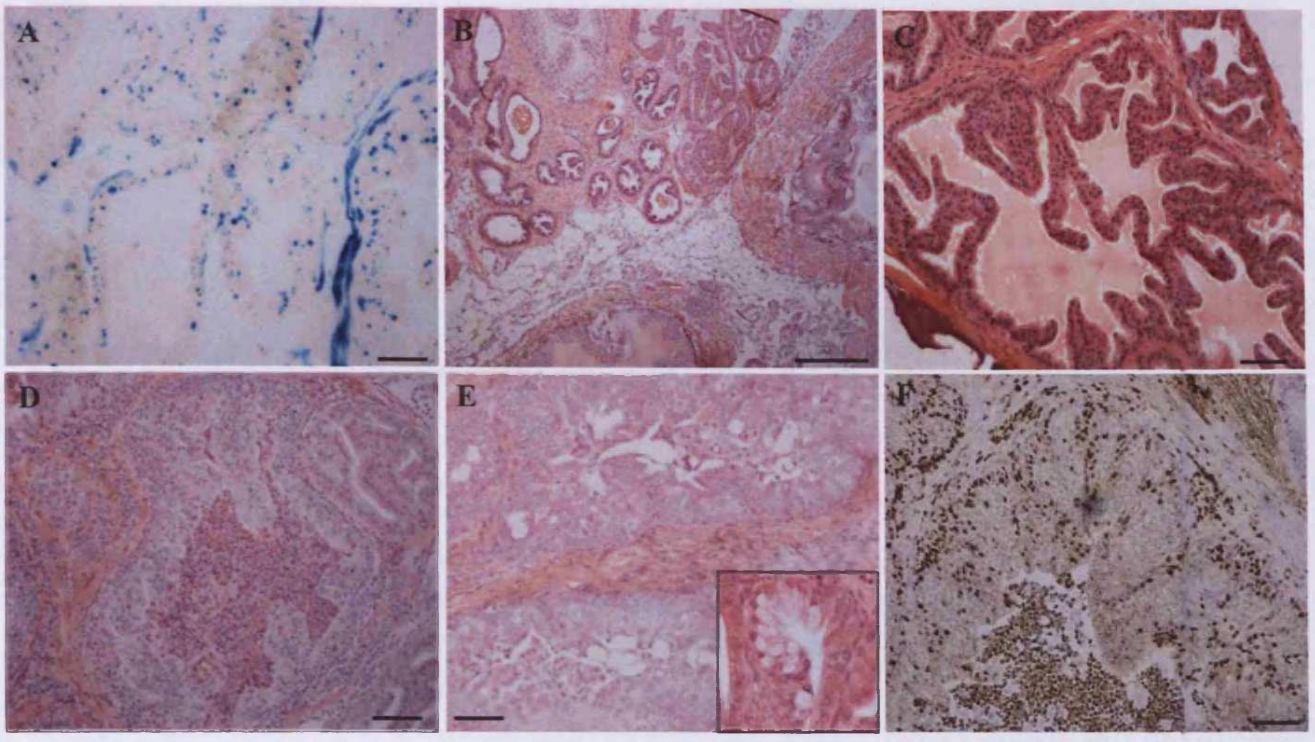

Figure 7.12 –Histology of *Lkb1*$^{fl/fl}$ AHCre+ male mice shows aberrant prostate phenotypes in conjunction with high level infection of the GU tract. **A,** Lacz staining of ventral prostate showing occasional blue positives (Scale bar =50μm). **B,** *Lkb1*$^{+/+}$ ventral prostate lobes surrounding bladder/urethral junction (Scale bar =100μm) **C,** *Lkb1*$^{+/+}$ vesicular gland (Scale bar =50μm) **D,** Coagulating gland neoplasia from *Lkb1*$^{fl/fl}$ male uninduced mouse aged 10-11weeks (Scale bar =100μm). **E,** Close up histopathology of coagulating gland neoplasia (Scale bar =100μm) inset sebaceous cell phenotype. **F,** Ki-67 immunohistochemistry staining for replicative capacity in coagulating gland neoplasia of *Lkb1*$^{fl/fl}$ male at 8 weeks.

Figure 7.12A LacZ staining indicates that low level recombination of the AHCre occurs in the prostate region of the GU tract. In addition to the intestinal phenotype, *Lkb1*$^{fl/fl}$ male mice develop prostate neoplasia at high penetrance (approximately 90%), and mice display signs of disease at a young age (between 7-12 weeks)(figure 7.12D-F). Neoplastic growth is accompanied by a high frequency of infection within the GU tract, which was diagnosed by pathogen screening as *Coagulase negative staphylococci*; an opportunistic pathogen (figure 7.12 D). Increased secretory or sebaceous looking cells and Ki-67 staining (marking proliferative index) were also observed in neoplastic areas (figures 7.12 E inset and F respectively).

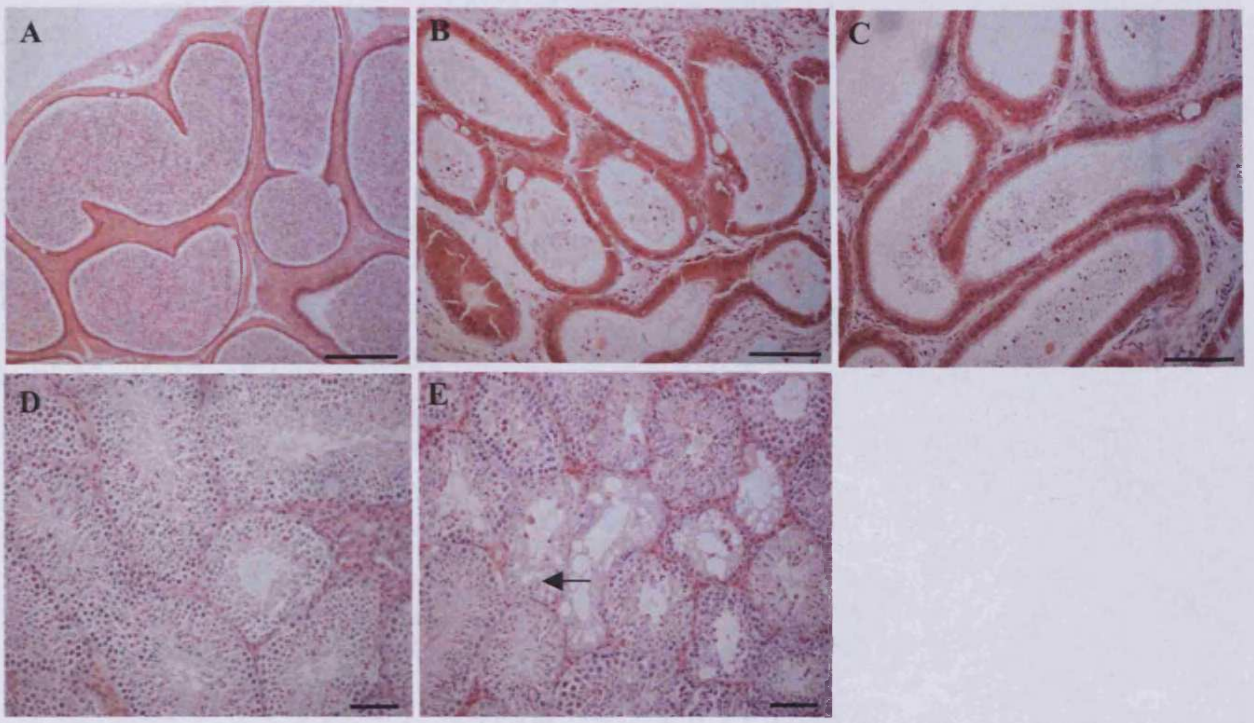

Figure 7.13– *Lkb1*$^{fl/fl}$ AHCre+/- male mice shows abnormal histology of the testis and epididymis. H&E of epididymis from **A,** *Lkb1*$^{+/fl}$ AHCre+ at 6 months B, *Lkb1*$^{fl/fl}$ AHCre+ at 10 weeks **C,** *Lkb1*$^{fl/fl}$ AHCre- at 10 weeks (scale bars = 100μm). **D,** *Lkb1*$^{+/+}$ **E,** *Lkb1*$^{fl/fl}$ AHCre+ H&E histology of testis (arrow denotes apoptotic figures, scale bars = 50μm).

Figure 7.13 shows histology of the epididymis and testis from *Lkb1*$^{fl/fl}$ mutant mice. *Lkb1*$^{+/+}$ AHCre+ and *Lkb1*$^{+/fl}$ AHCre+ mice are fertile and storage of sperm is seen in the epididymis (figure 7.13A). Both *Lkb1*$^{fl/fl}$ AHCre+ and *Lkb1*$^{fl/fl}$ AHCre– mice show no evidence of viable sperm in the epididymis and are therefore sterile (figure 7.13 B-C). Histological analysis of the testis showed sperm production to be apparently normal in *Lkb1*$^{fl/fl}$ AHCre+ and *Lkb1*$^{fl/fl}$ AHCre mice, however several apoptotic bodies were observed in the epithelium (figure 7.13 E).

7.3.12 Additional phenotypes

In addition to the phenotypes described in the intestine, *Lkb1*$^{fl/fl}$ mice developed fatty steatosis of the liver at the 5-6 month time point associated with hamartoma formation (identified by Oil-Red-O staining, figure 7.14 A-B). This phenotype was also observed in several *Lkb1*$^{fl/+}$ AHCre+ and *Lkb1*$^{+/fl}$ DelCre+ heterozygous mice, but

only at late time points of 18 months or more (figure 7.14 C-D). Upon closer examination of the kidney, proximal tubules appear vacuolated at 6 in $Lkb1^{fl/fl}$ and 18 months in $Lkb1^{+/fl}$ mice (figure 7.14E-F). These phenotypes were very rarely observed in $Lkb1^{+/+}$ mice of the same age.

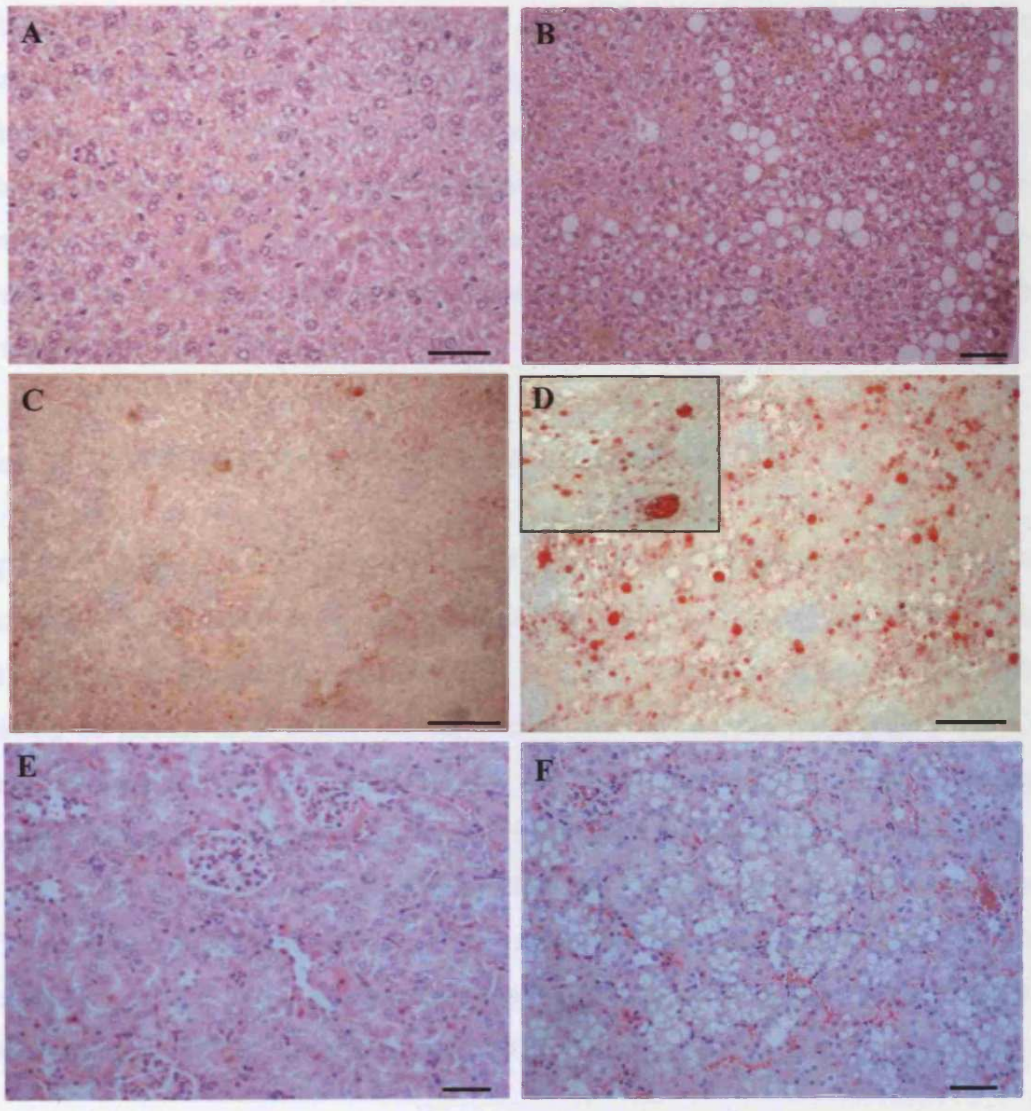

Figure 7.14 – Additional phenotypes associated with Lkb1 loss. H&E liver histology from: **A,** $Lkb1^{+/+}$ **B,** $Lkb1^{fl/fl}$ AHCre + mice 6 months following recombination with 0.8mg/kg β-napthoflavone. Oil red-O histological staining for intracellular fat storage in: **C,** $Lkb1^{+/+}$ **D,** $Lkb1^{fl/+}$ AHCre+ mice 18months following recombination with 4x80mg/kg β-napthoflavone (scale bars = 20μm). H&E Kidney histology in: **E,** $Lkb1^{+/+}$ **F,** $Lkb1^{fl/fl}$ AHCre + mice 6 months following recombination with 0.8mg/kg β-napthoflavone (all other scale bars = 50μm).

7.4 Discussion

7.4.1 Lkb1 floxing regimes

The low-level recombination technique employed to study long term tumourigenesis in *Lkb1*$^{fl/fl}$ mice was successful in permitting mice to age to 5-6 months. Recombination in a limited number of crypts with 1 injection or feeding with 0.8mg/kg β-napthoflavone resulted in stem cell recombination of approximately 10% of intestinal cells as observed from whole mount LacZ staining (figure 7.1 E). Floxing at lower levels results in *Lkb1* homozygosity in a subset of cells that may be of more clinical relevance to PJS patients; where an additional somatic hit to the LKB1 locus would be an infrequent event rather than occurring within 100% of cells as in the high level deletion protocol (chapter 5).

7.4.2 Tumourigenesis and Long term persistence of *Lkb1* loss

Figure 7.2 shows that heterozygote loss of Lkb1 6 days following recombination with 80mg/kg β-napthoflavone, fails to result in any significant change from *Lkb1*$^{+/+}$ tissue with regard to increased cellularity or increased secretory lineages. Alcian blue staining of goblet cells shows no significant increase in positives (figure 7.2 C-D) when compared with that of the highly dysplastic goblet cells in the homozygote mouse in Chapter 5 (figure 5.10). In addition when these mice were subsequently left to age, no signs of disease or unusual phenotype were apparent, furthermore mice failed to develop hamartomatous polyps at an age comparable with that previously reported by several other groups studying constitutive heterozygosity (Miyoshi *et al* 2002, Nakau *et al* 2002, Bardeesy *et al* 2002).

Upon H&E analysis of *Lkb1*$^{fl/fl}$ histology, I found that low levels of aberrant crypt structures were retained 6 months following *Lkb1* deletion with 0.8mg/kg β-napthoflavone (figure 7.3A-B) and that these aberrant structures were similar in appearance to crypts from *Lkb1*$^{fl/fl}$ animals at day 13 following recombination (figure 5.2). I also identified infrequent hamartomas at this time point (figure 7.3C-F), indicating that *Lkb1* deficiency confers a relatively stable phenotype, and may contribute to hamartoma formation.

Although mucosal prolaspse and hamartoma formation themselves are considered of low neoplastic potential, *Lkb1*$^{fl/fl}$ mice displayed signs of clinical disease at 6 months following low dose recombination. The physical obstruction of a hamartoma (although non-malignant) may well explain the rapid decline observed in these animals. Control mice for the feeding regime were *Lkb1*$^{+/+}$ and *Lkb1*$^{fl/+}$ AHCre+ heterozygote mice of the same age. These mice failed to develop any intestinal phenotype when harvested or through histological analysis, suggesting that haploinsufficiency does not necessarily predispose to hamartoma formation in the AHCre conditional model, or that the time frame of complete loss of Lkb1 may be important in hamartoma development.

7.4.3 Constitutive heterozygosity in *Lkb1*$^{+/fl}$ mice predisposes to hamartoma formation

Mice heterozygote for *Lkb1* with the Deleter Cre frequently developed hamartomas of the small intestine, in addition to a number of aberrant phenotypes (table 7.1). The mucinous polyps were distinctly different from adenomas such as those seen in Apc knockout models (figure 7.4 C-D)(Sansom *et al* 2004a), displaying a well differentiated cell type, mucosal prolapse, stromal outgrowths and frond like epithelial structures such as those described in section 1.5 (figure 7.4 A-B). The hypermucinous goblet cells are a common feature in PJS hamartomas and figures 7.3 C-F and 7.4 C, E-F reflect this. Hamartomas are classically considered benign due to the differentiated nature and limited proliferative capacity of the tissue in contrast to adenomas (Bosman *et al* 1998) (figure 7.4 D&F). Contrastingly LKB1 loss has been suggested to drive the transition from premalignant precursor to malignancy following the observation that loss of epithelial expression correlated with high-grade intestinal lesions (Ghaffar *et al* 2003).

Hamartomas were most frequently located at the proximal junction between stomach and small intestine, although several mice displayed polyps mid way down the small intestine and rarely colonic polyps. Hamartomas observed in stomach regions of Lkb1 deficient mice showed a different histology to those of the small intestine, being

highly glandular and lacking the stalk component, crypt-like overgrowths and blocked crypt structures associated with intestinal hamartomas (figure 7.7 A-D).

Knockout mouse models for LKB1 and Par1 homologues from the MARK/AMPK family have also been shown to result in epithelial prolapse (Hurd *et al* 2003, Bessone *et al* 1999), thereby leading to the suggestion that loss of polarity is an initiating factor in hamartoma formation, and that patients with PJS have a genetic predisposition to mucosal prolapse and polyp formation. As mentioned previously, PJS polyps are considered benign and rarely show loss of polarity. Certainly figure 7.8A-B confirms that the secretory cell types within hamartomas retain correct basolateral polarity when histology is compared to adenomatous lesions showing no clear nuclear polarization and a disorganised stacking structure of cells (figure 7.8 C-D).

Further to the discussion of chapter 6, impaired asymmetric division was also considered as a possible cause of hamartoma formation and Lkb1 loss may result in down regulation of 'stemness' thereby triggering aberrant differentiation. The long-term persistence of phenotypes within the crypt such as the secretory lineage (figure 7.3 A-B), suggests the clonal dominance of a stem cell that has aberrant asymmetric division or upon division produces fewer adsorptive progenitors in the progenitor mix.

Chi square statistical analysis confirms that there is a significant difference in hamartoma formation between AHCre mice harbouring epithelial Lkb1 deletion and DelCre mice with constitutive Lkb1 deletion ($p=<0.001$), with the majority of *Lkb1*$^{fl/+}$DelCre mice developing an intestinal phenotype. Constitutive deletion of Lkb1 with the deleter Cre colony may channel asymmetric division in stem cells towards the secretory lineage via alterations in paracrine signalling, surrounding growth factors and cytokines from the nearby mesenchymal cells (Leedham *et al* 2005). Another possibility is the window of development, with AHCre mediated Lkb1 deletion occurring in adult tissue and DelCre mice having lost Lkb1 during embryogenesis.

However, mice homozygote for *Lkb1* with the AHCre also develop hamartomas solely as a result of loss of Lkb1 within the epithelium, adding confusion to the mesenchymal loss hypothesis as a prerequisite for hamartoma development. Until further knowledge is gained of the stromal/ mesenchymal/ epithelial interactions within the crypt this question will be hard to address.

Haploinsufficiency and Lkb1 expression in polyps

LKB1 was previously thought to act as a recessive tumour suppressor gene in hamartoma formation similarly to *PTEN*, *P27* and *SMAD4*. Mice heterozygote for these genes are predisposed to tumour formation without loss of the remaining allele and in defiance of the Knudson's second hit hypothesis. However, *in situ* analysis of normal, malignant and hamartoma tissue from PJS patients has revealed heterogeneous results with regard to the cytoplasmic epithelial expression of LKB1 in the intestine. Previous groups have reported only a third of heterozygotes succumb to hamartoma formation and that Lkb1 protein was retained in all the polyps (Rowan *et al* 2000).

qRT-PCR analysis of $Lkb1^{fl/+}$ DelCre hamartomas for *Lkb1* transcripts showed of the 4 samples tested, *Lkb1* was only down regulated an average of 1.41 fold (+/-0.1SD). This may be due to dilution by somatic cell contamination, or may reflect up regulation of the remaining wild type allele to maintain normal levels of Lkb1. Given the late age of tumour formation in $Lkb1^{fl/+}$DelCre mice and the confusion surrounding stromal versus epithelial loss, it may be that clonal homozygote loss has occurred. Indeed as LKB1 was infrequently lost in polyps, complete loss is suggested to be secondary as a result of neoplastic progression (Rowan *et al* 2000).

Progression to malignancy

Although LOH of the remaining wild type *Lkb1* allele and loss of polarity have both been suggested to contribute to progression of tumours, it has been suggested that conventional initiation of tumourigenesis must occur for an alteration in LKB1 levels to become relevant. This may explain the benign nature of hamartomas and increased

risk of neoplastic progression to PJS patients. In support of this, JPS patients presenting with similar hamartomas as a result of dysfunctional gatekeeper genes such as Smad4 or BMP, develop further malignancies as a result of aberrant Wnt activation (Jansen *et al* 2005 in press). Interestingly potentially malignant microadenoma lesions are occasionally observed in PJS hamartomas (Jansen *et al* 2005 in press), and one *Lkb1*$^{fl/+}$DelCre mouse did show an unusual area of adenomatous-like cells within a hamartoma (figure 7.8 H). Furthermore, IHC for proliferative markers such as Ki-67 confirmed aberrant pockets of proliferative cells within the hamartoma structure, although this was mostly localised to the base of crypt-like structures (figure 7.8E-F). Staining for S6 ribosomal protein may also mark highly proliferative sub regions of the hamartoma, as isolated pockets of positive cells displayed S6K activity (figure 7.8 G), similar to that previously reported in PJS polyps (Shaw *et al* 2004b). Inhibition of BMP signalling in mice over expressing Noggin results in similar pockets of proliferation in aberrant crypt-like regions, suggesting that hamartoma formation may rely on both altered Notch signalling in the underlying mesenchymal tissue in conjunction with altered BMP inhibitors such as Noggin in the epithelium (Haramis *et al* 2003). Together these data cast doubt on reports that hamartomas present no neoplastic potential, and the disorganised nature of the structure and aberrant placing of stem cell compartments may play a role in cancer progression.

7.4.4 Lkb1 loss and lymphoid infiltration

The aberrant phenotypes described in figure 7.5 and table 7.1 are unusual and have been diagnosed as either marginal or mantle cell intestinal lymphomas. Screening for certain markers such as B cell proliferating CD20/CD79A, CD5,10, 23 Cyclin D1 – ve, Bcl-2 +ve (for marginal cell lymphoma) or CD5, Cyclin D1, Bcl-2+ve, CD10, 23-ve (for mantle cell/lymphomatous polyposis), will help to diagnose this phenotype. These aggressive lymphomas invade through the basement membrane of the intestine and appear to originate from the Peyer's patches, rather than as a secondary consequence of lymphoma external to the intestine. Furthermore, lymphoma occurrence in *Lkb1*$^{fl/+}$ DelCre and *Lkb1*$^{+/+}$ mice was a rare feature (figure 7.5E- F, table 7.1).

Intestinal lymph nodes (Peyer's patches) are formed as a result of lymphotoxin signalling from inducer cells via NF-κB signalling on the surrounding stromal tissue (Taylor *et al* 2004). $Pten^{+/-}$ mice are predisposed to a variety of neoplasias, and a recent report shows that the gastrointestinal tumours in heterozygote Pten or doubly mutant $Pten^{+/-}$ $p27^{+/-}$ mice occurred in association with underlying non-neoplastic hyperplasia of intestinal lymph nodes (Podsypanina *et al* 1999, DiCristofano *et al* 2001). This disturbance in the lymph node signalling to the overlying epithelium has been suggested to cause aberrant overgrowth observed in hamartomas (Podsypanina *et al* 1999). The interactions with the overlying epithelia may be critical in $Lkb1^{fl/+}$ DelCre mice where Lkb1 loss is heterozygous in all components of the intestinal tissue. Increased lymphoid follicles in p21 deficient mice has also been linked to the formation of ACF (Poole *et al* 2004). Interestingly M cells in the epithelium mediate expression of adhesive molecules between intraepithelial lymphocytes and the ECM in addition to cytokine production, which may correlate with some of the array changes noted in chapter 6.

Epithelial cells associated with defective proliferative stromal cells may become more susceptible to neoplastic transformation, and this may also be associated with loss of polarity and an increased inflammatory response (Kinzler and Vogelstein 1998). These immunosurvellance functions may be of importance when challenged by a pathological condition (Tlaskalova-Hogenova *et al* 1995), and indeed microenvironment is considered one of the most influential factors in tumourigenesis, outlining an additional landscaper tumour suppressor function for Lkb1.

It is of note to mention that JPS is also thought to arise from defective landscaper functions of BMP signalling in the mesenchymal region, however it was recently reported that homozygote loss of Smad4 solely in the epithelium in JPS and mice was also found to predispose to polyp formation. This finding suggests that polyp formation arises as a result of disrupted interpretation of mesenchymal signalling by the epithelium (Haramis *et al* 2003). However, lymph aggregates in $Lkb1^{fl/+}$ DelCre mice were infrequently observed in the absence of hamartoma formation, suggesting the phenotype in these mice to be coincidental to hamartoma formation, or merely at

an earlier stage of progression. Further genetic analysis of the stromal, paracrine and epithelial components of hamartomas is necessary to provide clues into the clonal or primary oncogenic origin of hamartomas (Kinzler and Vogelstein 1998).

The aberrant dysplasia of lymph nodes within the *Lkb1*$^{+/fl}$DelCre intestine may not underlie hamartoma formation, but provide a mechanism for neoplastic progression in PJS patients. My present studies of the *Lkb1*$^{+/fl}$DelCre heterozygous mice are insufficient to address this question as the majority of mice were harvested without signs of malignancies other than lymphoma, which may occur spontaneously in a small proportion of *Lkb1*$^{+/+}$ mice (approximately 10%) at 18 months.

Finally, *Lkb1* deficient mice are particularly susceptible to the protozoan gut parasite Giardia. The intestinal mucosal defence system against Giardia is independent of the immune system, and is directly controlled by paneth cell secretions. As mentioned in Chapter 5, poor exocytosis of paneth cell granules containing IgA, NO, α-defensins, angiogenins and lactoferrin or failure of proteolytic processing signals may underlie this susceptibility to giardia. Whatever the mechanism of action of Lkb1 within the intestine, the fact that the rederived 'clean' isolator mice show the same phenotype as giardia infected mice (figure 7.6), confirms that this phenotype is independent of infection and subsequent immune response.

7.4.5 Lkb1 hypomorphic and *in utero* phenotypes

Data produced by Dario Alessi outlines the hypomorphic nature of the unrecombined *Lkb1*^{fl} allele in skeletal muscle, heart and testis (Sakamoto *et al* 2005 in press). In the intestine I observed a clear reduction of Lkb1 kinase activity and also protein level from western blot analysis in the *Lkb1*$^{fl/fl}$ sample (figure 7.9). However, overall detection of Lkb1 expression within the gut is extremely variable between samples, even of the same genotype (samples 600 and 601 = *Lkb1*$^{+/+}$ mice, but show very different expression patterns, figure 7.9). This suggests that the extraction or assay protocol used may not be sensitive enough for reliable results in intestinal samples.

Non-mendalian genetics were observed for the *Lkb1*^{fl} transgene when crossed to the AHCre transgene. Chi square analysis revealed that there was a significant difference between the expected and observed genotypes of the mice (p=<0.001). This may be attributed to the hypomorphic nature of the allele and a reduction of *Lkb1* expression during development. Residual protein levels from the transgene may also possess dominant negative effects, this will be of particular importance if found to effect the regulatory C-terminal end of the protein, which has recently been suggested to determine activation of AMPK or polarity pathways (Forcet *et al* 2005).

The finding that liver samples show a hypomorphic phenotype may have implications for the survival of the mice at day 13. Other knockout models such as the *Apc*$^{fl/fl}$ mouse show signs of disease by day 8 attributed to liver function failure as a result of leakage of the AHCre (Sansom *et al* 2004a). Further investigation to address this point will involve liver function tests from blood samples. However, no gross abnormalities such as those observed in the *Apc*$^{fl/fl}$ mice are apparent at day 13 in Lkb1 deficient livers.

Preliminary data from figure 7.9 suggests the *Lkb1*^{fl} allele to show only 5% of normal activity in the intestine. However, *Lkb1*$^{+/+}$ and *Lkb1*$^{fl/fl}$AHCre- mice show no difference in crypt cell number, apoptosis or differentiation status in the intestine and qRT-PCR of *Lkb1* levels revealed expression in *Lkb1*$^{fl/fl}$ AHCre- mice was less than a 1.8 fold reduction compared to *Lkb1*$^{+/+}$ levels (see chapter 6, figure 6.8). As hypomorphic activity of the allele in the intestine is very slight and *Lkb1*$^{fl/fl}$ AHCre- female mice survive until 18 months of age without development of hamartomas, this argues against a haploinsufficiency requirement for hamartoma formation when Lkb1 is lost in the epithelium alone in the AHCre mouse. The appearance of hamartomas in the DelCre heterozygotes reflects either an epithelial versus non-epithelial difference or the loss of Lkb1 earlier in development.

Loss of Lkb1 *in utero*

If polyp formation were dependent of loss of polarity, one might expect germline loss of LKB1 during development to be the underlying cause of hamartoma formation. Additionally, the aberrant neural tube closure seen in constitutive Lkb1 knockouts is

associated with many genetic defects, particularly those involved in cell polarity, with Dishevelled (Dsh) knockout mice displaying a similar phenotype (Copp *et al* 2003). My limited *in utero* studies have not revealed neural tube defects, although one *Lkb1*$^{fl/+}$ heterozygote pup was born with midline closure failure. This is an unusual event, but mice doubly mutant for *Tgfβ2* and *Tgfβ3* display a similar phenotype and are viable to day 18.5 (Dunker and Krieglstein 2002).

As deletion of Lkb1 in adult epithelial tissue fails to predispose to tumours in heterozygous mice, the aging of mice with *in utero* heterozygote Lkb1 loss may provide evidence of a developmental dependence. Figure 7.10 shows that mice subjected to *in utero* floxing recapitulate the phenotype at day 18.5 of that observed in adult tissue with Lkb1 loss (figure 7.10 A-B). This is confirmed by alcian blue staining for goblet cells and Caspase 3 immunohistochemistry of apoptosis in *Lkb1*$^{fl/fl}$ mice (figure 7.10C-F). It is of note that *Lkb1*$^{fl/+}$AHCre mice show no intestinal *in utero* phenotype at day 18.5, and mice are currently being aged and monitored.

Upon closer examination of H&E *in utero* histology, it was clear that *Lkb1* null embryos displayed high levels of apoptosis. Figure 7.11 confirmed this phenotype by caspase 3 immunohistochemistry of several organs, Figure 7.11 C-D also shows that Lkb1 deficient mice exhibit high levels of apoptosis in addition to lack of obvious trabeculae in the lung, outlining an important role for Lkb1 in this tissue. Indeed there appears to be tissue specificity for different LKB1 responses, in particular apoptosis. Prostate cancer cells and pancreatic β cells are extremely sensitive to death following AMPK activator treatment with AICAR or Metformin. Lung cancer cells and astrocytes however lack significant LKB1 expression and are less sensitive to death as a result. Indeed glucose deprivation may be an advantage to some cancer cells as they are protected against apoptosis (Luo *et al* 2005). Therefore LKB1 action on AMPK can be both pro- and anti-apoptotic depending on tissue type. Ultimately exposure of Lkb1 null mice to DNA damaging agents such as those described in previous chapters with Mbd4 and Dapk null mice may help to elucidate the role of LKB1 in mediating the apoptotic response in different tissues.

7.4.6 Loss of Lkb1 predisposes to an aberrant GU phenotype

prostate

Prostate cancer is one of the largest causes of mortality in men, although still relatively little is known of the genetic defects that may underlie the disease. Multiple susceptibility genes have been identified including: *HPC1, HPC2, MSRI, BRCA1 and NBS1*. Many of these genes are involved in DNA damage signalling pathways, and patients that harbour germline heterozygote mutations in these genes may be of increased susceptibility to tumourigenesis (Cybulski *et al* 2004). Given the interactions of LKB1 with ATM and p53, LKB1 plays a role in DNA damage surveillance and may be a candidate susceptibility gene.

The development of the aberrant phenotypes described in figures 7.12 and 7.13 has been attributed to leakage of the AHCre prior to recombination with β-napthoflavone in several areas of the GU tract, particularly the ventral prostate (LacZ figure 7.12 A).

100% of $Lkb1^{fl/fl}$ mice developed a GU phenotype, most commonly opportunistic infection of glands in addition to early onset low grade prostate neoplasias, although the origin of neoplasia initiation is unclear. An increased immune response is seen in the stromal and urethral gland lining and the urethra wall is thickened. The pathogen identified in the GU tract was *Coagulase negative staphylococci,* which is an opportunistic infection of the skin and GU tract and is associated with immunodeficiency. Interestingly a report detailing phenotypes of *NOS2* knockout mice showed susceptibility to the same pathogen (Won *et al* 2002). Array data from Lkb1 null intestines showed increased NOS2 expression and this gene has been linked to an activated immune response, changes in fibronectin, laminins and MMP activity and may provide opportunity for infection by this pathogen (Shinji *et al* 1998). However, patients with PJS do not display any immunodeficiency problems, perhaps as a result of the far lower frequency of LKB1 loss predicted in humans compared to that of the $Lkb1^{fl/fl}$ mouse. Given the differences between mouse and human prostate the relevance of this data to the human situation is unclear as $Lkb1^{fl/fl}$ mice develop neoplasia predominantly of the coagulating gland, which is absent in humans.

Array analysis on prostate cancer cell lines has suggested upregulation of secretory differentiation factors MASH1 and Neurogenin3, and neuroendocrine cells (NE) in aggressive forms of the disease (Hu *et al* 2002). Given the parallels to changes in bHLH differentiation factors and secretory lineages in the intestinal molecular studies, array analysis of Lkb1 null prostate samples would perhaps prove useful in probing the molecular mechanisms of Lkb1 mediated prostate tumourigenesis.

Ki-67 positive staining has been correlated to aggressive forms of prostate neoplasia, and staining of $Lkb1^{fl/fl}$ prostate sections reveals that mitotic figures are frequent in the aberrant prostate and that areas of neoplastic tissue are hyperplastic (figure 7.12 F).

Prostate cancers often undergo metastasis to nearby bone by modulation of VEGF signalling by BMP. Noggin, an antagonist of BMP signalling was found to inhibit this interaction. Several BMP molecules have been found over expressed in prostate carcinogenesis (Dai *et al* 2004). This may reflect the role of Lkb1 in the BMP differentiation pathway described in chapter 6 and also provide some starting points to further characterise the prostate phenotype. At present it is hard to distinguish the point of origin of the neoplasia in $Lkb1^{fl/fl}$ mice. Treatment with anti-androgens or COX2 inhibitors may identify a hormonal dependency. Additionally, primary culture of prostate cells and treatment with pathway inhibitors may provide further mechanistic clues for Lkb1 signalling.

Testis

Testicular cancers from sporadic and PJS LKB1 mutations arise from a sertoli cell origin (Bergada *et al* 2001), and this process is crucial in the tumourigenic process. Figure 7.13 D-E shows increased apoptosis in this region of the testis and this sensitivity to Lkb1 loss may provide a safety mechanism to delete cells, hence why I did not observe any testicular tumours. Secondary mutations in this apoptotic response, or the DNA repair function of LKB1 may lead to malignant progression.

AMPK is a mammalian homologue of SNRK in yeast and both genes may be involved in regulating energy production. As AMPK is highly expressed in the testis it may be required for energy regulation of sperm motility and migration. Interestingly *Lkb1*$^{fl/fl}$ mice show low levels of sperm production, a large number of apoptotic cells and recently sperm from *Lkb1*$^{fl/fl}$ mice have been shown to exhibit low motility (unpublished observation, Alan Ashworth ICR).

The epididymis functions to store and mature sperm. There are several suggestions for the absence of sperm in the *Lkb1*$^{fl/fl}$ epididymis seen in figure 7.13 A-C. Firstly the movement of sperm from the testis to the epididymis is reliant upon microvilli-like structures termed stereocilia that brush the immature sperm along the ducts to storage. These structures may be reliant on Lkb1 for correct polarity, much the same as brush borders in the intestine. Furthermore, the hypomorphic nature of the allele, aberrant cell secretions or indeed impaired sperm maturation may be responsible for this phenotype.

7.4.7 Lkb1 loss and additional phenotypes

Hamartomas of the intestine are the most abundant phenotype in PJS, however hamartomatous polyps of the bladder, nasopharynx and respiratory tract are also common (Jansen *et al* 2005 in press). Although hamartomas of any other tissues were absent, figure 7.14 details the additional phenotypes observed in *Lkb1*$^{fl/fl}$ AHCre+ and *Lkb1*$^{fl/fl}$ AHCre– hypomorphic mice and *Lkb1*$^{fl/+}$ AHCre+ mice at 18 months. Typically homozygous Lkb1 nulls develop these phenotypes earlier than heterozygote mice (6 months) and in most cases are more severe.

Liver phenotype

Intracellular fatty steatosis was apparent from figure 7.14 A-B and confirmed by Oil Red-O fat staining (figure 7.14 C-D). Loss of LKB1 and hence AMPK activation may contribute to both insulin resistance and steatosis within the liver of these mice as well as intestinal tumourigenesis (Luo *et al* 2005).

The processes underlying development of liver steatosis are still poorly understood. Hyperammonemia and hypoglycaemia are associated with fatty steatosis of the liver (Yamazaki *et al* 2002), as is obesity and alcohol-induced disease. Insulin resistance arises as a result of insulin receptor substrate phosphorylation by a variety of inputs e.g. JNK, PI3K, mTOR, cJUN, PKC. Several genes of interest isolated from chapter 6 play a role in insulin resistance and fatty steatosis. Indeed certain inflammatory processes and cytokine activities have been linked to TNFα, MMP alterations and fatty liver formation in mice (Moseley 2004). Also NOS2 activity (previously mentioned in association with the GU infections discussed above) is associated with liver steatosis, mitochondrial and hepatic dysfunction (Venkatraman *et al* 2004). Furthermore, Pten deficiency results in steatosis and development of HCC in mice, due to changes in adipocyte specific differentiation genes and hepatocyte lipogenesis enzymes (Horie *et al* 2004). These processes are characteristic of AMPK inactivity and loss of Lkb1 appears to result in similar steatosis (figure 7.14 A-B).

As AMPK can be activated independently of LKB1, treatments such as Metformin/AICAR and rosiglitazone used by diabetics to increase glucose utilization in the liver and decrease fatty acid synthesis may alleviate this phenotype (Zhou *et al* 2001, Luo *et al* 2005).

Kidney phenotype

Figure 7.14E-F histology of the kidney shows a vacuolated phenotype of the proximal tubules in $Lkb1^{fl/fl}$ mice when compared to $Lkb1^{+/+}$ control animals. This phenotype was also apparent in the long term $Lkb1^{+/fl}$ AHCre and DelCre colonies when mice were harvested at 18 months or more. The phenotype has been difficult to define, although it shares some similarities with the defective tubules observed in glycogen storage diseases. Alternatively it may represent abnormalities in solute reabsorption, disruption of ATP gradients and proximal tubule transport. Hypokalemia results in vacuoles in proximal tubules, which sometimes resembles fat storage. The underlying cause of this syndrome is defective potassium channels, and since the array data from chapter 6 produced many changes in solute channel proteins, this may underlie the role of Lkb1 in the kidney (personal communication professor Geriant Williams).

7.5 Chapter summary and conclusions

- Selective survival of aberrant crypt structures and infrequent hamartomas in *Lkb1*$^{fl/fl}$ mice were evident 6 months following recombination.

- Lkb1 heterozygosity was found to contribute to tumourigenesis in constitutive *Lkb1*$^{+/fl}$DelCre mice, but not in AHCre epithelial knockout colonies.

- Additional Lkb1 loss in stromal tissue or during development may predispose to hamartoma development in DelCre+ mice,

- Homozygous Lkb1 loss in the epithelium also predisposed to infrequent hamartoma formation at an early age, suggesting sensitivity of the epithelium to complete Lkb1 loss, a process that may also occur in *Lkb1*$^{+/fl}$DelCre mice given the late stages of hamartoma onset. Furthermore, LOH was not observed in DelCre hamartomas indicating homozygousity is not the key route to polyp formation but reflects patches of LOH found in goblet cell rich areas of hamartomas (Hemminki *et al* 1997)

A threshold model may exist for Lkb1, similarly to Pten where the tumour suppressor function depends on the burden of mutant cells. A potential field effect may arise on the surrounding normal cells in mouse models. This situation is unlikely to occur in humans, which usually develop cancer as a result of a single transformed cell. However, the multi-step process of tumourigenesis and genetic heterogeneity of tumours in conjunction with the eventual formation of fields of cancer cells in humans suggest that the mouse field effect in combination with stromal and mesenchymal interactions may be of particular relevance after all to human disease (Trotman *et al* 2003).

A situation may arise where the effects of Lkb1 status depend on the stage of loss, stromal versus epithelial loss and tissue specificity, in addition to further genetic alterations and microenvironment challenges. Further understanding of these processes is required to elucidate the complex role of Lkb1 in tumourigenesis.

The immediate phenotype observed following Lkb1 loss from chapter 5 showed marked disruption of crypt villus architecture, sensitivity of enterocytes to cell death and an expansion of the secretory cell lineages, such as that observed in PJS hamartomas. This was found to be driven by deregulation of intestinal differentiation transcription factors, most importantly Math1 (chapter 6), implicating altered Notch signalling as an important pathway in intestinal tumourigenesis. Retention of these perturbed crypts and disrupted signalling environment ultimately predisposed to hamartoma formation in *Lkb1*$^{fl/fl}$ mice over a relatively short time period (figure 7.15). The combination of these intestinal phenotypes observed from chapters 5-7 parallels the susceptibility of Peutz-Jeghers patients to cancer, but also highlights an important role for Lkb1 in several other tissues such as the liver and prostate, to be further investigated.

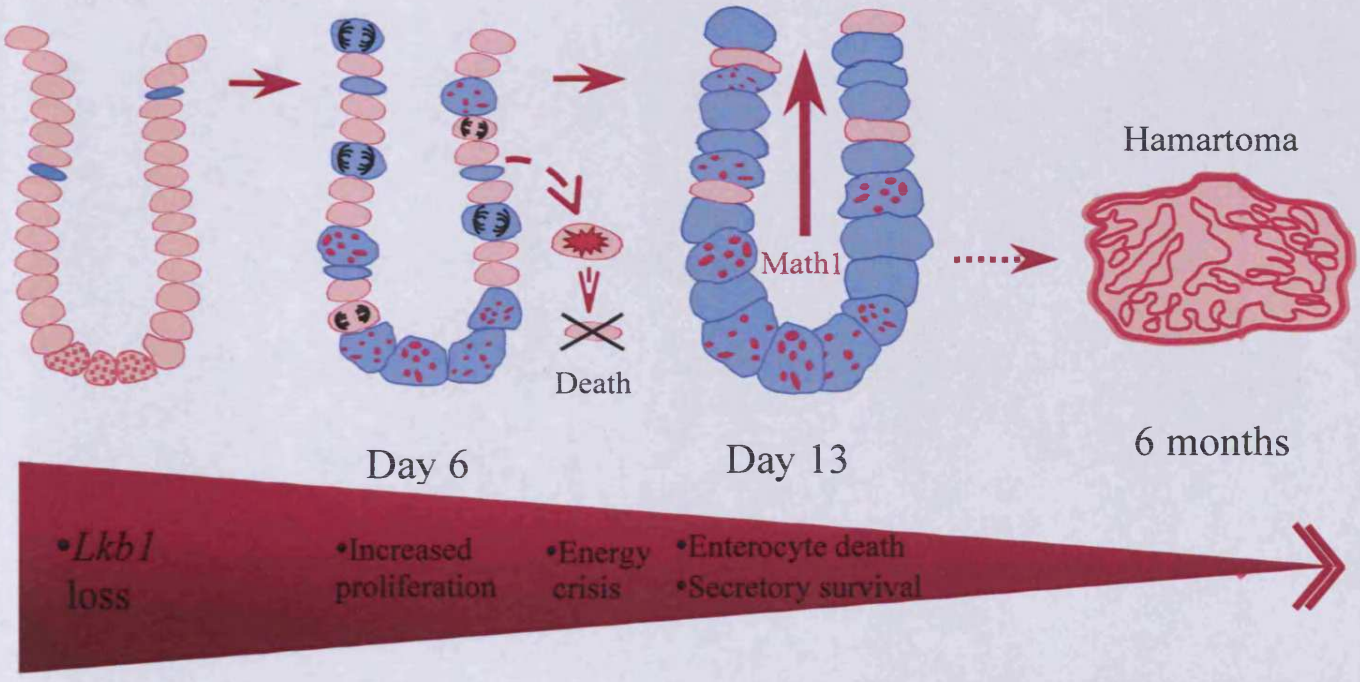

Figure 17- Schematic diagram illustrating long term consequences of *Lkb1* loss in the intestinal epithelium. Following an initial proliferative burst, the enterocyte lineage undergo an energy crisis and are channelled toward a cell death response. Secretory precursor cells are protected from this fate and with a coincident increase in *Math1* expression, expand and populate the crypt. The resultant mucin filled crypt shows long term persistence ultimately predisposing to hamartoma formation.

Thesis summary

The development of murine models with precisely defined genetic lesions is allowing a much better understanding of the cellular and molecular mechanisms that control cell death and underlie tumour suppressor gene function has greatly increased our understanding of the genetic control of apoptosis as well as raising new hypotheses and new potential routes to intervention.

Previous studies raised the attractive hypotheses that tumour predisposition may be explained in terms of failed cell death, and also that tumour regression may be initiated through activation of an apoptotic programme.

This thesis has investigated some significant questions relating to the apoptotic response elicited following DNA damage, and finds both *MBD4* and *DAPK* add to the increasing cohort of genes implicated in the control of DNA damage-induced death. However, it is clear that this represents the 'easy' part of these studies, and that the interpretation of the significance of these relationships is much more challenging.

It is clear from this thesis that MBD4, DAPK can act as damage sensors and initiate an apoptotic response. The ability to engage cell death even in a lesion dependent manner, partially explains the tumour suppressor activity of these genes. However, the failure to predict endpoints such as clonogenic survival for Mbd4 with temozolomide and ionising radiation and for Dapk with all agents, reinforces the complex nature of the apoptotic response and makes the relevance to tumour predisposition and regression hard to predict.

This conclusion is not surprising as indeed all cells must be considered within the context of interacting networks either at the molecular or cellular level, with complex endpoints necessarily difficult to predict. Indeed given the reports of DAPK in mediating intrinsic, extrinsic and now DNA damage induced death, it appears likely that this gene may lie at the crossroads between several death pathways, and some levels of redundancy may therefore exist.

Much of the challenge that remains lies in interpreting the physiological relevance of these observations. Investigations using high dose DNA damaging agents may be valuable to chemotherapy treatment but does not answer questions relating to loss of the gene and tumour predisposition at spontaneous levels of DNA damage, and indeed our ability to test the significance of apoptosis in such circumstances remains limited.

My investigations into LKB1 tumour suppressor function using conditional inactivation of the gene reflect a more physiologically relevant study. The very low level of Lkb1 activity achieved using the AHCre and DelCre transgenes and the conditional Lox-P system resulted in progression of intestinal hamartomas in LKB1 deficient mice that strongly resembled those observed in human PJS patients, and suggests a stromal element may also contribute to PJS hamartomas similarly to JPS.

Furthermore, a critical role for LKB1 in directing intestinal differentiation was identified from short term studies of Lkb1 loss in the normal intestinal epithelium, with Lkb1 loss also sensitizing certain cell populations to apoptosis. Data from chapter 5 and the immediate phenotype suggest that loss of LKB1 at the early initiation stages of tumourigenesis or in normal tissues would sensitize to apoptosis and hence protect against inappropriate survival. This argues against a role for LKB1 in tumour initiation, but confirms reports that loss of LKB1 at later stages of tumourigenesis may confer a selective advantage to tumour cells that loose apoptotic control during the course of tumourigenesis, and hence negate the safety mechanism of energy crisis induced apoptosis.

One further point of interest from the LKB1 microarray (chapter 6) and DelCre studies (chapter 7) was the attention drawn toward the crypt niche and its surrounding microenvironment in regulating intestinal homeostasis such as cell differentiation and death. Microarray analysis of LKB1 deficient RNA frequently pointed toward aberrant adhesion signalling and stromal interaction and consequently misinterpretation of signalling pathways such as Notch, TGF-β, BMP and Wnt, all of which are crucial in directing crypt homeostasis.

Further investigation is needed to try to elucidate many of the regulatory mechanisms still overlooked for these genes such as cell type specific interactions, binding

partners and pathway components, epigenetic regulation, and inhibitory family members or auto inhibitory structures within these proteins that may modulate activity.

References

Abed, A. A., K. Gunther, et al. (2001). "Mutation screening at the RNA level of the STK11/LKB1 gene in Peutz-Jeghers syndrome reveals complex splicing abnormalities and a novel mRNA isoform (STK11 c.597(insertion mark)598insIVS4)." Hum Mutat **18**(5): 397-410.

Adams, J. M., A. W. Harris, et al. (1985). "The c-myc oncogene driven by immunoglobulin enhancers induces lymphoid malignancy in transgenic mice." Nature **318**(6046): 533-8.

Altarejos, J. Y., M. Taniguchi, et al. (2005). "Myocardial ischemia differentially regulates LKB1 and an alternate 5'-AMP-activated protein kinase kinase." J Biol Chem **280**(1): 183-90.

Arango, D., G. A. Corner, et al. (2001). "c-myc/p53 interaction determines sensitivity of human colon carcinoma cells to 5-fluorouracil in vitro and in vivo." Cancer Res **61**(12): 4910-5.

Attardi, L. D. and T. Jacks (1999). "The role of p53 in tumour suppression: lessons from mouse models." Cell Mol Life Sci **55**(1): 48-63.

Attardi, L. D., S. W. Lowe, et al. (1996). "Transcriptional activation by p53, but not induction of the p21 gene, is essential for oncogene-mediated apoptosis." Embo J **15**(14): 3693-701.

Baas, A. F., J. Boudeau, et al. (2003). "Activation of the tumour suppressor kinase LKB1 by the STE20-like pseudokinase STRAD." Embo J **22**(12): 3062-72.

Baas, A. F., L. Smit, et al. (2004). "LKB1 tumor suppressor protein: PARtaker in cell polarity." Trends Cell Biol **14**(6): 312-9.

Back, W., S. Loff, et al. (1999). "Immunolocalization of beta catenin in intestinal polyps of Peutz-Jeghers and juvenile polyposis syndromes." J Clin Pathol **52**(5): 345-9.

Backman, S., V. Stambolic, et al. (2002). "PTEN function in mammalian cell size regulation." Curr Opin Neurobiol **12**(5): 516-22.

Bader, S., M. Walker, et al. (2000). "Most microsatellite unstable sporadic colorectal carcinomas carry MBD4 mutations." Br J Cancer **83**(12): 1646-9.

Bai, T., T. Tanaka, et al. (2004). "Reduced expression of death-associated protein kinase in human uterine and ovarian carcinoma cells." Oncol Rep **11**(3): 661-5.

Ballestar, E. and A. P. Wolffe (2001). "Methyl-CpG-binding proteins. Targeting specific gene repression." Eur J Biochem **268**(1): 1-6.

Bardeesy, N., M. Sinha, et al. (2002). "Loss of the Lkb1 tumour suppressor provokes intestinal polyposis but resistance to transformation." Nature **419**(6903): 162-7.

Baross-Francis, A., S. E. Andrew, et al. (1998). "Tumors of DNA mismatch repair-deficient hosts exhibit dramatic increases in genomic instability." Proc Natl Acad Sci U S A **95**(15): 8739-43.

Batlle, E., J. T. Henderson, et al. (2002). "Beta-catenin and TCF mediate cell positioning in the intestinal epithelium by controlling the expression of EphB/ephrinB." Cell **111**(2): 251-63.

Baylin, S. B. and J. G. Herman (2000). "DNA hypermethylation in tumorigenesis: epigenetics joins genetics." Trends Genet **16**(4): 168-74.

Bellacosa, A. (2001a). "Functional interactions and signaling properties of mammalian DNA mismatch repair proteins." Cell Death Differ **8**(11): 1076-92.

Bellacosa, A. (2001b). "Role of MED1 (MBD4) Gene in DNA repair and human cancer." J Cell Physiol **187**(2): 137-44.

Bessone, S., F. Vidal, et al. (1999). "EMK protein kinase-null mice: dwarfism and hypofertility associated with alterations in the somatotrope and prolactin pathways." Dev Biol **214**(1): 87-101.

Bialik, S., A. R. Bresnick, et al. (2004). "DAP-kinase-mediated morphological changes are localization dependent and involve myosin-II phosphorylation." Cell Death Differ **11**(6): 631-44.

Bienz, M. and H. Clevers (2000). "Linking colorectal cancer to Wnt signaling." Cell **103**(2): 311-20.

Bjerknes, M. and H. Cheng (1999). "Clonal analysis of mouse intestinal epithelial progenitors." Gastroenterology **116**(1): 7-14.

Blache, P., M. van de Wetering, et al. (2004). "SOX9 is an intestine crypt transcription factor, is regulated by the Wnt pathway, and represses the CDX2 and MUC2 genes." J Cell Biol **166**(1): 37-47.

Blanchard, C., S. Durual, et al. (2004). "IL-4 and IL-13 up-regulate intestinal trefoil factor expression: requirement for STAT6 and de novo protein synthesis." J Immunol **172**(6): 3775-83.

Blumer, J. B., M. L. Bernard, et al. (2003). "Interaction of activator of G-protein signaling 3 (AGS3) with LKB1, a serine/threonine kinase involved in cell polarity and cell cycle progression: phosphorylation of the G-protein regulatory (GPR) motif as a regulatory mechanism for the interaction of GPR motifs with Gi alpha." J Biol Chem **278**(26): 23217-20.

Bocker, T., J. Ruschoff, et al. (1999). "Molecular diagnostics of cancer predisposition: hereditary non-polyposis colorectal carcinoma and mismatch repair defects." Biochim Biophys Acta **1423**(3): O1-O10.

Bosman, F. T. (1999). "The hamartoma-adenoma-carcinoma sequence." J Pathol **188**(1): 1-2.

Boudeau, J., A. Kieloch, et al. (2003a). "Functional analysis of LKB1/STK11 mutants and two aberrant isoforms found in Peutz-Jeghers Syndrome patients." Hum Mutat **21**(2): 172.

Boudeau, J., A. F. Baas, et al. (2003b). "MO25alpha/beta interact with STRADalpha/beta enhancing their ability to bind, activate and localize LKB1 in the cytoplasm." Embo J **22**(19): 5102-14.

Boudeau, J., M. Deak, et al. (2003c). "Heat-shock protein 90 and Cdc37 interact with LKB1 and regulate its stability." Biochem J **370**(Pt 3): 849-57.

Brabletz, T., S. Spaderna, et al. (2004). "Down-regulation of the homeodomain factor Cdx2 in colorectal cancer by collagen type I: an active role for the tumor environment in malignant tumor progression." Cancer Res **64**(19): 6973-7.

Brajenovic, M., G. Joberty, et al. (2004). "Comprehensive proteomic analysis of human Par protein complexes reveals an interconnected protein network." J Biol Chem **279**(13): 12804-11.

Brugarolas, J. and W. G. Kaelin, Jr. (2004). "Dysregulation of HIF and VEGF is a unifying feature of the familial hamartoma syndromes." Cancer Cell **6**(1): 7-10.

Buermeyer, A. B., S. M. Deschenes, et al. (1999). "Mammalian DNA mismatch repair." Annu Rev Genet **33**: 533-64.

Buettner, V. L., H. Nishino, et al. (1997). "Spontaneous mutation frequencies and spectra in p53 (+/+) and p53 (-/-) mice: a test of the 'guardian of the genome' hypothesis in the Big Blue transgenic mouse mutation detection system." Mutat Res **379**(1): 13-20.

Bunz, F., P. M. Hwang, et al. (1999). "Disruption of p53 in human cancer cells alters the responses to therapeutic agents." J Clin Invest **104**(3): 263-9.

Burch, L. R., M. Scott, et al. (2004). "Phage-peptide display identifies the interferon-responsive, death-activated protein kinase family as a novel modifier of MDM2 and p21WAF1." J Mol Biol **337**(1): 115-28.

Campbell, S. J., F. Carlotti, et al. (1996). "Regulation of the CYP1A1 promoter in transgenic mice: an exquisitely sensitive on-off system for cell specific gene regulation." J Cell Sci **109 (Pt 11)**: 2619-25.

Carling, D. (2004). "The AMP-activated protein kinase cascade--a unifying system for energy control." Trends Biochem Sci **29**(1): 18-24.

Chan, M. W., L. W. Chan, et al. (2002). "Hypermethylation of multiple genes in tumor tissues and voided urine in urinary bladder cancer patients." Clin Cancer Res **8**(2): 464-70.

Chen, C. H., W. J. Wang, et al. (2005). "Bidirectional signals transduced by DAPK-ERK interaction promote the apoptotic effect of DAPK." Embo J **24**(2): 294-304.

Chen, X. D., L. W. Fisher, et al. (2004). "The small leucine-rich proteoglycan biglycan modulates BMP-4-induced osteoblast differentiation." Faseb J **18**(9): 948-58.

Cheng, S. W., L. G. Fryer, et al. (2004). "Thr2446 is a novel mammalian target of rapamycin (mTOR) phosphorylation site regulated by nutrient status." J Biol Chem **279**(16): 15719-22.

Chin, L., A. Tam, et al. (1999). "Essential role for oncogenic Ras in tumour maintenance." Nature **400**(6743): 468-72.

Clarke, A. R., M. C. Cummings, et al. (1995). "Interaction between murine germline mutations in p53 and APC predisposes to pancreatic neoplasia but not to increased intestinal malignancy." Oncogene **11**(9): 1913-20.

Clarke, A. R., S. Gledhill, et al. (1994). "p53 dependence of early apoptotic and proliferative responses within the mouse intestinal epithelium following gamma-irradiation." Oncogene **9**(6): 1767-73.

Clarke, A. R., L. A. Howard, et al. (1997). "p53, mutation frequency and apoptosis in the murine small intestine." Oncogene **14**(17): 2015-8.

Clarke, A. R., C. A. Purdie, et al. (1993). "Thymocyte apoptosis induced by p53-dependent and independent pathways." Nature **362**(6423): 849-52.

Cohen, O., E. Feinstein, et al. (1997). "DAP-kinase is a Ca2+/calmodulin-dependent, cytoskeletal-associated protein kinase, with cell death-inducing functions that depend on its catalytic activity." Embo J **16**(5): 998-1008.

Cohen, O., B. Inbal, et al. (1999). "DAP-kinase participates in TNF-alpha- and Fas-induced apoptosis and its function requires the death domain." J Cell Biol **146**(1): 141-8.

Collins, S. P., J. L. Reoma, et al. (2000). "LKB1, a novel serine/threonine protein kinase and potential tumour suppressor, is phosphorylated by cAMP-dependent protein kinase (PKA) and prenylated in vivo." Biochem J **345 Pt 3**: 673-80.

Cortellino, S., D. Turner, et al. (2003). "The base excision repair enzyme MED1 mediates DNA damage response to antitumor drugs and is associated with mismatch repair system integrity." Proc Natl Acad Sci U S A **100**(25): 15071-6.

Cory, S., D. C. Huang, et al. (2003). "The Bcl-2 family: roles in cell survival and oncogenesis." Oncogene **22**(53): 8590-607.

Crighton, D. and K. M. Ryan (2004). "Splicing DNA-damage responses to tumour cell death." Biochim Biophys Acta **1705**(1): 3-15.

Cybulski, C., B. Gorski, et al. (2004). "NBS1 is a prostate cancer susceptibility gene." Cancer Res **64**(4): 1215-9.

Dai, J., Y. Kitagawa, et al. (2004). "Vascular endothelial growth factor contributes to the prostate cancer-induced osteoblast differentiation mediated by bone morphogenetic protein." Cancer Res **64**(3): 994-9.

D'Cruz, C. M., E. J. Gunther, et al. (2001). "c-MYC induces mammary tumorigenesis by means of a preferred pathway involving spontaneous Kras2 mutations." Nat Med **7**(2): 235-9.

de Stanchina, E., E. Querido, et al. (2004). "PML is a direct p53 target that modulates p53 effector functions." Mol Cell **13**(4): 523-35.

Debatin, K. M. (2004). "Apoptosis pathways in cancer and cancer therapy." Cancer Immunol Immunother **53**(3): 153-9.

Debatin, K. M. and P. H. Krammer (2004). "Death receptors in chemotherapy and cancer." Oncogene **23**(16): 2950-66.

Degtyareva, N., D. Subramanian, et al. (2001). "Analysis of the binding of p53 to DNAs containing mismatched and bulged bases." J Biol Chem **276**(12): 8778-84.

Deiss, L. P., E. Feinstein, et al. (1995). "Identification of a novel serine/threonine kinase and a novel 15-kD protein as potential mediators of the gamma interferon-induced cell death." Genes Dev **9**(1): 15-30.

Di Cristofano, A., M. De Acetis, et al. (2001). "Pten and p27KIP1 cooperate in prostate cancer tumor suppression in the mouse." Nat Genet **27**(2): 222-4.

Dong, S. M., E. J. Lee, et al. (2005). "Progressive methylation during the serrated neoplasia pathway of the colorectum." Mod Pathol **18**(2): 170-8.

Dove, W. F., R. T. Cormier, et al. (1998). "The intestinal epithelium and its neoplasms: genetic, cellular and tissue interactions." Philos Trans R Soc Lond B Biol Sci **353**(1370): 915-23.

Drummond, J. T. and A. Bellacosa (2001). "Human DNA mismatch repair in vitro operates independently of methylation status at CpG sites." Nucleic Acids Res **29**(11): 2234-43.

Duckett, D. R., J. T. Drummond, et al. (1996). "Human MutSalpha recognizes damaged DNA base pairs containing O6-methylguanine, O4-methylthymine, or the cisplatin-d(GpG) adduct." Proc Natl Acad Sci U S A **93**(13): 6443-7.

Dunker, N. and K. Krieglstein (2002). "Tgfbeta2 -/- Tgfbeta3 -/- double knockout mice display severe midline fusion defects and early embryonic lethality." Anat Embryol (Berl) **206**(1-2): 73-83.

Eads, C. A., A. E. Nickel, et al. (2002). "Complete genetic suppression of polyp formation and reduction of CpG-island hypermethylation in Apc(Min/+) Dnmt1-hypomorphic Mice." Cancer Res **62**(5): 1296-9.

Escaffit, F., F. Boudreau, et al. (2005). "Differential expression of claudin-2 along the human intestine: Implication of GATA-4 in the maintenance of claudin-2 in differentiating cells." J Cell Physiol **203**(1): 15-26.

Esteller, M. (2005). "DNA methylation and cancer therapy: new developments and expectations." Curr Opin Oncol **17**(1): 55-60.

Esteller, M., E. Avizienyte, et al. (2000). "Epigenetic inactivation of LKB1 in primary tumors associated with the Peutz-Jeghers syndrome." Oncogene **19**(1): 164-8.

Esteller, M., P. G. Corn, et al. (2001). "A gene hypermethylation profile of human cancer." Cancer Res **61**(8): 3225-9.

Esteller, M. and J. G. Herman (2002). "Cancer as an epigenetic disease: DNA methylation and chromatin alterations in human tumours." J Pathol **196**(1): 1-7.

Esteller, M., M. Sanchez-Cespedes, et al. (1999). "Detection of aberrant promoter hypermethylation of tumor suppressor genes in serum DNA from non-small cell lung cancer patients." Cancer Res **59**(1): 67-70.

Fedier, A. and D. Fink (2004). "Mutations in DNA mismatch repair genes: implications for DNA damage signaling and drug sensitivity (review)." Int J Oncol **24**(4): 1039-47.

Felsher, D. W. and J. M. Bishop (1999). "Reversible tumorigenesis by MYC in hematopoietic lineages." Mol Cell **4**(2): 199-207.

Fernandes, N., Y. Sun, et al. (2005). "DNA damage-induced association of ATM with its target proteins requires a protein interaction domain in the N terminus of ATM." J Biol Chem **280**(15): 15158-64.

Fishel, R. (1999). "Signaling mismatch repair in cancer." Nat Med **5**(11): 1239-41.

Forcet, C., S. Etienne-Manneville, et al. (2005). "Functional analysis of Peutz-Jeghers mutations reveals that the LKB1 C-terminal region exerts a crucial role in regulating both the AMPK pathway and the cell polarity." Hum Mol Genet **14**(10): 1283-92.

Fridman, J. S. and S. W. Lowe (2003). "Control of apoptosis by p53." Oncogene **22**(56): 9030-40.

Friedberg, E. C., L. D. McDaniel, et al. (2004). "The role of endogenous and exogenous DNA damage and mutagenesis." Curr Opin Genet Dev **14**(1): 5-10.

Ghaffar, H., F. Sahin, et al. (2003). "LKB1 protein expression in the evolution of glandular neoplasia of the lung." Clin Cancer Res **9**(8): 2998-3003.

Ghebranious, N. and L. A. Donehower (1998). "Mouse models in tumor suppression." Oncogene **17**(25): 3385-400.

Giles, R. H., J. H. van Es, et al. (2003). "Caught up in a Wnt storm: Wnt signaling in cancer." Biochim Biophys Acta **1653**(1): 1-24.

Giuriato, S., K. Rabin, et al. (2004). "Conditional animal models: a strategy to define when oncogenes will be effective targets to treat cancer." Semin Cancer Biol **14**(1): 3-11.

Gong, J. G., A. Costanzo, et al. (1999). "The tyrosine kinase c-Abl regulates p73 in apoptotic response to cisplatin-induced DNA damage." Nature **399**(6738): 806-9.

Gossen, M. and H. Bujard (2002). "Studying gene function in eukaryotes by conditional gene inactivation." Annu Rev Genet **36**: 153-73.

Gozuacik, D. and A. Kimchi (2004). "Autophagy as a cell death and tumor suppressor mechanism." Oncogene **23**(16): 2891-906.

Guo, F., D. N. Gopaul, et al. (1997). "Structure of Cre recombinase complexed with DNA in a site-specific recombination synapse." Nature **389**(6646): 40-6.

Haramis, A. P., H. Begthel, et al. (2004). "De novo crypt formation and juvenile polyposis on BMP inhibition in mouse intestine." Science **303**(5664): 1684-6.

Hardie, D. G. (2005). "New roles for the LKB1-->AMPK pathway." Curr Opin Cell Biol **17**(2): 167-73.

Hawley, S. A., J. Boudeau, et al. (2003). "Complexes between the LKB1 tumor suppressor, STRAD alpha/beta and MO25 alpha/beta are upstream kinases in the AMP-activated protein kinase cascade." J Biol **2**(4): 28.

He, X. C., J. Zhang, et al. (2004). "BMP signaling inhibits intestinal stem cell self-renewal through suppression of Wnt-beta-catenin signaling." Nat Genet **36**(10): 1117-21.

Hedbacker, K., S. P. Hong, et al. (2004). "Pak1 protein kinase regulates activation and nuclear localization of Snf1-Gal83 protein kinase." Mol Cell Biol **24**(18): 8255-63.

Hehlgans, T. and K. Pfeffer (2005). "The intriguing biology of the tumour necrosis factor/tumour necrosis factor receptor superfamily: players, rules and the games." Immunology **115**(1): 1-20.

Hemminki, A., D. Markie, et al. (1998). "A serine/threonine kinase gene defective in Peutz-Jeghers syndrome." Nature **391**(6663): 184-7.

Hemminki, A., I. Tomlinson, et al. (1997). "Localization of a susceptibility locus for Peutz-Jeghers syndrome to 19p using comparative genomic hybridization and targeted linkage analysis." Nat Genet **15**(1): 87-90.

Hendrich, B. and A. Bird (1998). "Identification and characterization of a family of mammalian methyl-CpG binding proteins." Mol Cell Biol **18**(11): 6538-47.

Hendrich, B., U. Hardeland, et al. (1999). "The thymine glycosylase MBD4 can bind to the product of deamination at methylated CpG sites." Nature **401**(6750): 301-4.

Hendry, J. H., D. A. Broadbent, et al. (2000). "Effects of deficiency in p53 or bcl-2 on the sensitivity of clonogenic cells in the small intestine to low dose-rate irradiation." Int J Radiat Biol **76**(4): 559-65.

Hendry, J. H., W. B. Cai, et al. (1997). "p53 deficiency sensitizes clonogenic cells to irradiation in the large but not the small intestine." Radiat Res **148**(3): 254-9.

Hengartner, M. O. and H. R. Horvitz (1994). "Programmed cell death in Caenorhabditis elegans." Curr Opin Genet Dev **4**(4): 581-6.

Henis-Korenblit, S., N. L. Strumpf, et al. (2000). "A novel form of DAP5 protein accumulates in apoptotic cells as a result of caspase cleavage and internal ribosome entry site-mediated translation." Mol Cell Biol **20**(2): 496-506.

Herman, J. G., J. R. Graff, et al. (1996). "Methylation-specific PCR: a novel PCR assay for methylation status of CpG islands." Proc Natl Acad Sci U S A **93**(18): 9821-6.

Herzig, M. and G. Christofori (2002). "Recent advances in cancer research: mouse models of tumorigenesis." Biochim Biophys Acta **1602**(2): 97-113.

Hickman, M. J. and L. D. Samson (1999). "Role of DNA mismatch repair and p53 in signaling induction of apoptosis by alkylating agents." Proc Natl Acad Sci U S A **96**(19): 10764-9.

Hirao, A., A. Cheung, et al. (2002). "Chk2 is a tumor suppressor that regulates apoptosis in both an ataxia telangiectasia mutated (ATM)-dependent and an ATM-independent manner." Mol Cell Biol **22**(18): 6521-32.

Hong, S. P., F. C. Leiper, et al. (2003). "Activation of yeast Snf1 and mammalian AMP-activated protein kinase by upstream kinases." Proc Natl Acad Sci U S A **100**(15): 8839-43.

Horie, Y., A. Suzuki, et al. (2004). "Hepatocyte-specific Pten deficiency results in steatohepatitis and hepatocellular carcinomas." J Clin Invest **113**(12): 1774-83.

Hoyes, K. P., W. B. Cai, et al. (2000). "Effect of bcl-2 deficiency on the radiation response of clonogenic cells in small and large intestine, bone marrow and testis." Int J Radiat Biol **76**(11): 1435-42.

Hu, Y., J. E. Ippolito, et al. (2002). "Molecular characterization of a metastatic neuroendocrine cell cancer arising in the prostates of transgenic mice." J Biol Chem **277**(46): 44462-74.

Hurd, D. D. and K. J. Kemphues (2003). "PAR-1 is required for morphogenesis of the Caenorhabditis elegans vulva." Dev Biol **253**(1): 54-65.

Ijiri, K. and C. S. Potten (1987). "Further studies on the response of intestinal crypt cells of different hierarchical status to eighteen different cytotoxic agents." Br J Cancer **55**(2): 113-23.

Inbal, B., S. Bialik, et al. (2002). "DAP kinase and DRP-1 mediate membrane blebbing and the formation of autophagic vesicles during programmed cell death." J Cell Biol **157**(3): 455-68.

Inbal, B., O. Cohen, et al. (1997). "DAP kinase links the control of apoptosis to metastasis." Nature **390**(6656): 180-4.

Ireland, H., R. Kemp, et al. (2004). "Inducible Cre-mediated control of gene expression in the murine gastrointestinal tract: effect of loss of beta-catenin." Gastroenterology **126**(5): 1236-46.

Jang, C. W., C. H. Chen, et al. (2002). "TGF-beta induces apoptosis through Smad-mediated expression of DAP-kinase." Nat Cell Biol **4**(1): 51-8.

Jansen, M et al. (2005). "Mucosal prolapse in the pathogenesis of Peutz jegers polyposis." In press

Jenne, D. E., H. Reimann, et al. (1998). "Peutz-Jeghers syndrome is caused by mutations in a novel serine threonine kinase." Nat Genet **18**(1): 38-43.

Jenny, M., C. Uhl, et al. (2002). "Neurogenin3 is differentially required for endocrine cell fate specification in the intestinal and gastric epithelium." Embo J **21**(23): 6338-47.

Jensen, J., E. E. Pedersen, et al. (2000). "Control of endodermal endocrine development by Hes-1." Nat Genet **24**(1): 36-44.

Jimenez, A. I., P. Fernandez, et al. (2003). "Growth and molecular profile of lung cancer cells expressing ectopic LKB1: down-regulation of the phosphatidylinositol 3'-phosphate kinase/PTEN pathway." Cancer Res **63**(6): 1382-8.

Jin, Y., E. K. Blue, et al. (2001). "Identification of a new form of death-associated protein kinase that promotes cell survival." J Biol Chem **276**(43): 39667-78.

Jin, Y. and P. J. Gallagher (2003). "Antisense depletion of death-associated protein kinase promotes apoptosis." J Biol Chem **278**(51): 51587-93.

Jishage, K., J. Nezu, et al. (2002). "Role of Lkb1, the causative gene of Peutz-Jegher's syndrome, in embryogenesis and polyposis." Proc Natl Acad Sci U S A **99**(13): 8903-8.

Johnstone, R. W., A. A. Ruefli, et al. (2002). "Apoptosis: a link between cancer genetics and chemotherapy." Cell **108**(2): 153-64.

Kaestner, K. H., D. G. Silberg, et al. (1997). "The mesenchymal winged helix transcription factor Fkh6 is required for the control of gastrointestinal proliferation and differentiation." Genes Dev **11**(12): 1583-95.

Karuman, P., O. Gozani, et al. (2001). "The Peutz-Jegher gene product LKB1 is a mediator of p53-dependent cell death." Mol Cell **7**(6): 1307-19.

Katzenellenbogen, R. A., S. B. Baylin, et al. (1999). "Hypermethylation of the DAP-kinase CpG island is a common alteration in B-cell malignancies." Blood **93**(12): 4347-53.

Kerr, J. F., A. H. Wyllie, et al. (1972). "Apoptosis: a basic biological phenomenon with wide-ranging implications in tissue kinetics." Br J Cancer **26**(4): 239-57.

Kim, W. S., H. J. Son, et al. (2003). "Promoter methylation and down-regulation of DAPK is associated with gastric atrophy." Int J Mol Med **12**(6): 827-30.

Kimball, S. R. and L. S. Jefferson (2005). "Role of amino acids in the translational control of protein synthesis in mammals." Semin Cell Dev Biol **16**(1): 21-7.

Kimura, N., C. Tokunaga, et al. (2003). "A possible linkage between AMP-activated protein kinase (AMPK) and mammalian target of rapamycin (mTOR) signalling pathway." Genes Cells **8**(1): 65-79.

Kinzler, K. W. and B. Vogelstein (1996). "Lessons from hereditary colorectal cancer." Cell **87**(2): 159-70.

Kinzler, K. W. and B. Vogelstein (1998). "Landscaping the cancer terrain." Science **280**(5366): 1036-7.

Kissil, J. L., E. Feinstein, et al. (1997). "DAP-kinase loss of expression in various carcinoma and B-cell lymphoma cell lines: possible implications for role as tumor suppressor gene." Oncogene **15**(4): 403-7.

Kissil, J. L. and A. Kimchi (1998). "Death-associated proteins: from gene identification to the analysis of their apoptotic and tumour suppressive functions." Mol Med Today **4**(6): 268-74.

Kogel, D., J. H. Prehn, et al. (2001). "The DAP kinase family of pro-apoptotic proteins: novel players in the apoptotic game." Bioessays **23**(4): 352-8.

Komarova, E. A., R. V. Kondratov, et al. (2004). "Dual effect of p53 on radiation sensitivity in vivo: p53 promotes hematopoietic injury, but protects from gastro-intestinal syndrome in mice." Oncogene **23**(19): 3265-71.

Kondo, E., Z. Gu, et al. (2005). "The thymine DNA glycosylase MBD4 represses transcription and is associated with methylated p16(INK4a) and hMLH1 genes." Mol Cell Biol **25**(11): 4388-96.

Kuhn, R., F. Schwenk, et al. (1995). "Inducible gene targeting in mice." Science **269**(5229): 1427-9.

Kyriakis, J. M. (2003). "At the crossroads: AMP-activated kinase and the LKB1 tumor suppressor link cell proliferation to metabolic regulation." J Biol **2**(4): 26.

Ladner, R. D., F. J. Lynch, et al. (2000). "dUTP nucleotidohydrolase isoform expression in normal and neoplastic tissues: association with survival and response to 5-fluorouracil in colorectal cancer." Cancer Res **60**(13): 3493-503.

Lane, DP and Crawford, LV, 1979, "T antigen is bound to a host protein in SV40-transformed cells". Nature **278**: 261-263.

Laird, P. W., L. Jackson-Grusby, et al. (1995). "Suppression of intestinal neoplasia by DNA hypomethylation." Cell **81**(2): 197-205.

Laprise, P., P. Chailler, et al. (2002). "Phosphatidylinositol 3-kinase controls human intestinal epithelial cell differentiation by promoting adherens junction assembly and p38 MAPK activation." J Biol Chem **277**(10): 8226-34.

Le Meur, N., C. Martin, et al. (2004). "Complete germline deletion of the STK11 gene in a family with Peutz-Jeghers syndrome." Eur J Hum Genet **12**(5): 415-8.

Lee, S. and C. A. Schmitt (2003). "Chemotherapy response and resistance." Curr Opin Genet Dev **13**(1): 90-6.

Leedham, S. J., M. Brittan, et al. (2005). "Intestinal stem cells." J Cell Mol Med **9**(1): 11-24.

Lengauer, C., K. W. Kinzler, et al. (1998). "Genetic instabilities in human cancers." Nature **396**(6712): 643-9.

Leow, C. C., M. S. Romero, et al. (2004). "Hath1, down-regulated in colon adenocarcinomas, inhibits proliferation and tumorigenesis of colon cancer cells." Cancer Res **64**(17): 6050-7.

Levitt, N. C. and I. D. Hickson (2002). "Caretaker tumour suppressor genes that defend genome integrity." Trends Mol Med **8**(4): 179-86.

Levy-Strumpf, N. and A. Kimchi (1998). "Death associated proteins (DAPs): from gene identification to the analysis of their apoptotic and tumor suppressive functions." Oncogene **17**(25): 3331-40.

Li, E., T. H. Bestor, et al. (1992). "Targeted mutation of the DNA methyltransferase gene results in embryonic lethality." Cell **69**(6): 915-26.

Lijnen, H. R., B. Van Hoef, et al. (2004). "Neointima formation and thrombosis after vascular injury in transgenic mice overexpressing plasminogen activator inhibitor-1 (PAI-1)." J Thromb Haemost **2**(1): 16-22.

Lin, M. Y., I. A. Munshi, et al. (1992). "The defensin-related murine CRS1C gene: expression in Paneth cells and linkage to Defcr, the cryptdin locus." Genomics **14**(2): 363-8.

Lin-Marq, N., C. Borel, et al. (2005). "Peutz-Jeghers LKB1 mutants fail to activate GSK-3beta, preventing it from inhibiting Wnt signaling." Mol Genet Genomics **273**(2): 184-96.

Liu, W. K., C. Y. Chien, et al. (2003). "An LKB1-interacting protein negatively regulates TNFalpha-induced NF-kappaB activation." J Biomed Sci **10**(2): 242-52.

Livak, K. J. and T. D. Schmittgen (2001). "Analysis of relative gene expression data using real-time quantitative PCR and the 2(-Delta Delta C(T)) Method." Methods **25**(4): 402-8.

Lizcano, J. M., O. Goransson, et al. (2004). "LKB1 is a master kinase that activates 13 kinases of the AMPK subfamily, including MARK/PAR-1." Embo J **23**(4): 833-43.

Llambi, F., F. C. Lourenco, et al. (2005). "The dependence receptor UNC5H2 mediates apoptosis through DAP-kinase." Embo J **24**(6): 1192-201.

Lowe, S. W. (1999). "Activation of p53 by oncogenes." Endocr Relat Cancer **6**(1): 45-8.

Lowe, S. W., E. M. Schmitt, et al. (1993). "p53 is required for radiation-induced apoptosis in mouse thymocytes." Nature **362**(6423): 847-9.

Luo, Y., F. T. Lin, et al. (2004). "ATM-mediated stabilization of hMutL DNA mismatch repair proteins augments p53 activation during DNA damage." Mol Cell Biol **24**(14): 6430-44.

Luo, Z., A. K. Saha, et al. (2005). "AMPK, the metabolic syndrome and cancer." Trends Pharmacol Sci **26**(2): 69-76.

Luukko, K., A. Ylikorkala, et al. (1999). "Expression of LKB1 and PTEN tumor suppressor genes during mouse embryonic development." Mech Dev **83**(1-2): 187-90.

Lynch, J. P. and D. G. Silberg (2002). "To differentiate or proliferate? The interaction between PI3K/PTEN and Cdx2." Gastroenterology **123**(4): 1395-7.

Macleod, K. F., N. Sherry, et al. (1995). "p53-dependent and independent expression of p21 during cell growth, differentiation, and DNA damage." Genes Dev **9**(8): 935-44.

MacPhee, M., K. P. Chepenik, et al. (1995). "The secretory phospholipase A2 gene is a candidate for the Mom1 locus, a major modifier of ApcMin-induced intestinal neoplasia." Cell **81**(6): 957-66.

Mahmoud, N. N., A. J. Dannenberg, et al. (1998). "Aspirin prevents tumors in a murine model of familial adenomatous polyposis." Surgery **124**(2): 225-31.

Mak, B. C. and R. S. Yeung (2004). "The tuberous sclerosis complex genes in tumor development." Cancer Invest **22**(4): 588-603.

Makin, G. and J. A. Hickman (2000). "Apoptosis and cancer chemotherapy." Cell Tissue Res **301**(1): 143-52.

Marignani, P. A. (2005). "LKB1, the multitasking tumour suppressor kinase." J Clin Pathol **58**(1): 15-9.

Marignani, P. A., F. Kanai, et al. (2001). "LKB1 associates with Brg1 and is necessary for Brg1-induced growth arrest." J Biol Chem **276**(35): 32415-8.

Martin, S. G. and D. St Johnston (2003). "A role for Drosophila LKB1 in anterior-posterior axis formation and epithelial polarity." Nature **421**(6921): 379-84.

Martoriati, A., G. Doumont, et al. (2005). "dapk1, encoding an activator of a p19ARF-p53-mediated apoptotic checkpoint, is a transcription target of p53." Oncogene **24**(8): 1461-6.

McBurney, M. W. (1999). "Gene silencing in the development of cancer." Exp Cell Res **248**(1): 25-9.

McDonnell, T. J., N. Deane, et al. (1989). "bcl-2-immunoglobulin transgenic mice demonstrate extended B cell survival and follicular lymphoproliferation." Cell **57**(1): 79-88.

McShane, L. M., M. D. Radmacher, et al. (2002). "Methods for assessing reproducibility of clustering patterns observed in analyses of microarray data." Bioinformatics **18**(11): 1462-9.

Meehan, R. R., J. D. Lewis, et al. (1989). "Identification of a mammalian protein that binds specifically to DNA containing methylated CpGs." Cell **58**(3): 499-507.

Meniel, V., T. Hay, et al. (2005). "Mutations in Apc and p53 synergize to promote mammary neoplasia." Cancer Res **65**(2): 410-6.

Merritt, A. J., T. D. Allen, et al. (1997). "Apoptosis in small intestinal epithelial from p53-null mice: evidence for a delayed, p53-independent G2/M-associated cell death after gamma-irradiation." Oncogene **14**(23): 2759-66.

Meyers, M., A. Hwang, et al. (2004). "Role of DNA mismatch repair in apoptotic responses to therapeutic agents." Environ Mol Mutagen **44**(4): 249-64.

Meyers, M., M. W. Wagner, et al. (2005). "DNA mismatch repair-dependent response to fluoropyrimidine-generated damage." J Biol Chem **280**(7): 5516-26.

Mihara, M., S. Erster, et al. (2003). "p53 has a direct apoptogenic role at the mitochondria." Mol Cell **11**(3): 577-90.

Milano, J., J. McKay, et al. (2004). "Modulation of notch processing by gamma-secretase inhibitors causes intestinal goblet cell metaplasia and induction of genes known to specify gut secretory lineage differentiation." Toxicol Sci **82**(1): 341-58.

Millar, C. B., J. Guy, et al. (2002). "Enhanced CpG mutability and tumorigenesis in MBD4-deficient mice." Science **297**(5580): 403-5.

Mills, J. C., N. L. Stone, et al. (1998). "Apoptotic membrane blebbing is regulated by myosin light chain phosphorylation." J Cell Biol **140**(3): 627-36.

Miyaki, M., T. Iijima, et al. (2000). "Somatic mutations of LKB1 and beta-catenin genes in gastrointestinal polyps from patients with Peutz-Jeghers syndrome." Cancer Res **60**(22): 6311-3.

Miyazaki, T., M. Shen, et al. (2004). "Functional role of death-associated protein 3 (DAP3) in anoikis." J Biol Chem **279**(43): 44667-72.

Miyoshi, H., M. Nakau, et al. (2002). "Gastrointestinal hamartomatous polyposis in Lkb1 heterozygous knockout mice." Cancer Res **62**(8): 2261-6.

Modrich, P. (1994). "Mismatch repair, genetic stability, and cancer." Science **266**(5193): 1959-60.

Morin, C. I. and J. Huot (2004). "Recent advances in stress signaling in cancer." Cancer Res **64**(5): 1893-8.

Moseley, A. E., M. H. Cougnon, et al. (2004). "Attenuation of cardiac contractility in Na,K-ATPase alpha1 isoform-deficient hearts under reduced calcium conditions." J Mol Cell Cardiol **37**(5): 913-9.

Moser, A. R., C. Luongo, et al. (1995). "ApcMin: a mouse model for intestinal and mammary tumorigenesis." Eur J Cancer **31A**(7-8): 1061-4.

Moser, A. R., H. C. Pitot, et al. (1990). "A dominant mutation that predisposes to multiple intestinal neoplasia in the mouse." Science **247**(4940): 322-4.

Motoyama, N. and K. Naka (2004). "DNA damage tumor suppressor genes and genomic instability." Curr Opin Genet Dev **14**(1): 11-6.

Mueller, T., W. Voigt, et al. (2003). "Failure of activation of caspase-9 induces a higher threshold for apoptosis and cisplatin resistance in testicular cancer." Cancer Res **63**(2): 513-21.

Mukamel, Z. and A. Kimchi (2004). "Death-associated protein 3 localizes to the mitochondria and is involved in the process of mitochondrial fragmentation during cell death." J Biol Chem **279**(35): 36732-8.

Mummenbrauer, T., F. Janus, et al. (1996). "p53 Protein exhibits 3'-to-5' exonuclease activity." Cell **85**(7): 1089-99.

Nakanishi, C., T. Yamaguchi, et al. (2004). "Germline mutation of the LKB1/STK11 gene with loss of the normal allele in an aggressive breast cancer of Peutz-Jeghers syndrome." Oncology **67**(5-6): 476-9.

Nakatsuka, S., T. Takakuwa, et al. (2000). "Role of hypermethylation of DAP-kinase CpG island in the development of thyroid lymphoma." Lab Invest **80**(11): 1651-5.

Nakau, M., H. Miyoshi, et al. (2002). "Hepatocellular carcinoma caused by loss of heterozygosity in Lkb1 gene knockout mice." Cancer Res **62**(16): 4549-53.

Newlands, E. S., M. F. Stevens, et al. (1997). "Temozolomide: a review of its discovery, chemical properties, pre-clinical development and clinical trials." Cancer Treat Rev **23**(1): 35-61.

Ng, M. H., K. W. To, et al. (2001). "Frequent death-associated protein kinase promoter hypermethylation in multiple myeloma." Clin Cancer Res **7**(6): 1724-9.

Niiro, N. and M. Ikebe (2001). "Zipper-interacting protein kinase induces Ca(2+)-free smooth muscle contraction via myosin light chain phosphorylation." J Biol Chem **276**(31): 29567-74.

Nishisho, I., Y. Nakamura, et al. (1991). "Mutations of chromosome 5q21 genes in FAP and colorectal cancer patients." Science **253**(5020): 665-9.

Nittka, S., J. Gunther, et al. (2004). "The human tumor suppressor CEACAM1 modulates apoptosis and is implicated in early colorectal tumorigenesis." Oncogene **23**(58): 9306-13.

Ohanna, M., A. K. Sobering, et al. (2005). "Atrophy of S6K1(-/-) skeletal muscle cells reveals distinct mTOR effectors for cell cycle and size control." Nat Cell Biol **7**(3): 286-94.

Oniscu, A., N. Sphyris, et al. (2004). "p73alpha is a candidate effector in the p53 independent apoptosis pathway of cisplatin damaged primary murine colonocytes." J Clin Pathol **57**(5): 492-8.

Ossipova, O., N. Bardeesy, et al. (2003). "LKB1 (XEEK1) regulates Wnt signalling in vertebrate development." Nat Cell Biol **5**(10): 889-94.

Pao, W., D. S. Klimstra, et al. (2003). "Use of avian retroviral vectors to introduce transcriptional regulators into mammalian cells for analyses of tumor maintenance." Proc Natl Acad Sci U S A **100**(15): 8764-9.

Paris, F., Z. Fuks, et al. (2001). "Endothelial apoptosis as the primary lesion initiating intestinal radiation damage in mice." Science **293**(5528): 293-7.

Peek, R. M., Jr. (2004). "Prevention of colorectal cancer through the use of COX-2 selective inhibitors." Cancer Chemother Pharmacol **54 Suppl 1**: S50-6.

Pelengaris, S. and M. Khan (2001). "Oncogenic co-operation in beta-cell tumorigenesis." Endocr Relat Cancer **8**(4): 307-14.

Pelengaris, S., T. Littlewood, et al. (1999). "Reversible activation of c-Myc in skin: induction of a complex neoplastic phenotype by a single oncogenic lesion." Mol Cell **3**(5): 565-77.

Pelengaris, S., B. Rudolph, et al. (2000). "Action of Myc in vivo - proliferation and apoptosis." Curr Opin Genet Dev **10**(1): 100-5.

Pelled, D., T. Raveh, et al. (2002). "Death-associated protein (DAP) kinase plays a central role in ceramide-induced apoptosis in cultured hippocampal neurons." J Biol Chem **277**(3): 1957-61.

Peters, G. J., H. H. Backus, et al. (2002). "Induction of thymidylate synthase as a 5-fluorouracil resistance mechanism." Biochim Biophys Acta **1587**(2-3): 194-205.

Petronzelli, F., A. Riccio, et al. (2000a). "Investigation of the substrate spectrum of the human mismatch-specific DNA N-glycosylase MED1 (MBD4): fundamental role of the catalytic domain." J Cell Physiol **185**(3): 473-80.

Petronzelli, F., A. Riccio, et al. (2000b). "Biphasic kinetics of the human DNA repair protein MED1 (MBD4), a mismatch-specific DNA N-glycosylase." J Biol Chem **275**(42): 32422-9.

Pinto, D., A. Gregorieff, et al. (2003). "Canonical Wnt signals are essential for homeostasis of the intestinal epithelium." Genes Dev **17**(14): 1709-13.

Ramalho-Santos, M., D. A. Melton, et al. (2000). "Hedgehog signals regulate multiple aspects of gastrointestinal development." Development **127**(12): 2763-72.

Ranger, A. M., J. Zha, et al. (2003). "Bad-deficient mice develop diffuse large B cell lymphoma." Proc Natl Acad Sci U S A **100**(16): 9324-9.

Raveh, T., H. Berissi, et al. (2000). "A functional genetic screen identifies regions at the C-terminal tail and death-domain of death-associated protein kinase that are critical for its proapoptotic activity." Proc Natl Acad Sci U S A **97**(4): 1572-7.

Raveh, T., G. Droguett, et al. (2001). "DAP kinase activates a p19ARF/p53-mediated apoptotic checkpoint to suppress oncogenic transformation." Nat Cell Biol **3**(1): 1-7.

Raveh, T. and A. Kimchi (2001). "DAP kinase-a proapoptotic gene that functions as a tumor suppressor." Exp Cell Res **264**(1): 185-92.

Reichmann, A., P. Martin, et al. (1981). "Chromosomal banding patterns in human large bowel cancer." Int J Cancer **28**(4): 431-40.

Reitmair, A. H., J. C. Cai, et al. (1996). "MSH2 deficiency contributes to accelerated APC-mediated intestinal tumorigenesis." Cancer Res **56**(13): 2922-6.

Reya, T. and H. Clevers (2005). "Wnt signalling in stem cells and cancer." Nature **434**(7035): 843-50.

Riccio, A., L. A. Aaltonen, et al. (1999). "The DNA repair gene MBD4 (MED1) is mutated in human carcinomas with microsatellite instability." Nat Genet **23**(3): 266-8.

Rossi, D. J., A. Ylikorkala, et al. (2002). "Induction of cyclooxygenase-2 in a mouse model of Peutz-Jeghers polyposis." Proc Natl Acad Sci U S A **99**(19): 12327-32.

Rowan, A., M. Churchman, et al. (2000). "In situ analysis of LKB1/STK11 mRNA expression in human normal tissues and tumours." J Pathol **192**(2): 203-6.

Saadoun, S., M. C. Papadopoulos, et al. (2005). "Impairment of angiogenesis and cell migration by targeted aquaporin-1 gene disruption." Nature **434**(7034): 786-92.

Sakamoto, K., O. Goransson, et al. (2004). "Activity of LKB1 and AMPK-related kinases in skeletal muscle: effects of contraction, phenformin, and AICAR." Am J Physiol Endocrinol Metab **287**(2): E310-7.

Sakamoto, K., A. McCarthy, et al. (2005). "Deficiency of LKB1 in skeletal muscle prevents AMPK activation and glucose uptake during contraction." Embo J **24**(10): 1810-20.

Samuels-Lev, Y., D. J. O'Connor, et al. (2001). "ASPP proteins specifically stimulate the apoptotic function of p53." Mol Cell **8**(4): 781-94.

Sanchez-Cespedes, M., M. Esteller, et al. (2000). "Gene promoter hypermethylation in tumors and serum of head and neck cancer patients." Cancer Res **60**(4): 892-5.

Sanchez-Cespedes, M., P. Parrella, et al. (2002). "Inactivation of LKB1/STK11 is a common event in adenocarcinomas of the lung." Cancer Res **62**(13): 3659-62.
Sancho, E., E. Batlle, et al. (2003). "Live and let die in the intestinal epithelium." Curr Opin Cell Biol **15**(6): 763-70.

Sancho, E., E. Batlle, et al. (2004). "Signaling pathways in intestinal development and cancer." Annu Rev Cell Dev Biol **20**: 695-723.

Sansom, O. J., K. R. Reed, et al. (2004a). "Loss of Apc in vivo immediately perturbs Wnt signaling, differentiation, and migration." Genes Dev **18**(12): 1385-90.

Sansom, O. J., S. M. Bishop, et al. (2004b). "MBD4 deficiency does not increase mutation or accelerate tumorigenesis in mice lacking MMR." Oncogene **23**(33): 5693-6.

Sansom, O. J., S. M. Bishop, et al. (2003a). "Apoptosis and mutation in the murine small intestine: loss of Mlh1- and Pms2-dependent apoptosis leads to increased mutation in vivo." DNA Repair (Amst) **2**(9): 1029-39.

Sansom, O. J., J. Berger, et al. (2003b). "Deficiency of Mbd2 suppresses intestinal tumorigenesis." Nat Genet **34**(2): 145-7.

Sansom, O. J., J. Zabkiewicz, et al. (2003c). "MBD4 deficiency reduces the apoptotic response to DNA-damaging agents in the murine small intestine." Oncogene **22**(46): 7130-6.

Sansom, O. J. and A. R. Clarke (2002). "The ability to engage enterocyte apoptosis does not predict long-term crypt survival in p53 and Msh2 deficient mice." Oncogene **21**(38): 5934-9.

Sansom, O. J., L. A. Stark, et al. (2001a). "Suppression of intestinal and mammary neoplasia by lifetime administration of aspirin in Apc(Min/+) and Apc(Min/+), Msh2(-/-) mice." Cancer Res **61**(19): 7060-4.

Sansom, O. J., N. J. Toft, et al. (2001b). "Msh-2 suppresses in vivo mutation in a gene dose and lesion dependent manner." Oncogene **20**(27): 3580-4.

Sapkota, G. P., M. Deak, et al. (2002). "Ionizing radiation induces ataxia telangiectasia mutated kinase (ATM)-mediated phosphorylation of LKB1/STK11 at Thr-366." Biochem J **368**(Pt 2): 507-16.

Sapkota, G. P., A. Kieloch, et al. (2001). "Phosphorylation of the protein kinase mutated in Peutz-Jeghers cancer syndrome, LKB1/STK11, at Ser431 by p90(RSK) and cAMP-dependent protein kinase, but not its farnesylation at Cys(433), is essential for LKB1 to suppress cell vrowth." J Biol Chem **276**(22): 19469-82.

Satoh, A., M. Toyota, et al. (2002). "DNA methylation and histone deacetylation associated with silencing DAP kinase gene expression in colorectal and gastric cancers." Br J Cancer **86**(11): 1817-23.

Schmitt, C. A., C. T. Rosenthal, et al. (2000). "Genetic analysis of chemoresistance in primary murine lymphomas." Nat Med **6**(9): 1029-35.

Schori, H., E. Yoles, et al. (2002). "Immune-related mechanisms participating in resistance and susceptibility to glutamate toxicity." Eur J Neurosci **16**(4): 557-64.

Schroder, N. and A. Gossler (2002). "Expression of Notch pathway components in fetal and adult mouse small intestine." Gene Expr Patterns **2**(3-4): 247-50.

Screaton, R. A., S. Kiessling, et al. (2003). "Fas-associated death domain protein interacts with methyl-CpG binding domain protein 4: a potential link between genome surveillance and apoptosis." Proc Natl Acad Sci U S A **100**(9): 5211-6.

Searfoss, G. H., W. H. Jordan, et al. (2003). "Adipsin, a biomarker of gastrointestinal toxicity mediated by a functional gamma-secretase inhibitor." J Biol Chem **278**(46): 46107-16.

Sedgwick, S. G. and S. J. Smerdon (1999). "The ankyrin repeat: a diversity of interactions on a common structural framework." Trends Biochem Sci **24**(8): 311-6.

Shani, G., L. Marash, et al. (2004). "Death-associated protein kinase phosphorylates ZIP kinase, forming a unique kinase hierarchy to activate its cell death functions." Mol Cell Biol **24**(19): 8611-26.

Shaw, R. J., M. Kosmatka, et al. (2004a). "The tumor suppressor LKB1 kinase directly activates AMP-activated kinase and regulates apoptosis in response to energy stress." Proc Natl Acad Sci U S A **101**(10): 3329-35.

Shaw, R. J., N. Bardeesy, et al. (2004b). "The LKB1 tumor suppressor negatively regulates mTOR signaling." Cancer Cell **6**(1): 91-9.

Shen, Z., X. F. Wen, et al. (2002). "The tumor suppressor gene LKB1 is associated with prognosis in human breast carcinoma." Clin Cancer Res **8**(7): 2085-90.

Shibata, H., K. Toyama, et al. (1997). "Rapid colorectal adenoma formation initiated by conditional targeting of the Apc gene." Science **278**(5335): 120-3.

Shibue, T., K. Takeda, et al. (2003). "Integral role of Noxa in p53-mediated apoptotic response." Genes Dev **17**(18): 2233-8.

Shimodaira, H., A. Yoshioka-Yamashita, et al. (2003). "Interaction of mismatch repair protein PMS2 and the p53-related transcription factor p73 in apoptosis response to cisplatin." Proc Natl Acad Sci U S A **100**(5): 2420-5.

Shin, M. S., H. S. Kim, et al. (2002). "Alterations of Fas-pathway genes associated with nodal metastasis in non-small cell lung cancer." Oncogene **21**(26): 4129-36.

Shinji, H., J. Sakurada, et al. (1998). "Different effects of fibronectin on the phagocytosis of Staphylococcus aureus and coagulase-negative staphylococci by murine peritoneal macrophages." Microbiol Immunol **42**(12): 851-61.

Shohat, G., T. Spivak-Kroizman, et al. (2001). "The pro-apoptotic function of death-associated protein kinase is controlled by a unique inhibitory autophosphorylation-based mechanism." J Biol Chem **276**(50): 47460-7.

Simpson, D. J., R. N. Clayton, et al. (2002). "Preferential loss of Death Associated Protein kinase expression in invasive pituitary tumours is associated with either CpG island methylation or homozygous deletion." Oncogene **21**(8): 1217-24.

Slee, E. A., D. J. O'Connor, et al. (2004). "To die or not to die: how does p53 decide?" Oncogene **23**(16): 2809-18.

Smith, D. P., S. I. Rayter, et al. (2001). "LIP1, a cytoplasmic protein functionally linked to the Peutz-Jeghers syndrome kinase LKB1." Hum Mol Genet **10**(25): 2869-77.

Smith, D. P., J. Spicer, et al. (1999). "The mouse Peutz-Jeghers syndrome gene Lkb1 encodes a nuclear protein kinase." Hum Mol Genet **8**(8): 1479-85.

Soria, J. C., M. Rodriguez, et al. (2002). "Aberrant promoter methylation of multiple genes in bronchial brush samples from former cigarette smokers." Cancer Res **62**(2): 351-5.

Soriano, P. (1999). "Generalized lacZ expression with the ROSA26 Cre reporter strain." Nat Genet **21**(1): 70-1.

Spicer, J., S. Rayter, et al. (2003). "Regulation of the Wnt signalling component PAR1A by the Peutz-Jeghers syndrome kinase LKB1." Oncogene **22**(30): 4752-6.

Stappenbeck, T. S., J. C. Mills, et al. (2003). "Molecular features of adult mouse small intestinal epithelial progenitors." Proc Natl Acad Sci U S A **100**(3): 1004-9.

Stiegler, G. L. and L. C. Stillwell (1993). "Big Blue transgenic mouse lacI mutation analysis." Environ Mol Mutagen **22**(3): 127-9.

Strasser, A., A. W. Harris, et al. (1990). "Novel primitive lymphoid tumours induced in transgenic mice by cooperation between myc and bcl-2." Nature **348**(6299): 331-3.

Strathdee, G., M. J. MacKean, et al. (1999). "A role for methylation of the hMLH1 promoter in loss of hMLH1 expression and drug resistance in ovarian cancer." Oncogene **18**(14): 2335-41.

Su, L. K., K. W. Kinzler, et al. (1992). "Multiple intestinal neoplasia caused by a mutation in the murine homolog of the APC gene." Science **256**(5057): 668-70.

Sun, T. Q., B. Lu, et al. (2001). "PAR-1 is a Dishevelled-associated kinase and a positive regulator of Wnt signalling." Nat Cell Biol **3**(7): 628-36.

Sun, X. M., M. MacFarlane, et al. (1999). "Distinct caspase cascades are initiated in receptor-mediated and chemical-induced apoptosis." J Biol Chem **274**(8): 5053-60.

Takaku, K., M. Sonoshita, et al. (2000). "Suppression of intestinal polyposis in Apc(delta 716) knockout mice by an additional mutation in the cytosolic phospholipase A(2) gene." J Biol Chem **275**(44): 34013-6.

Tanaka, F., T. Fukuse, et al. (2000). "The history, mechanism and clinical use of oral 5-fluorouracil derivative chemotherapeutic agents." Curr Pharm Biotechnol **1**(2): 137-64.

Tang, X., F. R. Khuri, et al. (2000). "Hypermethylation of the death-associated protein (DAP) kinase promoter and aggressiveness in stage I non-small-cell lung cancer." J Natl Cancer Inst **92**(18): 1511-6.

Taylor, E. B., W. J. Ellingson, et al. (2005). "Long-chain acyl-CoA esters inhibit phosphorylation of AMP-activated protein kinase at threonine-172 by LKB1/STRAD/MO25." Am J Physiol Endocrinol Metab **288**(6): E1055-61.

Taylor, R. T., A. Lugering, et al. (2004). "Intestinal cryptopatch formation in mice requires lymphotoxin alpha and the lymphotoxin beta receptor." J Immunol **173**(12): 7183-9.

Tee, A. R. and J. Blenis (2005). "mTOR, translational control and human disease." Semin Cell Dev Biol **16**(1): 29-37.

Tiainen, M., A. Ylikorkala, et al. (1999). "Growth suppression by Lkb1 is mediated by a G(1) cell cycle arrest." Proc Natl Acad Sci U S A **96**(16): 9248-51.

Tlaskalova-Hogenova, H., M. A. Farre-Castany, et al. (1995). "The gut as a lymphoepithelial organ: the role of intestinal epithelial cells in mucosal immunity." Folia Microbiol (Praha) **40**(4): 385-91.

Toft, N. J., L. J. Curtis, et al. (2002). "Heterozygosity for p53 promotes microsatellite instability and tumorigenesis on a Msh2 deficient background." Oncogene **21**(41): 6299-306.

Toft, N. J., D. J. Winton, et al. (1999). "Msh2 status modulates both apoptosis and mutation frequency in the murine small intestine." Proc Natl Acad Sci U S A **96**(7): 3911-5.

Tomlinson, I. P. and R. S. Houlston (1997). "Peutz-Jeghers syndrome." J Med Genet **34**(12): 1007-11.

Totafurno, J., M. Bjerknes, et al. (1987). "The crypt cycle. Crypt and villus production in the adult intestinal epithelium." Biophys J **52**(2): 279-94.

Toyooka, S., K. O. Toyooka, et al. (2003). "Epigenetic down-regulation of death-associated protein kinase in lung cancers." Clin Cancer Res **9**(8): 3034-41.

Trojan, J., A. Brieger, et al. (2000). "5'-CpG island methylation of the LKB1/STK11 promoter and allelic loss at chromosome 19p13.3 in sporadic colorectal cancer." Gut **47**(2): 272-6.

Trotman, L. C., M. Niki, et al. (2003). "Pten dose dictates cancer progression in the prostate." PLoS Biol **1**(3): E59.

Tsujimoto, Y., L. R. Finger, et al. (1984). "Cloning of the chromosome breakpoint of neoplastic B cells with the t(14;18) chromosome translocation." Science **226**(4678): 1097-9.

Tusher, V. G., R. Tibshirani, et al. (2001). "Significance analysis of microarrays applied to the ionizing radiation response." Proc Natl Acad Sci U S A **98**(9): 5116-21.

Udd, L., P. Katajisto, et al. (2004). "Suppression of Peutz-Jeghers polyposis by inhibition of cyclooxygenase-2." Gastroenterology **127**(4): 1030-7.

Ulrich, C. M., J. Bigler, et al. (2002). "Thymidylate synthase promoter polymorphism, interaction with folate intake, and risk of colorectal adenomas." Cancer Res **62**(12): 3361-4.

van de Wetering, M., E. Sancho, et al. (2002). "The beta-catenin/TCF-4 complex imposes a crypt progenitor phenotype on colorectal cancer cells." Cell **111**(2): 241-50.

van Den Brink, G. R., P. de Santa Barbara, et al. (2001). "Development. Epithelial cell differentiation--a Mather of choice." Science **294**(5549): 2115-6.

van Es, J. H., M. E. van Gijn, et al. (2005a). "Notch/gamma-secretase inhibition turns proliferative cells in intestinal crypts and adenomas into goblet cells." Nature **435**(7044): 959-63.

van Es, J. H., P. Jay, et al. (2005b). "Wnt signalling induces maturation of Paneth cells in intestinal crypts." Nat Cell Biol **7**(4): 381-6.

Velcich, A., G. Corner, et al. (2005). "Quantitative rather than qualitative differences in gene expression predominate in intestinal cell maturation along distinct cell lineages." Exp Cell Res **304**(1): 28-39.

Velcich, A., W. Yang, et al. (2002). "Colorectal cancer in mice genetically deficient in the mucin Muc2." Science **295**(5560): 1726-9.

Velentza, A. V., A. M. Schumacher, et al. (2001). "A protein kinase associated with apoptosis and tumor suppression: structure, activity, and discovery of peptide substrates." J Biol Chem **276**(42): 38956-65.

Villunger, A., E. M. Michalak, et al. (2003). "p53- and drug-induced apoptotic responses mediated by BH3-only proteins puma and noxa." Science **302**(5647): 1036-8.

Wade, P. A. (2001). "Methyl CpG binding proteins: coupling chromatin architecture to gene regulation." Oncogene **20**(24): 3166-73.

Wan, H., K. H. Kaestner, et al. (2004). "Foxa2 regulates alveolarization and goblet cell hyperplasia." Development **131**(4): 953-64.

Wang, W. J., J. C. Kuo, et al. (2002). "DAP-kinase induces apoptosis by suppressing integrin activity and disrupting matrix survival signals." J Cell Biol **159**(1): 169-79.

Wang, Z. J., F. Taylor, et al. (1998). "Genetic pathways of colorectal carcinogenesis rarely involve the PTEN and LKB1 genes outside the inherited hamartoma syndromes." Am J Pathol **153**(2): 363-6.

Watson, A. J. and D. M. Pritchard (2000). "Lessons from genetically engineered animal models. VII. Apoptosis in intestinal epithelium: lessons from transgenic and knockout mice." Am J Physiol Gastrointest Liver Physiol **278**(1): G1-5.

Watts, J. L., D. G. Morton, et al. (2000). "The C. elegans par-4 gene encodes a putative serine-threonine kinase required for establishing embryonic asymmetry." Development **127**(7): 1467-75.

Wei, C., C. I. Amos, et al. (2003). "Correlation of staining for LKB1 and COX-2 in hamartomatous polyps and carcinomas from patients with Peutz-Jeghers syndrome." J Histochem Cytochem **51**(12): 1665-72.

Wheeler, J. M., W. F. Bodmer, et al. (2000). "DNA mismatch repair genes and colorectal cancer." Gut **47**(1): 148-53.

Won, Y. S., H. J. Kwon, et al. (2002). "Identification of Staphylococcus xylosus isolated from C57BL/6J-Nos2(tm1Lau) mice with dermatitis." Microbiol Immunol **46**(9): 629-32.

Wong, G. T., D. Manfra, et al. (2004). "Chronic treatment with the gamma-secretase inhibitor LY-411,575 inhibits beta-amyloid peptide production and alters lymphopoiesis and intestinal cell differentiation." J Biol Chem **279**(13): 12876-82.

Wong, W. M., G. W. Stamp, et al. (2000). "Proliferative populations in intestinal metaplasia: evidence of deregulation in Paneth and goblet cells, but not endocrine cells." J Pathol **190**(1): 107-13.

Woodford-Richens, K. L., S. Halford, et al. (2001). "CDX2 mutations do not account for juvenile polyposis or Peutz-Jeghers syndrome and occur infrequently in sporadic colorectal cancers." Br J Cancer **84**(10): 1314-6.

Wyllie, A. H., J. F. Kerr, et al. (1980). "Cell death: the significance of apoptosis." Int Rev Cytol **68**: 251-306.

Yamada, S., H. Kojima, et al. (2001). "Differentiation of immature enterocytes into enteroendocrine cells by Pdx1 overexpression." Am J Physiol Gastrointest Liver Physiol **281**(1): G229-36.

Yamamoto, M., T. Hioki, et al. (2002). "DAP kinase activity is critical for C(2)-ceramide-induced apoptosis in PC12 cells." Eur J Biochem **269**(1): 139-47.

Yamazaki, H., H. Iketaki, et al. (2002). "Activities of cytochrome p450 enzymes in liver and kidney microsomes from systemic carnitine deficiency mice with a gene mutation of carnitine/organic cation transporter." Drug Metab Pharmacokinet **17**(1): 47-53.

Yang, H. Y., Y. Y. Wen, et al. (2003). "14-3-3 sigma positively regulates p53 and suppresses tumor growth." Mol Cell Biol **23**(20): 7096-107.

Yang, Q., N. A. Bermingham, et al. (2001). "Requirement of Math1 for secretory cell lineage commitment in the mouse intestine." Science **294**(5549): 2155-8.

Yang, T. L., Y. R. Su, et al. (2004). "High-resolution 19p13.2-13.3 allelotyping of breast carcinomas demonstrates frequent loss of heterozygosity." Genes Chromosomes Cancer **41**(3): 250-6.

Yi, F., P. L. Brubaker, et al. (2005). "TCF-4 mediates cell type-specific regulation of proglucagon gene expression by beta-catenin and glycogen synthase kinase-3beta." J Biol Chem **280**(2): 1457-64.

Ylikorkala, A., E. Avizienyte, et al. (1999). "Mutations and impaired function of LKB1 in familial and non-familial Peutz-Jeghers syndrome and a sporadic testicular cancer." Hum Mol Genet **8**(1): 45-51.

Yonish-Rouach, E., D. Resnitzky, et al. (1991). "Wild-type p53 induces apoptosis of myeloid leukaemic cells that is inhibited by interleukin-6." Nature **352**(6333): 345-7.

Yoo, L. I., D. C. Chung, et al. (2002). "LKB1--a master tumour suppressor of the small intestine and beyond." Nat Rev Cancer **2**(7): 529-35.

Yukawa, K., K. Hoshino, et al. (2005). "Deletion of the kinase domain from death-associated protein kinase attenuates p53 expression in chronic obstructive uropathy." Int J Mol Med **16**(3): 389-93.

Zeng, M., L. Narayanan, et al. (2000). "Ionizing radiation-induced apoptosis via separate Pms2- and p53-dependent pathways." Cancer Res **60**(17): 4889-93.

Zhou, G., R. Myers, et al. (2001). "Role of AMP-activated protein kinase in mechanism of metformin action." J Clin Invest **108**(8): 1167-74.

Oncogene (2003) 22, 7130–7136

www.nature.com/onc

MBD4 deficiency reduces the apoptotic response to DNA-damaging agents in the murine small intestine

Owen James Sansom[1], Joanna Zabkiewicz[1], Stefan Mark Bishop[1], Jackie Guy[2], Adrian Bird[2] and Alan Richard Clarke*,[1]

[1]*Cardiff School of Biosciences, Cardiff University, PO Box 911, Cardiff CF10 3US, UK;* [2]*Wellcome Trust Centre for Cell Biology, Kings Buildings, Edinburgh University, Edinburgh EH9 3JR, UK*

MBD4 was originally identified through its methyl binding domain, but has more recently been characterized as a thymine DNA glycosylase that interacts with the mismatch repair (MMR) protein MLH1. *In vivo*, MBD4 functions to reduce the mutability of methyl-CpG sites in the genome and mice deticient in MBD4 show increased intestinal tumorigenesis on an $Apc^{Min/+}$ background. As MLH1 and other MMR proteins have been functionally linked to apoptosis, we asked whether MBD4 also plays a role in mediating the apoptotic response within the murine small intestine. Mice deficient for MBD4 showed significantly reduced apoptotic responses 6 h following treatment with a range of cytotoxic agents including γ-irradiation, cisplatin, temozolomide and 5-fluorouracil (5-FU). This leads to increased clonogenic survival *in vivo* in $Mbd4^{-/-}$ mice following exposure to either 5-FU or cisplatin. We next analysed the apoptotic response to 5-FU and temozolomide in doubly mutant $Mbd4^{-/-}$, $Mlh1^{-/-}$ mice but observed no additive decrease. The results imply that MBD4 and MLH1 lie in the same pathway and therefore that MMR-dependent apoptosis is mediated through MBD4. MBD4 deficiency also reduced the normal apoptotic response to γ-irradiation, which we show is independent of *Mlh1* status (at least in the murine small intestine), so suggesting that the reliance upon MBD4 may extend beyond MMR-mediated apoptosis. Our results establish a novel functional role for MBD4 in the cellular response to DNA damage and may have implications for its role in suppressing neoplasia.
Oncogene (2003) **22,** 7130–7136. doi:10.1038/sj.onc.1206850

Keywords: MBD4; mismatch repair; apoptosis; DNA methylation; p53

Introduction

The mammalian protein MBD4 contains a methyl-CpG binding domain (Hendrich and Bird, 1998) and can also enzymatically remove T or U from a mismatched CpG site *in vitro* (Hendrich *et al.*, 1999; Petronzelli *et al.*, 2000). Recently, we confirmed that MBD4 functions *in vivo* to minimize the mutability of 5-methycytosine (m^5C) by showing that the frequency of mutation at m^5CpG dinucleotides in a murine transgene is significantly increased in $Mbd4^{-/-}$ mice (Millar *et al.*, 2002). The *MBD4* gene has also been found to be mutated in a high frequency of human mismatch repair-deficient colorectal cancers, although this is rarely a biallelic event (Riccio *et al.*, 1999; Bader *et al.*, 1999, 2000). Furthermore, Millar *et al.* (2002) have shown that deficiency of MBD4 accelerates tumorigenesis on an Apc^{Min} background. Analysis of these tumours showed an increased frequency of CpG mutation at the *Apc* allele, but that this was not fully penetrant. This raised the possibility that MBD4 may do more than just initiate repair of TG mismatches.

In addition to its role as a thymine glycosylase, MBD4 has been shown to interact with the MMR protein MLH1 (Bellacosa *et al.*, 1999). To date, the functional basis of this interaction is poorly understood. Since canonical mammalian mismatch repair (MMR) is independent of methylation status and the mutation rate and spectra are very different between $Mbd4^{-/-}$ mice and MMR-deficient mice (Millar *et al.*, 2002), it appears that the interaction between MMR and MBD4 cannot be simply explained by a role for MBD4 in MMR (Bellacosa, 2001; Drummond and Bellacosa, 2001).

A second possibility is that the MBD4–MMR interaction is associated with the normal damage response. The MMR proteins have been shown to be essential for the normal response to a wide spectrum of agents. These include oxidative damage, ionizing radiation (at least in primary fibroblasts), cisplatin, 6-TG, UV and 5-FU damage (Buermeyer *et al.*, 1999). Indeed the MMR proteins have been shown to bind directly to O6 methylguanine (O6meG) lesions (which are thought to mimic a mismatch as the O6meG pairs with a T) and signal apoptosis either directly or through cycles of futile repair (Karran and Bignami, 1992; Fishel, 1999).

We have previously shown that MMR-deficient mice have a compromised apoptotic response to a range of DNA-damaging agents *in vivo* including the alkylating agents temozolomide, NMNU and MNNG, cisplatin and nitrogen mustard (Toft *et al.*, 1999; Sansom *et al.*, 2001; Sansom and Clarke, 2002). Here we ask whether

*Correspondence: AR Clarke; E-mail: clarkear@cf.ac.uk
Received 4 April 2003; revised 30 May 2003; accepted 6 June 2003

MBD4 mediates MMR-dependent apoptosis in the murine small intestine, and furthermore whether MBD4 is a general mediator of the apoptotic response.

Materials and methods

Mice

Mbd4 and *Mlh1* mutant animals were derived from a colony segregating for Ola/129 and C57BL6J genomes, but which was had been backcrossed four generations onto the C57BL6J background and so were predominantly (93.75%) C57/BL6J. Mice were genotyped by PCR as previously described (Prolla *et al.*, 1998; Millar *et al.*, 2002), and in all experiments littermate controls were used. To rule out the possibility that differences in the apoptotic response were due to SV129-derived genes linked to the *Mbd4* locus, we determined if there was any difference in apoptotic response of purebred 129SV and C57Bl/6 mice 6 h following exposure to either cisplatin (mean apoptotic bodies per 50 half crypts $\pm$ s.d. values of 179 ± 28.5 and 131 ± 34.4, respectively) or temozolomide (112 ± 8.5 and 139 ± 32.4, respectively). For both agents, genetic background was not found to influence the apoptotic response compared to wild-type out-bred values (cisplatin: Mann–Whitney U-test, $P = 0.66$ for SV129 and $P = 0.19$ for C57B16; temozolomide: Mann–Whitney U-test, $P = 0.39$ for SV129 and $P = 1.0$ for C57B16). Furthermore, the levels of apoptosis seen for either cisplatin- or temozolomide-treated SV129 and C57B16 mice remained significantly higher than those for the out-bred *Mbd4* null mice ($P < 0.04$ for all combinations).

Reagents and administration

Mice, 8 to 12 weeks old, were given intraperitoneal (i.p.) cisplatin (10–20 mg/kg), temozolomide (100 mg/kg) and 5-FU (400 mg/kg × 2). The two injections of 5-FU were administered 6 h apart according to Pritchard *et al.* (1998). Cisplatin and 5-FU were obtained from David Bull Laboratories/Faulding Pharmaceuticals, while temozolomode was a gift from Malcolm Stevens. Mice were exposed to γ-irradiation using two different ^{137}Cs sources. These delivered γ-irradiation at 0.27 Gy/min or at 0. 423 Gy/min. Irrespective of the source used, animals were exposed such that they received a dose of either 5, 10 or 15 Gy.

Quantitation of apoptosis

At each indicated time point following injection, a minimum of three animals were killed and the small intestine removed, flushed with water and fixed overnight in methacam (four parts methanol, two parts chloroform, one part acetic acid). Histological sections were made and apoptosis scored as previously described (Toft *et al.*, 1999). A minimum of 50 half crypts were scored per animal. This method was used in preference to indirect assessments of apoptosis because the apoptotic response within the intestine has previously been well defined using this approach (Potten, 1990; Hendry *et al.*, 1997; Toft *et al.*, 1999). All data were counted in a double-blinded manner.

Microcolony assay of clonogenic survival

The microcolony assay was performed as previously described (Potten, 1990; Hendry *et al.*, 1997). Briefly, 72 h after injection with cytotoxic agents the murine small intestines were removed. The top third was then cut into small pieces and bound into a bundle with 3M surgical tape. These were fixed in 10% formalin and embedded. Histological cross-sections were made and the numbers of surviving crypts were then counted around the circumference of the intestines. Crypts were scored as viable if they contained more than five consecutive live cells. As all mice were harvested at the same time and comparison between genotypes are being made, there was no rationale for applying any correction factor (Ijiri and Potten, 1983). Doses of 15 and 20 mg/kg were used for cisplatin and 400 mg/kg × 2 5-FU according to Ijiri and Potten (1983) and Pritchard *et al.* (1998). All data were counted in a double-blinded manner.

BrdU immunohistochemistry

Mice were injected with 0.25 ml of bromodeoxyuridine (BrdU) (Amersham) 2 h prior to harvesting. The staining was done on paraffin-embedded, methacarn-fixed intestines. Briefly, after a quick wash in water, slides were shaken at 60°C for 10 min in 1 M HCl for antigen retrieval. They were washed in PBS and then blocked for 20 min in 1.5% H_2O_2. Slides were incubated in 1% BSA/PBS for 20 min and then incubated in BrdU conjugate (Roche) diluted to one part in 50. Slides were washed in PBS and then developed in DAB. All data were counted in a double-blinded manner.

Results and discussion

Reduced apoptosis in Mbd4*-deficient mice*

We analysed the influence of *Mbd4* status upon the apoptotic response of intestinal enterocytes following exposure to a range of different cytotoxic agents to fully characterize any reliance upon MBD4 function. For all these agents, we investigated the response 6 h following exposure, as this has previously been shown to report the maximal or near-maximal apoptotic response (e.g. Toft *et al.*, 1999; Sansom and Clarke, 2002). In the case of ionizing radiation, gene deficiency has been linked with a delayed apoptotic response, for example, in the absence of p53 (Toft *et al.*, 1999). Therefore, for this agent we also investigated the levels of apoptosis at 72 h. Mice null for *Mbd4* showed a markedly reduced apoptotic response following exposure to ionizing radiation at 6 h ($P = 0.001$), cisplatin ($P = 0.01$) and the alkylating agent temozolomide ($P = 0.01$) (Figure 1). With respect to the 72 h time point, we found no evidence for a delayed wave of apoptosis following ionizing radiation in the absence of MBD4.

These data therefore establish a role for Mbd4 in mediating the maximal or near-maximal apoptotic response to a series of different cytotoxic agents. To further investigate the kinetics of these responses, we analysed an extended time course for two agents, temozolomide and cisplatin. For temozolomide, a reduction in the apoptotic response was observed at both 6 and 11 h following treatment in the absence of MBD4 ($P < 0.01$; Mann–Whitney U-test). For cisplatin, similar reductions were observed at 6 and 10 h ($P < 0.04$; Mann–Whitney U-test). This extended analysis therefore confirms not only a role for MBD4 in mediating the normal programme of cell death following exposure to a range of DNA-damaging agents, but also shows that significant MBD4-independent apoptosis does occur following exposure to these agents.

One possible interpretation of these data is that MBD4 deficiency leads directly to mutations in other proapoptotic genes, such that frequent somatic mutation impairs the ability to engage apoptosis. Although we cannot formally rule out

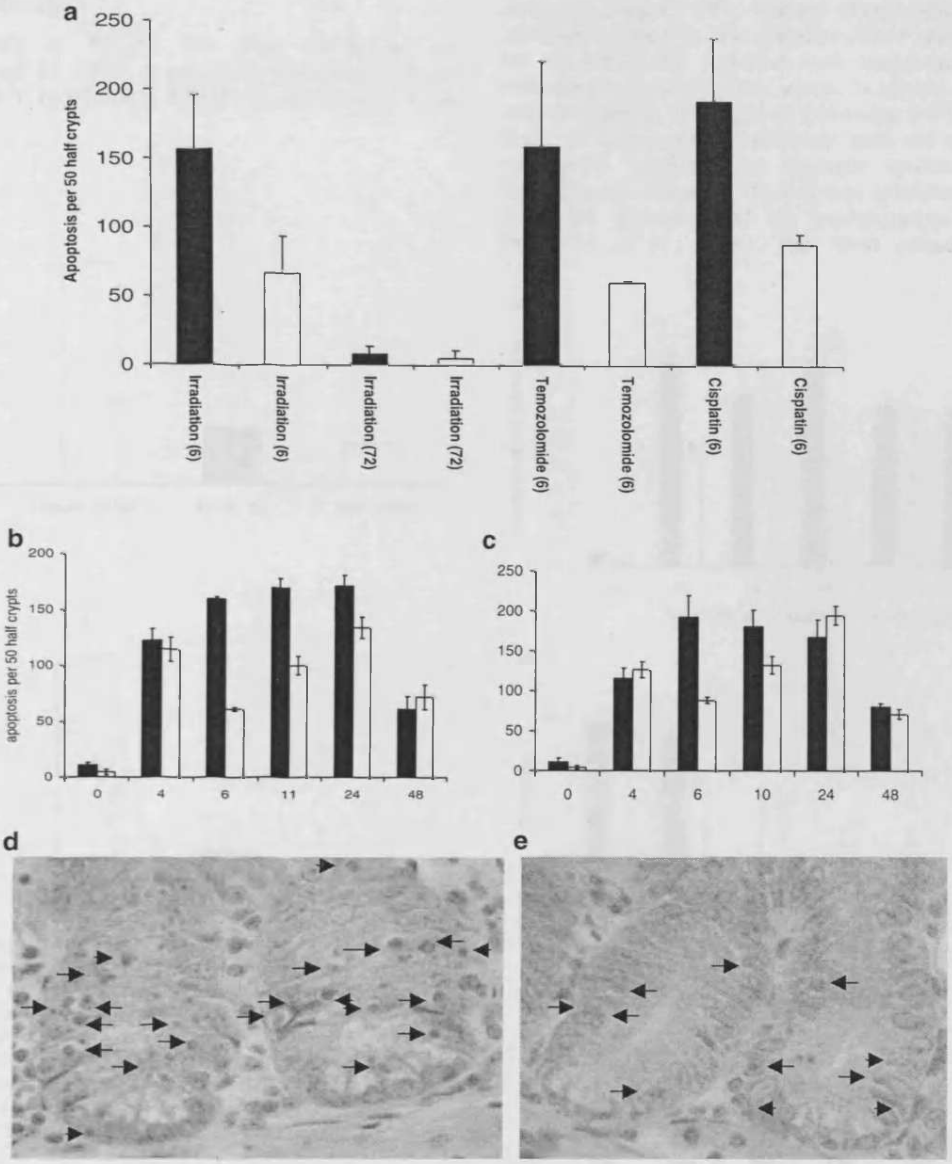

Figure 1 (**a**) Apoptosis scored per 50 half crypts following 5 Gy γ-irradiation, 10 mg/kg cisplatin and 100 mg/kg temozolomide treatment. Black bars, wild-type mice; open bars, *Mbd4*$^{-/-}$ mice. At least three mice were used for every time point and error bars represent s.d. *Mbd4*$^{-/-}$ mice had a significantly reduced apoptotic response at 6 h following all drugs used (γ-irradiation, $n=8$, $P=0.001$, temozolomide and cisplatin $n=5$, $P=0.001$). There was no gene dependency at 72 h ($P=0.68$, $n=3$). All statistical analyses were performed using the Mann–Whitney U-test. (**b**) Apoptosis scored per 50 half crypts over a 48 h period following 10 mg/kg temozolomide. Black bars, wild-type mice; open bars, *Mbd4*$^{-/-}$ mice. At least three mice were used for every time point and error bars represent s.e.m. (**c**) Apoptosis scored per 50 half crypts over a 48 h period following 100 mg/kg cisplatin treatment. Black bars, wild-type mice; open bars, *Mbd4*$^{-/-}$ mice. At least three mice were used for every time point and error bars represent s.e.m. (**d**) Representative photograph of apoptosis induced within wild-type intestinal crypts 6 h following exposure to cisplatin. Haematoxylin and eosin stained section, arrows indicate apoptotic bodies. (**e**) Representative photograph of apoptosis induced within MBD4 deficient intestinal crypts 6 h following exposure to cisplatin. Haematoxylin and eosin stained section, arrows indicate apoptotic bodies

this possibility, this hypothesis seems unlikely, as the reported elevation in mutation rate in the absence of MBD4 is almost certainly too low to generate sufficient numbers of mutant clones to modulate the apoptotic response (Millar *et al*., 2002). It seems more likely that MBD4 plays a direct role in mediating apoptosis, a hypothesis supported by the reported interaction between MBD4 and FADD (Screaton *et al*., 2003).

The observed reduction in the apoptotic response of *Mbd4* mutant mice implies that a proportion of cells fail to be appropriately deleted in the absence of MBD4. This in turn implies that clonogenic survival would be increased in *Mbd4* null mice. Figure 2 details the results of intestinal microcolony assays following exposure to DNA damage. MBD4 deficiency leads to no observable difference following exposure to 10 and 15 Gy γ-radiation (Figure 2a). However, increased clonogenic survival was observed following exposure to 15 mg/kg cisplatin (Figure 2b), indicating that *Mbd4* status can influence long-term *in vivo* survival, albeit in a damage-type-dependent manner.

MBD4 and 5-FU damage

Recently, deficiency of MLH1 has been implicated in resistance to damage by 5-FU, a cytotoxic ribosomal poison (Meyers *et al*., 2001). In addition, MBD4 has previously been shown to bind to 5-FU damage (Petronzelli *et al*., 2000). We therefore wished to test whether *Mbd4* status was important for the apoptotic response and long-term survival *in vivo* following exposure to this agent. It should be noted that the normal kinetics of apoptosis following 5-FU differ somewhat from the other agents used here, with the apoptotic response potentially mediated by multiple mechanisms of action, including inhibition of thymidylate synthase, which gives rise to DNA damage, and by incorporation into RNA (e.g. Pritchard *et al*., 1998). For these reasons the apoptotic

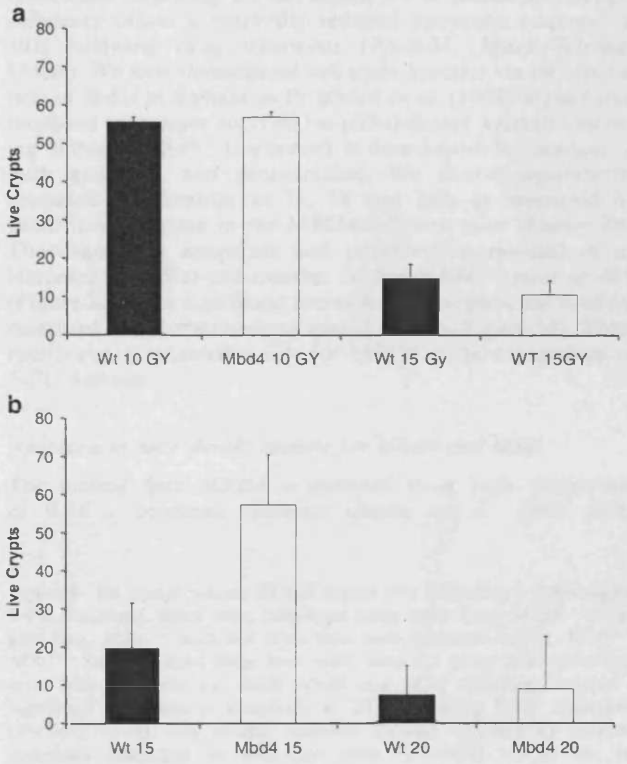

Figure 2 (**a**) Clonogenic survival scored following 10 and 15 Gy γ-irradiation. Black bars, wild-type mice; open bars, *Mbd4*$^{-/-}$ mice. At least three mice were used for every time point and error bars represent s.d. MBD4 deficiency did not affect crypt survival at either dose (10 Gy, $P=0.66$, $n=4$, 15 Gy, $P=0.38$). (**b**) Clonogenic survival following 15 and 20 mg/kg cisplatin treatment. Black bars, wild-type mice; open bars, *Mbd4*$^{-/-}$ mice. At least three mice were used for every time point and error bars represent s.d. MBD4 deficiency caused a significant increase in crypt survival following exposure to 15 mg/kg cisplatin ($P=0.03$, $n=6$). All statistical analyses were performed using the Mann–Whitney U-test

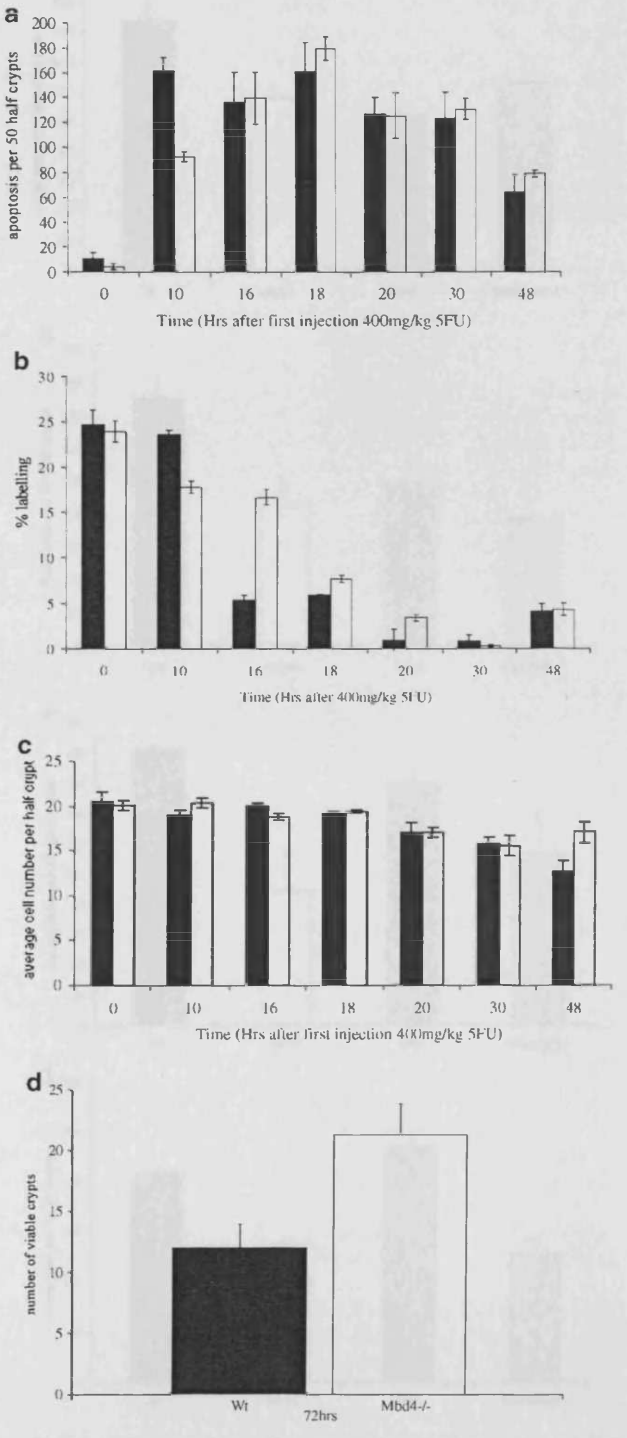

Figure 3 (**a**) Apoptosis per 50 half crypts following 2 × 400 mg/kg 5-FU treatment. Black bars, wild-type mice; open bars, *Mbd4*$^{-/-}$ mice. At least three mice were used for every time point and error bars represent s.d. MBD4 deficiency caused a significant reduction in apoptosis at 10 h following 5-FU treatment ($P=0.001$, $n=8$). (**b**) S phase incorporation per 50 half crypts following 2 × 400 mg/kg 5-FU treatment. Black bars, wild-type mice; open bars, *Mbd4*$^{-/-}$ mice. At least three mice were used for every time point and error bars represent s.d. MBD4 deficiency caused a significant increase in BrdU labelling at 16, 18 and 20 h following 5-FU treatment ($P<0.05$, $n=3$). (**c**) Average epithelial cell number per half crypt. Black bars, wild-type mice; open bars, *Mbd4*$^{-/-}$ mice. At least 3 mice were used for every time point and error bars represent s.d. MBD4 deficiency caused a significant increase in epithelial cell number 48 h following 5-FU treatment ($P<0.05$, $n=3$). (**d**) Clonogenic survival of intestinal crypts 72 h following 2 × 400 mg/kg 5-FU treatment. Black bars, wild-type mice; open bars, *Mbd4*$^{-/-}$ mice. At least three mice were used for every time point and error bars represent s.d. MBD4 deficiency caused a significant increase crypt survival following 5-FU treatment ($P=0.02$, $n=6$). All statistical analyses were performed using the Mann–Whitney U-test

response is potentially more complex than following other cytotoxic drugs and we therefore analysed the requirement for MBD4 over an extended time course, and also assessed changes in crypt cellularity and S-phase labelling.

Figure 3a displays the apoptotic response scored over a 48 h timecourse following 2 × 400 mg/kg 5-FU treatment. MBD4 deficiency causes a markedly reduced apoptotic response at 10 h following drug treatment ($P=0.01$; Mann–Whitney U-test). We next investigated cell cycle kinetics via incorporation of BrdU at S phase as Pritchard *et al.* (1998) argued that increased enterocyte survival (in p53-deficient animals following 400 mg/kg 5-FU treatment) is determined by changes in both apoptosis and proliferation. We found significantly increased proliferation at 16, 18 and 20 h as measured by BrdU incorporation in the MBD4-deficient mice (Figure 3b). The changes in apoptosis and proliferation resulted in an increased epithelial cell number in the *Mbd4*$^{-/-}$ mice at 48 h (Figure 3c) and a significant increase in clonogenic survival (as measured by the microcolony assay) at 72 h (Figure 3d). These results clearly establish a role for MBD4 in the recognition of 5-FU damage.

Apoptosis in mice doubly mutant for Mbd4 *and* Mlh1

The finding that *MBD4* is mutated in a high proportion of RER+ intestinal tumours (Bader *et al.*, 1999, 2000; Riccio *et al.*, 1999), together with the reported physical interaction between MLHl and MBD4 (Bellacosa *et al.*, 1999), prompted us to address the interdependence of MBD4 and MLH1 in signalling apoptosis. We therefore generated mice doubly mutant for *Mbd4* and *Mlh1*. If MBD4 and MLH1 operate in separate pathways, one would predict an additive decrease in the levels of apoptosis. Levels of apoptosis were

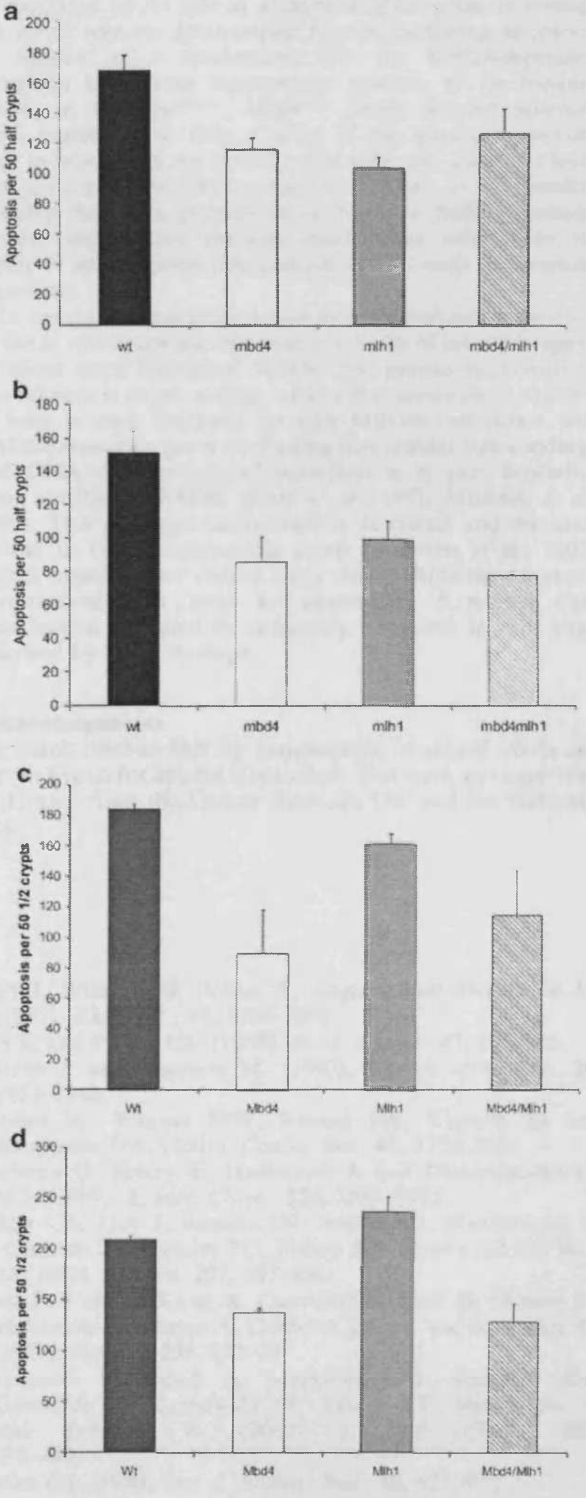

Figure 4 (**a**) Apoptosis per 50 half crypts 10 h following 2 × 400 mg/kg 5-FU treatment. Black bars, wild-type mice; open bars, *Mbd4*$^{-/-}$ mice; grey bars, *Mlh1*$^{-/-}$ mice and open bars with diagonal stripes, *Mbd4*$^{-/-}$ *Mlh1*$^{-/-}$ mice. At least three mice were used for every time point and error bars represent s.d. Both *Mbd4* and *Mlh1* deficiency caused a significant reduction in apoptosis at 10 h following 5-FU treatment ($P<0.01$, $n=6$). The double mutants showed significantly reduced apoptosis compared to wild-type mice ($P=0.04$, $n=3$), but no significant reduction compared to either *Mlh1*$^{-/-}$ ($P=0.38$, $n=3$) or *Mbd4*$^{-/-}$ mice ($P=0.65$, $n=3$). (**b**) Apoptosis per 50 half crypts 6 h following 100 mg/kg temozolomide treatment. At least three mice were used for every time point and error bars represent s.d. Black bars, wild-type mice; open bars, *Mbd4*$^{-/-}$ mice; grey bars, *Mlh1*$^{-/-}$ mice and open bars with diagonal stripes, *Mbd4*$^{-/-}$ *Mlh1*$^{-/-}$ mice, *Mbd4* and *Mlh1* deficiency caused a significant reduction in apoptosis at 6 h following cisplatin treatment ($P=0.01$, $n=5$). Double mutants showed reduced apoptosis compared to wild-type mice ($P=0.04$; Mann–Whitney U-test, $n=3$), but there was no significant reduction compared to either *Mlh1*$^{-/-}$ ($P=0.765$, $n=3$) or *Mbd4*$^{-/-}$ mice ($P=0.365$, $n=3$). All statistical analyses were performed using the Mann–Whitney U-test. (**c**) Apoptosis per 50 half crypts 6 h following 10 mg/kg cisplatin treatment. At least three mice were used for every time point and error bars represent s.d. Black bars, wild-type mice; open bars, *Mbd4*$^{-/-}$ mice; grey bars, *Mlh1*$^{-/-}$ mice and open bars with diagonal stripes, *Mbd4*$^{-/-}$ *Mhl1*$^{-/-}$ mice. *Mbd4* and *Mlh1* deficiency caused a significant reduction in apoptosis at 6 h following cisplatin treatment ($P=0.04$, $n=3$). *Mbd4*$^{-/-}$ mice showed significantly lower levels of apoptosis compared to *Mlh1*$^{-/-}$ mice ($P=0.04$, $n=3$). Double mutants showed significantly reduced apoptosis compared to wild-type and *Mlh1*$^{-/-}$ mice ($P=0.04$, $n=3$), but there was no significant reduction compared to *Mbd4*$^{-/-}$ mice ($P=0.45$, $n=3$). (**d**) Apoptosis per 50 half crypts 6 h following 5 Gy γ-irradiation. These experiments yielded higher overall levels of apoptosis as compared to Figure 1, as a different Cs^{137} source was used with a higher dose rate (see Materials and methods). At least three mice were used for every time point and error bars represent s.d. Black bars, wild-type mice; open bars, *Mbd4*$^{-/-}$ mice; grey bars, *Mlh1*$^{-/-}$ mice and open bars with diagonal stripes, *Mbd4*$^{-/-}$ *Mlh1*$^{-/-}$ mice, *Mbd4* deficiency caused a significant reduction in apoptosis at 6 h following γ-irradiation ($P=0.001$, $n=4$). *Mlh1*$^{-/-}$ mice showed no significant reduction compared to wild-types ($P=0.45$, $n=4$). Double mutants showed significantly reduced apoptosis compared to wild-type and *Mlh1*$^{-/-}$ mice ($P=0.01$, $n=4$), but there was no significant reduction compared to *Mbd4*$^{-/-}$ mice ($P=0.55$, $n=4$)

scored at time points selected to reflect maximal induction of the apoptotic response in singly mutated *Mbd4*$^{-/-}$ and *Mlh1*$^{-/-}$ mice and also in the double null (*Mbd4*$^{-/-}$, *Mlh1*$^{-/-}$) mice following exposure to 5-FU (Figure 4a), temozolomide (4B), cisplatin (4C) and γ-irradiation (4D). Following exposure to 5-FU and temozolomide both single mutants showed significantly reduced apoptosis, but this effect was not enhanced by simultaneous mutation of both genes (Figure 4a,b). The failure to see an additive effect argues that, for these agents, MBD4 operates within the same pathway as MLHl-dependent apoptosis.

Following cisplatin the reduction in apoptosis observed in the *Mlh1*$^{-/-}$ mice was very small (Figure 4c), similar to that previously observed in the *Msh2*$^{-/-}$ mice (Toft *et al*., 1999). MBD4 deficiency results in a significantly greater impairment of the apoptotic response than MLHl deficiency ($P = 0.04$; Mann–Whitney U-test), suggesting that MBD4 can also mediate MMR-independent apoptosis. This notion is further supported by analysis of the response to ionizing radiation that was shown to be dependent on MBD4 but not MLHl (Figure 4d), although we have not formally ruled out the possibility that other molecules in the MMR system may be involved in this response.

Significance of MBD4-mediated apoptosis

We and others have shown that the failure to engage apoptosis does not necessarily predict long-term intestinal enterocyte survival in *vivo*, so raising concerns about the precise relevance of failed apoptosis to carcinogenesis (Hendry *et al*., 1997; Sansom and Clarke, 2000, 2002). However, the finding that MBD4 deficiency leads to both diminished apoptosis and increased clonogenic survival after both cisplatin and 5-FU exposure clearly demonstrates an important role in deleting (presumably damaged) cells following DNA damage. We have previously shown that deficiency of MSH2 does not increase long-term survival following cisplatin damage (as assessed by the microcolony assay, Sansom *et al*., 2001), again indicating that loss of MBD4 can lead to a more substantial phenotype than MMR deficiency. The failure to see an MBD4-dependent increase in survival following γ-irradiation is not surprising given the recent findings of Paris *et al*. (2001), who showed endothelial cell survival is the prime determinant of long-term clonogenic survival in the intestine following γ-irradiation. Indeed, complete loss of the immediate apoptotic response in the epithelium of p53-deficient mice only weakly influences clonogenic survival following γ-irradiation (Hendry *et al*., 1997).

With respect to neoplasia, we recently demonstrated that MBD4 suppresses intestinal tumorigenesis in the *Apc*$^{Min/+}$ mouse (Millar *et al*., 2002). This suppression may be mediated by its role as a thymine glycosylase or through the novel role we demonstrate here in mediating apoptosis. In support of a mechanistic role for MBD4-dependent apoptosis in tumour suppression, analysis of the tumours arising in the *Apc*$^{Min/+}$, *Mbd4*$^{-/-}$ mouse showed enhanced CpG mutability in only a third of the tumours analysed, with in most cases the initially wild-type *Apc* allele still being lost through loss-of-heterozygosity (LOH). It is therefore possible that in a proportion of tumours MBD4 mediates tumour suppression through mechanisms other than the repair of spontaneous deamination events, such as apoptotic signalling.

In conclusion, we have shown that a significant proportion of the *in vivo* apoptotic response to a range of cytotoxic agents is reliant upon functional MBD4. The precise mechanism of this reliance is as yet unclear, although it seems likely that it is at least in part mediated through MBD4s interaction with FADD; especially given the finding that cellular stress-induced and DNA damage-induced apoptosis is in part dependent upon functional FADD (Herr *et al*., 1997; Micheau *et al*., 1999). This potential mechanism is described and discussed further in the accompanying paper (Screaton *et al*., 2003). Taken together, our results argue that MBD4 may suppress tumorigenesis not only by suppressing 5 methyl CpG deamination but also by mediating apoptosis in cells characterised by DNA damage.

Acknowledgements
We thank Nathan Hill for maintenance of animal stocks and Steven Frisch for helpful discussions. This work was supported by Grants from the Cancer Research UK and the Wellcome trust.

References

Bader S, Walker M and Harrison D. (2000). *Br. J. Cancer*, **83,** 1646–1649.
Bader S, Walker M, Heindrich B, Bird A, Bird C, Hooper M and Wyllie A. (1999). *Oncogene*, **18,** 8044–8047.
Bellacosa A. (2001). *J. Cell. Physiol.*, **187,** 137–144.
Bellacosa A, Cicchillitti L, Schepis F, Riccio A, Yeung AT, Matsumoto Y, Golemis EA, Genuardi M and Neri G. (1999). *Proc. Natl. Acad. Sci. USA*, **96,** 3969–3975.
Buermeyer AB, Deschennes SM, Baker SM and Liskay RM. (1999). *Annu. Rev. Genet.*, **33,** 533–564.
Drummond JT and Bellacosa A. (2001). *Nucleic Acid Res.*, **29,** 2234–2243.
Fishel R. (1999). *Nat. Med.*, **5,** 1239–1241.
Hendrich B and Bird A. (1998). *Mol. Cell. Biol.*, **18,** 6538–6547.
Hendrich B, Hardeland U, Ng HH, Jiricny J and Bird A. (1999). *Nature*, **401,** 301–304.
Hendry JH, Cai WB, Roberts SA and Potten CS. (1997). *Radiat. Res.*, **148,** 254–259.
Herr I, Wilhelm D, Bohler T, Angel P and Debatin K-M. (1997). *EMBO J.*, **16,** 6200–6208.
Ijiri K and Potten CS. (1983). *Br. J. Cancer*, **47,** 175–185.
Karran P and Bignami M. (1992). *Nucleic Acid Res.*, **20,** 2933–2940.
Meyers M, Wagner MW, Hwang HS, Kinsella TJ and Boothman DA. (2001). *Cancer Res.*, **61,** 5193–5201.
Micheau O, Solary E, Hammann A and Dimanche-Boitrel MT. (1999). *J. Biol. Chem.*, **274,** 7987–7992.
Millar CB, Guy J, Sansom OJ, Selfridge J, MacDougall E, Hendrich B, Keightley PD, Bishop SM, Clarke AR and Bird A. (2002). *Science*, **297,** 403–405.
Paris F, Fuks Z, Kang A, Capodieci P, Juan G, Ehleiter D, Haimovitz-Friedman A, Cordon-Cardo C and Kolesnick R. (2001). *Science*, **293,** 293–297.
Petronzelli F, Riccio A, Markham GD, Seeholzer SH, Genuardi M, Karbowski M, Yeung AT, Matsumoto Y and Bellacosa A. (2000). *J. Biol. Chem.*, **185,** 473–480.
Potten CS. (1990). *Int. J. Radiat. Biol.*, **58,** 925–973.

Pritchard DM, Potten CS and Hickman JA. (1998). *Cancer Res.*, **58,** 5453–5465.

Prolla TA, Baker SM, Harris AC, Tsao EL, Yao X, Bronner CE, Zheng BH, Gordon M, Reneker J, Amheim N, Shibata D, Bradley A and Liskay RM. (1998). *Nat. Genet.*, **18,** 276–279.

Riccio A, Aaltonen LA, Godwin AK, Loukola A, Percesepe A, Salovaara R, Masciullo V, Genuardi M, Paravatou-Petsotas M, Bassi DE, Ruggeri BA, Klein-Szanto AJP, Testa JR, Neri G and Bellacosa A. (1999). *Nat. Genet.*, **23,** 266–268.

Sansom OJ and Clarke AR. (2000). *Mutation Res.-Fundam. Mol. Mech. Mutagen.*, **452,** 149–162.

Sansom OJ and Clarke AR. (2002). *Oncogene*, **21,** 5934–5399.

Sansom OJ, Toft NJ, Winton DJ and Clarke AR. (2001). *Oncogene*, **20,** 3580–3584.

Screaton RA, Kiessling S, Sansom OJ, Millar CB, Maddison K, Bird A, Clarke AR, Frisch SM. (2003). *Proc. Natl. Acad. USA*, **100,** 5211–5216.

Toft NJ, Winton DJ, Kelly J, Howard LA, Dekker M, Riele HT, Arends MJ, Wyllie AH, Margison GP and Clarke AR. (1999). *Proc. Natl. Acad. USA*, **96,** 3911–3915.

Available online at www.sciencedirect.com

SCIENCE DIRECT

Biochimica et Biophysica Acta 1705 (2004) 17–25

BIOCHIMICA ET BIOPHYSICA ACTA
BBA

http://www.elsevier.com/locate/bba

Review

DNA damage-induced apoptosis: insights from the mouse

Joanna Zabkiewicz, Alan R. Clarke*

Cardiff School of Biosciences, Cardiff School of Biosciences. Biomedical Building, Museum Avenue, P.O. Box 911, Cardiff CF10 3US, UK

Available online 30 September 2004

Abstract

The availability of murine models with precisely defined genetic lesions has greatly increased our understanding of the genetic control of cell death, with functional dependence established for a wide range of genes including (amongst others) the p53 and Bcl-2 gene family members, the mismatch repair (MMR) genes and the methyl binding domain family member Mbd4. These studies raised the attractive hypotheses that tumour predisposition may be explained in terms of failed cell death, and also that tumour regression may be initiated through activation of an apoptotic programme. The studies that have addressed these notions have revealed complex consequences of a failed death programme, such that these simple hypotheses have not always been supported. Remarkably, however, some tissues show more predictable responses than others, most apparent in the contrast between the intestine and the haematopoietic system. This review will focus upon a discussion of these relationships, and will also consider the relevance of some of these findings to tumour predisposition and regression.

Keywords: p53; Mismatch repair; Apoptosis; Murine model; Tumorigenesis; Clonogenic survival; Mutation

Contents

* Corresponding author. Tel.: +44 2920 874 609; fax: +44 2920 874 116.
E-mail address: Clarkear@cf.ac.uk (A.R. Clarke).

0304-419X/$ - see front matter © 2004 Elsevier B.V. All rights reserved.
doi:10.1016/j.bbcan.2004.09.002

1. Introduction

The majority of neoplasias develop as a result of a complex accumulation of genetic alterations. The precise contribution played by each mutation remains unclear, although many associations have been made between gene mutation and disease stage, such as the sequential genetic events proposed to underlie colorectal cancer. A key challenge has therefore been to link individual genetic changes with the cellular mechanisms underlying disease. One such mechanism, frequently found perturbed at different stages of disease, is the ability to engage apoptosis. Indeed, this has led to the notion of a global 'gatekeeping' role for several tumour suppressor genes, which prevent neoplasia through the initiation of cell death. Our understanding of the relevance of apoptosis to disease initiation and progression has been tempered by both the limitations of ex vivo studies and the complexities of in vivo analysis. The advent of genetically defined murine models has alleviated some of these problems, and indeed the increasing sophistication of this approach is leading to remarkable insights into the relevance of apoptosis, which are discussed below. Many models have been utilised to address the role of candidate genes in inducing spontaneous apoptosis, whilst others have focused on elucidating the genetic control of apoptosis in response to DNA damage. As discussed, these approaches can relatively easily be used to demonstrate particular genetic dependencies. However, much of the challenge that remains lies in interpreting the physiological relevance of these observations, perhaps most clearly illustrated by analysis of the p53 tumour suppressor gene, the biology of which frequently defies the simple interpretation as a 'gatekeeper' functioning through the initiation of apoptosis. This review will summarise some of the information obtained from these models, and will specifically address the hypothesis that perturbation of the ability to engage apoptosis is a critical determinant of tumour predisposition.

2. Murine model systems

The first transgenic mouse models of human neoplasia were generated through pronuclear injection and relied upon overexpression of a given candidate sequence. This strategy provided the first real insights into genetic predisposition, and although it continues to provide invaluable data, it has been augmented by the availability of knockout strains, and then by the generation of models that allow both spatial and temporal control of both transgenes and endogenous genes. Some of the more recent technologies include the delivery of conditional transgene expression by the Tet on/off system [1], or by controlling transgene activity through fusion to a tamoxifen sensitive mutant of the Estradiol Receptor. The latter approach has proven particularly successful in studying conditional c-Myc, with extremely rapid transgene activation in tissues such as skin, pancreas and lymphocytes [2]. Conditional expression of endogenous alleles has also been achieved with the Cre–LoxP and Flp–Frt systems, and combinations of all of these systems are now being successfully used, for example in the analysis of co-operativity in tumourigenesis. These strategies, allied with the use of viral delivery systems and reporter genes such as LacZ and luciferase, are proving invaluable in monitoring tumour initiation, development, metastasis and regression [2].

3. p53

The tumour suppressor gene p53 has been described as 'a guardian of the genome' as a consequence of its multiple roles in DNA repair, senescence and apoptosis [3]. p53 appears to mediate death through a variety of mechanisms. These include down-regulation of the anti-apoptotic genes Bcl-2, Map4 and survivin, and up-regulation of pro-apoptotic genes Bax, IGF-BP3, DR5, Fas, Apaf1 and various other apoptosome components [4]. p53 can also up-regulate PTEN, a negative regulator of the PI3K/AKT survival pathway [5]; indeed, PTEN knockout mouse embryonic fibroblasts (MEFS) show reduced p53-dependent apoptosis [6].

P53 does not, however, exclusively mediate death through transcriptional control, as experiments using actinomycin D and transcriptionally inactive mutants show clear uncoupling of transcription factor function from the apoptotic response [4]. Similarly, there is evidence for the translocation of stress-induced p53 directly to the mitochondria to induce apoptosis via Bcl-2/Bcl-xl-mediated cytochrome *c* release, demonstrating multiple roles for p53 in mediating cell death [7].

Given the central nature of p53 to the apoptotic response, it is perhaps not surprising that perturbations of proteins known to regulate p53 also impact on the apoptotic programme. Thus, the 14-3-3 protein, which can stabilize p53 after DNA damage and which also antagonises Mdm2 function, can inhibit oncogene-induced tumourigenesis in vivo [8]. Similarly, mice null for the p53 activator Chk2 show defects in ionising radiation-induced apoptosis [9], and cells deficient for the upstream regulator PML (promyelocytic leukaemia gene) show decreased senescence and apoptosis in response to p53 activation [10]. Further details on p53-dependent apoptosis are given in the succeeding sections.

3.1. p53-deficient mice

To test the function of p53 in vivo, null mice have been generated by several different groups, all of which show essentially similar patterns of spontaneous tumour predisposition. The availability of these strains has allowed a clear demonstration of the in vivo requirement for p53 in mediating

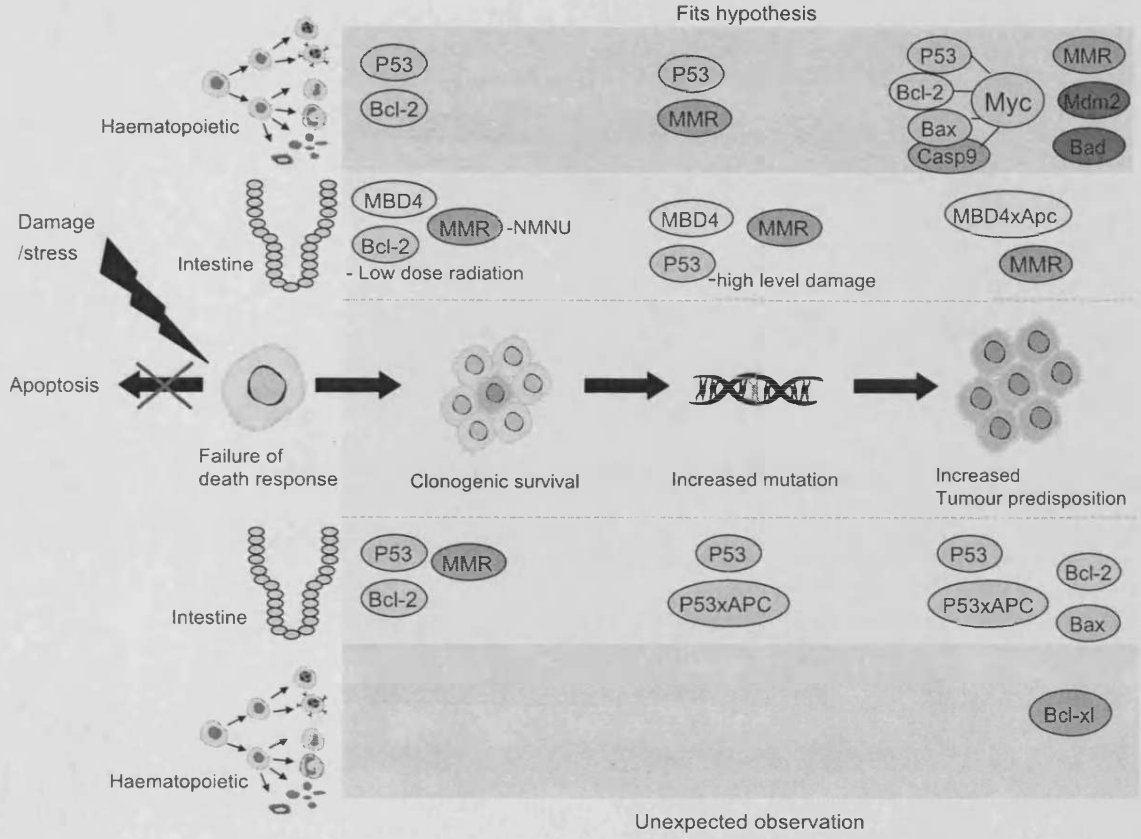

Fig. 1. Schematic diagram illustrating experimental data contributing to the hypothesis that defects in the apoptotic programme can underlie tumour predisposition. This hypothesis has a number of predictions if apoptosis is compromised: first, increased clonogenic survival; second, increased mutation burden; and finally, increased tumour predisposition. The diagram indicates those genes for which the data either supports or refutes this hypothesis, within some cases genes appearing multiple times to reflect opposing results. One notable phenomenon is the strong tissue specific differences, indicated here by the differences observed between the intestinal epithelium and cells of the haematopoietic system.

apoptosis following DNA damage (e.g., Refs. [11,12]). These observations formed the basis of a relatively simple hypothesis: namely that p53 deficiency leads to the inappropriate survival of cells that carry an increased DNA damage burden and are therefore predisposed to develop into neoplasia. This hypothesis has a number of readily testable endpoints: first, that the apoptotic response to DNA damaging agents is compromised; second, that this translates into differences in long-term survival; third, that there is an increase in the mutation burden within the surviving cells; and finally, that this leads to an increased predisposition to neoplasia (Fig. 1).

3.2. p53 and haematopoietic cell death

p53-deficient mice appear particularly prone to haematological malignancies, with lymphomagenesis the prominent tumour predisposition in null mice. Analysis of both thymocytes and pre-B cells [12,13] revealed a strong p53-dependent apoptotic response to ionising radiation. Critically, this was shown to lead to increased clonogenic survival and an increased mutation burden [13]. Notably, this increase in mutation burden directly reflected increased clonogenic survival, rather than a change in mutation rate. The important implication here is that any increase in the number of mutant bearing clones arises due to a defect in the death programme rather than an altered ability to repair DNA damage.

Within the haematopoietic lineages, the simple hypothesis of predisposition through failure to engage the death programme therefore appears to be of value. This conclusion is underlined by studies addressing the potential of p53-dependent apoptosis in neoplasia. Thus, p53 deficiency has been shown to enhance lymphomagenesis in Eμ-Myc transgenics through loss of the apoptotic response [14]; and similar enhanced lymphomagenesis has been reported following disruption of the apoptotic programme downstream of p53 through mutation of Bcl-2 or Caspase 9 [14]. Furthermore, perturbation of p53 function through deregulation of the p53 inhibitors Mdm2 and Mdm4 has been shown to be relevant to neoplasia, with overexpression of Mdm2 leading to lymphoma development [15].

3.3. p53 and intestinal cell death

p53 function has also been extensively examined within the intestine. In this tissue, p53 again mediates the

immediate apoptotic response to various forms of DNA damage, including ionising radiation, alkylation agents and 5FU [16–18]. In the absence of p53, there is almost no detectable apoptotic response to these agents immediately following exposure, which was assumed to reflect a complete abrogation of the response. However, closer analysis of the kinetics revealed this not to be the case, with a delayed p53-independent response identified which appears specific to the intestine [16,18]. There is growing evidence that this delayed response may be mediated by the p53 family members p63 and p73, overexpression of either of which induces apoptosis and up-regulates various p53 targets. Indeed, p73alpha was recently proposed as a candidate to mediate p53-independent death in colonocytes following exposure to cisplatin [19]. A direct assessment of the roles of both p73 and p63 is somewhat complicated as mice deficient for both genes exhibit severe developmental abnormalities. However, these mice have been used to show that combined loss of p63 and p73 blocks at least some forms of p53-dependent cell death [20]. The interdependency between the p53 family members is therefore rather complex with apparently differing roles in development and tumour suppression. However, it is clear that these genes have some overlapping functionality, with p63 and p73 suggested as being able to partially substitute for p53 deficiency and perhaps even to compensate for p53 loss during development [5].

Unlike in the haematopoietic system, it is not possible to directly address clonogenic survival using intestinal cultures, but an indication of survival can be gained from the microcolony assay, which essentially scores the ability of an entire crypt structure to survive insult. Using this approach, several different groups have shown either a weak or absent dependence upon p53 status following a range of insults (e.g., Refs. [21–24]), with perhaps the most marked dependence seen for cisplatin. Some of this failure to directly relate apoptosis with crypt survival may arise as a consequence of the assay system itself. This is clearly the case with ionising radiation, as survival of the endothelial cells rather than of the crypt epithelium itself appears to be the determinant of whole crypt survival [25].

The somewhat confused relationship between apoptosis and survival is further compounded if the endpoint of whole animal survival is considered. Surprisingly, p53 deficiency has been found to sensitise mice to higher doses of ionising radiation, causing lethal gastro-intestinal syndrome characterised by accelerated cell death and destruction of the villi [26]. This has been interpreted to occur as a consequence of failure of a protective p21-dependent cell cycle arrest. Notably, the opposite is observed in haematopoietic lineages, with p53-deficient mice showing reduced sensitivity to lethal haematopoietic syndrome.

Several assays have been developed to score mutation frequency within the intestine in vivo, either based around transgenic systems such as 'Big Blue' [27], or by scoring mutation frequency at the endogenous Dlb-1 locus [28]. Using either of these strategies, it has not been possible to show an increased mutation burden at spontaneous levels of damage [29], and following DNA damage differences have only been noted at extreme levels of damage [30]. We therefore see an apparent failure of the simple hypothesis within the intestine, which perhaps explains why p53 deficiency only weakly predisposes to increased intestinal neoplasia on the APC^{min} background, despite showing strong co-operativity with Apc deficiency in other tissues such as the pancreas [31] and the mammary gland [32].

3.4. p53 and tissue specificity

From the above, it is clear that p53 plays very different functional roles in intestinal and haematopoietic cells, irrespective of the fact that these are both cell types which may be described as being 'primed to die'. Indeed, there are even dramatic differences in the control of death between rather similar cell types, such as the small and large intestine, with the latter showing increased p53-dependence for clonogenic survival [21]. The mechanisms underlying these differences remain to be elucidated, but they are likely to reflect differences in p53 biology itself, for example in protein conformation, modification and promoter interactions which may all be specified by cell type or tissue [33,4]. These differences can certainly be shown to lead to different patterns of expression in p53 response genes, for example with good correlations observed between activation of the apoptotic targets of p53 and tissue sensitivity [34,35]. Tissue specificity must also be imposed through differences in interacting networks, as p53 biology cannot be considered in isolation. The most obvious candidates for such interactions are controlling and compensatory pathways, such as those mediated through the other p53 family members and the Mdm proteins, respectively.

It seems likely that tissue specificity therefore arises from both innate cellular predispositions as well as differences in microenvironment [5]. In the light of this, one might question the value of direct extrapolation of results from normal cells within genetically engineered mice to other tissues and to neoplasias. Indeed, given the marked differences between tissue types, one might logically expect clear differences between different tumour stages [36].

4. The relevance of damage response studies to neoplasia?

For p53, the relationship between initiation of cell death and predisposition to neoplasia is clearly not simple, and appears to be radically different in different cell types. Given this scenario, it is reasonable to ask how informative the murine studies of drug exposure have been to the prediction of both tumour predisposition and tumour responsiveness to chemotherapy.

Consistent with the observations in the null mice, p53 status does appear relevant to haematological tumour cell development and the efficacy of cancer therapy in vivo [37]. Furthermore, this reliance is suggested to be dependent upon functionality of the apoptotic response rather than cell cycle arrest, as p21 null mice rarely develop neoplasia of the same kind to p53 knockout animals [4].

Again, much of the tissue type dependency observed in normal tissues can readily be demonstrated within different tumour types, with Kemp and Sun [38] showing DNA damage to elicit p53-dependent apoptosis in T-cell lymphomas, intestinal adenomas and mammary tumours, but not in lung or liver adenomas.

In terms of drug resistance, p53 loss can be shown to confer de novo resistance to drug- and ionising radiation-induced damage in vitro and in vivo [39]. p53 null tumour cells have also been reported to be extremely resistant to 5FU-induced damage [40]. However, as may be inferred from the complexity discussed above, the true clinical situation is inevitably complex with p53 status not directly predicting chemoresistance [41].

5. Mismatch repair (MMR)

The MMR proteins function to repair DNA lesions which arise as a result of oxidative, alkylating or base cross-linking damage. Mammalian cells have six MMR genes: MSH2, MLH1, PMS1, PMS2, MSH3 and GTBP, inactivation of each has been linked to human neoplasia, most convincingly through the association with the hereditary cancer syndrome HNPCC. A role for the MMR system in eliciting apoptosis was first suggested by the observation of reduced sensitivity to cytotoxic DNA damaging agents in MMR defective tumours [42]. This again raised the hypothesis that MMR deficiency may predispose to neoplasia through failed apoptosis as well as failed DNA repair.

MMR null mice have been generated and shown to be susceptible to both lymphoma and intestinal tumourigenesis, although the predisposition to intestinal neoplasia is gene-dependent, with the lowest predisposition seen in mice singly mutant for Pms2 [43]. Analysis of the apoptotic response following exposure to DNA damage shows defective responses in Pms2, Msh2 and Mlh1 nulls, but with damage-specific and gene dose-dependent differences in the requirement for each of these MMR components [18,44]. For example, at high levels of alkylation damage, Msh2 is required for signalling the apoptotic response whereas Mlh1 and Pms2 appear redundant. In contrast, lower levels of damage appear dependent on Mlh1 and Pms2 [45]. These studies therefore show clear reliance upon functional MMR for the in vivo induction of apoptosis, but reveal significant complexity in this reliance.

The precise mechanism by which MMR mediates cell death remains unclear, with both futile cycles of repair and direct signalling proposed [46]. There is clear evidence for mediation through p53, for example with the MMR machinery proposed to activate p53 in response to radiation damage, and recently the Mlh1–Pms1 heterodimer linked to regulation of p53 [47]. Evidence of interdependency from the mouse is, however, somewhat contradictory, with very clear p53 dependency for the response to alkylation damage [18], but with cells from mice mutant for Pms2 and p53 reported only showing additive decreases in the apoptotic response to radiation, suggesting independent roles [48].

In terms of clonogenic survival, this has again been assessed in the intestine through the micro-colony assay. As with p53, this assay revealed a failure to directly predict survival from apoptosis data, with MMR-dependent differences only enhancing clonogenic survival after a single agent (NMNU), despite apoptotic dependency being observed for a range of agents (cisplatin, nitrogen mustard and NMNU). This failure may again reflect the presence of a delayed wave of MMR-independent apoptosis [24]. In support of this, Pms2 has been shown to stabilize p73 and relocalise it to the nuclear compartment. This interaction was found to increase upon treatment with cisplatin, indicating that this p73/Pms2 interaction may contribute to the delayed p53-independent apoptotic response seen in the intestine [49].

In terms of mutation and tumour predisposition, there is very clear data showing MMR deficiency to lead to increased mutability and neoplastic predisposition in both the intestine and haemopoietic lineages [50–54]. However, precisely which elements of these increases relate to the failed engagement of apoptosis as opposed to failed repair remains to be elucidated.

5.1. Parp-1

Parp-1 is a double-stranded break repair enzyme, and has been shown to mediate the immediate response to DNA damage, as well as being a principal target of caspase cleavage. Deficiency of Parp-1 may therefore have been predicted to have a similar effect to the other repair deficiencies discussed above. However, although exposure of Parp-1 null mice to ionising radiation leads to the delayed activation of p53, this appears not to influence the immediate apoptotic response but rather leads to enhanced crypt death, indicating a role in promoting intestinal cell survival [55]. Given the central hypothesis within this review, this argues against a role for Parp-1 as a 'tumour suppressor' by the mechanisms discussed above for p53 and the MMR proteins. In terms of its contribution to tumourigenesis some confusion exists, as Parp-1 has been shown to both increase [56] and decrease tumour latency via upstream phosphorylation of p53 [57,58].

5.2. Mbd4

Mbd4 is a thymine glycoslyase of the base excision repair system, capable of binding and signalling GT

mismatches associated with spontaneous ^{me}5C deamination events within the genome. As such, Mbd4 clearly possesses a DNA repair function; however, it is also known to strongly associate with components of the MMR system, which may also reflect a role in eliciting cell death. Analysis of Mbd4 null mice shows Mbd4 to mediate the apoptotic response in the small intestine. However, the range of damaging agents showing Mbd4-dependent death is wider than that predicted from any MMR interaction. This strongly implies that Mbd4 has dual functionality in its DNA repair and apoptosis activities, with the latter possibly explained through the recently recognised interaction with FADD [59]. Whatever the mechanism of Mbd4-mediated death, its significance is underlined by the observation of increased clonogenic survival in the intestine following exposure to both 5FU and cisplatin [60].

Mbd4 deficiency perturbs survival in the intestine, but does this translate into increased tumour predisposition? This question has been addressed by crossing onto the APC^{min} background, where Mbd4 deficiency leads to accelerated intestinal adenoma development [61]. This experiment shows Mbd4 to act as a tumour suppressor; however, this may simply reflect its DNA repair activities, as suggested by the observed shift towards point mutation at the remaining wild-type Apc allele. It seems likely that the potential contribution of Mbd4-dependent apoptosis to tumour suppression will only be clarified through dissecting the individual repair and death activities away from each other.

6. The Bcl-2 family

The Bcl-2 family of proteins comprise both anti-apoptotic and pro-apoptotic members, and it is thought that the ratio of these family members is critical to the cellular decision to live or die. Thus, Bcl-2, Bcl-xL and Bcl-w inhibit apoptosis and promote cellular growth [15], hence predicting their oncogenic role if overexpressed. Pro-apoptotic members of the family include Bax, Bak, Bok and the BH3 subfamily comprising Bik, Bad, Bid, Bim, Noxa and Puma.

The complexity of reliance upon individual Bcl-2 family members becomes apparent from an examination of the apoptotic responses within the intestine. In this tissue, spontaneous and induced apoptosis is independent of Bax status. However, Bcl-2 null animals showed elevated sensitivity within the stem cell compartment of the large intestine [62]. By contrast, apoptosis within the small intestine is seen to be regulated by the anti-apoptotic family member Bcl-w, with elevated levels of apoptosis following either 5FU or ionising radiation [63]. Such differential reliance upon the Bcl-2 family members may reflect the differential patterns of expression of each family member [64].

At least part of the association between Bcl-2 proteins and cell death may arise as a consequence of p53 status, as several members of the Bcl-2 family including Bax, Noxa and Bid are regulated by p53. Consistent with this, both Bax and Noxa null MEFs show resistance to oncogene-induced p53-dependent apoptosis [5,65]. Noxa null mice also show resistance to irradiation-induced apoptosis of the small intestine, reinforcing the role of Noxa in p53-mediated apoptosis [66]. Noxa has also been shown to be involved in oncogene-independent apoptosis mediated via p21.

In terms of clonogenic survival within the small intestine, Bcl-2 deficiency has been reported to reduce crypt survival following low dose-rate radiation, although this was reported only following a low dose-rate regimen [22]. At higher dose rates, no difference in clonogenic survival was noted in the small intestine, although interestingly reduced survival was seen in the bone marrow [67].

These associations within normal tissues again raise the relevance of these proteins to neoplasias, and here, as with p53, it is clear that results cannot simply be extrapolated from to neoplasias. For example, in contrast to the mouse model, Bax-deficient tumours show marked resistance to therapy, suggesting Bax function may change depending on genetic environment or following oncogenic stimulation [68]. Similarly, cell lines can be rendered chemosensitive in vivo by overexpressing Bcl-xL yet prove to be chemoresistant in vivo, a phenomenon which may indicate that tumour micro-environment is all critical in predicting response to chemotherapy [69]. Perhaps the clearest correlation between Bcl-2 family perturbation and drug resistance comes from analyses of the effects of Bcl-2 expression itself within a model of Myc-driven lymphomagenesis, where overexpression produces multi-drug resistance [70].

Despite these complexities, it is clear that perturbation of the Bcl-2 family can accelerate neoplasia, for example through Bcl-2 overexpression [64]. This demonstrates a general principal that inhibition of an apoptotic programme on its own or in the context of other mutations can strongly promote neoplasia. Thus, Bad knockout mice developed B cell lymphomas, and showed clear acceleration of lymphomagenesis following exposure to γ-irradiation [71]. Similarly, Bim deficiency accelerates neoplasia in the context of overexpression of c-Myc, and Bax null mice develop tumours in cooperation with other oncogenes such as E1A, Sv40, or Myc [64].

7. Intrinsic apoptotic signalling and death receptors

It is clear from the above that there is a series of molecules that can act as damage sensors and initiate an apoptotic response. However, there is also emerging data in support of cross talk between the damage sensing pathways and intrinsic apoptotic signalling.

Death receptor ligation and subsequent intrinsic apoptotic cascades are activated in response to a wide variety of stimuli

including stress, cytotoxic drugs, ionising radiation, and withdrawal of survival factors. However, the contribution of exogenous and endogenous apoptotic signalling to drug-induced cell death is still unclear. Certainly cisplatin, 5FU and other cytotoxic agents have been shown to invoke auto and paracrine signalling to tumour cell death receptors to stimulate apoptosis. Indeed, p53 has been shown to up-regulate CD95, FADD, Procaspase8 and the DISC complex proteins, and more recently the MBD4 protein has been shown to interact directly with FADD [59]. In vivo, $FADD^{-/-}$ and $Casp8^{-/-}$ MEFs are still drug-sensitive, although clearly independently of death receptor stimulation. In contrast, $Apaf1^{-/-}$ and $Casp9^{-/-}$ MEFs are sensitive to death receptor triggers but show resistance to cytotoxic drugs [41]. See Section 5 for more details on the death receptor pathway.

8. Apoptosis and spontaneous tumour regression: Ras and Myc

The above discussion has focussed upon genes that control the short-term apoptotic response to very high levels of DNA damage, partially in an attempt to address the relevance of gene function to clinical tumour responsiveness. The significance of these studies to tumour development is perhaps less clear, as spontaneous neoplasias usually arise in a much lower DNA-damage environment.

High quality data relating to spontaneous neoplasia has, however, been obtained for two genes known to be integral to the apoptotic response. The first of these is C-Myc, which mediates apoptosis by a range of mechanisms, including the Bax-mediated release of cytochrome *c*, and the activation of a wide range of pro-apoptotic molecular targets, such as Arf and FADD.

The in vivo consequences of overexpression of c-Myc were first shown through the development of early onset lymphomagenesis in transgenic mice [72]. Adaptation of the Eμ-Myc mouse transgene by combination with the Tet on/off system showed overexpression of c-Myc to lead to T cell lymphomas and acute myeloid leukaemias, but that subsequent inactivation of c-Myc led to 90% tumour regression via terminal differentiation and apoptosis [73,74].

Similar scenarios have been reported in other cell types, with conditional expression of c-Myc in keratinocytes leading to the rapid development of skin lesions, which regressed following tamoxifen withdrawal [75,74]. D'cruz et al. [76] have also shown similar full reversal of Myc-induced invasive mammary carcinomas. Parallel experiments in pancreatic β cells showed Myc expression to drive both apoptosis and proliferation, but only to result in neoplasia following co-expression of Bcl-xL, which inhibited apoptosis [74,77]. The precise role played by c-Myc-driven apoptosis in initiation and regression remains somewhat unclear, but is clearly context-dependent. In the skin model described above, both tumour growth and regression were not associated with markedly changed levels of apoptosis. However, the predominant scenario, as in the pancreatic model described above, is one of strong selection against Myc-driven death [74]. Indeed, consistent with this, cells with amplified Myc expression are sensitive to 5FU-induced apoptosis [78].

Somewhat similar data has been generated for mutant Ras alleles, with several different groups using conditional strategies to control mutant Ras gene expression. Thus, Chin et al. used the Tet system to drive expression of the mutant H-ras V12G allele which resulted in melanoma development within 2 months. Upon doxycycline withdrawal, tumours spontaneously regressed showing high levels of apoptosis, but rapidly reestablished if doxycycline was readministered [79]. Parallel results have been obtained from a model dependent upon p53-deficient fibroblasts transfected with a doxycycline regulable tet-o-K-Ras4b^{G12D} allele and subsequently infected with avian retrovirus carrying the rtTA component. In these circumstances, withdrawal of doxycycline resulted in reduced expression of the mutant K-ras allele and initiated regression of tumours in vivo [80].

These studies therefore show critical roles for at least two genes in controlling the death programme within neoplasias. Notably these phenomena are reported in the absence of exogenous DNA damage, although modified DNA damage responses can be observed. These studies therefore contrast with the bulk of those discussed here and raise a fundamental question about how we can interpret data derived from exposure to high levels of DNA damage. The potential relevance of such data to chemotherapy does appear clear. However, the interpretation for tumour predisposition at spontaneous levels of DNA damage remains much less obvious, and indeed our ability to test the significance of apoptosis in such circumstances remains limited.

9. Conclusions

The development of increasingly sophisticated genetic models is allowing a much better understanding of the molecular mechanisms that control cell death. This review has summarised a relatively small portion of that data relating to apoptosis elicited following DNA damage, yet it is clear that there is a rapidly increasing cohort of genes implicated in the control of DNA damage-induced death. It is increasingly obvious that we will soon be able to identify many of those genes whose loss or mis-expression is relevant to death. However, it is also becoming clear that this represents the 'easy' part of these studies, and that it is the interpretation of the significance of these relationships which is much more challenging.

This review began with a discussion of p53-dependent apoptosis, a gene for which there is perhaps the clearest data linking function to cell death. This association gave rise to the simple hypothesis that the ability to engage cell death at least partially explained tumour suppressor activity. However, the

data that has subsequently been generated has shown this hypothesis to be naïve, with failed predictions in some tissues, yet good support for the hypothesis from other tissues, such as in the haematopoietic system. The inevitable conclusion from these studies must be that a similar scenario will be replicated for other genes, with the ability to engage apoptosis in normal cells often failing to predict endpoints such as survival and tumour predisposition and regression. Such a conclusion should not be seen as surprising as all genes and indeed all cells must be considered within the context of interacting networks either at the molecular or cellular level, with complex endpoints necessarily difficult to predict. Nor should this be taken as an argument to ignore the genetic dependency of apoptosis as a predictive tool, as clearly there is good evidence that modulation of the apoptotic response can have powerful effects upon tumour predisposition and therapy, such as that demonstrated in spontaneous regression.

In summary, studies of DNA damage-induced cell death are giving us a basic insight into the molecular control of cell death as well as raising new hypotheses and new potential routes to intervention. They must, however, be interpreted with some caution and be used as the basis for subsequent hypotheses rather than as directly predictive tools.

References

[1] M. Gossen, H. Bujard, Tight control of gene expression in mammalian cells by tetracycline-responsive promoters, Proc. Natl. Acad. Sci. U. S. A. 89 (1992) 5547–5551.

[2] S. Giuriato, K. Rabin, et al., Conditional animal models: a strategy to define when oncogenes will be effective targets to treat cancer, Semin. Cancer Biol. 14 (2004) 3–11.

[3] S.W. Lowe, Activation of p53 by oncogenes, Endocr.-Relat. Cancer 6 (1999) 45–48.

[4] E.A. Slee, D.J. O'Connor, et al., To die or not to die: how does p53 decide? Oncogene 23 (2004) 2809–2818.

[5] J.S. Fridman, S.W. Lowe, Control of apoptosis by p53, Oncogene 22 (2003) 9030–9040.

[6] V.D. Stambolic, MacPherson, et al., Regulation of PTEN transcription by p53, Mol. Cell 8 (2001) 317–325.

[7] M. Mihara, S. Mihara, et al., p53 has a direct apoptogenic role at the mitochondria, Mol. Cell 11 (2003) 577–590.

[8] H.Y. Yang, Y.Y. Wen, et al., 14-3-3 sigma positively regulates p53 and suppresses tumor growth, Mol. Cell. Biol. 23 (2003) 7096–7107.

[9] A. Hirao, A. Cheung, et al., Chk2 is a tumor suppressor that regulates apoptosis in both an ataxia telangiectasia mutated (ATM)-dependent and an ATM-independent manner, Mol. Cell. Biol. 22 (2002) 6521–6532.

[10] E. de Stanchina, E. Querido, et al., PML is a direct p53 target that modulates p53 effector functions, Mol. Cell 13 (2004) 523–535.

[11] S.W. Lowe, E.M. Schmitt, et al., p53 is required for radiation-induced apoptosis in mouse thymocytes, Nature 362 (1993) 847–849.

[12] A.R. Clarke, C.A. Purdie, et al., Thymocyte apoptosis induced by p53-dependent and independent pathways, Nature 362 (1993) 849–852.

[13] S.D. Griffiths, S.J. Marsden, et al., Lethality and mutagenesis of B lymphocyte progenitor cells following exposure to alpha-particles and X-rays, Int. J. Radiat. Biol. 66 (1994) 197–205.

[14] C.A. Schmitt, J.S. Fridman, et al., Dissecting p53 tumor suppressor functions in vivo, Cancer Cell 1 (2002) 289–298.

[15] M. Herzig, G. Christofori, Recent advances in cancer research: mouse models of tumorigenesis, Biochim. Biophys. Acta 1602 (2002) 97–113.

[16] A.R. Clarke, S. Gledhill, et al., p53 dependence of early apoptotic and proliferative responses within the mouse intestinal epithelium following gamma-irradiation, Oncogene 9 (1994) 1767–1773.

[17] D.M. Pritchard, C.S. Potten, et al., The relationships between p53-dependent apoptosis, inhibition of proliferation, and 5-fluorouracil-induced histopathology in murine intestinal epithelia, Cancer Res. 58 (1998) 5453–5465.

[18] N.J. Toft, D.J. Winton, et al., Msh2 status modulates both apoptosis and mutation frequency in the murine small intestine, Proc. Natl. Acad. Sci. U. S. A. 96 (1999) 3911–3915.

[19] A. Oniscu, N. Sphyris, et al., p73alpha is a candidate effector in the p53 independent apoptosis pathway of cisplatin damaged primary murine colonocytes, J. Clin. Pathol. 57 (2004) 492–498.

[20] E.R. Flores, K.Y. Tsai, et al., p63 and p73 are required for p53-dependent apoptosis in response to DNA damage, Nature 416 (2002) 560–564.

[21] J.H. Hendry, W.B. Cai, et al., p53 deficiency sensitizes clonogenic cells to irradiation in the large but not the small intestine, Radiat. Res. 148 (1997) 254–259.

[22] J.H. Hendry, D.A. Broadbent, et al., Effects of deficiency in p53 or bcl-2 on the sensitivity of clonogenic cells in the small intestine to low dose-rate irradiation, Int. J. Radiat. Biol. 76 (2000) 559–565.

[23] D.M. Pritchard, C.S. Potten, et al., The relationships between p53-dependent apoptosis, inhibition of proliferation, and 5-fluorouracil-induced histopathology in murine intestinal epithelia, Cancer Res. 58 (1998) 5453–5465.

[24] O.J. Sansom, A.R. Clarke, The ability to engage enterocyte apoptosis does not predict long-term crypt survival in p53 and Msh2 deficient mice, Oncogene 21 (2002) 5934–5939.

[25] F. Paris, Z. Fuks, et al., Endothelial apoptosis as the primary lesion initiating intestinal radiation damage in mice, Science 293 (2001) 293–297.

[26] E.A. Komarova, R.V. Kondratov, et al., Dual effect of p53 on radiation sensitivity in vivo: p53 promotes hematopoietic injury, but protects from gastro-intestinal syndrome in mice, Oncogene 23 (2004) 3265–3271.

[27] S.W. Kohler, G.S. Provost, et al., Spectra of spontaneous and mutagen-induced mutations in the lacI gene in transgenic mice, Proc. Natl. Acad. Sci. U. S. A. 88 (1991) 7958–7962.

[28] D.J. Winton, N.J. Gooderham, et al., Mutagenesis of mouse intestine in vivo using the Dlb-1 specific locus test: studies with 1,2-dimethylhydrazine, dimethylnitrosamine, and the dietary mutagen 2-amino-3,8-dimethylimidazo[4,5-f]quinoxaline, Cancer Res. 50 (1990) 7992–7996.

[29] V.L. Buettner, H. Nishino, et al., Spontaneous mutation frequencies and spectra in p53 (+/+) and p53 (−/−) mice: a test of the 'guardian of the genome' hypothesis in the Big Blue transgenic mouse mutation detection system, Mutat. Res. 379 (1997) 13–20.

[30] A.R. Clarke, L.A. Howard, et al., p53, mutation frequency and apoptosis in the murine small intestine, Oncogene 14 (1997) 2015–2018.

[31] A.R. Clarke, M.C. Cummings, et al., Interaction between murine germline mutations in p53 and APC predisposes to pancreatic neoplasia but not to increased intestinal malignancy, Oncogene 11 (1995) 1913–1920.

[32] Meniel et al., submitted for publication.

[33] G. Ferbeyre, E. de Stanchina, et al., Oncogenic ras and p53 cooperate to induce cellular senescence, Mol. Cell. Biol. 22 (2002) 3497–3508.

[34] P. Fei, E.J. Bernhard, et al., Tissue-specific induction of p53 targets in vivo, Cancer Res. 62 (2002) 7316–7327.

[35] P.J. Coates, S.A. Lorimore, et al., Tissue-specific p53 responses to ionizing radiation and their genetic modification: the key to tissue-specific tumour susceptibility? J. Pathol. 201 (2003) 377–388.

[36] A.R. Clarke, O.J. Sansom, Analyzing tumor suppressor activities in the murine small intestine, Oncol. Res. 13 (2003) 333–337.
[37] S.W. Lowe, S. Bodis, et al., p53 status and the efficacy of cancer therapy in vivo, Science 266 (1994) 807–810.
[38] C.J. Kemp, S. Sun, et al., p53 induction and apoptosis in response to radio- and chemotherapy in vivo is tumor-type-dependent, Cancer Res. 61 (2001) 327–332.
[39] C.A. Schmitt, S.W. Lowe, Apoptosis and therapy, J. Pathol. 187 (1990) 127–137.
[40] F. Bunz, P.M. Hwang, et al., Disruption of p53 in human cancer cells alters the responses to therapeutic agents, J. Clin. Invest. 104 (1999) 263–269.
[41] K.M. Debatin, P.H. Krammer, Death receptors in chemotherapy and cancer, Oncogene 23 (2004) 2950–2966.
[42] A. Fedier, D. Fink, Mutations in DNA mismatch repair genes: implications for DNA damage signaling and drug sensitivity, Int. J. Oncol. 24 (2004) 1039–1047.
[43] T.A. Prolla, S.M. Baker, et al., Tumour susceptibility and spontaneous mutation in mice deficient in Mlh1, Pms1 and Pms2 DNA mismatch repair, Nat. Genet. 18 (1998) 276–279.
[44] C. Colussi, S. Fiumicino, et al., 1,2-Dimethylhydrazine-induced colon carcinoma and lymphoma in msh2(−/−) mice, J. Natl. Cancer Inst. 93 (2001) 1534–1540.
[45] O.J. Sansom, S.M. Bishop, et al., Apoptosis and mutation in the murine small intestine: loss of Mlh1- and Pms2-dependent apoptosis leads to increased mutation in vivo, DNA Repair (Amst.) 2 (2003) 1029–1039.
[46] R. Fishel, Signaling mismatch repair in cancer, Nat. Med. 5 (1999) 1239–1241.
[47] Y. Luo, F.T. Lin, et al., ATM-mediated stabilization of hMutL DNA mismatch repair proteins augments p53 activation during DNA damage, Mol. Cell. Biol. 24 (2004) 6430–6444.
[48] M. Zeng, L. Narayanan, et al., Ionizing radiation-induced apoptosis via separate Pms2- and p53-dependent pathways, Cancer Res. 60 (2000) 4889–4893.
[49] H. Shimodaira, A. Yoshioka Yamashita, et al., Interaction of mismatch repair protein PMS2 and the p53-related transcription factor p73 in apoptosis response to cisplatin, Proc. Natl. Acad. Sci. U. S. A. 100 (2003) 2420–2425.
[50] O.J. Sansom, N.J. Toft, et al., Msh-2 suppresses in vivo mutation in a gene dose and lesion dependent manner, Oncogene 20 (2001) 3580–3584.
[51] A. Baross-Francis, N. Makhani, et al., Elevated mutant frequencies and increased C: G→T: a transitions in Mlh1−/− versus Pms2−/− murine small intestinal epithelial cells, Oncogene 20 (2001) 619–625.
[52] O.J. Sansom, S.M. Bishop, et al., Apoptosis and mutation in the murine small intestine: loss of Mlh1- and Pms2-dependent apoptosis leads to increased mutation in vivo, DNA Repair 2 (2003) 1029–1039.
[53] X. Qin, D. Shibata, et al., Heterozygous DNA mismatch repair gene PMS2-knockout mice are susceptible to intestinal tumor induction with *N*-methyl-*N*-nitrosourea, Carcinogenesis 21 (2000) 833–838.
[54] C. Shao, M. Yin, et al., Loss of heterozygosity and point mutation at Aprt. locus in T cells and fibroblasts of Pms2−/− mice, Oncogene 21 (2002) 2840–2845.
[55] S. Ishizuka, K. Martin, et al., Poly(ADP-ribose) polymerase-1 is a survival factor for radiation-exposed intestinal epithelial stem cells in vivo, Nucleic Acids Res. 31 (2003) 6198–6205.
[56] M. Masutani, T. Nozaki, et al., The response of Parp knockout mice against DNA damaging agents, Mutat Res. 462 (2000) 159–166.
[57] M.T. Valenzuela, R. Guerrero, et al., PARP-1 modifies the effectiveness of p53-mediated DNA damage response, Oncogene 21 (2002) 1108–1116.
[58] A.R. Clarke, M. Hollstein, Mouse models with modified p53 sequences to study cancer and ageing, Cell Death Differ. 10 (2003) 443–450.
[59] R.A. Screaton, S. Kiessling, et al., Fas-associated death domain protein interacts with methyl-CpG binding domain protein 4: a potential link between genome surveillance and apoptosis, Proc. Natl. Acad. Sci. U. S. A. 100 (2003) 5211–5216.
[60] O.J. Sansom, J. Zabkiewicz, et al., MBD4 deficiency reduces the apoptotic response to DNA-damaging agents in the murine small intestine, Oncogene 22 (2003) 7130–7136.
[61] C.B. Millar, J. Guy, et al., Enhanced CpG mutability and tumorigenesis in MBD4-deficient mice, Science 297 (2002) 403–405.
[62] A.J. Watson, D.M. Pritchard, Lessons from genetically engineered animal models. VII. Apoptosis in intestinal epithelium: lessons from transgenic and knockout mice, Am. J. Physiol.: Gasterointest. Liver Physiol. 278 (2000) G1–G5.
[63] D.M. Pritchard, C. Print, et al., Bcl-w is an important determinant of damage-induced apoptosis in epithelia of small and large intestine, Oncogene 19 (2000) 3955–3959.
[64] S. Cory, D.C. Huang, et al., The Bcl-2 family: roles in cell survival and oncogenesis, Oncogene 22 (2003) 8590–8607.
[65] A. Villunger, E.M. Michalak, et al., p53- and drug-induced apoptotic responses mediated by BH3-only proteins puma and noxa, Science 302 (2003) 1036–1038.
[66] T. Shibue, K. Takeda, et al., Integral role of Noxa in p53-mediated apoptotic response, Genes. Dev. 17 (2003) 2233–2238.
[67] K.P. Hoyes, W.B. Cai, et al., Effect of bcl-2 deficiency on the radiation response of clonogenic cells in small and large intestine, bone marrow and testis, Int. J. Radiat. Biol. 76 (2000) 1435–1442.
[68] D.M. Pritchard, C.S. Potten, et al., Damage-induced apoptosis in intestinal epithelia from bcl-2-null and bax-null mice: investigations of the mechanistic determinants of epithelial apoptosis in vivo, Oncogene 18 (1999) 7287–7293.
[69] R.W. Johnstone, A.A. Ruefli, et al., Apoptosis: a link between cancer genetics and chemotherapy, Cell 108 (2002) 153–164.
[70] C.A. Schmitt, C.T. Rosenthal, et al., Genetic analysis of chemoresistance in primary murine lymphomas, Nat. Med. 6 (2000) 1029–1035.
[71] A.M. Ranger, J. Zha, et al., Bad-deficient mice develop diffuse large B cell lymphoma, Proc. Natl. Acad. Sci. U. S. A. 100 (2003) 9324–9329.
[72] J.M. Adams, A.W. Harris, et al., The c-myc oncogene driven by immunoglobulin enhancers induces lymphoid malignancy in transgenic mice, Nature 318 (1985) 533–538.
[73] D.W. Felsher, J.M. Bishop, Reversible tumorigenesis by MYC in hematopoietic lineages, Mol. Cell 4 (1999) 199–207.
[74] S. Pelengaris, B. Rudolph, et al., Action of Myc in vivo-proliferation and apoptosis, Curr. Opin. Genet. Dev. 10 (2000) 100–105.
[75] S. Pelengaris, T. Littlewood, et al., Reversible activation of c-Myc in skin: induction of a complex neoplastic phenotype by a single oncogenic lesion, Mol. Cell 3 (1995) 565–577.
[76] C.M. D'Cruz, E.J. Gunther, et al., c-MYC induces mammary tumorigenesis by means of a preferred pathway involving spontaneous Kras2 mutations, Nat. Med. 7 (2001) 235–239.
[77] S. Pelengaris, M. Khan, et al., Suppression of Myc-induced apoptosis in beta cells exposes multiple oncogenic properties of Myc and triggers carcinogenic progression, Cell 109 (2002) 321–334.
[78] D. Arango, G.A. Corner, et al., c-myc/p53 interaction determines sensitivity of human colon carcinoma cells to 5-fluorouracil in vitro and in vivo, Cancer Res. 61 (2001) 4910–4915.
[79] L. Chin, A. Tam, et al., Essential role for oncogenic Ras in tumour maintenance, Nature 400 (1999) 468–472.
[80] W. Pao, D.S. Klimstra, et al., Use of avian retroviral vectors to introduce transcriptional regulators into mammalian cells for analyses of tumor maintenance, Proc. Natl. Acad. Sci. U. S. A. 100 (2003) 8764–8769.